I. KINETIC AND MECHANISTIC STUDIES OF DYNAMIC ALKYNE METATHESIS
II. TOWARDS REGENERATIVE THERMOSETS USING FRONTAL RING-OPENING OLEFIN METATHESIS POLYMERIZATION

BY

ANDREW JAMES GREENLEE

DISSERTATION

Submitted in partial fulfillment of the requirements
for the degree of Doctor of Philosophy in Chemistry
in the Graduate College of the
University of Illinois Urbana-Champaign, 2023

Urbana, Illinois

Doctoral Committee:

Professor Jeffrey S. Moore, Chair
Professor Damien Guironnet
Professor Catherine J. Murphy
Dr. Leah N. Appelhans

ABSTRACT

In recent years, dynamic covalent chemistry (DCC) has seen the synthesis of increasingly complex cyclooligomers, polymers, and diverse compound libraries. The reversible formation of covalent bonds characteristic of DCC reactions favors thermodynamic product distributions for simple unitopic reactions. Traditionally, it was also assumed that DCC self-assembly processes with multitopic precursors were also wholly governed by thermodynamic factors. However, evidence suggests that kinetic effects are increasingly influential in reactions of increasingly complex substrates. Part I of this Dissertation describes mechanistic investigations into dynamic alkyne metathesis (AM) with the aim of elucidating factors leading to pathway-dependency in AM self-assembly reactions. Kinetic studies reveal the kinetic regime occupied by AM and serve as the basis for a rule-based computational model of dynamic self-assembly. To explore the relationship between catalyst loading and assembly efficiency, we developed a pulsed addition technique to determine the kinetic profile of AM catalyst deactivation. We found that prototypical AM catalysts are deactivated in solution on a timescale comparable to that of a self-assembly reaction, potentially leading to inefficient thermodynamic error correction.

In our exploration of more robust catalysts, we also established the orthogonality of dynamic imine exchange and AM. We hypothesized that tridentate AM "canopy" catalysts developed by Zhang, Fürstner, and Lee for AM would remain metathesis-active in the presence of Lewis basic moieties involved in other dynamic exchange reactions. Catalysts using a rigid trityl-derived ligand scaffold were found to successfully engender the metathesis of imine-bearing substrates, while catalysts using a relatively flexible triphenolsilane ligand were not. The former catalyst was found to be stable to imine moieties, but metathesis-inactive in the presence of basic

amines, excess water, and Lewis acidic co-catalysts. Assembly and disassembly of a molecular ladder prepared via tandem DCC in one pot was demonstrated in the presence and absence of a Lewis acid catalyst.

Part II of this Dissertation describes a novel approach to the design and manufacture of "regenerative" polymer thermosets and novel upcycling strategies for such species. While recent work has enabled the synthesis of thermosets with degradable linkages, current strategies for end-of-life management of these materials is still limited to upcycling strategies. Sustainability initiatives would benefit tremendously from the development of chemical strategies to regenerate polymer functionality through the restoration of the original polymerizable moieties, enabling reuse of degradation products in repeated polymerizations. We hypothesized that derivatives of dicyclopentadiene (DCPD) and its corresponding polymer possessing a potent dienophilic moiety, namely an enone motif, would be amenable to reactivation for ring opening metathesis polymerization (ROMP) by Diels-Alder reaction with cyclopentadiene. We found that a ketone-functionalized DCPD derivative forms persistent chelates in solution-phase ROMP, slowing the reaction. This diminished propagation rate, coupled with the crystallinity of the monomer, prohibited its application in frontal polymerization. Attempts at post-polymerization modification of oligo(oxaDCPD) via Diels-Alder reaction with cyclopentadiene failed to furnish the desired product, yielding instead chain end-functionalized oligomers as determined by advanced mass analysis. These data provide insight into the pitfalls of both monomer design and reactivation strategies for future regenerative thermosets.

ACKNOWLEDGMENTS

I consider it the privilege of a lifetime to have studied at the University of Illinois. That I got to do it with the with the support of the mentors, friends, and colleagues listed here is more than I could have ever asked for. The work I present in this dissertation would not have been possible without you.

First and foremost, I am tremendously grateful for the guidance of my advisor, Jeff Moore. I am grateful for the opportunity to study what I wanted to study, as abstract as that may have been, and for the standards you set for my work. I aspire to, one day, match your thorough understanding of both organic chemistry and the scientific method. I am also grateful for the calm you imparted to me in the times when my back was against the wall. Work felt like play in your lab, and I intend to take that spirit with me into future research endeavors. I also want to thank the University professors who served on my committee for their guidance and insight. Professors Cathy Murphy, Damien Guironnet, and Steve Zimmerman: thank you for setting the bar high.

I am indebted to the staff at the University of Illinois who made research not only doable, but fun as well. I want to thank Dean Olson, Lingyang Zhu, Furong Sun, Xiuli Mao, and Nikki Duay. To the administrators of the Inorganic/Materials/Physical/Analytical Chemistry office: thank you for all you do to meet the needs of the student body. Finally, to the administrator of the Moore group, Ashley Trimmell: thank you for holding the group together. Everyone who has come through the Moore group in your time here owes a large part of their success to you.

Most of my training as a chemist has been in the lab under the guiding hands of several incredible mentors. Drs. Chris Pattillo, Josh Laffoon, and Chloe Wendell: I owe my synthetic skills entirely to you. Thank you for your patience and generosity, welcoming me into your ranks. Dr.

Morgan Cencer: your rigorous approach to data analysis and experimental design is a Platonic ideal to which I aspire. I feel incredibly lucky to have worked alongside you all.

I was fortunate enough to have two research careers in my time as a graduate student, and I am incredibly grateful for the opportunity to try something new at Sandia National Labs. I am thankful to Dr. Sam Leguizamon for teaching me to shoot from the hip. Your hustle and apparently boundless creativity are matched only by your kindness. To Dr. Leah Appelhans, I am grateful not only for your wisdom in guiding my research, but for stepping in as a committee member, your thoroughness in reviewing my research output, and for welcoming me to New Mexico. To you, and the other team members at the Advanced Materials Laboratory, I want to express how wonderful an experience it was to be a Sandian, even for a short time.

My amazing friends and coworkers have carried me through every trial in the last five years. Kevin, Hannah, Joe, Kelly, Frank, Elliot, Annie, Will, Alison, Eric, Troy, and Justine, thank you for the memories. I'm sure there will be more to come. To the members of the Moore group, especially Katie, Morgan, Josh, Billy, Yuting, Yunyan, Brittany, Jose, Oleg, and Betty, thank you for making it fun to go to work every day.

To my parents, Alan and Muffy, thank you for everything. Your relentless empathy and optimism made me feel like I could do anything, even when research was difficult. To my sister, Sarah, thank you for being so cool. To my grandparents, Dee and Denny, thank you for your overwhelming love and support. To all of you, as well as Andy, Kevin, Benjie, and Jimmy, thank you for pretending to find my work interesting. I love you all.

To my sister and best friend, Sarah

TABLE OF CONTENTS

CHAPTER 1: INTRODUCTION TO KINETIC AND THERMODYNAMIC CONTROL IN DYNAMIC COVALENT CHEMISTRY

1.1 Introduction to Dynamic Covalent Chemistry (DCC)

1.1.1 Dynamic Covalent Chemistry (DCC)

Dynamic covalent chemistry (DCC) is an efficient synthetic strategy that utilizes multitopic precursors designed to form reversible covalent bonds, combining advantages of error correction during synthesis with the stability of a covalent compound as the final product.[†] It has enabled the synthesis of a variety of molecular architectures, often isolated as a single, discrete species, including macrocycles,[1] cages,[2] and covalent organic frameworks.[3,4] A literature survey on 1,100 papers acquired through a search of the term "dynamic covalent" indicates that polymers are the most common target, followed by cages, macrocycles, and COFs.[5] Reversible bonds commonly in use include imine, boronic ester, hydrazine, disulfide, alkyne, oxime and alkene exchange, listed in order of their frequency. These structures have found applications in host-guest chemistry,[6] organic electronic materials,[7] information storage and retrieval,[8] catalysis,[9] biological applications,[10] chemical sensing,[11] and as building blocks for other materials, such as nanofibers.[12]

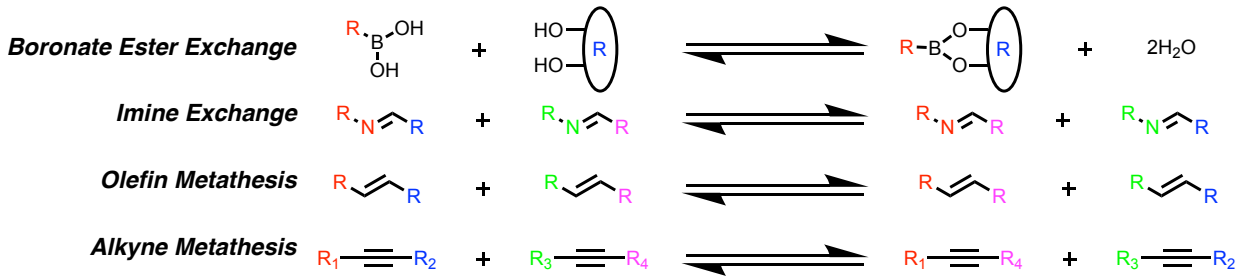

Figure 1.1. Selected examples of DCC reactions.

[†] This chapter has been adapted from the following publication: Greenlee, A. J.; Wendell, C. I.; Cencer, M. M.; Laffoon, S. D.; Moore, J. S. Kinetic and Thermodynamic Control in Dynamic Covalent Synthesis. *Trends Chem.* **2020**, *2* (12), 1043–1051. DOI: 10.1016/j.trechm.2020.09.005

Most targets of DCC are constructed from a small number of different types of repeating units. Thus, DCC is commonly a cyclooligomerization process. The combination of a bimolecular oligomerization and intramolecular cyclization in the same reaction represents one challenge of dynamic covalent synthesis. Another challenge stems from the multitopic nature of DCC precursors. While the individual bond forming events are reversible, incorrectly joined structures may require multiple bond breakages to release an incorrectly placed precursor. Some erroneous structures fall out of dynamic equilibrium with the rest of the reaction network. Nonetheless, overcoming these challenges unleashes DCC's tremendous gain in synthetic efficiency reflected by the number of bonds made per operational step. Moreover, DCC product yields may approach quantitative, whereas cyclooligomerizations relying on strong irreversible bond formations tend to give low yields of final product, presumably because error correction is key to synthetic success.[13]

Due to the reversibility of each bond forming event, DCC is generally thought to operate under thermodynamic control. The same literature survey mentioned above found that thermodynamic products and pathways are mentioned twice as much as kinetic products and pathways. However, as DCC advances to increasingly complex targets, there is good reason to suggest that kinetic factors may become more important. In this regard, there is an analogy between dynamic covalent synthesis and Levinthal's paradox for protein folding.[14] Levinthal's paradox states that because of the very large number of degrees of freedom in an unfolded polypeptide chain, the possible conformations are too vast to explore them all on the way to its native folded state. In a similar vein, the concatenation of multitopic precursors gives rise to a large number of structures on the way to the target product. These structures include polyhedra, polymers, and networks, and they may have very similar energies. This suggests a flat landscape, but complexes exhibiting multiple persistent bonds are stabilized, which produces a vast landscape with

somewhat regular variation. Given the complexity of DCC reaction networks and associated energy landscapes, synthetic intuition is unsuited to predict the outcome. Failures in experimental DCC often come at a high cost because multitopic, complex precursors require considerable structural optimization and synthetic overhead.[9] Predicting outcomes is therefore essential and may require computational modeling to ensure a full understanding of the underlying factors that shape the energy landscape.

1.1.2 Thermodynamically Controlled DCC

The ability of dynamic systems to undergo reversible component exchange is key to the utility of DCC. Under thermodynamic control, even off-pathway intermediates typically error correct toward favorable product distributions on the timescale of the reaction (Figure 1.2).[15] Work from the Swager group recently demonstrated the reversibility of nucleophilic aromatic substitution (S_NAr) in the synthesis of macrocycles and covalent organic frameworks from both free starting material and off-pathway kinetic intermediates.[16] Accessing the product distribution regardless of entry point into the reaction landscape is a necessary condition to classify the product distribution as a thermodynamic equilibrium. In a second example, arylene ethynylene macrocycles are formed both by alkyne metathesis cyclooligomerization and by depolymerization-macrocyclization of linear poly(arylene ethynylene) species.[17]

Thermodynamic control of DCC systems enables certain applications. For example, Swager and coworkers demonstrate the dynamic covalent synthesis of surfactants in situ in order to generate double emulsions.[18] One component of the surfactant is water soluble and the other is oil soluble; the surfactant itself forms at the interface of the three phases. The surfactant remains in dynamic equilibrium, allowing the incorporation of antibodies for biosensing applications.

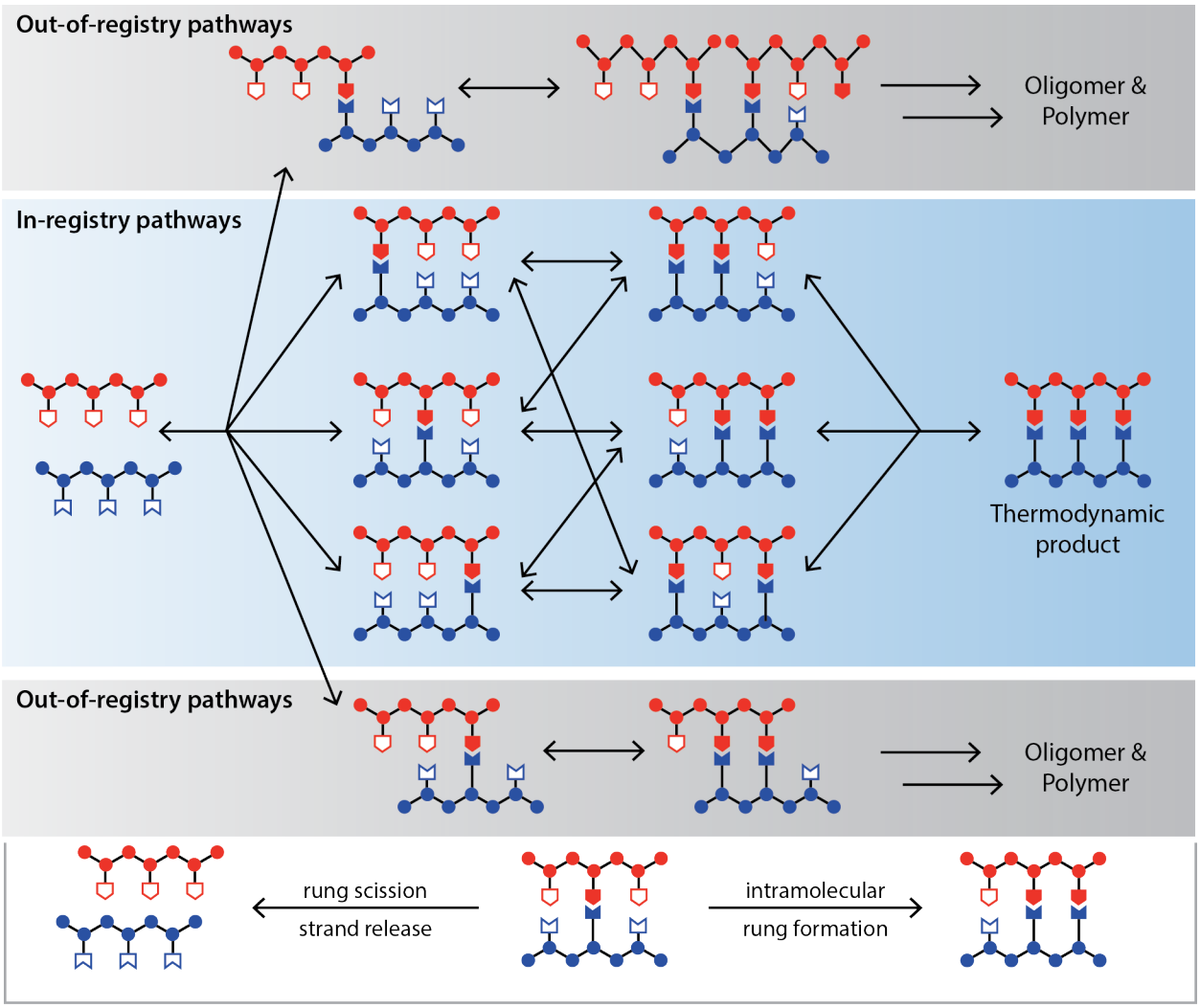

Figure 1.2. Reaction network of ladder formation under DCC. In-registry intermediates and products have correctly matched rungs where outer rungs bond to other outer rungs, and center rungs bond to other center rungs between two strands. Out-of-registry products have mismatched rung formation. Mismatched intermediates revert to free strands if rung scission is faster than intramolecular rung formation. Reproduced with permission from ref. 5. Copyright 2020, Cell Press.

Systems under thermodynamic control favor distributions that maximize entropy by generating structures with the fewest possible number of building blocks while minimizing angle strain of the resultant structures. These principles have enabled the intuitive design of a wide variety of cyclic molecular architectures on the basis of precursor topicity and geometry.[19] Furthermore, in systems with very flat energy landscapes, slight differences in thermodynamic

stability lead to self-sorting and large amplifications of product concentrations, which can be further improved by increased catalyst loading and thermal cycling.[17,20–23] Our group and the Cooper group demonstrated that small energetic differences arising from chiral recognition are sufficient to direct the homochiral self-sorting of dynamic covalent libraries (DCLs) composed of racemic building blocks.[23,24] Zhang and coworkers recently demonstrated the synthesis of a cyclic porphyrin macrocycle via dynamic alkyne metathesis, which yielded the desired trimer in 82% compared to a mixture of trimer (18%) and dimer (20%) via a kinetically controlled cross-coupling cyclooligomerization.[25]

While design principles are generally reliable predictors of product topology and stability, occasionally this thinking belies the nuances of DCC energy landscapes. Cooper and coworkers recently designed a computational screening procedure to predict the outcomes of imine condensation reactions based on product stability.[26] While most combinations of aldehyde and amine precursors produced the predicted imine cages, several pairings of precursors led to structures with unexpected topologies. In these cases, the less thermodynamically favored product was observed, and the energetic preference for the predicted structures was determined to be small (around 5 kJ mol^{-1}) compared to the observed products. The Zhang group reported similar phenomena in the synthesis of arylene ethynylene cages.[27] Slight variations in monomer size yielded structures with drastically different topologies, despite a consistent face-to-edge angle between substrates. Taken together, these results suggest that intuitive design rules are unreliable predictors of complex reaction outcomes, and that pathway-dependence may contribute to DCC syntheses in largely unexplored ways. Advancing DCC as a robust and reliable synthetic approach will likely benefit from extending the existing computational tools (*vide infra*).

1.1.3 Kinetically Controlled DCC

The reversible bonds used in DCC enable systems to undergo error correction. The faster the rate of exchange, the less prone the resulting system is to kinetic traps (Figure 1.3). A ladder with hydrogen bonded rungs demonstrates much higher fidelity (98% vs. 62%) than an imine-linked ladder with an identical backbone, due in part to the high exchange rate of hydrogen bonding.[28,29] However, while rapid exchange speed rescues a system from a putative kinetic trap, all covalent bonds are susceptible to trapping under some circumstances. Rigid complex architectures, such as COFs and cages, typically synthesized via DCC tend to be predisposed towards kinetic control due to precursor multitopicity. Macrocycles with ditopic precursors require two bond breakage events before a precursor is released. After the first bond breakage, the two resulting reactive moieties are in close proximity and so have a faster rate of recombination than two unlinked precursors, an effect which is exacerbated by the rigidity of the structures. If the rate of bond reformation is faster than the breakage of the second bond, the macrocycle may behave as a kinetic trap. Kinetic trap behavior is even more likely for structures which require three or four bond breakages, where precursors are tritopic or tetratopic and the partially broken structures have higher rigidity.[2,30] This is apparent in the synthesis of ladder compounds, which generally have n-topic precursors, where n is the number of rungs. These studies show that beyond a certain number of rungs the structures can no longer undergo error correction and tend to form myriad mismatched products instead.[8,31,32]

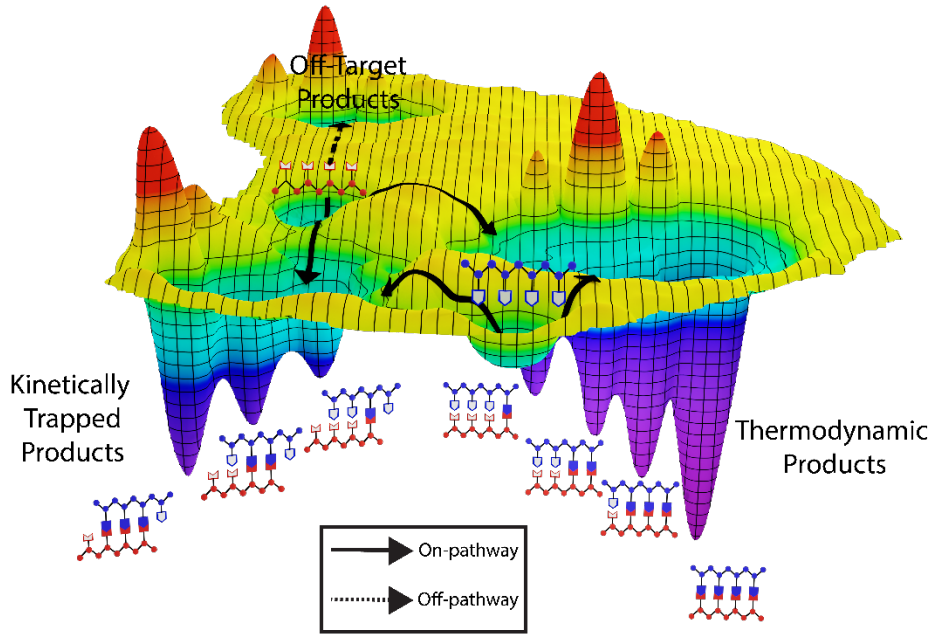

Figure 1.3. Generic energy landscape of ladder formation. In reactions with complex energy landscapes, species can become kinetically trapped even if reversible chemistry is used. Kinetic traps can persist if small barriers funnel material back to the trapped structure rather than out of the kinetic trap and toward a thermodynamic minimum. In the case of molecular ladders, out-of-registry products may be kinetic traps if rung scission is immediately followed by reformation of the rung. Kinetic factors such as proximity-induced high effective concentration prevent error correction in a dynamic system where the thermodynamic product is desired. Reproduced with permission from ref. 5. Copyright 2020, Cell Press.

Rigidity also influences reaction outcomes by rendering certain transition states geometrically inaccessible. This is particularly relevant for reactions with conformationally restrictive transition states, such as the transition state leading to the metallacyclobutadiene intermediate in alkyne metathesis. Work by our group to synthesize a molecular Möbius strip has demonstrated total kinetic diastereoselectivity because only one of the two possible diastereomeric intermediates could form the key metallacylobutadiene transition state (Figure 1.4).[33]

Solubility is an ever-present consideration in the synthesis of complex architectures. Large structures common in DCC have decreased kinetic solubility. Heavily conjugated structures are common because they are rigid enough to be shape-persistent, but large, planar π surfaces

contribute to insolubility due to π-π stacking, removing the compound from dynamic equilibrium and promoting its formation. Dichtel and coworkers developed a system which produces macrocycle only when it is insoluble in the reaction solvent; dissolving the macrocycle and bringing it back into dynamic equilibrium leads to conversion into polymer, the putative thermodynamic product.[1] Many DCC syntheses are driven by precipitation.[6,34–37] Adding solubilizing groups or changing the size and planarity of the π surface allows modulation of solubility. Northrop and coworkers produce a planar and non-planar version of the same boronate ester cage by inserting ethynylene units into a biaryl backbone with a 90° twist.[37] They demonstrate that the more planar version is less soluble and more stable to protic solvents.

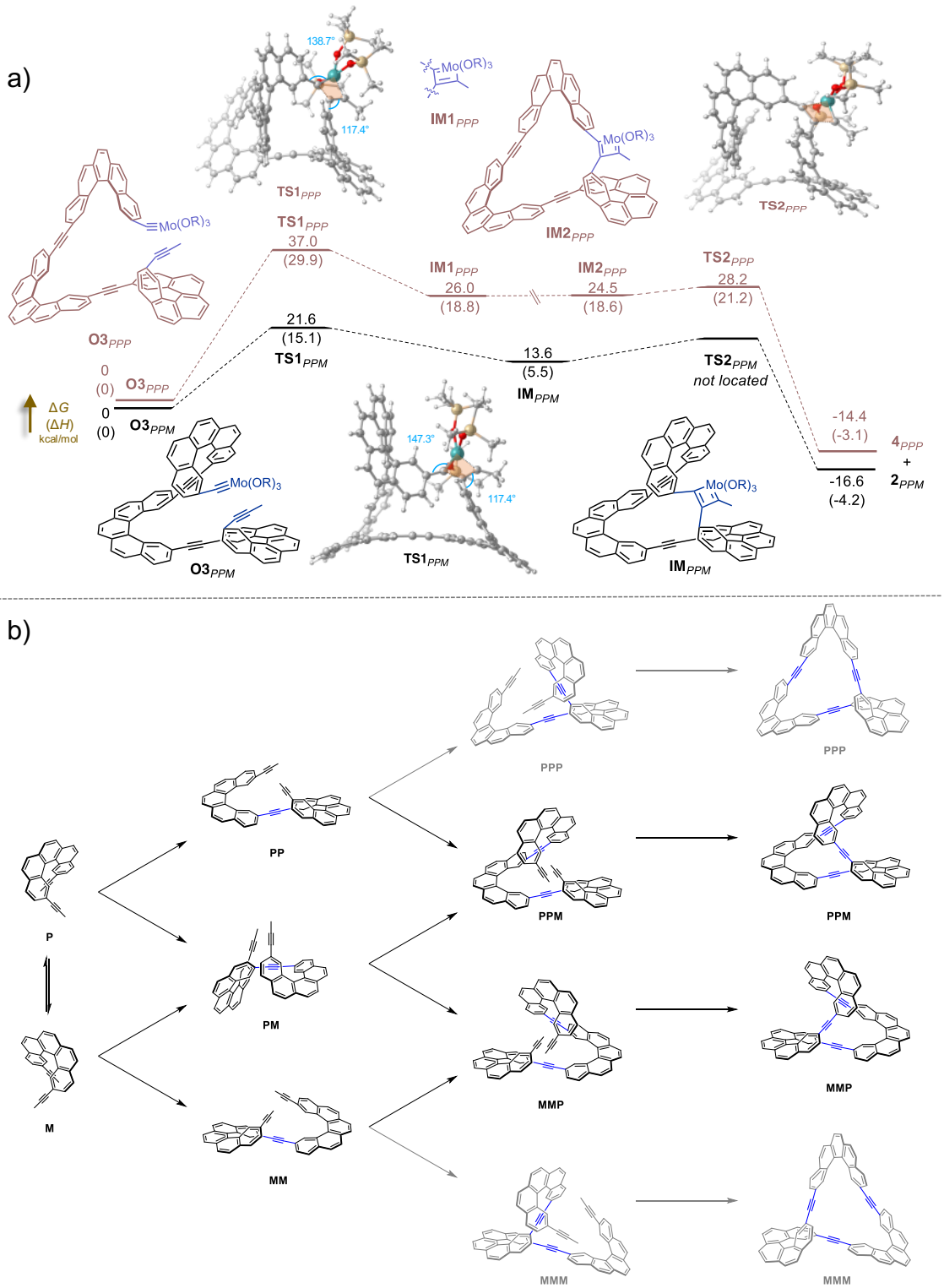

Figure 1.4. Reaction pathways leading to molecular Möbius strip. (a) Energy profile demonstrating kinetic diastereoselectivity in macrocyclization (b) reaction network showing intermediates leading to all possible stereoisomers. Structures in gray were not observed as products of the reaction. Reproduced with permission from ref. 33. Copyright 2020, American Chemical Society.

Supramolecular interactions in solution also affect the product distribution in some systems. The enthalpic benefit of the interactions themselves drive the equilibrium toward compounds that promote more stabilizing supramolecular interactions.[1] These interactions arise between species within the dynamic pool or through external selection. Work from the Sanders group demonstrates the utility of a kinetic template in addition to hydrophobic π-π interactions in the synthesis of a [3]-catenane inaccessible through thermodynamic control.[38]

In addition, supramolecular structures that form between cages and other complex products affect exchange rates. Dichtel and coworkers report an imine macrocycle that assembles into nanotubes which prevent further imine exchange, and Otto and coworkers report a similar effect.[12,39] In the synthesis of knots and catenanes from a DCL, multiple products are kinetically trapped as a result of intramolecular π-π stacking in ambiphilic molecules, analogous to the hydrophobic effect in protein folding.[40]

While kinetic traps may introduce synthetic obstacles, they sometimes provide products in higher yields than the same system under thermodynamic control. In some cases, the kinetic trap is also the thermodynamic product.[2,41] In other cases, the pathway-dependence of kinetically controlled systems can be leveraged. Multiple products may be accessible from the same precursors under different conditions, especially useful given the high synthetic overhead of DCC precursors.[12] Otto and coworkers have provided evidence that mechanical agitation has a strong influence on product distribution.[11,34] Slow addition of monomer has been demonstrated to produce COFs with larger crystal domains than a single-addition protocol.[41]

Kinetic control also allows improved information storage. Scott and coworkers show that a high-fidelity synthesis of an information-bearing five rung imine ladder is only achieved by increasing and then decreasing the concentration of scandium (III) triflate, commonly used to

promote imine exchange.[32] This sort of chemical annealing is reminiscent of thermal annealing of DNA.[32] Keeping the concentration at the same low levels throughout the reaction leads to mismatched byproducts instead; this dependence on pathway suggests that the information-bearing ladders are kinetic products. Lehn and coworkers have developed libraries of acyl hydrazones and imines generated from simple aldehyde, acyl hydrazine, and aniline building blocks.[8] In the presence of a metal cation with the appropriate coordination geometry, kinetically trapped species were favored. Upon precipitation of the directing metals, the libraries were expected to return to equilibrium, favoring formation of the more stable acyl hydrazone. However, because the exchange rate of imines and acyl hydrazones is on the order of weeks, the composition of the DCL remained unchanged on a relevant laboratory timescale, or until it was erased by thermal cycling. Furthermore, the library could be trained to adopt an altered kinetic equilibrium through the addition of a different metal cation, demonstrating the versatility of a simple system for information storage. In this case, kinetic factors allow access not only to targeted materials, but also to emergent properties from simple chemical systems.

In many biological and synthetic systems, molecular recognition events are triggered by a slow, irreversible step which occurs due to a perturbation of a system previously under thermodynamic control. This perturbation occurs either through internal or external selection, and the resulting irreversible step removes kinetically trapped species from the dynamic pool, shifting equilibrium to favor their formation. This phenomenon, referred to as dynamic systemic resolution (DSR), is one way to combine the adaptive nature of thermodynamic control with the selectivity of kinetic control.[10] As an extension of classical dynamic kinetic resolution, this technique has been used for chiral resolution of epimers,[42] as well as in biomimetic applications to amplify strong binders in the presence of receptor molecules.[43]

Unlike thermodynamic DCC syntheses, the selectivity of DSR arises from reaction kinetics rather than product stability. Thus, the external kinetic stimulus must be chosen judiciously: it must be selective enough to operate quickly on the fastest-responding component of the DCL without directly affecting the rest of the DCL or halting the ongoing thermodynamic equilibrium.[15] Osowa and Miljanić used irreversible oxidation to enable self-sorting of a DCL of imines.[44] Slow oxidation of the imine species ensured that only the fastest-reacting amine and aldehyde pairs were removed from the dynamic pool, enabling highly efficient resolution of three discrete products from a library capable of producing nine different imines. Similar processes have been reported by Rizzuto and Nitschke in the synthesis of imine-based coordination cages.[45] Antagonistic amplification of thermodynamically disfavored structures by kinetic requisition of more reactive imines resulted in the self-assembly of heteroleptic cages inaccessible by straightforward DCC synthesis. A major goal for DCC would be to use such DSR strategies to access and amplify kinetically trapped structures with low symmetry and unique functionality.[46]

1.1.4 Computational Studies

Most efforts at rationally designing DCC systems have utilized thermodynamic modeling. Computational predictions of reaction outcomes based on thermodynamic driving forces have been used to design precursors and generally rely on the assumption that reactions will reach their thermodynamic end point. The most common approach to thermodynamic modeling uses density functional theory (DFT) to locate the energy of the various possible structures that could be formed in a given reaction network. The lowest energy structure is then assigned as the expected product. However, this approach does not always account for features of product stability, such as permanent porosity in the case of molecular cages. Furthermore, few approaches to computational

modeling account for kinetic factors, namely reaction barriers to key assembly steps along competing reaction pathways, which may dictate product distributions.[3,24,26]

A common approach to kinetic modeling, which involves manually calculating a reaction network and generating a master equation for all species in solution, is well-explored for biological systems but difficult to apply to DCC processes, which typically proceed *via* cyclooligomerization and thus involve a theoretically infinite number of unique reaction intermediates.[45] Monte Carlo algorithms, which have been used to provide insight into the mechanism of covalent organic framework formation, ignore the reaction network and use repeated random sampling and subsequent statistical analysis to obtain insight into key intermediates and the rate determining step in product formation.[41,43,46] In an example of correlating thermodynamic and kinetic considerations, the Lively group used DFT to determine the formation energies of key intermediates along competing imine cage assembly pathways in order to rationalize scrambled product distributions.[43]

In DCC syntheses where kinetic traps are common, kinetic models may provide superior synthetic guidance compared to thermodynamic models but may be difficult to generate or computationally costly if many intermediates populate the dynamic pool or if the mechanism of error correction is unclear. Rule-based modeling combines the stochasticity of Monte Carlo modeling with the reaction network information provided by traditional kinetic modeling. The heart of a rule-based model is the rules, a set of simplified descriptors of the reactive chemistry of the system. These indicate changes in the bonding or state of reaction components. Once a set of rules sufficiently captures the attributes of a system, the model generates a reaction network and stochastically determines the time-dependent concentrations of all species in the course of a reaction simulation. Algorithmic generation of the reaction network ensures that it is complete and

accurate. Though rule-based models have been most widely applied to biological systems, this strategy is also uniquely suited to use in DCC assembly reactions, which involve comparably large and complex reaction networks.[30]

1.2 Alkyne Metathesis for the Synthesis of Nanostructures and Materials

1.2.1 Alkyne Metathesis

Alkyne metathesis (AM), the redistribution of the alkylidene units of a pair of acetylene derivatives with the aid of a transition metal catalyst, is a close relative of the contemporary and tremendously successful olefin metathesis reaction. It was first reported in 1968 using a heterogeneous WO_3/silica catalyst to engender the thermodynamic disproportionation of 2-pentyne at high temperatures (200-400 ºC).[47] Nearly a decade later, Mortreux and Blanchard documented the first heterogeneous AM catalyst system, which employed molybdenum hexacarbonyl and a phenol additive at slightly less extreme temperatures (160 ºC in the original report).[48] The advent of high-valent transition metal alkylidyne complexes ("Schrock alkylidynes") in the 1980s enabled mechanistic studies,[49–51] which provided evidence suggesting that the reaction proceeds through a [2+2] cycloaddition, followed by isomerization of the metallacyclobutadiene intermediate and liberation of the product by [2+2] cycloreversion (Figure 1.5a). These studies also indicated that the choice of ancillary ligands about the alkylidyne unit is a critical determinant of catalytic activity.

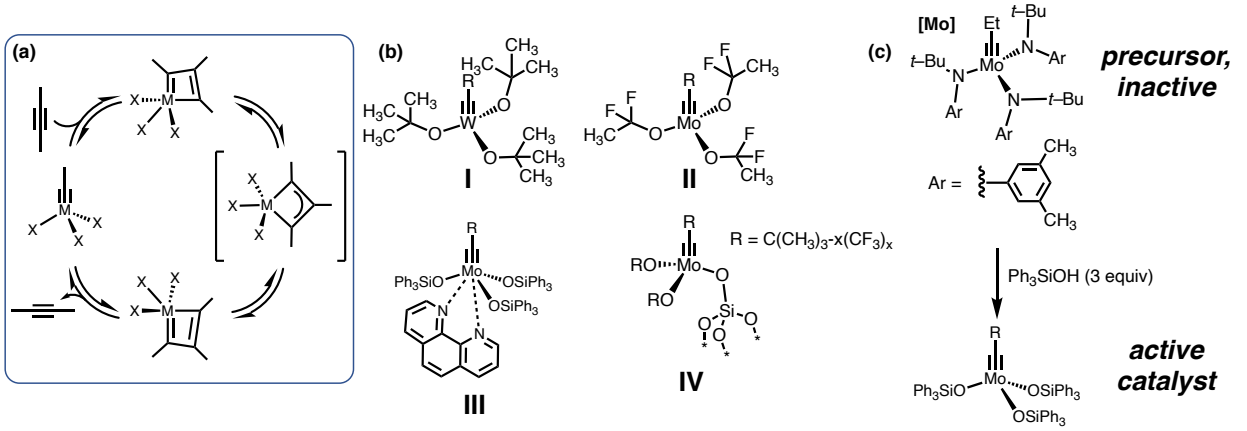

Figure 1.5. Alkyne metathesis mechanism and representative catalysts. (a) Reaction mechanism of AM. (b) Early Schrock type carbynes (**I** and **II**) paved the way for the more active siloxy-based catalysts, including bench-stable phanthroline adduct **III** and silica-supported species **IV**. (c) The archetypal AM catalyst generated from precursor **[Mo]** and triphenylsilanol.

The first well-defined AM alkylidyne complexes developed by Schrock and co-workers employed tungsten or molybdenum (VI) metal centers with (perfluorinated) tert-alkoxide ligands (**I** and **II**).[52–55] In the search for more highly active and functional group-tolerant catalyst systems, it was discovered that siloxy groups offer adaptive electronic characteristics ideal for metathesis. The "floppy" nature of the metal-oxygen-silicon linkage allows the oxygen atom to shuttle between the extremes of sp and sp^3 hybridization throughout the course of reaction, thus changing the donor ability of the ligand at each elementary step in the catalytic cycle. Synthetic routes to catalysts of this type, including pyridine and phenanthroline-stabilized alkylidene (**III**) and nitride adducts exhibiting remarkable storage lifetimes in ambient conditions,[56,57] as well as silica-supported complexes (**IV**),[58] have enabled the exploration of a wide range of chemical space with regards to catalyst design.[59–62] For example, the hypothesized metallacyclobutadiene intermediate generated from the archetypal **[Mo]**/$(Ph_3SiOH)_3$ alkylidyne complex was recently isolated and characterized by single crystal x-ray diffraction.[63] The state of the art of AM catalyst development is discussed in Chapter 3 (vide infra).

As a synthetic tool, AM possesses certain advantages over the more popular analog olefin metathesis. Despite considerable progress towards kinetically *E*- and *Z*-selective olefin metathesis catalysts, setting desired alkene geometry with high fidelity, particularly at a late stage of a synthetic endeavor, is still compromised by the lack of decent stereochemical resolution. Alkyne metathesis followed by stereoselective semireduction, or any other postmetathetic transformation of the triple bond, provides an alternate answer to this challenge. Indeed, Fürstner and coworkers have demonstrated the utility of a ring closing alkyne metathesis (RCAM) strategy in the total synthesis of a variety of macrocyclic natural products.[64–66]

1.2.2 Molecular Architectures via Alkyne Metathesis

In addition to their utility as synthetic handles, the ethynylene moiety possesses rigidity and linear geometry. These features make AM uniquely suited to generate shape-persistent nanoscale architectures with mechanical rigidity as well as thermal and chemical robustness. These facets, combined with the characteristic thermodynamic error-correction of DCC, has enabled the synthesis of a wide variety of functional alkynyl macrocylces, cages, and polymers in the last two decades (Figure 1.6).[67]

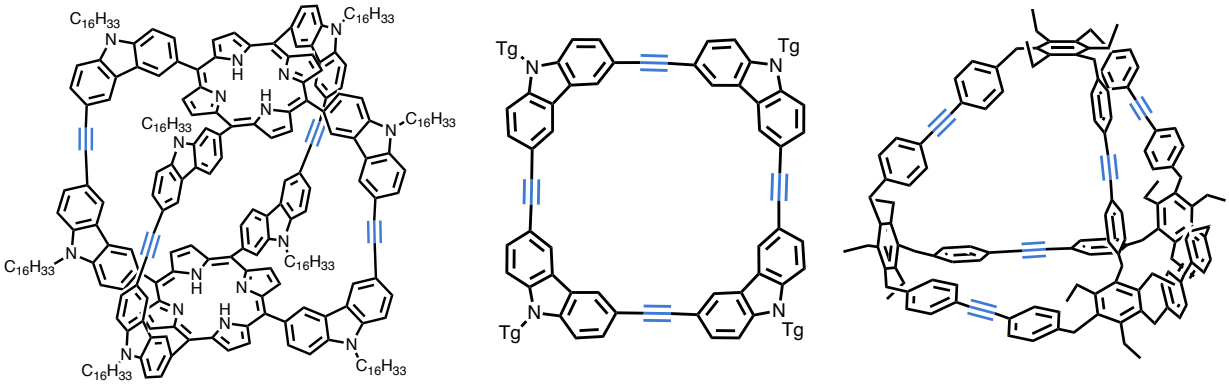

Figure 1.6. Selected nanoscale structures prepared via AM. Reproduced from references 25 (left), 68 (middle), and 2 (right).

Because AM is an equilibrium reaction, product formation requires a kinetic driving force. Thus, strategies to remove AM byproducts occurred concurrently with catalyst development. Early strategies involved the removal of small alkyne byproducts using a dynamic vacuum, though this entailed changes in solvent concentration and was found to be inefficient for reactions of larger scale. Moore and coworkers demonstrated that the removal of large, insoluble alkynes through precipitation circumvents potential catalyst poisoning by small molecules and enabled gram-scale synthesis of arylene ethynylene macrocycles, albeit with poor atom economy.[68] In 2010, Fürstner and coworkers demonstrated that 5 Å molecular sieves (MS) could be used to trap 2-butyne, a byproduct of AM of the propyne group.[57] Despite the practical inconvenience of installing the propyne group, this strategy has become the most widely used in AM DCC.

Despite the abundance of research towards highly active catalysts and controlling the equilibria of AM reactions, factors giving rise to contrathermodynamic AM reaction outcomes are still poorly understood. Work by the Zhang group demonstrated that precursor geometry plays a critical role in determining product outcomes for AM cage assembly.[57] Specifically, it was observed through dynamic scrambling experiments that fast macrocyclization of multitopic alkynyl precursors hinder the conversion of certain intermediates to others, leading to kinetically favored, but not kinetically trapped, products. Our group demonstrated that slight variations in the bite angle of reactive AM pendant groups can direct assembly away from discrete products and towards oligomers.[19]

It is speculated that this apparent kinetic sensitivity of AM DCC arises from the high strain barriers associated with the formation of confined 2- and 3D cage structures with mechanically rigid ethynylene building blocks. However, this assumption may belie the complexity of AM self-assembly. Exploration of factors related to kinetic control in self-assembly, including catalyst

activity and lifetime, templating effects of solvent or other guest molecule additives, and the effects of monomer design, including the addition of chelating, protic, or strong electron-withdrawing groups, all merit further study. Kinetic control may allow access to thermodynamically inaccessible structures, such as those with lower symmetries. Since AM is a homocoupling reaction, and thus lacks directionality (unlike imine condensation, e.g.), novel strategies to access these architectures will be required. For example, the development of unsymmetrical end groups with different kinetic behavior and catalyst systems capable of activating heteroatom-containing triple bonds deserve more attention, as they would increase the substrate pool considerably. Applications of kinetic control in AM to generate novel structures with shape persistency, extended conjugation, and well-defined internal cavities are anticipated.

1.3 References

(1) Chavez, A. D.; Evans, A. M.; Flanders, N. C.; Bisbey, R. P.; Vitaku, E.; Chen, L. X.; Dichtel, W. R. Equilibration of Imine-Linked Polymers to Hexagonal Macrocycles Driven by Self-Assembly. *Chem. – A Eur. J.* **2018**, *24* (16), 3989–3993.

(2) Lee, S.; Yang, A.; Moneypenny, T. P.; Moore, J. S. Kinetically Trapped Tetrahedral Cages via Alkyne Metathesis. *J. Am. Chem. Soc.* **2016**, *138* (7), 2182–2185.

(3) Gasparini, G.; Dal Molin, M.; Lovato, A.; Prins, L. J. Dynamic Covalent Chemistry. In *Supramolecular Chemistry*; John Wiley & Sons, Ltd: Chichester, UK, 2012.

(4) Ma, T.; Kapustin, E. A.; Yin, S. X.; Liang, L.; Zhou, Z.; Niu, J.; Li, L.-H.; Wang, Y.; Su, J.; Li, J.; Wang, X.; Wang, W. D.; Wang, W.; Sun, J.; Yaghi, O. M. Single-Crystal x-Ray Diffraction Structures of Covalent Organic Frameworks. *Science (80-.).* **2018**, *361* (6397), 48–52.

(5) Greenlee, A. J.; Wendell, C. I.; Cencer, M. M.; Laffoon, S. D.; Moore, J. S. Kinetic and

Thermodynamic Control in Dynamic Covalent Synthesis. *Trends Chem.* **2020**, *2* (12), 1043–1051.

(6) Slater, A. G.; Little, M. A.; Briggs, M. E.; Jelfs, K. E.; Cooper, A. I. A Solution-Processable Dissymmetric Porous Organic Cage. *Mol. Syst. Des. Eng.* **2018**, *3* (1), 223–227.

(7) Savino, C.; Ryan, R. P.; Knee, J. L.; Jimenez-Hoyos, C. A.; Northrop, B. H. Electronic Spectroscopy of 2-Phenyl-1,3,2-Benzodioxaborole and Its Derivatives: Important Building Blocks of Covalent Organic Frameworks. *J. Phys. Chem. A* **2020**, *124* (3), 529–537.

(8) Holub, J.; Vantomme, G.; Lehn, J.-M. Training a Constitutional Dynamic Network for Effector Recognition: Storage, Recall, and Erasing of Information. *J. Am. Chem. Soc.* **2016**, *138* (36), 11783–11791.

(9) Turcani, L.; Greenaway, R. L.; Jelfs, K. E. Machine Learning for Organic Cage Property Prediction. *Chem. Mater.* **2019**, *31* (3), 714–727.

(10) Herrmann, A. Dynamic Combinatorial/Covalent Chemistry: A Tool to Read, Generate and Modulate the Bioactivity of Compounds and Compound Mixtures. *Chem. Soc. Rev.* **2014**, *43* (6), 1899–1933.

(11) Evans, J. D.; Jelfs, K. E.; Day, G. M.; Doonan, C. J. Application of Computational Methods to the Design and Characterisation of Porous Molecular Materials. *Chem. Soc. Rev.* **2017**, *46* (11), 3286–3301.

(12) Pal, A.; Malakoutikhah, M.; Leonetti, G.; Tezcan, M.; Colomb-Delsuc, M.; Nguyen, V. D.; van der Gucht, J.; Otto, S. Controlling the Structure and Length of Self-Synthesizing Supramolecular Polymers through Nucleated Growth and Disassembly. *Angew. Chemie*

Int. Ed. **2015**, *54* (27), 7852–7856.

(13) Mastalerz, M. Porous Shape-Persistent Organic Cage Compounds of Different Size, Geometry, and Function. *Acc. Chem. Res.* **2018**, *51* (10), 2411–2422.

(14) Dill, K. A.; Chan, H. S. From Levinthal to Pathways to Funnels. *Nat. Struct. Mol. Biol.* **1997**, *4* (1), 10–19.

(15) *Dynamic Covalent Chemistry*; Zhang, W., Jin, Y., Eds.; Wiley, 2017.

(16) Ong, W. J.; Swager, T. M. Dynamic Self-Correcting Nucleophilic Aromatic Substitution. *Nat. Chem.* **2018**, *10* (10), 1023–1030.

(17) Gross, D. E.; Moore, J. S. Arylene–Ethynylene Macrocycles via Depolymerization–Macrocyclization. *Macromolecules* **2011**, *44* (10), 3685–3687.

(18) Zentner, C. A.; Anson, F.; Thayumanavan, S.; Swager, T. M. Dynamic Imine Chemistry at Complex Double Emulsion Interfaces. *J. Am. Chem. Soc.* **2019**, *141* (45), 18048–18055.

(19) Moneypenny, T. P.; Yang, A.; Walter, N. P.; Woods, T. J.; Gray, D. L.; Zhang, Y.; Moore, J. S. Product Distribution from Precursor Bite Angle Variation in Multitopic Alkyne Metathesis: Evidence for a Putative Kinetic Bottleneck. *J. Am. Chem. Soc.* **2018**, *140* (17), 5825–5833.

(20) Hartley, C. S.; Elliott, E. L.; Moore, J. S. Covalent Assembly of Molecular Ladders. *J. Am. Chem. Soc.* **2007**, *129* (15), 4512–4513.

(21) Wei, T.; Furgal, J. C.; Jung, J. H.; Scott, T. F. Long, Self-Assembled Molecular Ladders by Cooperative Dynamic Covalent Reactions. *Polym. Chem.* **2017**, *8* (3), 520–527.

(22) Liu, X.; Warmuth, R. Solvent Effects in Thermodynamically Controlled Multicomponent Nanocage Syntheses. *J. Am. Chem. Soc.* **2006**, *128* (43), 14120–14127.

(23) Sisco, S. W.; Moore, J. S. Homochiral Self-Sorting of BINOL Macrocycles. *Chem. Sci.*

2014, *5* (1), 81–85.

(24) Greenaway, R. L.; Santolini, V.; Pulido, A.; Little, M. A.; Alston, B. M.; Briggs, M. E.; Day, G. M.; Cooper, A. I.; Jelfs, K. E. From Concept to Crystals via Prediction: Multi-Component Organic Cage Pots by Social Self-Sorting. *Angew. Chemie Int. Ed.* **2019**, *58* (45), 16275–16281.

(25) Yu, C.; Long, H.; Jin, Y.; Zhang, W. Synthesis of Cyclic Porphyrin Trimers through Alkyne Metathesis Cyclooligomerization and Their Host–Guest Binding Study. *Org. Lett.* **2016**, *18* (12), 2946–2949.

(26) Greenaway, R. L.; Santolini, V.; Bennison, M. J.; Alston, B. M.; Pugh, C. J.; Little, M. A.; Miklitz, M.; Eden-Rump, E. G. B.; Clowes, R.; Shakil, A.; Cuthbertson, H. J.; Armstrong, H.; Briggs, M. E.; Jelfs, K. E.; Cooper, A. I. High-Throughput Discovery of Organic Cages and Catenanes Using Computational Screening Fused with Robotic Synthesis. *Nat. Commun.* **2018**, *9* (1), 2849.

(27) Wang, Q.; Yu, C.; Zhang, C.; Long, H.; Azarnoush, S.; Jin, Y.; Zhang, W. Dynamic Covalent Synthesis of Aryleneethynylene Cages through Alkyne Metathesis: Dimer, Tetramer, or Interlocked Complex? *Chem. Sci.* **2016**, *7* (5), 3370–3376.

(28) Swain, J. A.; Iadevaia, G.; Hunter, C. A. H-Bonded Duplexes Based on a Phenylacetylene Backbone. *J. Am. Chem. Soc.* **2018**, *140* (36), 11526–11536.

(29) Elliott, E. L.; Hartley, C. S.; Moore, J. S. Covalent Ladder Formation Becomes Kinetically Trapped beyond Four Rungs. *Chem. Commun.* **2011**, *47* (17), 5028.

(30) Cencer, M. M.; Greenlee, A. J.; Moore, J. S. Quantifying Error Correction through a Rule-Based Model of Strand Escape from an [n]-Rung Ladder. *J. Am. Chem. Soc.* **2020**, *142* (1), 162–168.

(31) Furgal, J. C.; van Dijck, J. M.; Leguizamon, S. C.; Scott, T. F. Accessing Sequence Specific Hybrid Peptoid Oligomers with Varied Pendant Group Spacing. *Eur. Polym. J.* **2019**, *118*, 306–311.

(32) Leguizamon, S. C.; Scott, T. F. Sequence-Selective Dynamic Covalent Assembly of Information-Bearing Oligomers. *Nat. Commun.* **2020**, *11* (1), 784.

(33) Jiang, X.; Laffoon, J. D.; Chen, D.; Pérez-Estrada, S.; Danis, A. S.; Rodríguez-López, J.; Garcia-Garibay, M. A.; Zhu, J.; Moore, J. S. Kinetic Control in the Synthesis of a Möbius Tris((Ethynyl)[5]Helicene) Macrocycle Using Alkyne Metathesis. *J. Am. Chem. Soc.* **2020**, *142* (14), 6493–6498.

(34) Komáromy, D.; Stuart, M. C. A.; Monreal Santiago, G.; Tezcan, M.; Krasnikov, V. V.; Otto, S. Self-Assembly Can Direct Dynamic Covalent Bond Formation toward Diversity or Specificity. *J. Am. Chem. Soc.* **2017**, *139* (17), 6234–6241.

(35) Ortiz, M.; Yu, C.; Jin, Y.; Zhang, W. Poly(Aryleneethynylene)s: Properties, Applications and Synthesis Through Alkyne Metathesis. *Top. Curr. Chem.* **2017**, *375* (4), 69.

(36) Chavez, A. D.; Smith, B. J.; Smith, M. K.; Beaucage, P. A.; Northrop, B. H.; Dichtel, W. R. Discrete, Hexagonal Boronate Ester-Linked Macrocycles Related to Two-Dimensional Covalent Organic Frameworks. *Chem. Mater.* **2016**, *28* (14), 4884–4888.

(37) Smith, M. K.; Goldberg, A. R.; Northrop, B. H. The Dynamic Assembly of Covalent Organic Polygons: Finding the Optimal Balance of Solubility, Functionality, and Stability. *European J. Org. Chem.* **2015**, *2015* (13), 2928–2941.

(38) Cougnon, F. B. L.; Jenkins, N. A.; Pantoş, G. D.; Sanders, J. K. M. Templated Dynamic Synthesis of a [3]Catenane. *Angew. Chemie Int. Ed.* **2012**, *51* (6), 1443–1447.

(39) Strauss, M. J.; Evans, A. M.; Castano, I.; Li, R. L.; Dichtel, W. R. Supramolecular

Polymerization Provides Non-Equilibrium Product Distributions of Imine-Linked Macrocycles. *Chem. Sci.* **2020**, *11* (7), 1957–1963.

(40) Ponnuswamy, N.; Cougnon, F. B. L.; Pantoş, G. D.; Sanders, J. K. M. Homochiral and Meso Figure Eight Knots and a Solomon Link. *J. Am. Chem. Soc.* **2014**, *136* (23), 8243–8251.

(41) Li, H.; Chavez, A. D.; Li, H.; Li, H.; Dichtel, W. R.; Bredas, J.-L. Nucleation and Growth of Covalent Organic Frameworks from Solution: The Example of COF-5. *J. Am. Chem. Soc.* **2017**, *139* (45), 16310–16318.

(42) Castano, I.; Evans, A. M.; Li, H.; Vitaku, E.; Strauss, M. J.; Brédas, J.-L.; Gianneschi, N. C.; Dichtel, W. R. Chemical Control over Nucleation and Anisotropic Growth of Two-Dimensional Covalent Organic Frameworks. *ACS Cent. Sci.* **2019**, *5* (11), 1892–1899.

(43) Zhu, G.; Liu, Y.; Flores, L.; Lee, Z. R.; Jones, C. W.; Dixon, D. A.; Sholl, D. S.; Lively, R. P. Formation Mechanisms and Defect Engineering of Imine-Based Porous Organic Cages. *Chem. Mater.* **2018**, *30* (1), 262–272.

(44) Berardo, E.; Greenaway, R. L.; Turcani, L.; Alston, B. M.; Bennison, M. J.; Miklitz, M.; Clowes, R.; Briggs, M. E.; Cooper, A. I.; Jelfs, K. E. Computationally-Inspired Discovery of an Unsymmetrical Porous Organic Cage. *Nanoscale* **2018**, *10* (47), 22381–22388.

(45) Matsumura, Y.; Hiraoka, S.; Sato, H. A Reaction Model on the Self-Assembly Process of Octahedron-Shaped Coordination Capsules. *Phys. Chem. Chem. Phys.* **2017**, *19* (31), 20338–20342.

(46) Li, H.; Evans, A. M.; Castano, I.; Strauss, M. J.; Dichtel, W. R.; Bredas, J.-L. Nucleation–Elongation Dynamics of Two-Dimensional Covalent Organic Frameworks. *J. Am. Chem. Soc.* **2020**, *142* (3), 1367–1374.

(47) Pennella, F.; Banks, R. L.; Bailey, G. C. Disproportionation of Alkynes. *Chem. Commun.* **1968**, No. 23, 1548.

(48) Mortreux, A.; Blanchard, M. Metathesis of Alkynes by a Molybdenum Hexacarbonyl–Resorcinol Catalyst. *J. Chem. Soc., Chem. Commun.* **1974**, No. 19, 786–787.

(49) Schrock, R. R. High-Oxidation-State Molybdenum and Tungsten Alkylidyne Complexes. *Acc. Chem. Res.* **1986**, *19* (11), 342–348.

(50) Schrock, R. R. High Oxidation State Multiple Metal−Carbon Bonds. *Chem. Rev.* **2002**, *102* (1), 145–180.

(51) Schrock, R. R. Multiple Metal–Carbon Bonds for Catalytic Metathesis Reactions (Nobel Lecture). *Angew. Chemie Int. Ed.* **2006**, *45* (23), 3748–3759.

(52) Listemann, M. L.; Schrock, R. R. Multiple Metal Carbon Bonds. 35. A General Route to Tri-Tert-Butoxytungsten Alkylidyne Complexes. Scission of Acetylenes by Ditungsten Hexa-Tert-Butoxide. *Organometallics* **1985**, *4* (1), 74–83.

(53) Schrock, R. R.; Murdzek, J. S.; Freudenberger, J. H.; Churchill, M. R.; Ziller, J. W. Multiple Metal-Carbon Bonds. 39. Preparation of Molybdenum and Tungsten Neopentylidyne Complexes of the Type M(CCMe3)(O2CR)3, Their Reactions with Acetylenes, and the x-Ray Structure of the .Eta.3-Cyclopropenyl Complex W[C3(CMe3)Et2](O2CCH3)3. *Organometallics* **1986**, *5* (1), 25–33.

(54) Pedersen, S. F.; Schrock, R. R.; Churchill, M. R.; Wasserman, H. J. Reaction of Tungsten(VI) Alkylidyne Complexes with Acetylenes to Give Tungstenacyclobutadiene and Cyclopentadienyl Complexes. *J. Am. Chem. Soc.* **1982**, *104* (24), 6808–6809.

(55) Wengrovius, J. H.; Sancho, J.; Schrock, R. R. Metathesis of Acetylenes by Tungsten(VI)-Alkylidyne Complexes. *J. Am. Chem. Soc.* **1981**, *103* (13), 3932–3934.

(56) Heppekausen, J.; Stade, R.; Kondoh, A.; Seidel, G.; Goddard, R.; Fürstner, A. Optimized Synthesis, Structural Investigations, Ligand Tuning and Synthetic Evaluation of Silyloxy-Based Alkyne Metathesis Catalysts. *Chem. - A Eur. J.* **2012**, *18* (33), 10281–10299.

(57) Heppekausen, J.; Stade, R.; Goddard, R.; Fürstner, A. Practical New Silyloxy-Based Alkyne Metathesis Catalysts with Optimized Activity and Selectivity Profiles. *J. Am. Chem. Soc.* **2010**, *132* (32), 11045–11057.

(58) Estes, D. P.; Gordon, C. P.; Fedorov, A.; Liao, W.-C.; Ehrhorn, H.; Bittner, C.; Zier, M. L.; Bockfeld, D.; Chan, K. W.; Eisenstein, O.; Raynaud, C.; Tamm, M.; Copéret, C. Molecular and Silica-Supported Molybdenum Alkyne Metathesis Catalysts: Influence of Electronics and Dynamics on Activity Revealed by Kinetics, Solid-State NMR, and Chemical Shift Analysis. *J. Am. Chem. Soc.* **2017**, *139* (48), 17597–17607.

(59) Zhang, W.; Kraft, S.; Moore, J. S. Highly Active Trialkoxymolybdenum(VI) Alkylidyne Catalysts Synthesized by a Reductive Recycle Strategy. *J. Am. Chem. Soc.* **2004**, *126* (1), 329–335.

(60) Zhang, W.; Kraft, S.; Moore, J. S. A Reductive Recycle Strategy for the Facile Synthesis of Molybdenum(VI) Alkylidyne Catalysts for Alkyne MetathesisElectronic Supplementary Information (ESI) Available: Spectral Data. See Http://Www.Rsc.Org/Suppdata/Cc/B2/B212405j/. *Chem. Commun.* **2003**, No. 7, 832–833.

(61) McDermott, G. A.; Dorries, A. M.; Mayr, A. Synthesis of Carbyne Complexes of Chromium, Molybdenum, and Tungsten by Formal Oxide Abstraction from Acyl Ligands. *Organometallics* **1987**, *6* (5), 925–931.

(62) Mayr, A.; McDermott, G. A. Oxidative Transformation of Monobromotetracarbonyl(Alkylidyne) Complexes of Molybdenum and Tungsten into

Tribromo(Alkylidyne) Complexes. *J. Am. Chem. Soc.* **1986**, *108* (3), 548–549.

(63) Haack, A.; Hillenbrand, J.; Leutzsch, M.; van Gastel, M.; Neese, F.; Fürstner, A. Productive Alkyne Metathesis with "Canopy Catalysts" Mandates Pseudorotation. *J. Am. Chem. Soc.* **2021**, *143* (15), 5643–5648.

(64) Fürstner, A.; Stelzer, F.; Rumbo, A.; Krause, H. Total Synthesis of the Turrianes and Evaluation of Their DNA-Cleaving Properties. *Chem. - A Eur. J.* **2002**, *8* (8), 1856.

(65) Fürstner, A.; Grela, K.; Mathes, C.; Lehmann, C. W. Novel and Flexible Entries into Prostaglandins and Analogues Based on Ring Closing Alkyne Metathesis or Alkyne Cross Metathesis. *J. Am. Chem. Soc.* **2000**, *122* (48), 11799–11805.

(66) Fürstner, A.; Dierkes, T. Concise Synthesis of (S,S)-(+)-Dehydrohomoancepsenolide. *Org. Lett.* **2000**, *2* (16), 2463–2465.

(67) Huang, S.; Lei, Z.; Jin, Y.; Zhang, W. By-Design Molecular Architectures via Alkyne Metathesis. *Chem. Sci.* **2021**, *12* (28), 9591–9606.

(68) Pattillo, C. C.; Cencer, M. M.; Moore*, J. S. Discussion Addendum for: Preparation of a Carbazole-Based Macrocycle Via Precipitation-Driven Alkyne Metathesis. In *Organic Syntheses*; Wiley, 2019; pp 231–239.

CHAPTER 2: KINETIC AND MECHANISTIC STUDIES OF ALKYNE METATHESIS

2.1 Introduction

Escaping a kinetic trap may represent the rate-limiting step of a DCC synthesis.[‡] Thus, understanding the mechanisms of error correction or escaping from a particular kinetic trap can provide useful guidance on optimal reaction conditions to increase the yield of a targeted product. The ability of a given DCC system to "error-correct," or remove a misconnection between constituents which is not consistent with the topology of the desired product, is highly dependent on the nature of the system. Higher valency precursors are more susceptible to kinetic trapping, since increasing the number of misconnections decreases the probability of disconnecting them all simultaneously. Molecular rigidity also contributes to kinetic trapping: if exchange components are held in close proximity to each other after an initial bond breakage, the rate of intramolecular recombination will be faster than that of two unlinked moieties. The interplay of each of these factors with the rate of dynamic exchange determines both the probability of, and time required for, successful error correction.

The complex relationship between exchange chemistries and molecular rigidity is apparent in molecular ladder systems, which generally have *n*-topic precursors, where *n* is the number of ladder rungs. Above a certain number of rungs, the system may lose the capacity for error correction and instead form a myriad of mismatched products, depending on the backbone and exchange chemistries chosen. For example, oligo(arylene ethynylene) ladders with hydrogen bonded rungs demonstrates much higher fidelity (98% versus 62%) than an imine-linked ladder with an identical backbone, due in part to the high exchange rate of hydrogen bonding (Figure

[‡] Elements of the work in section 2.2.2 were previously published in Quantifying Error Correction through a Rule-Based Model of Strand Escape from an [n]-Rung Ladder. Morgan M. Cencer, Andrew J. Greenlee, and Jeffrey S. Moore. Journal of the American Chemical Society 2020 142 (1), 162-168. DOI: 10.1021/jacs.9b08958. I contributed kinetic data for alkyne metathesis reactions for this manuscript.

2.1).[1,2] Furthermore, imine-linked ladders with flexible peptoid backbones exhibit fidelity up to 16 rungs, whereas rigid oligo(arylene ethynylene) imine ladders yield misregistered products above five rungs.[3] Ladder registration is therefore a useful diagnostic tool for identifying the relationship between dynamic exchange chemistries and the likelihood of kinetic traps, as the "in-register" ladder (defined as the duplex of single ladder strands in which all rungs of one strand are aligned with the corresponding rungs of the opposite strand) is typically assumed to be the thermodynamic product.

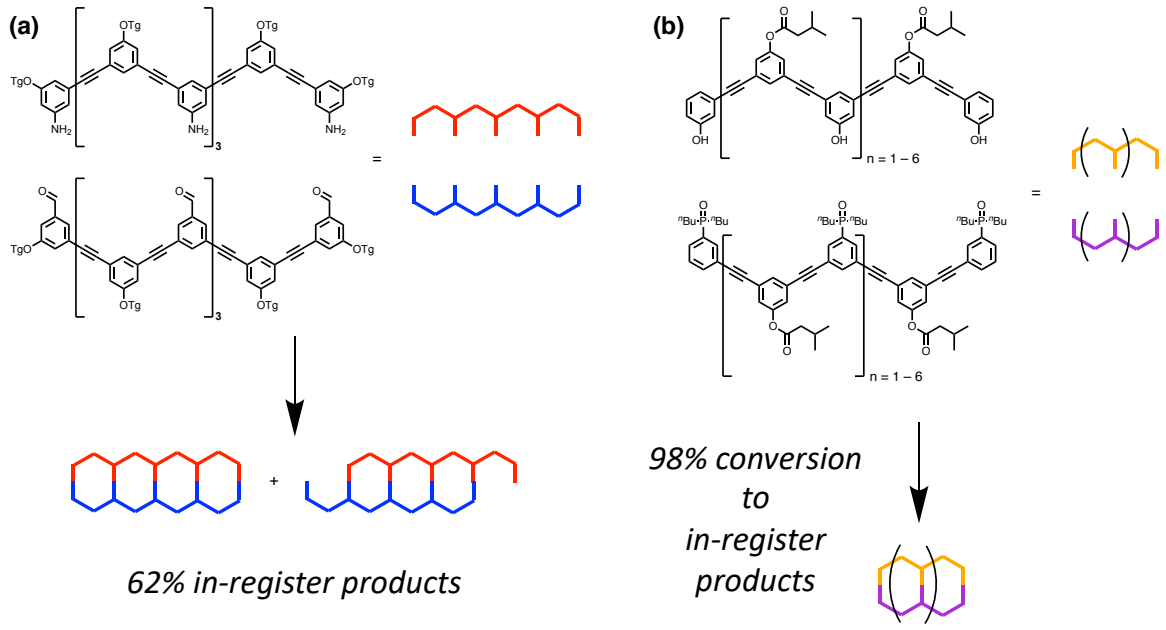

Figure 2.1. Oligo(arylene ethynylene) molecular ladders may exhibit kinetic trapping if the exchange chemistry of hybridization is not sufficiently fast. (a) Imine molecular ladders are trapped above four rungs whereas (b) hydrogen bonding ladders exhibit fidelity at much higher rung counts. Adapted from ref. 1, Copyright 2018, American Chemical Society, and ref. 2, Copyright 2011, Royal Society of Chemistry.

Despite the wealth of studies regarding ladder registration, mechanisms of ladder error correction are still poorly understood. In a study of amine and aldehyde ladder strand hybridization, Scott and coworkers found that ladder strands associate quickly and indiscriminately to form a mixture of high molecular weight oligomers, then gradually error correct.[3] On the basis of Førster Resonance Energy Transfer and MALDI experiments, it was

posited that registration proceeds *via* rapid initial association, followed by "handshake line"-type shuffling (Figure 2.2). Dr. Christopher Pattillo observed a similar cyclooligomerization process in the assembly of alkyne-bearing oligo(ester) ladder strands.[4] In this case, however, it was observed that ladders failed to register above only two rungs. Mass peaks corresponding to back-biting oligomers (e.g. cyclic trimers) and network-type precursors were also observed in the MALDI mass spectrum of the reaction mixture, suggesting that ladder strand oligomerization occurs concomitantly with oligomer self-association and higher-order network formation when the geometry of the oligomers permits folding. In a related body of work, Hunter and coworkers observed that the equilibria between self-association and oligomerization of hydrogen bonding oligo(arylene ethynylene) ladder strands can affect the distribution of species between different assembly channels, and thus the ultimate product distribution.[5] In cases like these, where products arise which would not be expected simply through consideration of thermodynamics, understanding the mechanisms of error correction is crucial to improving the yield of the target product.

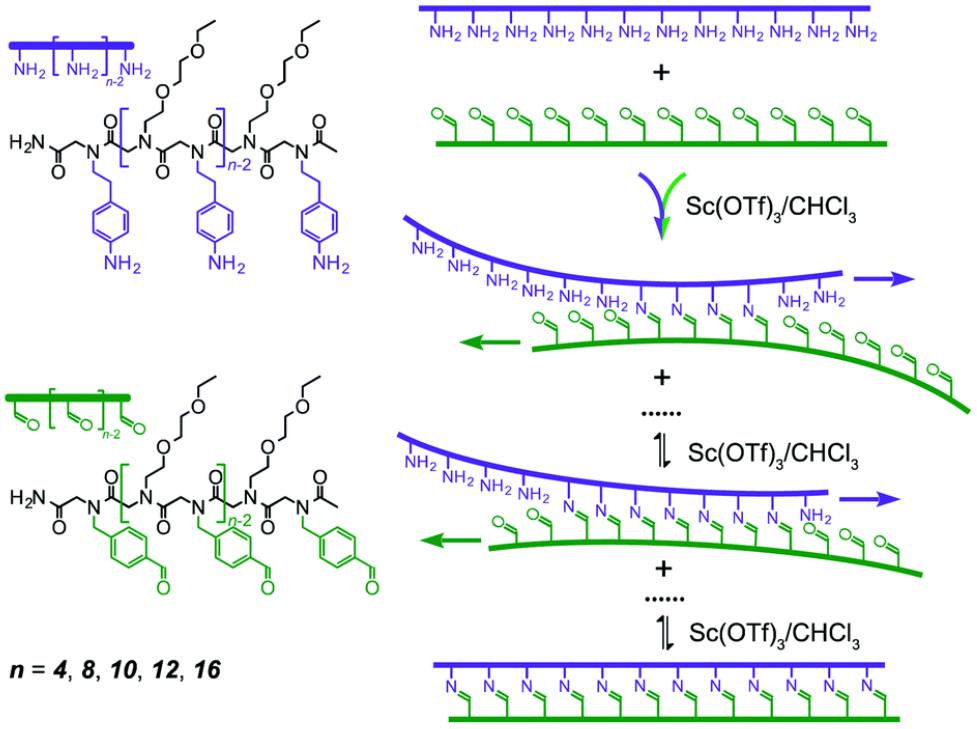

Figure 2.2. Proposed "handshake line" shuffling of peptoid-based imine molecular ladders. Following fast, indiscriminate association, ladders are assumed to pass through multiple misregistered hybridization states, which may be kinetically trapped. The flexibility of the peptoid backbone, compared to the rigid arylene ethynylene moiety, was proposed to contribute to the improved fidelity of longer ladders. Adapted from ref. 3. Copyright 2017, Royal Society of Chemistry.

Given the apparent system-dependency of error correction on exchange chemistries and backbone flexibilities, rationally predicting the outcome of ladder assembly reactions remains a challenge. DCC synthesis of molecular ladders, and more generally structures susceptible to kinetic trapping, would benefit from 1) quantitative understanding of chemical design principles facilitating escape from kinetic traps and 2) a rational approach to synthetic planning of routes to DCC. We sought to address these challenges through quantification of the rates of AM reactions, as well as other features of this reaction potentially associated with kinetic trapping. Specifically, we aimed to study the effects of precursor structure on reaction kinetics, as well as the kinetic profile of catalyst degradation. By integrating the results of these studies with a rule-based model,

we also envisioned creating an *in-silico* predictive tool to forecast yields and potential kinetic traps of AM self-assembly reactions, allowing a more rational approach to planning DCC syntheses.

2.2 Mechanistic Studies of Alkyne Metathesis Reaction Kinetics

2.2.1 Design of Alkynyl Molecular Ladders with Kinetic "Primers"

The Curtin-Hammett principle states that, for a reaction that has a pair of reactive intermediates that interconvert rapidly but react irreversibly to form two different products, the product distribution will depend on the difference in energy between the two rate-limiting transition states.[6] By analogy, if the formation of a particular kinetic trap is irreversible for a given DCC system, the product distribution may depend on the difference in the energy barriers between rate-limiting on- and off-pathway assembly steps, as well as the persistence of the corresponding oligomeric conformers. When the speed of subunit exchange is not sufficiently faster than the rate of bond formation, and thus the reaction is not under thermodynamic control, the formation of a kinetic trap may effectively remove the resultant species from the dynamic pool, shifting the reaction equilibrium to favor its amplification. Indeed, coupling an irreversible, kinetically controlled step with thermodynamic error correction has been demonstrated to induce resolution of complex dynamic libraries.[7–11] Though often associated with synthetic failure, we reasoned that leveraging this phenomenon might allow access to otherwise synthetically challenging, kinetically trapped structures.

In the same way that primary structure directs folding pathways of proteins and assembly of viral capsids,[12–14] we wondered if sequence definition in artificial oligomers could direct self-assembly pathways to favor certain kinetically trapped structures over others.[15] Hunter and coworkers demonstrated that the use of a covalent primer in the template oligomerization of supramolecular ladder strands improves the rate and fidelity of template-directed synthesis.[16]

Inspired by this work, we sought to investigate the effects of mixing pendant group reactivity in an AM ladder system. Specifically, we aimed to investigate the feasibility of a dynamic alkyne "primer" strategy, whereby one rung of a given ladder strand reacts more quickly than others in an initial association event, directing subsequent intramolecular rung "zipping" to favor in-register species.

2.2.2 Kinetic Studies of Metathesis

To better understand factors governing the rates of alkyne exchange, we began our investigation with a mechanistic study of AM. Early studies of AM catalysts indicated that catalyst productivity decreases for electron-poor systems.[17,18] Fischer and coworkers also demonstrated that the electronic character of molybdenum carbyne metathesis catalysts determines the rate of initiation in ring opening alkyne metathesis polymerization.[19] We therefore reasoned that the electronic character of alkynyl substrates would provide a convenient handle to control the initial rates of exchange in AM assembly systems. To investigate this notion, a library of isosteric *para*-substituted prop-1-yn-1-ylbenzene derivatives spanning the Hammett parameter space was prepared by Sonogashira cross-couplings. Then, these substrates were subjected to catalytic metathesis in the presence of 1 mol% tris(tert-butyl(3,5-dimethylphenyl)amino)(propylidyne)molybdenum precatalyst, abbreviated as **[Mo]**, and 6 mol% triphenylsiloxy ligand. Rates of alkyne exchange for each substrate were determined by measuring the conversion of the propynyl species to their corresponding diphenylacetylene derivative by ^{1}H NMR, then fitting the time-dependent concentration of substrate at the onset of reaction to the integrated first-order rate law (Figure 2.3a).[20]

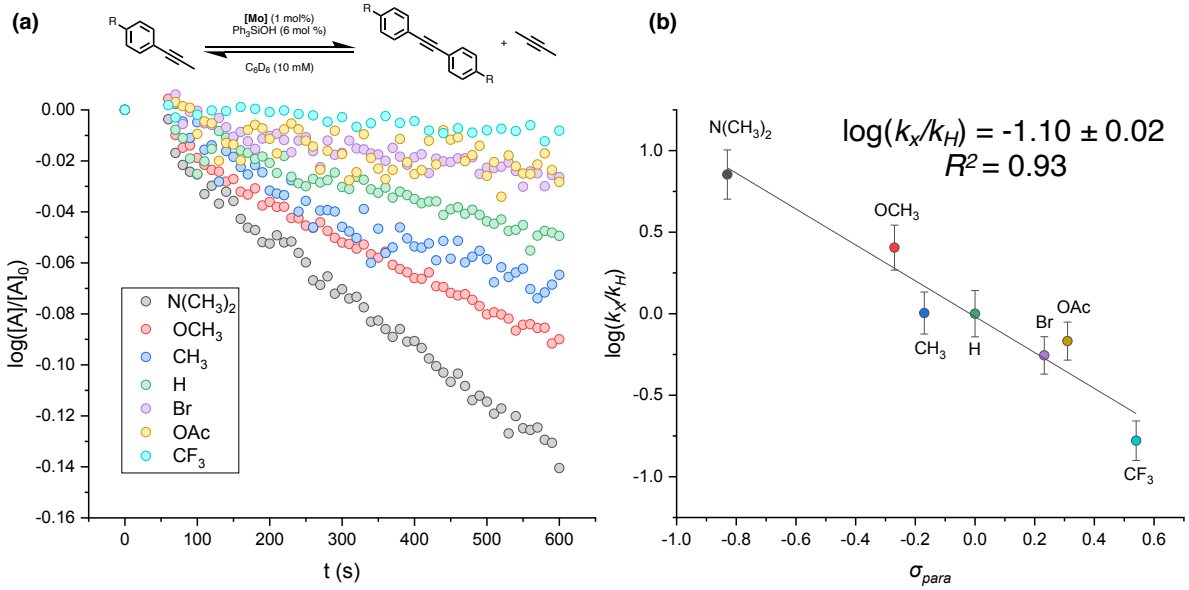

Figure 2.3. Metathesis of *para*-substituted propynylbenzene derivatives spanning the Hammett parameter space. (a) Representative kinetic traces of the metathesis of propynyl substrates. (b) Linear free-energy analysis of the average forward rate coefficients determined for each substrate.

It was determined that electron-rich derivatives reacted at a faster rate than the electron-poor species. Linear free-energy relationship (LFER) analysis of the forward rates of reaction for each species in the library provides further insight into the mechanism giving rise to this phenomenon (Figure 2.3b). A negative Hammett constant of -1.10 ± 0.02 indicates either the buildup of positive charge or a decrease in negative charge in the rate determining transition state. For unstrained alkynes, it has been demonstrated that the rate-determining step in metathesis is the initial cycloaddition to form a metallacyclobutadiene intermediate.[21] Thus, we reasoned that the electronic character of the alkyne contributes to the rate of metathesis in two ways:

1) Metathesis starting from molybdenum alkylidyne species may proceed *via* either productive or unproductive routes. In the productive route, the carbyne transfer occurs with regioselectivity favoring placement of the relatively electron rich aryl alkyne next to the relatively electron-deficient Mo(VI) metal center. The activation barrier to this step is putatively lowered for more electron-rich aryl alkynes, which are expected to better stabilize the buildup of positive

charge on the α-carbon in the rate-determining transition state. Thus, productive metathesis is favored for electron-rich species, while such regioselectivity likely decreases for electron-poor species.

2) Molybdenum benzylidyne species produced *in situ* by initial productive metathesis steps may also undergo either productive or unproductive metathesis. Here, regioselectivity of the cycloaddition placing the arene substrate next to the metal center results in unproductive metathesis. By the same logic outlined above, this regioselectivity would be favored for electron-rich substrates. However, we speculate that more electron-rich benzylidyne ligands better stabilize the buildup of positive charge in the rate-determining transition states of both productive and unproductive metathesis routes. Thus, electron-rich substrates are expected to generate more active benzylidyne species, which exhibit greater turnover frequencies and more net instances of productive metathesis compared to electron-poor species (Figure 2.4).

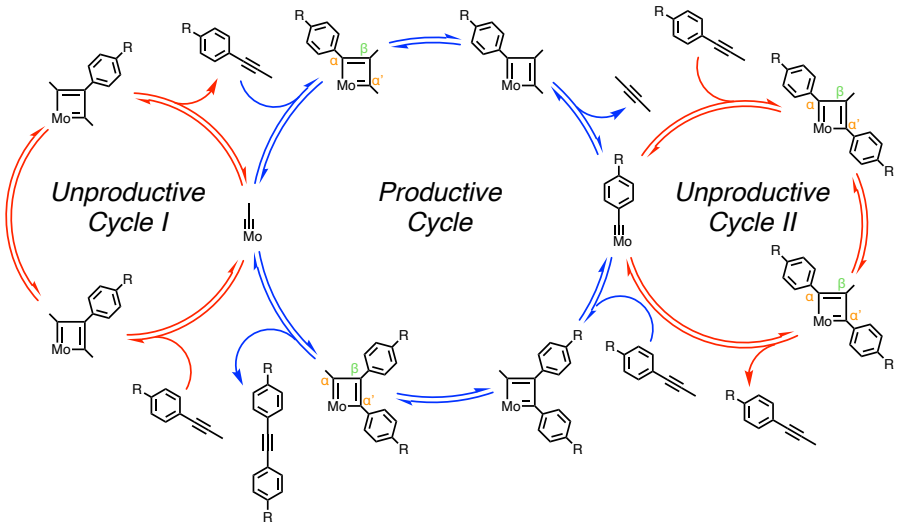

Figure 2.4. Productive (blue) and unproductive (red) metathesis pathways starting from molybdenum alkylidyne and molybdenum benzylidyne species. Ligands on the molybdenum metal center are omitted for clarity. We posit that electron-rich substrates facilitate more rapid catalyst turnover by stabilizing the buildup of positive charge on the α and α' carbons (indicated in orange) in rate-determining transition states.

To further support this hypothesis, kinetic experiments were repeated at slightly elevated catalyst loadings and longer reaction times. Global fitting of the reaction traces with the integrated reversible first-order rate law gave both forward and reverse rate coefficients for the reaction. Reverse rate coefficients were found to correlate with forward rate coefficients, indicating that electron-rich substrates undergo metathesis more rapidly in both the forward and reverse directions (Figure 2.5b). This result is consistent with our mechanistic analysis, and suggests that varying the electronic character of alkynyl substrates allows access to a wide range of kinetic behavior in AM.

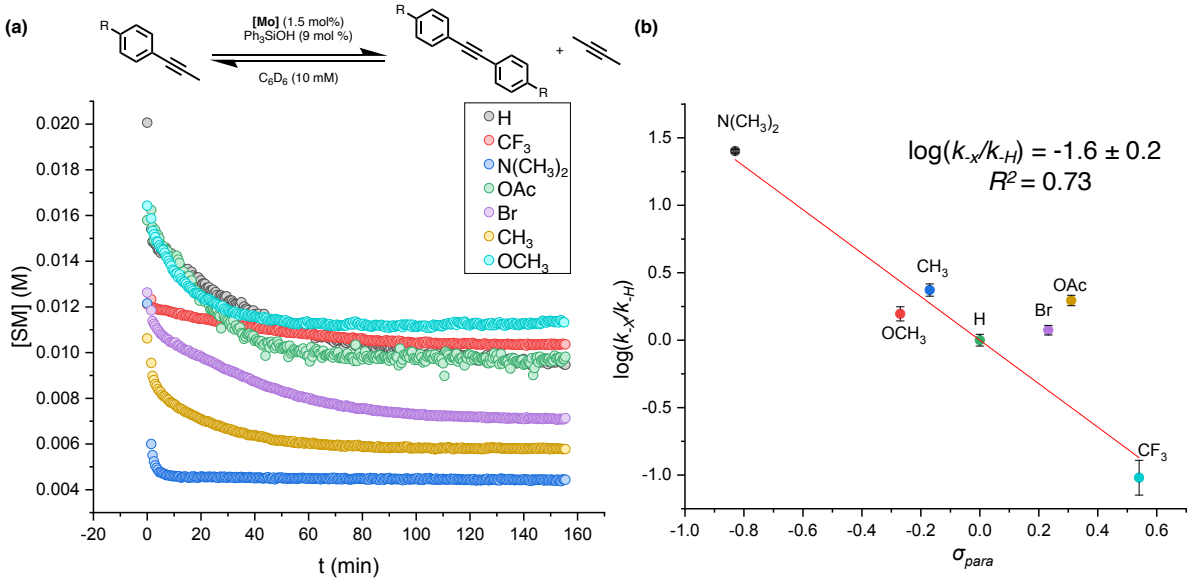

Figure 2.5. Reaction traces and LFER of extended metathesis studies. (a) Reaction traces of *para*-substituted propynylbenzene derivatives allowed to reach equilibrium over 2.5 h. (b) LFER of reverse rate coefficients determined by global fitting of the kinetic traces using the reversible first order rate law.

This newfound understanding of AM also allows us to draw quantitative comparisons between AM and other DCCs. Comparison by Dr. Morgan Cencer of experimentally derived AM rate coefficients to those found in literature for other dynamic exchange chemistries (and normalized for catalyst loadings) reveals that AM is orders of magnitude slower than other typical DCCs.[22] This analysis provides insight into the apparent relative frequency of kinetic trapping

phenomena in AM self-assembly literature, as kinetic trapping is known to occur more commonly in systems with slow exchange chemistries.[23]

2.2.3 Attempts to Synthesize Primed Alkynyl Molecular Ladders

In order to investigate the effects of varying rung reactivity in an AM ladder system, we next attempted to synthesize a series of three- and five-rung oligo(ester) ladders bearing relatively electron-rich propyne pendant groups on the central rung. We hypothesized that sufficiently different rates of reaction between central and peripheral rungs would direct assembly to favor the in-register three-rung molecular ladders. In collaboration with Dr. Joshua Laffoon, synthetic routes to *para*-N(CH_3), -O(CH_3), and -CH_3 ladder rung monomers were devised (Figure 2.6). However, the demanding synthesis of the *para*-methoxy and -methyl derivatives, as well as the synthetic intractability of the *para*-dimethylamino derivative, impeded our ability to test our hypothesis. Future work in this area will benefit from an operationally simple synthetic route to length- and sequence-defined molecular ladder strands.

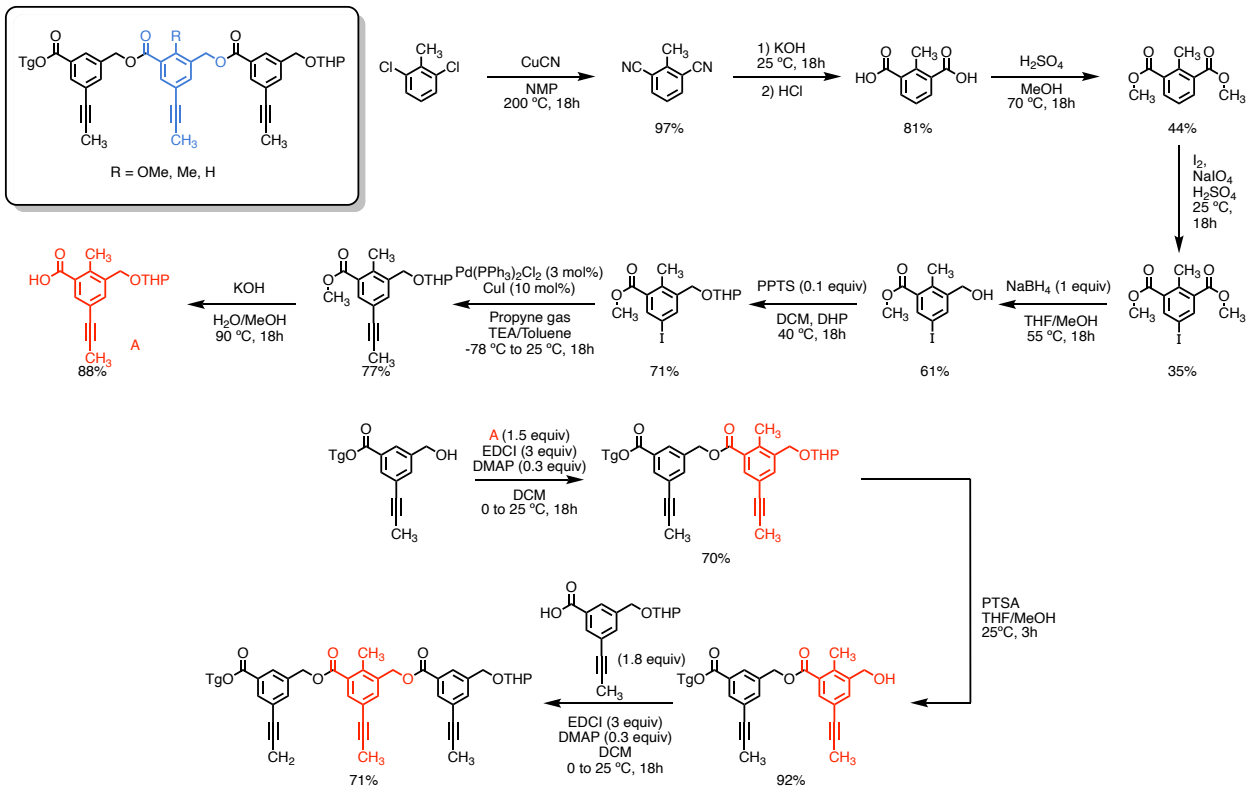

Figure 2.6. Synthesis of oligo(ester) alkynyl molecular ladders with mixed reactivity. The *para*-methyl three-rung ladder was synthesized in 1.6% overall yield.

2.3 Determination of the Kinetic Profile of AM Catalyst Decomposition

DCC assembly reactions typically employ high catalyst loadings to accelerate error correction, as slow rates of dynamic exchange are known to contribute to the formation of off-target, kinetically persistent byproducts. For the same reason, long reaction times are also employed to allow ample opportunities for intermediates to error correct.[24] However, this strategy is contingent on the assumption that a sufficiently high concentration of catalyst is active throughout the duration of the reaction to continually facilitate dynamic exchange. If catalyst deactivation occurs competitively with dynamic error correction, self-assembly may stall out.

Determination of the kinetic profiles of DCC catalyst deactivation would provide tremendous insight into strategies for improving self-assembly. For example, the Scott group demonstrated that alternately raising and lowering scandium triflate concentrations mitigated

kinetic trapping in the hybridization of imine-based peptoid molecular ladders.[25] Similarly, self-assembly reactions using catalysts susceptible to deactivation at high concentrations might benefit from slow rates of addition of catalyst as opposed to high initial loadings. This knowledge would also inform theoretical frameworks of DCC assembly reactions employing kinetic parameters.

Despite the need for greater understanding of catalyst deactivation in DCC self-assembly reactions, this problem remains largely unaddressed, due in part to practical difficulties associated with determining instantaneous catalyst activity in dynamic exchange reactions. Most AM catalysts are susceptible to poisoning by air, water, Lewis basic functional groups, ring-expansion polymerization of 2-butyne,[17] and bimolecular decomposition.[26,27] It is therefore likely that AM catalysts decompose to some degree during self-assembly reactions, but accurate identification of all possible decomposition products renders quantification of total catalyst deactivation challenging. Rational design of DCC syntheses would benefit from a generalizable, operationally simple approach to determine catalyst death profiles.

2.3.1 Design of Pulsed Addition Experiments

Taking inspiration from Grubbs and coworkers' studies of catalyst deactivation in the pulsed-addition ring opening metathesis polymerization (PA-ROMP) of norbornene imides,[28] we have developed a technique to determine the rate of catalyst deactivation in an AM reaction. In analogy to the PA-ROMP system, which enables calculation of initiator deactivation as a function of polymer molecular weight, we reasoned that catalyst death in an AM system could be determined indirectly as a function of time-dependent changes in catalyst activity. Specifically, we expected that solution aging of an AM reaction mixture would result in catalyst deactivation, as indicated by decreases in the rates of conversion of an alkynyl probe in an irreversible cross-metathesis reaction. Since the rate of metathesis is first order in catalyst for an irreversible reaction

(eq 1), the anticipated attrition of observed rate coefficients (k_{obs}) upon solution aging would directly reflect changes in the concentration of active catalyst (eq 2):

$$-\frac{d[A]}{dt} = k_{obs,x}[A][Mo] \quad (1)$$

$$\frac{k_{obs,x}}{k_{obs,0}} = \frac{[Mo]_x}{[Mo]_0} = \frac{[Mo]_0 - [Mo]_{deactivated}}{[Mo]_0} \quad (2)$$

where *A* is the alkynyl substrate, *Mo* is the metathesis catalyst, and *x* is the solution aging time. Thus, we anticipated that pulsed addition of an alkynyl analyte at predetermined intervals would enable quantification of the instantaneous degree of catalyst death.

2.3.2 Quantifying Catalyst Death Using Pulsed Addition Experiments

Benzoyl biphenyl-substituted propyne **7** was selected as the probe for these studies, owing to its unique AM reaction profile. Upon cross-metathesis, this species generates 2-butyne, which is scavenged by 5 Å molecular sieves, and bis(benzoyl biphenyl) acetylene **8**, which is insoluble in typical AM reaction solvents (Figure 2.7a). Removal of metathesis products from the dynamic pool by sequestration and precipitation renders the reaction irreversible, allowing a simple first-order approximation of the reaction kinetics. Metathesis of **7** in the presence of 5 Å molecular sieves and 5 mol% AM catalyst generated from molybdenum precatalyst **[Mo]** and Ph_3SiOH resulted in near quantitative conversion of the substrate within 10 minutes, as indicated by HPLC analysis. The reaction profile was fit with the integrated first-order rate law to afford a $k_{obs,0}$ of 0.48 ± 0.09 min^{-1}. This value represents the activity of a fresh catalyst solution in which no deactivation has occurred (Figure 2.7b).

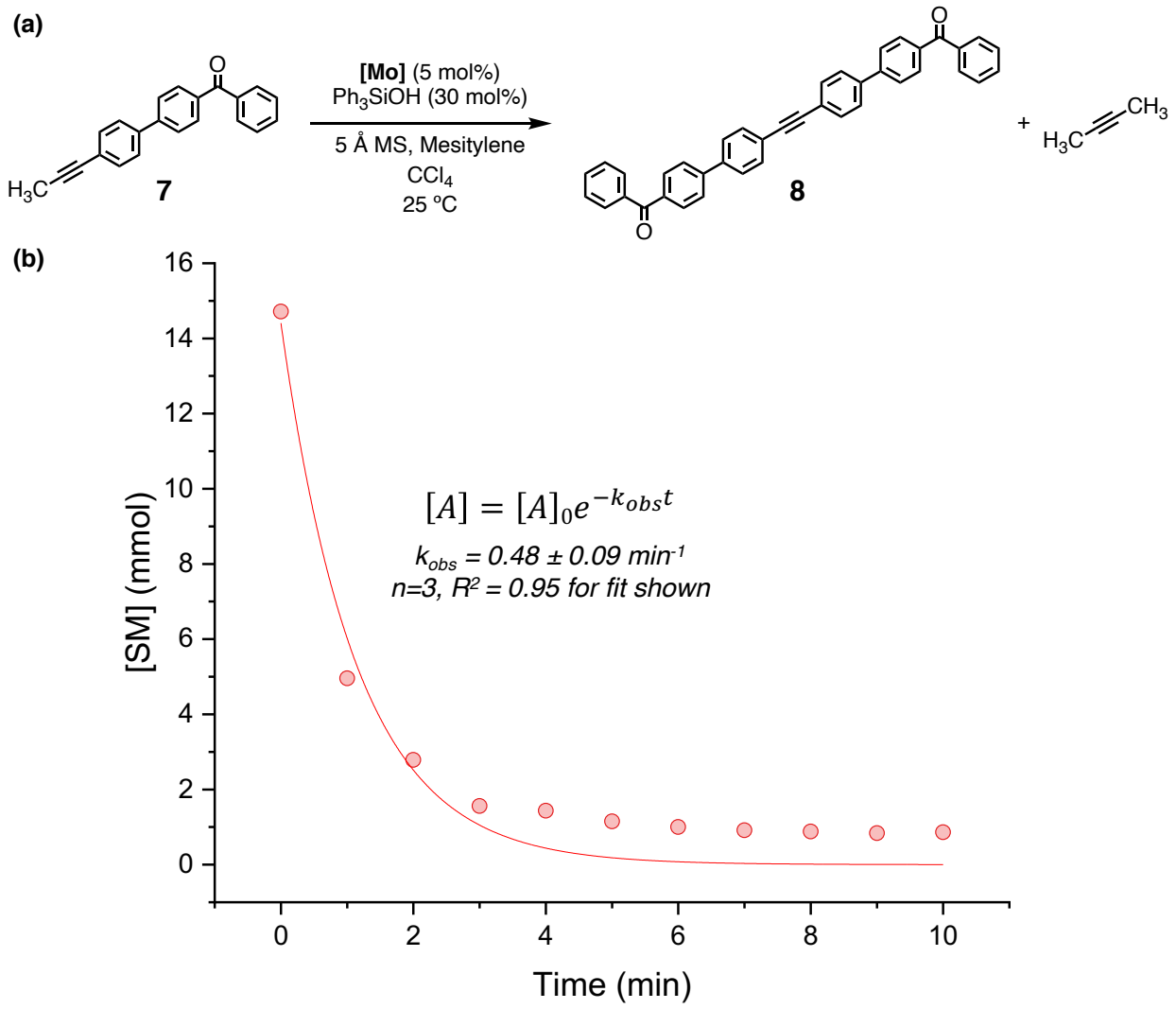

Figure 2.7. Metathesis of **7** to generate **8** and 2-butyne. (a) Reaction conditions. Both products are removed from the dynamic pool, rendering metathesis irreversible. (b) Representative kinetic trace of the conversion of **7** used to determine $k_{obs,0}$.

Next, PA experiments were performed. To simulate conditions of an AM self-assembly reaction, one equivalent of **7** was allowed to react with the preactivated catalyst in the presence of molecular sieves. After a period of solution aging ranging between one and six hours, another equivalent of **7** was added to the reaction mixture and substrate conversion was measured by HPLC. Each reaction trace was fit with a unique rate coefficient, $k_{obs,x}$, using the integrated first-order rate law. The rate of conversion of **7** was observed to decrease with extended solution aging. We attribute this effect to catalyst deactivation. Comparison of the rate coefficients determined

from PA experiments to that of the fresh catalyst solution, $k_{obs,0}$, using eq 2 revealed a roughly exponential decay profile of catalyst activity (Figure 2.8). The rate coefficient of catalyst death for this fit was determined to be 0.31 ± 0.01 s^{-1}. However, it was found that the decay profile could also be sufficiently described by the integrated second-order rate law, precluding determination of both the order in catalyst and primary mechanism of catalyst deactivation.

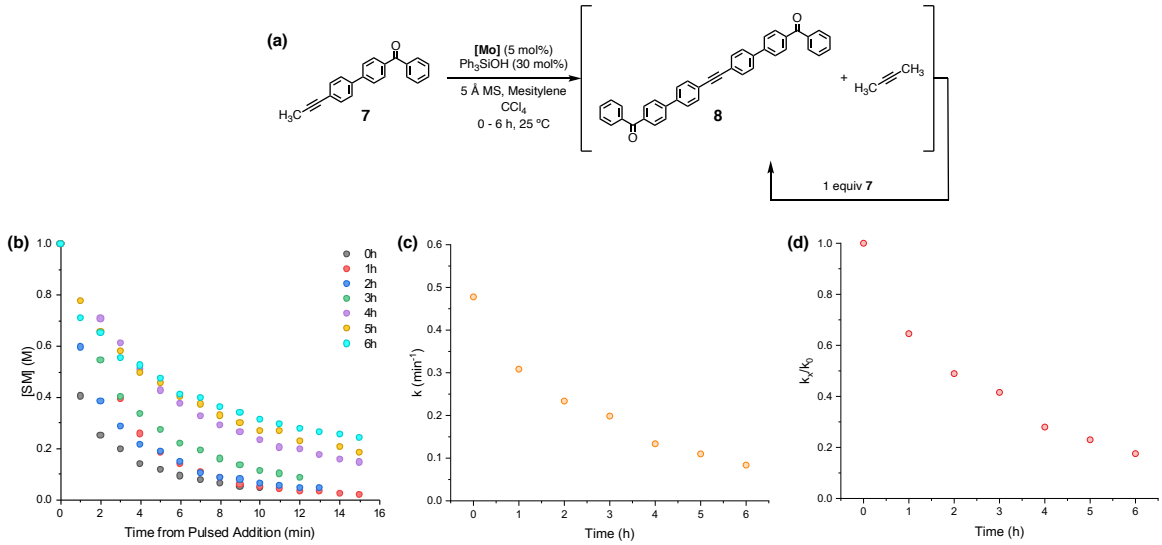

Figure 2.8. Reaction traces and kinetic analysis of pulsed addition experiments. (a) Reaction conditions. (b) Kinetic traces of the conversion of **7** after 0 – 6 hours of catalyst deactivation. (c) Rate coefficients determined from pulsed addition trials *vs.* time allowed for catalyst deactivation. The attrition (d) Ratios of rate coefficients for reactions using fresh and deactivated catalyst. This ratio is directly related to the instantaneous degree of catalyst death in the reaction mixture.

Given that PA reactions were run with molecular sieves under anhydrous conditions, we reasoned that the contributions of hydrolysis and ring expansion polymerization of 2-butyne to the observed catalyst death were likely minimal. Catalyst deactivation events associated with metathesis, such as the formation of persistent metallacycle intermediates, were similarly ruled out, as the concentration of alkyne in the dynamic pool prior to each PA was small (micromolar) and consistent between trials. We therefore hypothesized that catalyst death in our system was

primarily the result of bimolecular decomposition, and thus likely influenced by the initial concentration of catalyst.

To determine the relationship between initial catalyst concentration and deactivation rate, PA experiments were performed again using a catalyst loading of 10 mol% relative to **7**. Again, each trace was fit to a first-order decay profile and compared to the rate of conversion of **7** by fresh catalyst at 10 mol% loading. As evidenced by the more rapid decrease of $k_{obs,x}/k_{obs,0}$ compared to 5 mol% catalyst loading trials, higher initial catalyst loadings accelerate catalyst deactivation (Figure 2.9). This is consistent with our hypothesis that bimolecular decomposition contributes significantly to catalyst deactivation in this system. Fitting the time-dependent change in $k_{obs,x}/k_{obs,0}$ to both first- and second-order rate equations revealed that the rate of catalyst deactivation was better described by a first-order decay profile and afforded a rate coefficient of 0.53 ± 0.03 s^{-1}. Doubling the initial concentration of catalyst from 5 to 10 mol % increased the rate of catalyst deactivation by a factor of 1.7 ± 0.1.

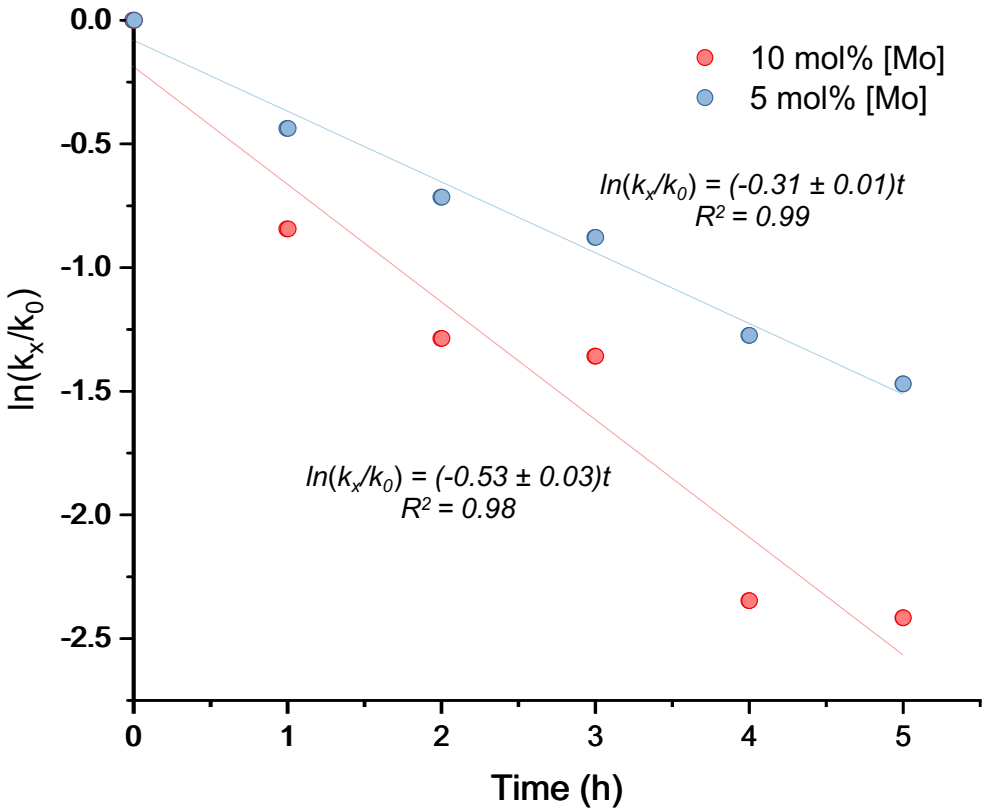

Figure 2.9. First order decay profiles for pulsed addition experiments using 5 and 10 mol% catalyst loading.

Together, these data suggest that catalyst deactivation is between zeroth and first order in catalyst. This could be the result of predominantly unimolecular decomposition pathways or saturation kinetics in the formation of inactive catalytic species. The latter explanation is consistent with the mechanism of bimolecular decomposition of metal-alkylidyne species proposed and later demonstrated on canopy-type systems by Fürstner and coworkers,[26,27] who determined that the collision of two active catalyst entities reversibly forms a dimetallatetrahedrane, which may either undergo the retro dimerization or liberate a disubstituted acetylene and M≡M complex (Scheme 2.1). Our data is consistent with the notion that catalyst deactivation occurs in the absence of a large dynamic pool, and thus through processes not associated with metathesis.

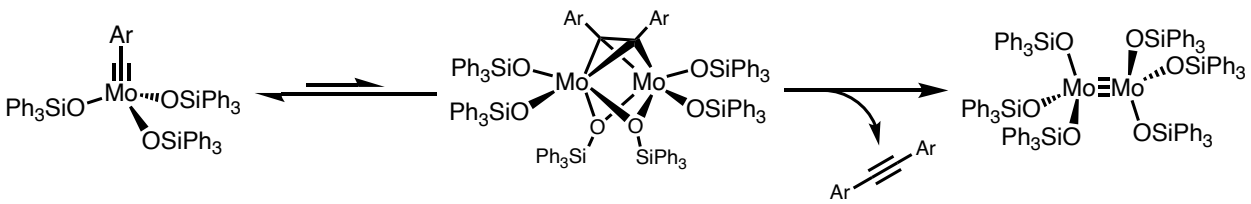

Scheme 2.1. Putative bimolecular decomposition pathway of molybdenum alkylidyne catalyst **[Mo]**/Ph_3SiOH.

It must be noted that the catalyst deactivation profile observed in this system does not likely represent the profile for a typical AM self-assembly reaction for several reasons. In the presence of a molar excess of alkyne relative to catalyst, saturation of active catalyst species by alkynes would decrease the frequency of bimolecular collisions of metal-carbynes. Furthermore, reversible deactivation pathways associated with the metathesis process, such as the formation of off-pathway metallatetrahedranes observed for some catalyst species,[29] are unaccounted for in our system, as are the effects of temperature in shifting deactivation equilibria. Future work should seek to elucidate the contributions of each of these phenomena to the overall kinetic profile of catalyst deactivation.

Our results imply that the rate of catalyst deactivation must be considered in DCC self-assembly reactions. If the kinetic profile of catalyst deactivation is on the order of a reaction timescale, longer reaction times may not improve the yield of targeted thermodynamic products, as it is commonly assumed. Slow addition of catalyst, for example, might enable a more economical approach to higher yields of DCC structures than increasing initial catalyst loadings. In analogy to thermal cycling, which has been demonstrated to facilitate thermodynamic error correction of nucleotide duplexes as well as scrambling of alkynyl macrocycles,[30–32] periodic additions of small amounts of catalyst might also be considered.

2.4 Conclusion

In this chapter, we report kinetic and mechanistic studies of AM in service of improving our understanding of kinetic control in DCC self-assembly. Our initial study was envisioned to proceed through a systematic evaluation of the effects of electronic character on the rates of initial and steady-state dynamic alkyne exchange. The rates of metathesis of a library of *para*-substituted propynylbenzene derivatives spanning the Hammett parameter space were measured and a linear free-energy relationship was observed. Electron-rich alkynes were determined to undergo metathesis more rapidly, likely due to the stabilization of positive charge in the rate-determining cycloaddition transition state. Comparison of the range of AM exchange rates to those of other well-studied DCCs indicated that AM is significantly slower than other typical DCC systems. This result is consistent with observations that AM systems are highly susceptible to kinetic trapping. Unfortunately, attempts to quantify differences in the efficiency of self-assembly of molecular ladders bearing alkyne rungs of mixed reactivity were impeded by lengthy and inefficient synthetic routes to ladder strand precursors.

We also demonstrated a generalizable pulsed addition strategy to elucidate the instantaneous degree of catalyst activity, and thus total catalyst deactivation, of an AM catalyst. We found that the prototypical AM catalyst **[Mo]**/$(Ph_3SiOH)_3$, in the absence of a dynamic pool, is deactivated on a timescale comparable to a typical AM reaction, and that increased catalyst loading accelerates catalyst deactivation. Based on catalyst loading experiments, we reason that this deactivation is likely the result of bimolecular decomposition.

These studies further demonstrate the importance of considering kinetic aspects of self-assembly in planning DCC syntheses. Understanding the range of dynamic behaviors of a given exchange chemistry is crucial to designing DCC systems capable of escaping kinetic traps. When

kinetic trapping is inevitable, as it may be in systems limited by slow exchange chemistries, promoting the kinetic selectivity of certain assembly pathways using precursors with mixed reactivity may improve the yield of targeted products. Similarly, awareness of factors leading to attrition of efficient error-correction are crucial to improving product yields. In an AM system, for example, slow addition of catalyst, as opposed to high initial loadings, may mitigate premature catalyst deactivation. This study further complements our previously reported synthetic and computational studies on ladder molecular cage formation, as well as key pathways considerations in 2- and 3D systems. We envision that these studies will lead to further studies on pathway control in DCC systems. We are particularly interested in studying in more detail whether varying and mixing precursor reactivity can affect product outcomes.

2.5 Supporting Information

2.5.1 General Considerations

All reactions were performed in oven (c.a. 165 ºC) or flame-dried glassware under an atmosphere of dry argon or nitrogen unless otherwise noted. All solvents used were either anhydrous commercial grade (Aldrich/Fisher) or purified by a solvent purification system unless otherwise noted. All alkyne metathesis reactions were conducted in an argon- filled glovebox in oven-dried glassware, using anhydrous (Aldrich), argon-degassed solvents. All reagents were purchased from commercial sources and used without further purification. Molybdenum(VI) propylidyne precatalyst **[Mo]** was prepared according to published literature procedures. Chromatographic purifications were conducted via MPLC on a Biotage Isolera 1 using Silicycle SiliaSep cartridges (230-400 mesh, 40-63 μm). Column separation conditions are reported in column volumes (CV) of gradient solvent mixtures. ^{1}H and ^{13}C NMR spectra were recorded on a Carver B500 Bruker Avance III HD NMR spectrometer at room temperature (298 K) and chemical shifts were

referenced to the residual solvent peak ($CDCl_3$ ^1H NMR δ = 7.26 ppm). Kinetic experiments were performed using a Varian Unity INOVA 400 MHz NMR spectrometer and are referenced to residual solvent peaks (C_6D_6 ^1H NMR δ = 7.16 ppm). Mass spectra were obtained through the Mass Spectrometry Facility, School of Chemical Sciences, University of Illinois. High resolution electron impact (EI) mass spectra were obtained on a Micromass 70-VSE TOF spectrometer and electrospray ionization (ESI) mass spectra were obtained on a Waters Synapt G2-Si TOF spectrometer. ^1H and ^{13}C NMR were processed using MestReNova software v12.0.4-22023. Reported yields are of isolated material which in some cases were corrected for trace residual solvent.

2.5.2 Synthesis and Characterization of Compounds

General Procedure for Synthesis of *para*-Substituted (prop-1-yn-1-yl)benzene Derivatives

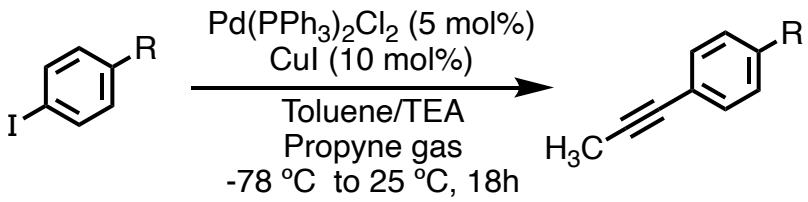

A 100 mL Schlenk flask was charged with magnetic stir bar, $Pd(PPh_3)_2Cl_2$ (35 mg, 0.05 mmol), CuI (19 mg, 0.1 mmol), and the appropriate 4-iodobenzene precursor (1 mmol) in dry toluene (12.5 mL). Dry triethylamine (12.5 mL) was added, and the reaction was cooled to -78 ºC. Propyne gas was bubbled into the reaction mixture and the system was stirred at -78 °C for ten minutes and 25 °C for 18 hours. The reaction was quenched with saturated aqueous NH_4Cl (50 mL) and extracted with CH_2Cl_2 (3 × 25 mL). The organic layer was washed with brine, dried over Na_2SO_4, and concentrated in vacuo. The crude oil was purified by flash column chromatography in hexanes only to afford the corresponding propynyl species.

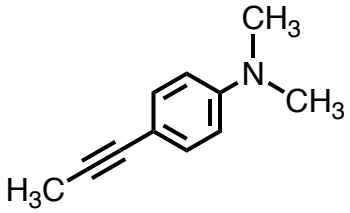

***N*,*N*-dimethyl-4-(prop-1-yn-1-yl)aniline:** Yellow solid; Yield 93%; ^{1}H NMR (500 MHz, $CDCl_3$) δ 7.33 (d, J = 8.7 Hz, 2H), 6.66 (d, J = 8.7 Hz, 2H), 2.99 (s, 6H), 2.09 (s, 3H); $^{13}C\{^1H\}$ NMR (126 MHz, $CDCl_3$) δ 149.73, 132.48, 111.99, 111.21, 83.01, 80.32, 40.32, 4.43; HRMS (EI) m/z: $[C_{11}H_{13}N]^+$ calculated: 159.1048; found: 159.1051.

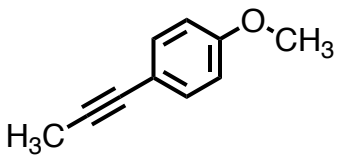

1-methoxy-4-(prop-1-yn-1-yl)benzene: Yellow oil; Yield 95%; ^{1}H NMR (500 MHz, $CDCl_3$) δ 7.32 (d, *J* = 8.8 Hz, 2H), 6.81 (d, *J* = 8.8 Hz, 1H), 3.79 (s, 3H), 2.03 (s, 3H); $^{13}C\{^1H\}$ NMR (126 MHz, $CDCl_3$) δ 159.14, 132.93, 116.31, 113.95, 84.23, 79.55, 77.41, 77.16, 76.91, 55.36, 4.42; HRMS (EI) m/z: $[C_{10}H_{10}O]^+$ calculated: 146.0732; found: 146.0732.

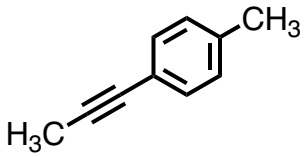

1-methyl-4-(prop-1-yn-1-yl)benzene: Colorless oil; Yield 36%; ^{1}H NMR (500 MHz, $CDCl_3$) δ 7.29 (d, *J* = 8.2 Hz, 2H), 7.09 (d, *J* = 8.2 Hz, 1H), 2.34 (s, 3H), 2.05 (s, 3H); $^{13}C\{^1H\}$ NMR (126 MHz, $CDCl_3$) δ 137.61, 131.49, 129.10, 121.06, 85.08, 79.87, 77.41, 77.16, 76.91, 21.52, 4.45; HRMS (EI) m/z: $[C_{10}H_{10}]^+$ calculated: 130.0783; found: 130.0779.

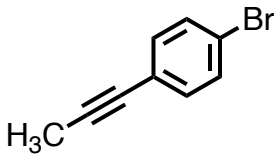

1-bromo-4-(prop-1-yn-1-yl)benzene: Yellow oil; Yield 89%; ^{1}H NMR (500 MHz, $CDCl_3$) δ 7.41 (d, *J* = 8.4 Hz, 2H), 7.24 (d, *J* = 8.5 Hz, 2H), 2.03 (s, 3H); $^{13}C\{^1H\}$ NMR (126 MHz, $CDCl_3$) δ 133.11, 131.57, 123.14, 121.74, 87.28, 78.90, 77.41, 77.16, 76.91, 4.50 ppm; HRMS (EI) m/z: $[C_9H_7Br]^+$ calculated: 193.9731; found: 193.97365.

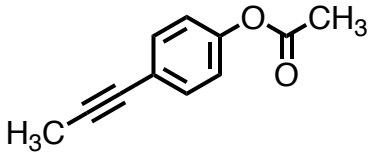

4-(prop-1-yn-1-yl)phenyl acetate: Brow solid, Yield 93%; ^{1}H NMR (500 MHz, $CDCl_3$) δ 7.39 (d, *J* = 8.7 Hz, 2H), 7.01 (d, *J* = 8.6 Hz, 2H), 2.29 (s, 3H), 2.04 (s, 3H); $^{13}C\{^1H\}$ NMR (126 MHz,

$CDCl_3$) δ 169.36, 150.02, 132.73, 121.89, 121.64, 86.04, 79.05, 77.41, 77.16, 76.91, 21.27, 4.45; HRMS (EI) m/z: $[C_{11}H_{10}O_2]^+$ calculated: 174.0681; found: 174.0683.

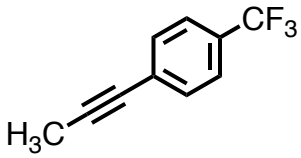

1-(prop-1-yn-1-yl)-4-(trifluoromethyl)benzene: Colorless oil; Yield 65%; 1H NMR (500 MHz, $CDCl_3$) δ 7.54 (d, J = 8.2 Hz, 2H), 7.48 (d, J = 8.2 Hz, 2H), 2.07 (s, 3H) ppm; $^{13}C\{^1H\}$ NMR (126 MHz, $CDCl_3$) δ 131.87, 129.32, 128.08, 125.25, 123.10, 88.87, 78.82, 4.44 ppm; ^{19}F NMR (470 MHz, CDCl3) δ 5.78 (s, 3F) ppm; HRMS (EI) m/z: $[C_{10}H_7F_3]^+$ calculated: 184.0500; found: 184.0501.

General Procedure for Kinetic Measurements of Alkyne Metathesis

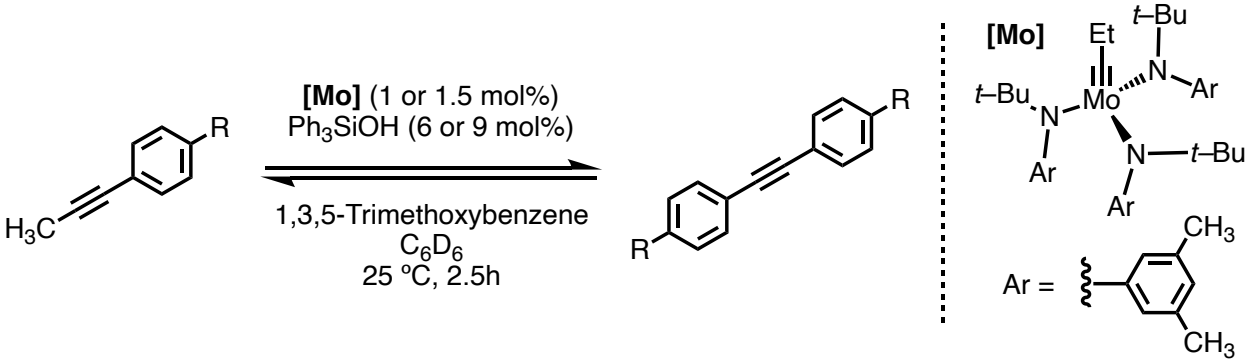

In an Ar-filled glovebox, a 500 mHz NMR tube was charged with *para*-substituted (prop-1-yn-1-yl)benzene derivative (0.01 mmol) and 1,3,5-trimethoxybenzene (0.005 mmol) in 0.6 mL C_6D_6 and sealed with a septum cap. After locking and shimming, an initial ^1H NMR spectrum was acquired, the sample was ejected, and 100 µL of stock solution of **[Mo]** (0.1 mM) and triphenylsilanol (0.6 mM) in C_6D_6 was injected. The tube was inverted to mix and reinserted into the probe. After 30 s of shimming adjustment, ^1H NMR spectra were acquired every 20s at ambient temperature. Concentrations of the propynyl substrate were determined using 1,3,5-trimethoxybenzene as an internal standard. Forward rate coefficients k_a were determined by fitting the first-order integrated rate law to the time-dependent concentration of the propynyl substrate observed at the beginning of the reaction. Reported rate coefficients and associated errors were

determined by the average of three trials. To determine reverse rate coefficients, k_d, the same procedure was repeated using 150 μL of stock solution of **[Mo]** and triphenylsilanol. ^{1}H spectra were acquired every 20 s for 160 min at ambient temperature. Reverse rate coefficients and thus equilibrium constants *K*, were calculated by fitting the first-order reversible integrated rate law to the time-dependent concentration of the propynyl substrate.

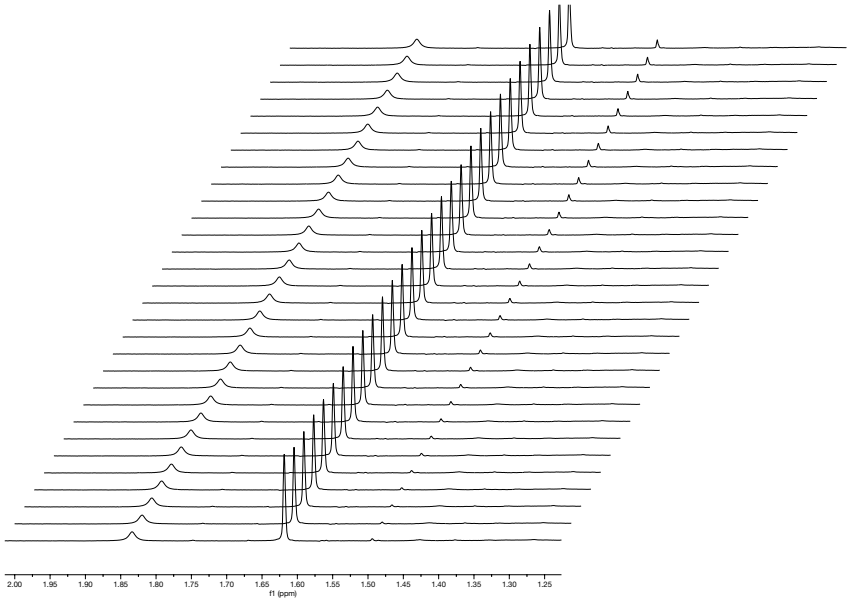

Figure 2.10. Representative array of the first 30 spectra acquired in the metathesis of prop-1-yn-1-ylbenzene. Formation of the 2-butyne byproduct is indicated by the increasing intensity of the singlet peak at δ = 1.50 ppm.

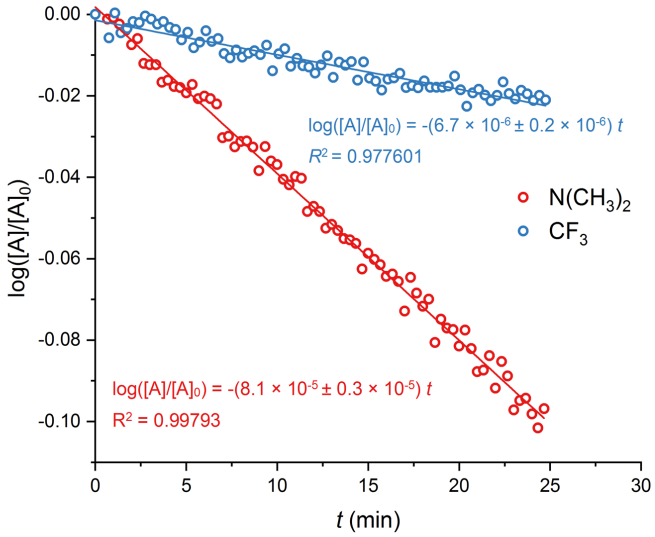

Figure 2.11. Representative kinetic traces and fits for the metathesis of *N*,*N*-dimethyl-4-(prop-1-yn-1-yl)aniline (blue) and 1-(prop-1-yn-1-yl)-4-(trifluoromethyl)benzene (red).

Substrate	σ_{para}	$k_a \times 10^4$ (s^{-1})	$\log(k_a/k_H)$
$N(CH_3)_2$	-0.83	4.5 ± 0.1	0.85 ± 0.02
OCH_3	-0.27	1.60 ± 0.04	0.41 ± 0.01
CH_3	-0.17	0.63 ± 0.02	0.004 ± 0.02
H	0	0.63 ± 0.01	0.00 ± 0.01
Br	0.232	0.348 ± 0.005	-0.256 ± 0.01
OAc	0.31	0.426 ± 0.04	-0.17 ± 0.04
CF_3	0.54	0.104 ± 0.004	-0.7 ± 0.03

Table 2.1. Forward rate coefficients and associated errors determined by initial rate studies.

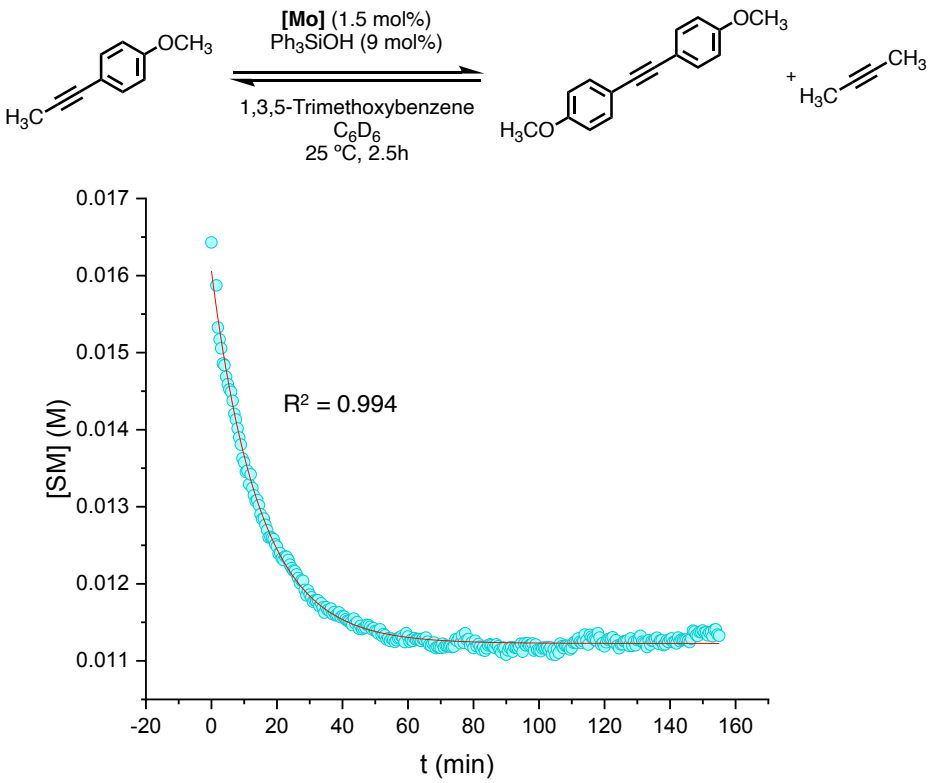

Figure 2.12. Representative reaction trace of the metathesis of *para*-methoxy propynylbenzene derivative with global fitting to the reversible first-order integrated rate law. Equilibrium concentrations of substrate $[A]_{eq}$ were determined by ^{1}H NMR using 1,3,5-trimethoxybenzene as an internal standard. Association constants k_a determined from initial studies and normalized for catalyst loading (assuming the rate of metathesis is first order in catalyst) were used to calculate the corresponding k_d values.

Substrate	$k_d \times 10^4$ (s^{-1})	$\log(k_d/k_{-H})$
$N(CH_3)_2$	25.3 ± 0.4	1.20 ± 0.01
OCH_3	1.57 ± 0.04	-0.009 ± 0.05
CH_3	2.4 ± 0.2	0.17 ± 0.05
H	1.6 ± 0.2	0.00 ± 0.04
Br	1.19 ± 0.02	-0.13 ± 0.04
OAc	2.0 ± 0.1	0.09 ± 0.04
CF_3	0.096 ± 0.007	-1.2 ± 0.3

Table 2.2. Reverse rate coefficients and associated errors determined by global fitting of AM reaction traces to the first order reversible rate law.

Synthesis of phenyl(4'-(prop-1-yn-1-yl)-[1,1'-biphenyl]-4-yl)methanone (7):

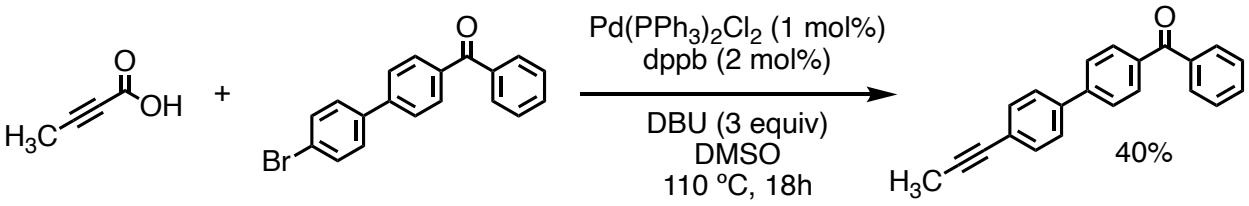

A 50 mL Schlenk flask was charged with 4-benzoyl-4'-bromobiphenyl (1.35 g, 4 mmol, 1 equiv), 2-butynoic acid (420 mg, 4 mmol, 1.25 equiv), 1,4-bis(diphenylphosphino)butane (34 mg, 0.08 mmol, 0.02 equiv), and $Pd(PPh_3)_2Cl_2$ (28 mg, 0.04 mmol, 0.01 equiv). Reagents were dissolved in DMSO (12 mL), then DBU (1.8 mL, 12 mmol, 3 equiv) was added in one portion. The reaction was then sealed and heated at 110 ºC overnight in an oil bath. After cooling to room temperature, saturated NH_4Cl was added. The layers were then separated and the aqueous layer was extracted 3x with DCM. The combined organic layers were washed with water and brine, dried with Na_2SO_4, and filtered over celite. The reaction mixture was purified *via* silica gel chromatography using

DCM to afford **7** as a yellow solid (470 mg, 40% yield). ^{1}H NMR (500 MHz, $CDCl_3$) δ 7.89 (d, *J* = 8.4 Hz, 2H), 7.83 (d, *J* = 8.4 Hz, 2H), 7.69 (d, *J* = 8.4 Hz, 2H), 7.64 – 7.60 (m, 1H), 7.58 (d, *J* = 8.4 Hz, 2H), 7.53 – 7.47 (m, 4H), 2.09 (s, 3H); ^{13}C{^{1}H} NMR (126 MHz, $CDCl_3$) δ 196.43, 144.61, 139.06, 137.87, 136.52, 132.56, 132.23, 130.91, 130.15, 128.47, 127.22, 126.93, 124.19, 87.42, 79.56, 77.41, 77.16, 76.91, 4.61; HRMS (ESI) m/z: $[C_{22}H_{17}O]^+$ calculated: 297.1279; found: 297.1274.

General Procedure for Pulsed Addition Experiments

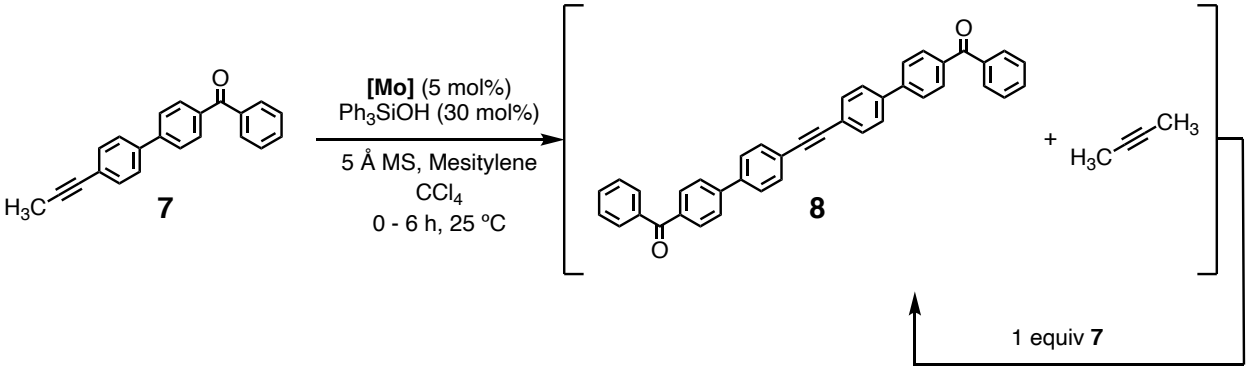

Determination of $k_{obs,0}$: All setup was performed in an Ar-filled glovebox. In a 20 mL scintillation vial, **7** (22 mg, 0.075 mmol, 1 equiv) and mesitylene (4 μL, 0.0375 mmol, 0.5 equiv) were dissolved in CCl_4 (2 mL). In a third, 2-dram vial, **[Mo]** (11 mg, 0.017 mmol) and Ph_3SiOH (28 mg, 102 mmol) were dissolved in CCl_4 (3.5 mL). The catalyst solution was allowed to pre-stir for 15 minutes, then 1.5 mL was transferred to the vial containing substrate **7**. 100 μL aliquots of the reaction were taken every 30s and passed over a short silica plug and diluted to a volume of 1 mL with CCl_4, then submitted for HPLC analysis. The time-dependent concentration of substrate was determined by HPLC using mesitylene as an internal standard.

Pulsed Addition Experiments: In a 20 mL scintillation vial, **7** (22 mg, 0.075 mmol, 1 equiv) and mesitylene (4 μL, 0.0375 mmol, 0.5 equiv) was dissolved in CCl_4 (2 mL). An identical stock solution was prepared in a separate 20 mL vial for later use. In a third, 2-dram vial, **[Mo]** (11 mg,

0.017 mmol) and Ph_3SiOH (28 mg, 102 mmol) were dissolved in CCl_4 (3.5 mL). The catalyst solution was allowed to pre-stir for 15 minutes, then 1.5 mL was transferred to one vial containing substrate **7**. The reaction was allowed to proceed for a predetermined time period between 1 and 6 hours, at which point the stock solution of **7** was added to the reaction mixture. Reaction progress was then monitored for 15 minutes.

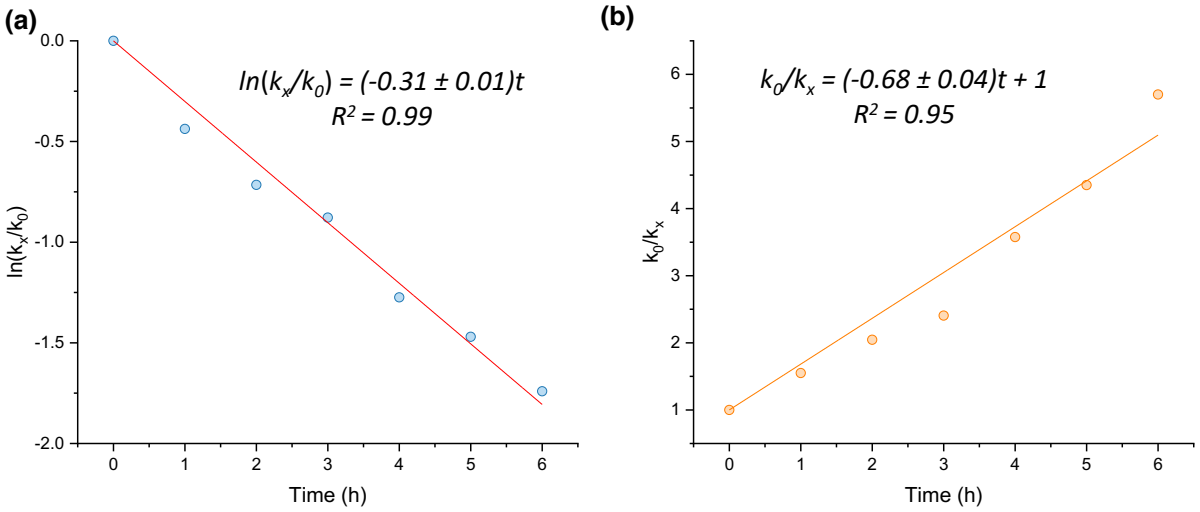

Figure 2.13. (a) First- and (b) second-order fit of catalyst deactivation for 5 mol% catalyst loading PA experiments.

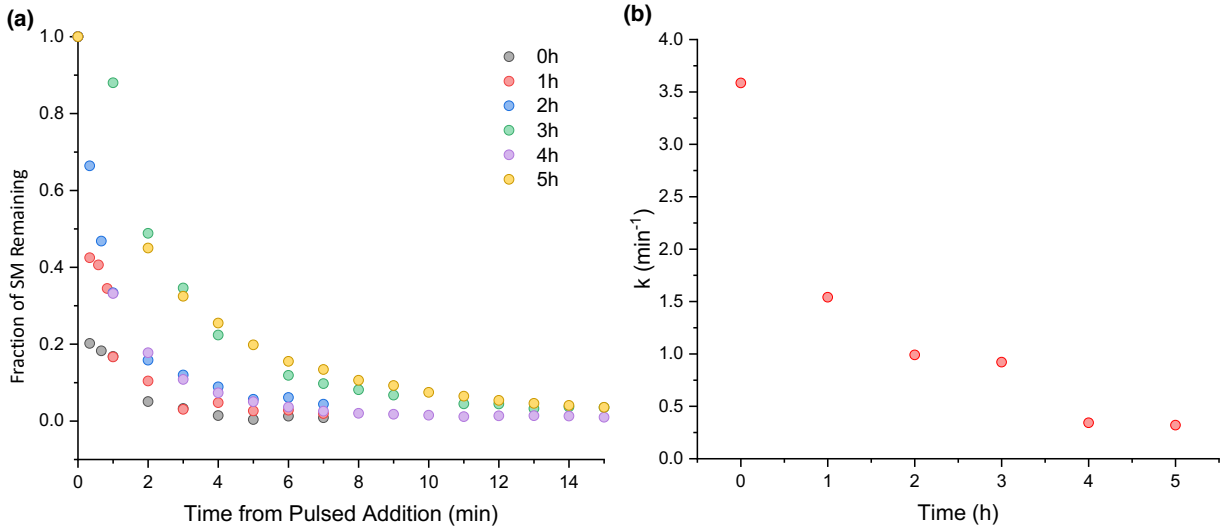

Figure 2.14. Pulsed addition experiments using 10 mol% initial catalyst loading. (a) Reaction traces for the conversion of substrate **7** after 0-5 hours of catalyst deactivation. (b) Rate coefficients, $k_{obs,x}$, determined for each pulsed addition experiment.

2.5.3 NMR Spectra

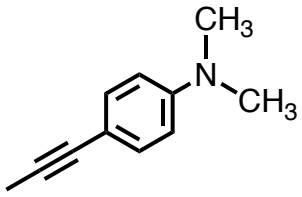

(^{1}H NMR, $CDCl_3$, 500 MHz)

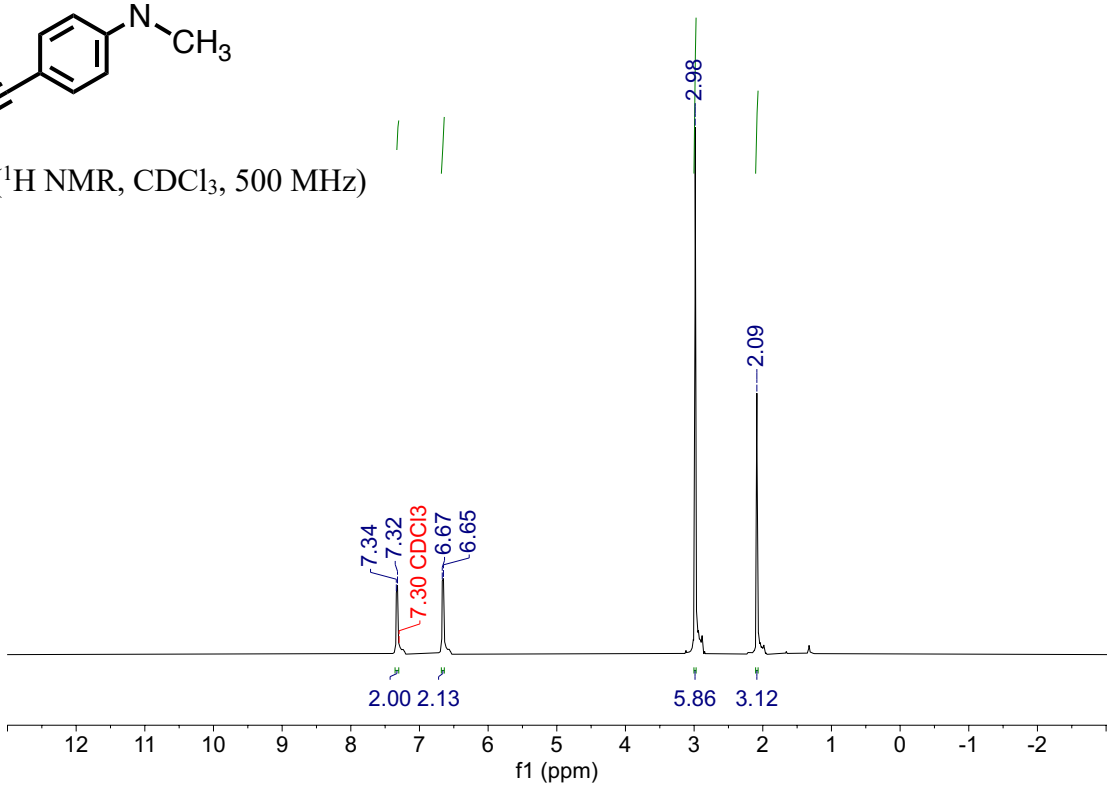

(^{13}C{^{1}H} NMR, $CDCl_3$, 126 MHz)

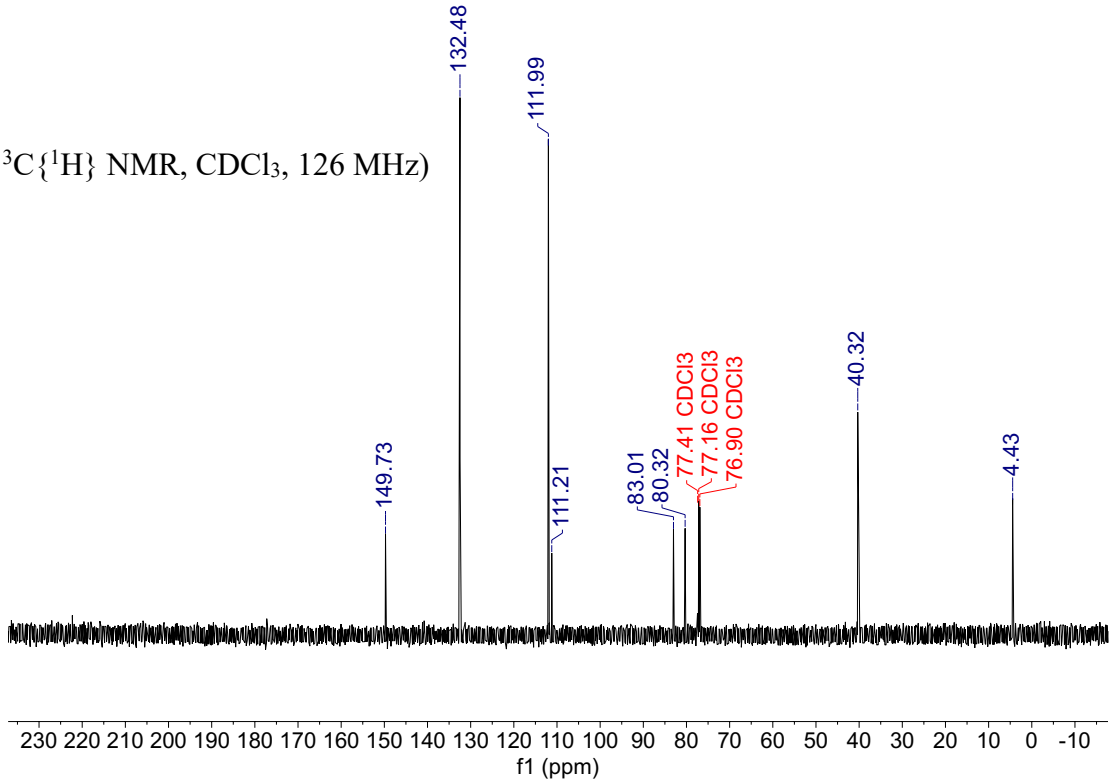

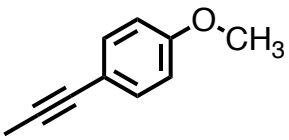

(^{1}H NMR, $CDCl_3$, 500 MHz)

(^{13}C{^{1}H} NMR, $CDCl_3$, 126 MHz)

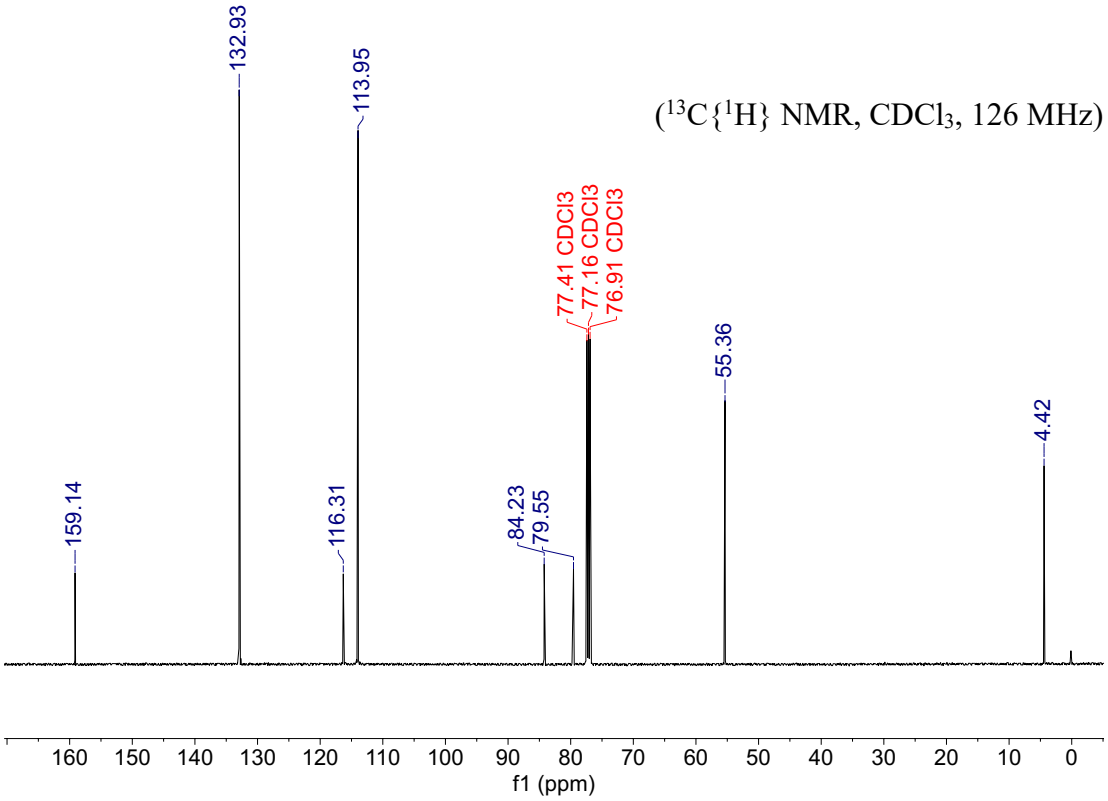

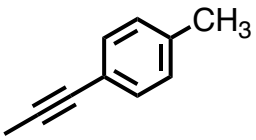

(^{1}H NMR, $CDCl_3$, 500 MHz)

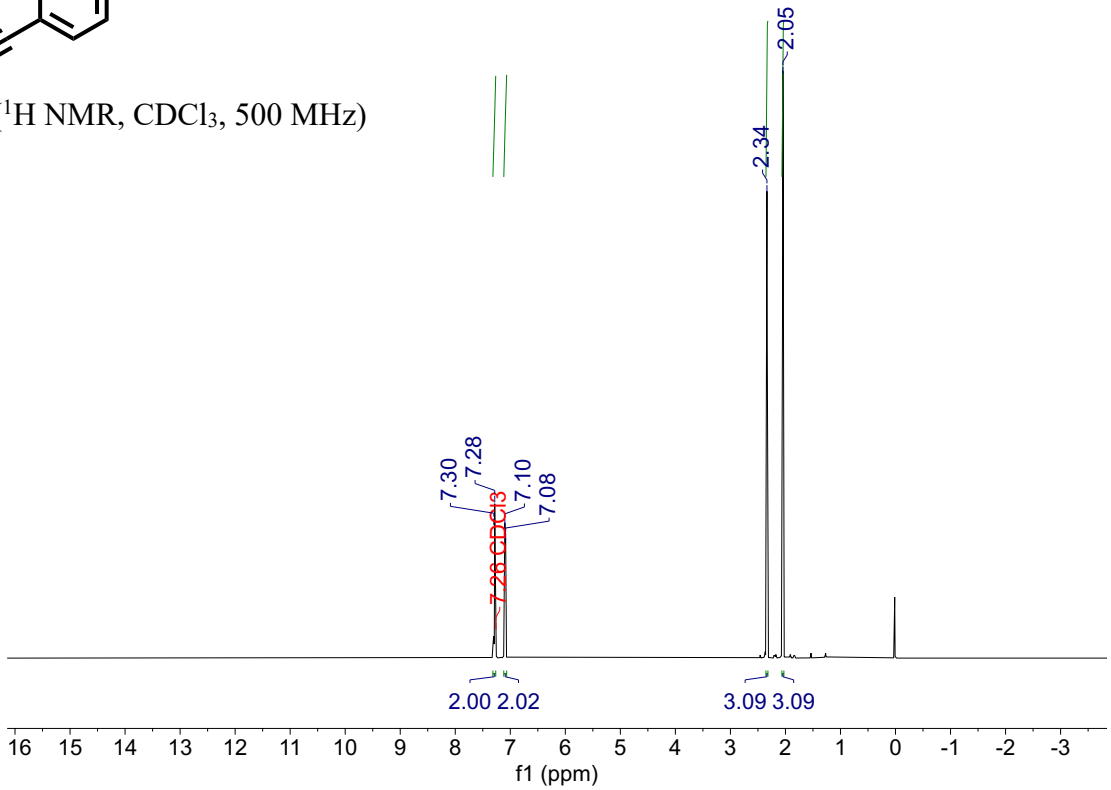

(^{13}C{^{1}H} NMR, $CDCl_3$, 126 MHz)

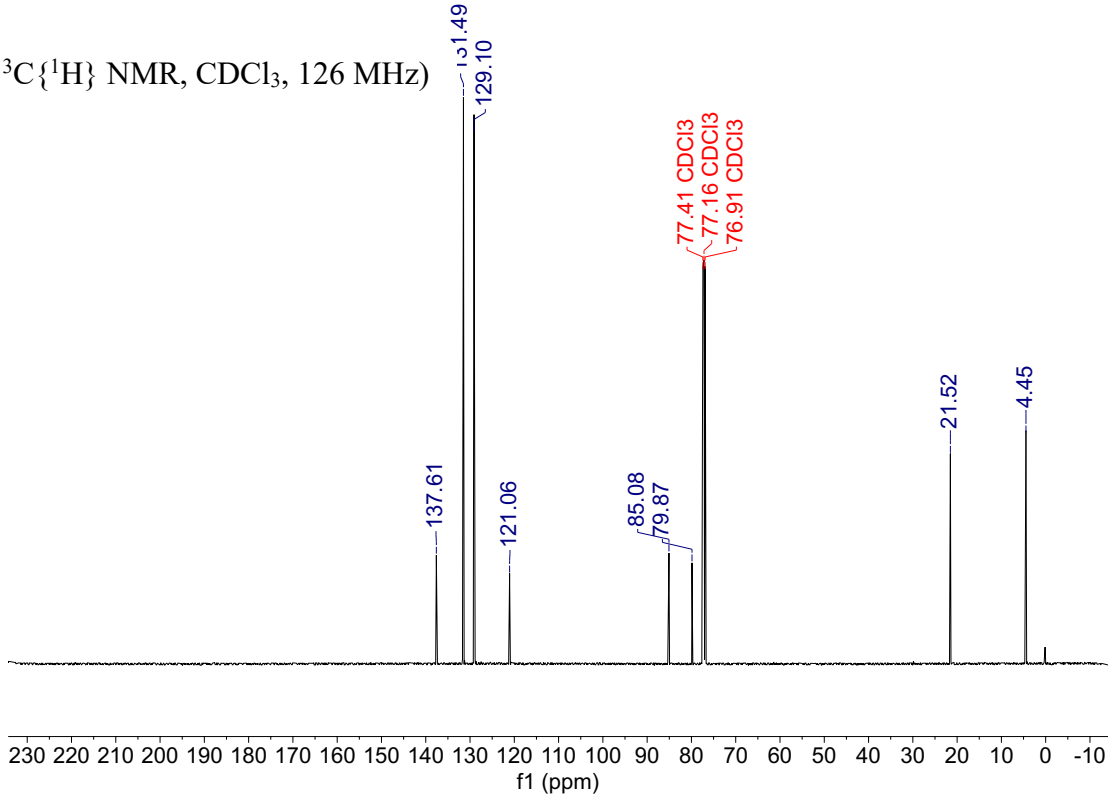

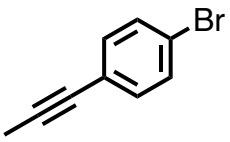

(^{1}H NMR, $CDCl_3$, 500 MHz)

(^{13}C{^{1}H} NMR, $CDCl_3$, 126 MHz)

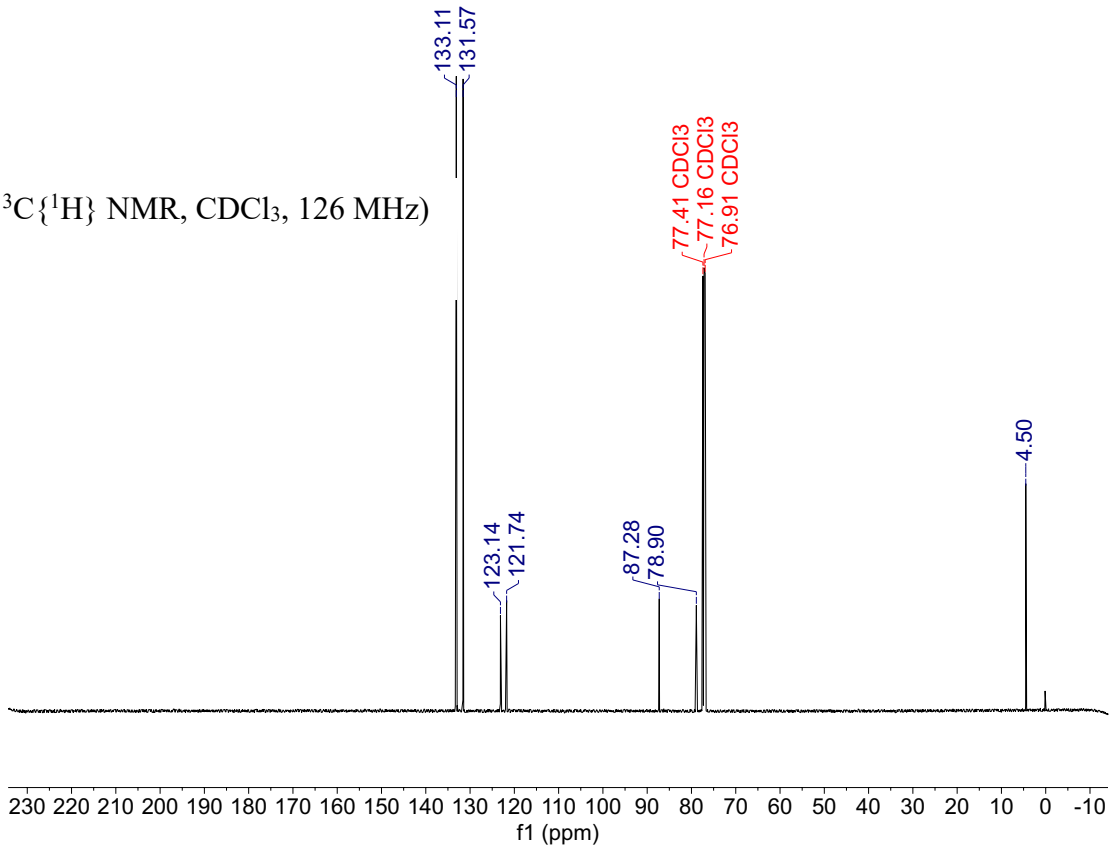

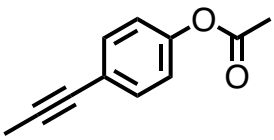

(^{1}H NMR, $CDCl_3$, 500 MHz)

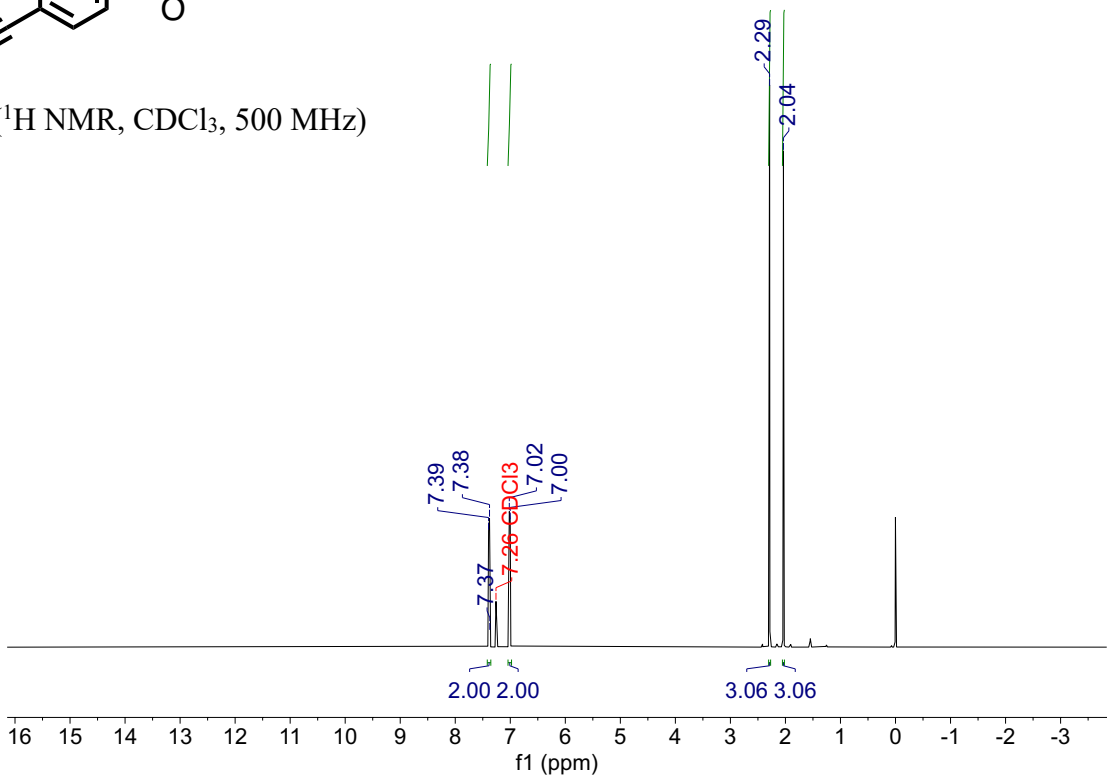

(^{13}C{^{1}H} NMR, $CDCl_3$, 126 MHz)

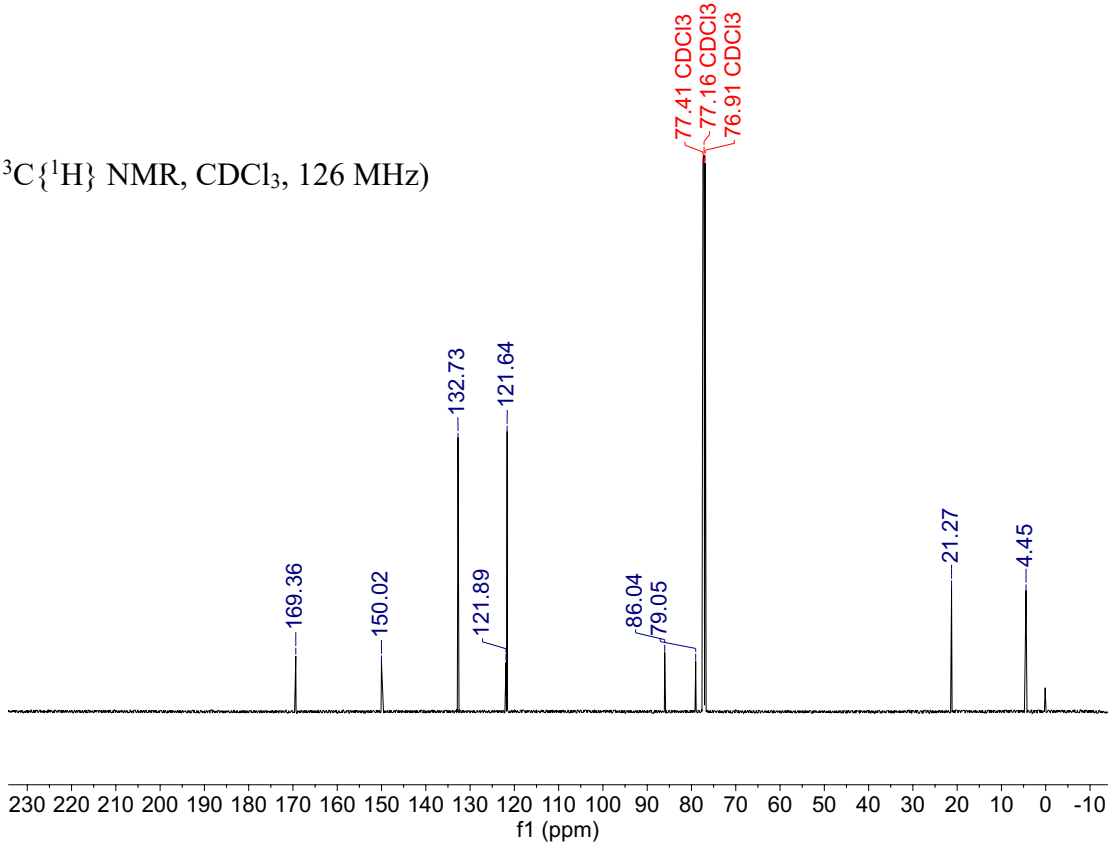

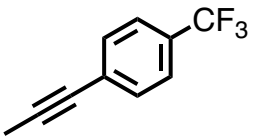

(^{1}H NMR, $CDCl_3$, 500 MHz)

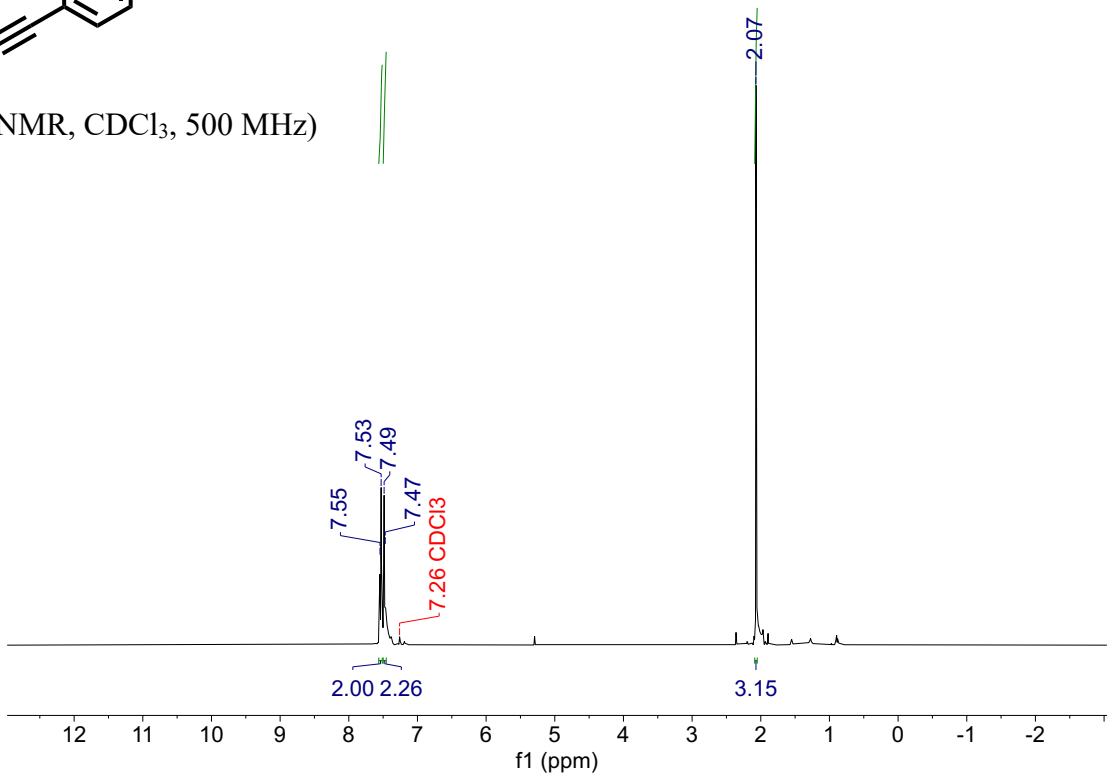

(^{13}C{^{1}H} NMR, $CDCl_3$, 126 MHz)

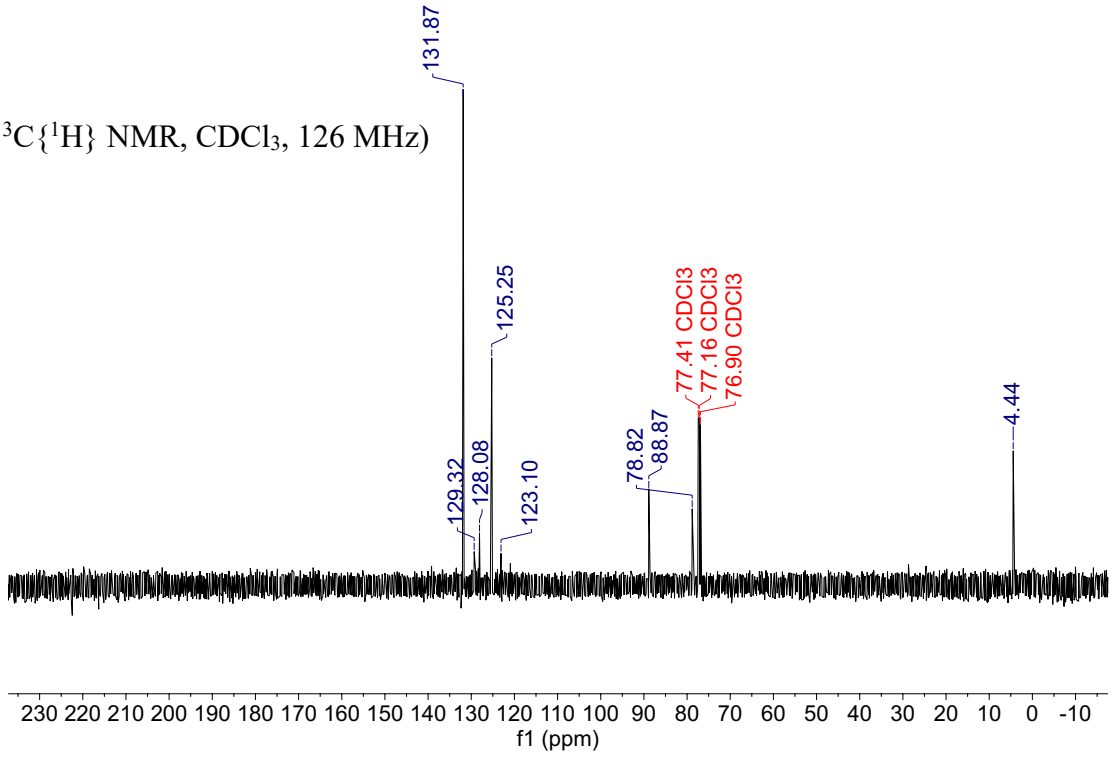

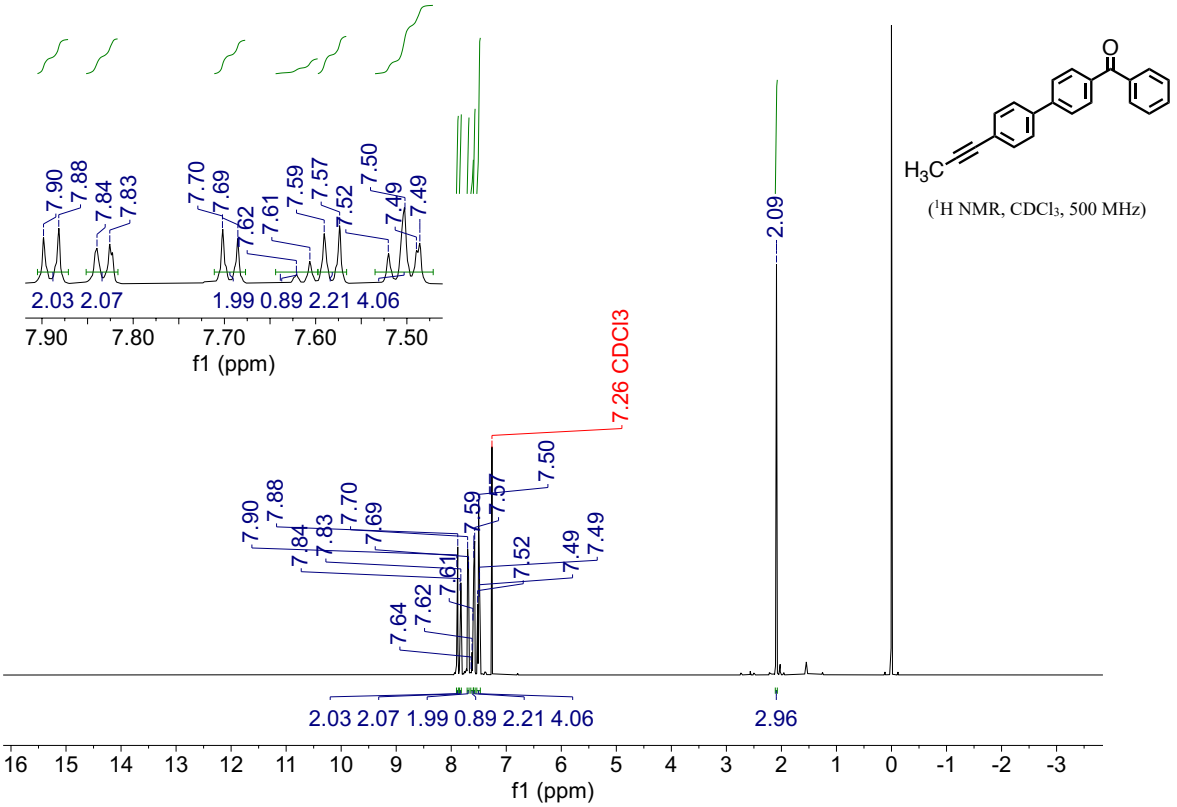

($^{13}C\{^{1}H\}$ NMR, $CDCl_3$, 126 MHz)

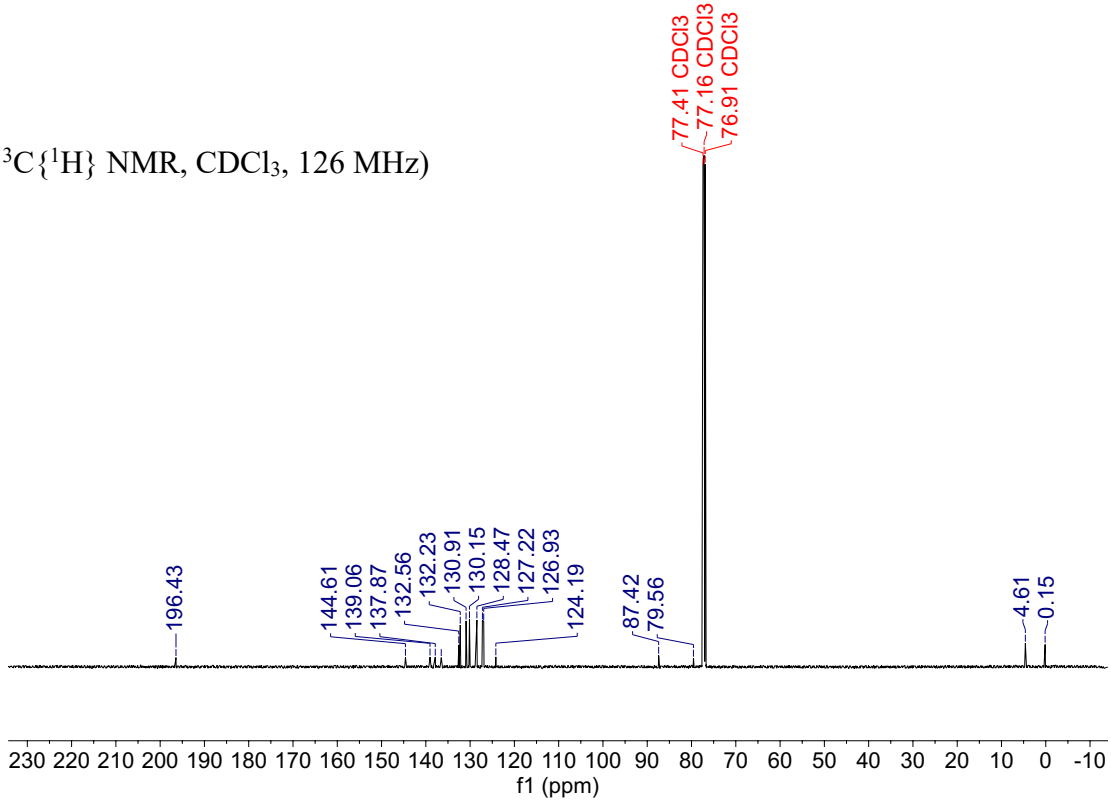

2.6 References

(1) Swain, J. A.; Iadevaia, G.; Hunter, C. A. H-Bonded Duplexes Based on a Phenylacetylene Backbone. *J. Am. Chem. Soc.* **2018**, *140* (36), 11526–11536.

(2) Elliott, E. L.; Hartley, C. S.; Moore, J. S. Covalent Ladder Formation Becomes Kinetically Trapped beyond Four Rungs. *Chem. Commun.* **2011**, *47* (17), 5028.

(3) Wei, T.; Furgal, J. C.; Jung, J. H.; Scott, T. F. Long, Self-Assembled Molecular Ladders by Cooperative Dynamic Covalent Reactions. *Polym. Chem.* **2017**, *8* (3), 520–527.

(4) Pattillo, C. C. Synthetic and Mechanistic Studies to Expand the Scope of Alkyne Metathesis Dynamic Covalent Chemistry, University of Illinois at Urbana-Champaign, 2019.

(5) Iadevaia, G.; Swain, J. A.; Núñez-Villanueva, D.; Bond, A. D.; Hunter, C. A. Folding and Duplex Formation in Mixed Sequence Recognition-Encoded m -Phenylene Ethynylene Polymers. *Chem. Sci.* **2021**, *12* (30), 10218–10226.

(6) Curtin, D. Y. Stereochemical Control of Organic Reactions. Differences in Behavior of Diastereoisomers. I. Ethane Derivatives. The Cis Effect. *Rec. Chem. Prog.* **1954**, No. 15, 111–128.

(7) Osowska, K.; Miljanić, O. Š. Self-Sorting of Dynamic Imine Libraries during Distillation. *Angew. Chemie Int. Ed.* **2011**, *50* (36), 8345–8349.

(8) Osowska, K.; Miljanić, O. Š. Oxidative Kinetic Self-Sorting of a Dynamic Imine Library. *J. Am. Chem. Soc.* **2011**, *133* (4), 724–727.

(9) Lirag, R. C.; Osowska, K.; Miljanić, O. Š. Precipitation-Driven Self-Sorting of Imines. *Org. Biomol. Chem.* **2012**, *10* (25), 4847.

(10) Hsu, C.-W.; Miljanić, O. Š. Adsorption-Driven Self-Sorting of Dynamic Imine Libraries.

Angew. Chemie Int. Ed. **2015**, *54* (7), 2219–2222.

(11) Ji, Q.; Miljanić, O. Š. Distillative Self-Sorting of Dynamic Ester Libraries. *J. Org. Chem.* **2013**, *78* (24), 12710–12716.

(12) Arai, K.; Takei, T.; Shinozaki, R.; Noguchi, M.; Fujisawa, S.; Katayama, H.; Moroder, L.; Ando, S.; Okumura, M.; Inaba, K.; Hojo, H.; Iwaoka, M. Characterization and Optimization of Two-Chain Folding Pathways of Insulin via Native Chain Assembly. *Commun. Chem.* **2018**, *1* (1), 26.

(13) Endres, D.; Miyahara, M.; Moisant, P.; Zlotnick, A. A Reaction Landscape Identifies the Intermediates Critical for Self-Assembly of Virus Capsids and Other Polyhedral Structures. *Protein Sci.* **2009**, *14* (6), 1518–1525.

(14) Zlotnick, A. Theoretical Aspects of Virus Capsid Assembly. *J. Mol. Recognit.* **2005**, *18* (6), 479–490.

(15) Covalent Assembly of Molecular Ladders. *J. Am. Chem. Soc.* **2007**, *129* (15), 4512–4513.

(16) Núñez-Villanueva, D.; Hunter, C. A. H-Bond Templated Oligomer Synthesis Using a Covalent Primer. *J. Am. Chem. Soc.* **2022**, *144* (37), 17307–17316.

(17) Zhang, W.; Kraft, S.; Moore, J. S. Highly Active Trialkoxymolybdenum(VI) Alkylidyne Catalysts Synthesized by a Reductive Recycle Strategy. *J. Am. Chem. Soc.* **2004**, *126* (1), 329–335.

(18) Koy, M.; Elser, I.; Meisner, J.; Frey, W.; Wurst, K.; Kästner, J.; Buchmeiser, M. R. High Oxidation State Molybdenum N -Heterocyclic Carbene Alkylidyne Complexes: Synthesis, Mechanistic Studies, and Reactivity. *Chem. - A Eur. J.* **2017**, *23* (61), 15484–15490.

(19) von Kugelgen, S.; Sifri, R.; Bellone, D.; Fischer, F. R. Regioselective Carbyne Transfer to Ring-Opening Alkyne Metathesis Initiators Gives Access to Telechelic Polymers. *J. Am.*

Chem. Soc. **2017**, *139* (22), 7577–7585.

(20) Cencer, M. M.; Greenlee, A. J.; Moore, J. S. Quantifying Error Correction through a Rule-Based Model of Strand Escape from an [n]-Rung Ladder. *J. Am. Chem. Soc.* **2019**.

(21) Zhu, J.; Jia, G.; Lin, Z. Theoretical Investigation of Alkyne Metathesis Catalyzed by W/Mo Alkylidyne Complexes. *Organometallics* **2006**, *25* (7), 1812–1819.

(22) Cencer, M. M.; Greenlee, A. J.; Moore, J. S. Quantifying Error Correction through a Rule-Based Model of Strand Escape from an [n]-Rung Ladder. *J. Am. Chem. Soc.* **2020**, *142* (1), 162–168.

(23) Wang, Q.; Yu, C.; Zhang, C.; Long, H.; Azarnoush, S.; Jin, Y.; Zhang, W. Dynamic Covalent Synthesis of Aryleneethynylene Cages through Alkyne Metathesis: Dimer, Tetramer, or Interlocked Complex? *Chem. Sci.* **2016**, *7* (5), 3370–3376.

(24) Greenlee, A. J.; Wendell, C. I.; Cencer, M. M.; Laffoon, S. D.; Moore, J. S. Kinetic and Thermodynamic Control in Dynamic Covalent Synthesis. *Trends Chem.* **2020**, *2* (12), 1043–1051.

(25) Leguizamon, S. C.; Scott, T. F. Sequence-Selective Dynamic Covalent Assembly of Information-Bearing Oligomers. *Nat. Commun.* **2020**, *11* (1), 784.

(26) Hillenbrand, J.; Korber, J. N.; Leutzsch, M.; Nöthling, N.; Fürstner, A. Canopy Catalysts for Alkyne Metathesis: Investigations into a Bimolecular Decomposition Pathway and the Stability of the Podand Cap. *Chem. – A Eur. J.* **2021**, *27* (56), 14025–14033.

(27) Heppekausen, J.; Stade, R.; Kondoh, A.; Seidel, G.; Goddard, R.; Fürstner, A. Optimized Synthesis, Structural Investigations, Ligand Tuning and Synthetic Evaluation of Silyloxy-Based Alkyne Metathesis Catalysts. *Chem. - A Eur. J.* **2012**, *18* (33), 10281–10299.

(28) Matson, J. B.; Virgil, S. C.; Grubbs, R. H. Pulsed-Addition Ring-Opening Metathesis

Polymerization: Catalyst-Economical Syntheses of Homopolymers and Block Copolymers. *J. Am. Chem. Soc.* **2009**, *131* (9), 3355–3362.

(29) Thompson, R. R.; Rotella, M. E.; Du, P.; Zhou, X.; Fronczek, F. R.; Kumar, R.; Gutierrez, O.; Lee, S. Siloxide Podand Ligand as a Scaffold for Molybdenum-Catalyzed Alkyne Metathesis and Isolation of a Dynamic Metallatetrahedrane Intermediate. *Organometallics* **2019**, *38* (21), 4054–4059.

(30) Kreysing, M.; Keil, L.; Lanzmich, S.; Braun, D. Heat Flux across an Open Pore Enables the Continuous Replication and Selection of Oligonucleotides towards Increasing Length. *Nat. Chem.* **2015**, *7* (3), 203–208.

(31) Mast, C. B.; Schink, S.; Gerland, U.; Braun, D. Escalation of Polymerization in a Thermal Gradient. *Proc. Natl. Acad. Sci.* **2013**, *110* (20), 8030–8035.

(32) Jiang, X.; Laffoon, J. D.; Chen, D.; Pérez-Estrada, S.; Danis, A. S.; Rodríguez-López, J.; Garcia-Garibay, M. A.; Zhu, J.; Moore, J. S. Kinetic Control in the Synthesis of a Möbius Tris((Ethynyl)[5]Helicene) Macrocycle Using Alkyne Metathesis. *J. Am. Chem. Soc.* **2020**, *142* (14), 6493–6498.

CHAPTER 3: ONE-POT IMINE FORMATION AND ALKYNE METATHESIS ENABLED BY CATALYST CHOICE

3.1 Introduction

Typically, DCC syntheses rely on a single type of chemical transformation leading to highly symmetric architectures containing only one type of functionality.[§] By contrast, orthogonal DCC (ODCC) offers great potential to construct molecular architectures with low symmetry and well-defined chemical functionalities.[1,2] However, explorations of ODCC have been hindered by the lack of functional group tolerance and chemical incompatibilities of multi-component dynamic exchange reactions.

Alkyne metathesis (AM) in particular, owing to the sensitivity of typical operative metal carbyne complexes to poisoning by air, water, and polar moieties, suffers from poor tolerance to even relatively mildly Lewis basic functional groups. Recently, the Fürstner,[3] Lee,[4] and Zhang[5–8] groups made considerable AM catalyst advances using tripodal ligand frameworks (Chart 3.1). Through the chelating effect, these scaffolds engender molybdenum carbyne species with improved robustness to hydrolysis and deleterious coordination to the metal center.[3,9] These studies have yielded a library of catalysts with impressive functional group tolerance and activity, which we posit will enable AM to operate in parallel with other dynamic covalent reactions. Recently, we reported the synthesis of a molecular cage via sequential imine condensation and AM using a canopy catalyst developed by Zhang et al. (Figure 3.1).[10] However, the sensitivity of the metathesis catalyst to poisoning by unreacted amine groups mandated extensive purification between steps. Because one of the unique advantages of DCC is its operational simplicity, it is

[§] The work in this chapter was adapted from the following publication: Tandem Imine Formation and Alkyne Metathesis Enabled by Catalyst Choice. Andrew J. Greenlee, Heyu Chen, Chloe I. Wendell, and Jeffrey S. Moore. The Journal of Organic Chemistry 2022 87 (13), 8429-8436. DOI: 10.1021/acs.joc.2c00538

desirable to avoid such purifications whenever possible. The development of ODCC for AM would streamline procedures for synthetically challenging multifunctional architectures.

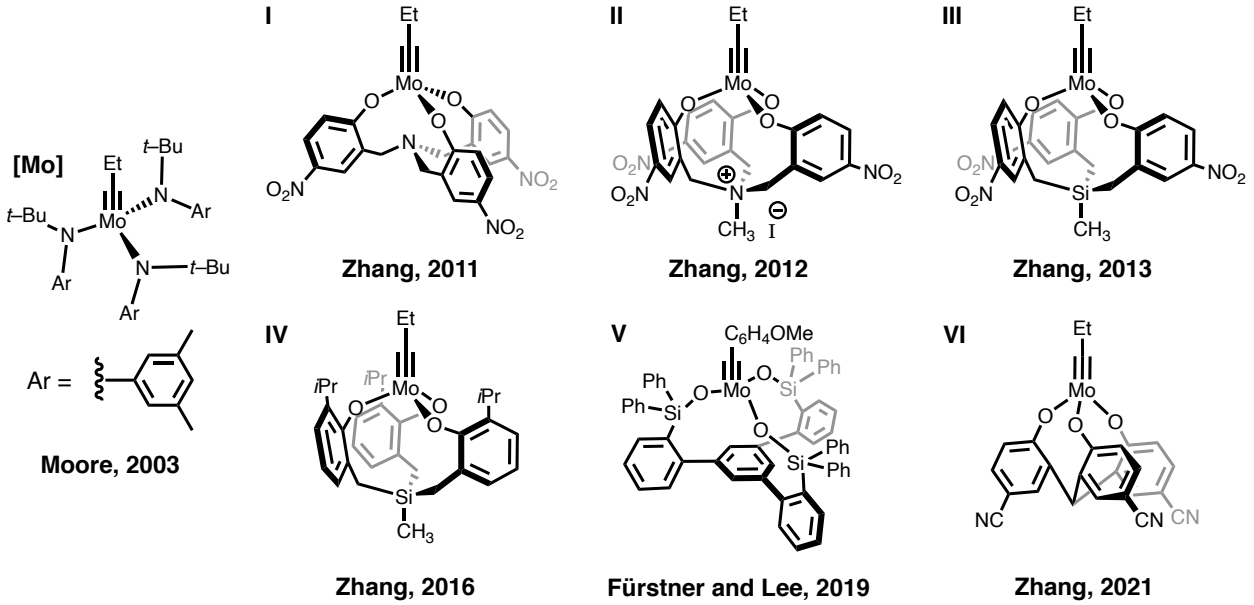

Chart 3.1. Representative alkyne metathesis catalysts generated from precursor [Mo] and tripodal ligand scaffolds.

Another rarely explored advantage of ODCC is the ability to leverage differences in reaction rates, or orders of addition, to achieve preorganization in self-assembly. This general strategy is used in nature to direct protein folding: fast, dynamic exchange processes (e.g. H-bond exchange) are often coupled with slower dynamic reactions (e.g. disulfide exchange) to lock proteins into their native tertiary structures.[11] Analogous reaction strategies have been used in the synthesis of structures like hydrogels[12] and nanowires,[13] as well as in the resolution of complex dynamic libraries,[14,15] but rarely have these strategies been explored in the dynamic covalent synthesis of discrete, well-controlled molecular architectures. AM, in particular, is well-suited for this strategy, as it is considerably slower than many common DCC reactions.[16] However, its kinetic sensitivity is underutilized in DCC syntheses.[17] Development of ODCC synthetic strategies involving AM might therefore also allow access to its underexplored kinetic manifold.

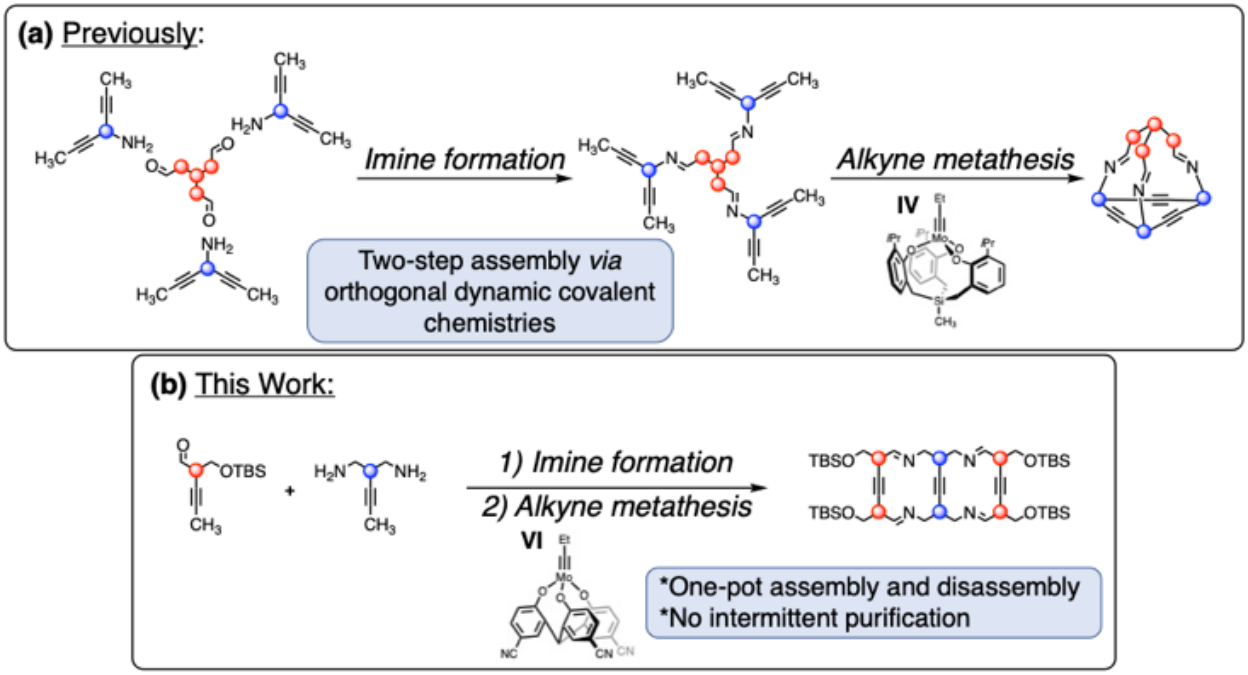

Figure 3.1. Developments in AM ODCC. (a) A molecular cage prepared via sequential orthogonal imine formation and alkyne metathesis. Reprinted from ref. 10. Copyright 2019, Royal Society of Chemistry. (b) A molecular ladder prepared via one-pot ODCC without intermittent isolation and purification.

To these ends, we sought to investigate the cross-reactivity of AM and imine formation and to develop protocols for one-pot syntheses of molecular structures via AM ODCC. Herein, we report the first example of AM operating in the same pot as another dynamic covalent reaction applied to the synthesis of a three-rung molecular ladder.

3.2 Orthogonal Imine Exchange and Alkyne Metathesis

3.2.1 Compatibility of AM Canopy Catalysts with Imine Exchange

Imine formation was selected as the orthogonal complement to AM because it is relatively well established and amenable to a variety of functional groups and reaction conditions.[18] We reasoned that 5 Å molecular sieves, included in AM reactions for removal of the 2-butyne byproduct,[19,20] might also effectively remove condensate generated by imine formation. Furthermore, molecular sieves have been shown to catalyze imine formation via redistribution of adventitious acid in

reaction media.[21] Thus, we anticipated that imine exchange would likely tolerate AM reaction conditions, while the sensitivity of AM catalysts might create challenges for one-pot ODCC. Specifically, we envisioned that imine or primary amine functionalities might poison the catalyst, as would hydrolysis by water generated from condensation reactions.

We began our study by investigating the efficacy of two different AM canopy catalysts in the assembly of an imine-bearing 3-rung molecular ladder. Precursor **7**, a single strand of ladder **8**, was synthesized from diamine **3** and aldehyde **6** (Scheme 3.1). Imine linkages form the strand segment with alkyne rungs as pendant groups. Ladder assembly was attempted using catalyst **III** or **VI**, generated from the corresponding ligand scaffold (**L-III** or **L-VI**) and molybdenum-trisamide alkylidyne precatalyst **[Mo]**. High (30 mol%) catalyst loadings were used to ensure thermodynamic error correction. The resulting mixture was heated at 40 °C for 18 h, then analyzed by MALDI-MS and size exclusion chromatography (SEC). The mass spectrum of the reaction mixture containing catalyst **III** showed only low molecular weight peaks, indicating that cyclooligomerization via AM likely did not occur. By contrast, the mass spectrum of the reaction containing catalyst **VI** showed a single peak corresponding to the target molecular ladder **8** (Figure 3.2). SEC analysis of the reaction mixture using catalyst **VI** also showed conversion to a higher molecular weight species, presumed to be ladder **8**. A high molecular weight tail is present in the metathesis reaction mixtures.

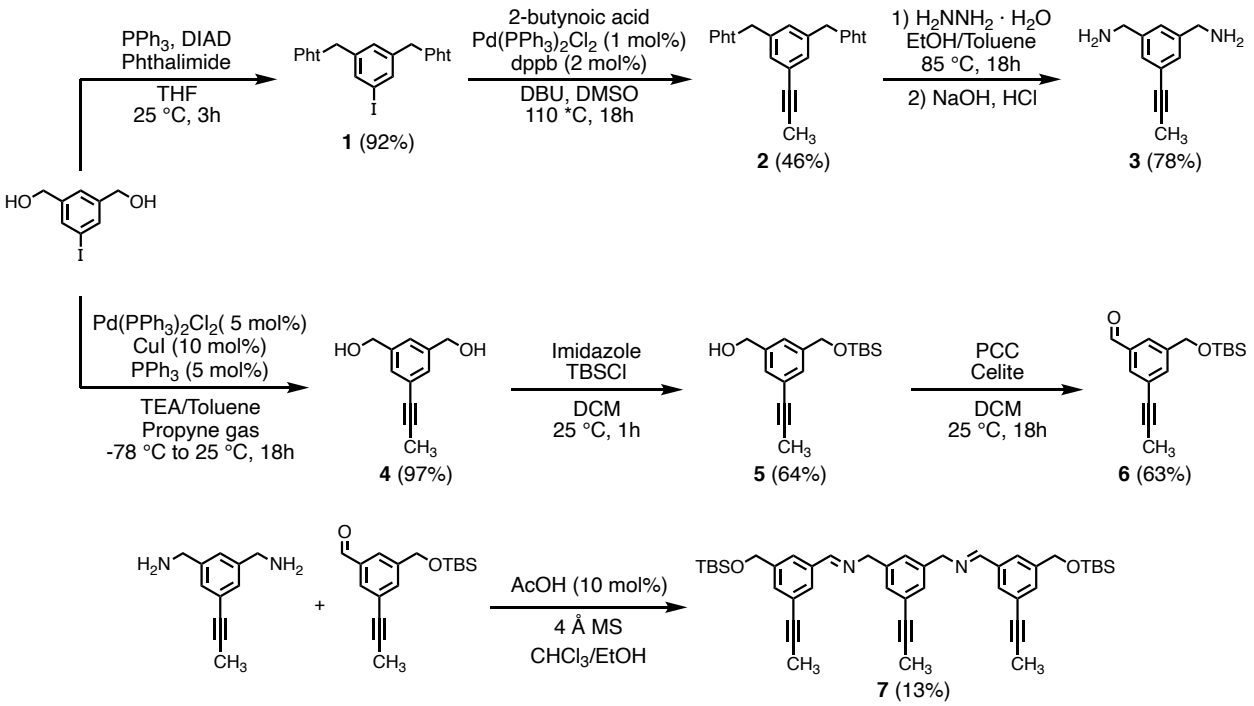

Scheme 3.1. Synthesis of ladder precursor **7** from diamine **3** and aldehyde **6**.

From these results, we concluded that the reportedly more active and robust catalyst **VI** can achieve AM of imine-bearing species, while the silyl analog **III** cannot. Independently, Zhang, Fürstner, and Lee have suggested that the differences in activity of these canopy catalysts may arise from ligand flexibility, though these effects are not yet completely understood.[5,22,23] It has been suggested that the inability of ancillary ligands to distort limits catalyst geometries that contribute to the formation off-pathway intermediates. It is possible that the flexibility of ligand **L-III** also negates some of the stabilizing effects imparted by its "canopy" design, such as tightly blocking active binding sites. This notion is supported by the ability of the more rigid analog **IV** to catalyze the metathesis of imine-bearing substrates,[10] although these ligands show drastically different sensitivities to steric and electronic effects and therefore defy direct comparison. This discrepancy will require a more nuanced follow-up study in the future.

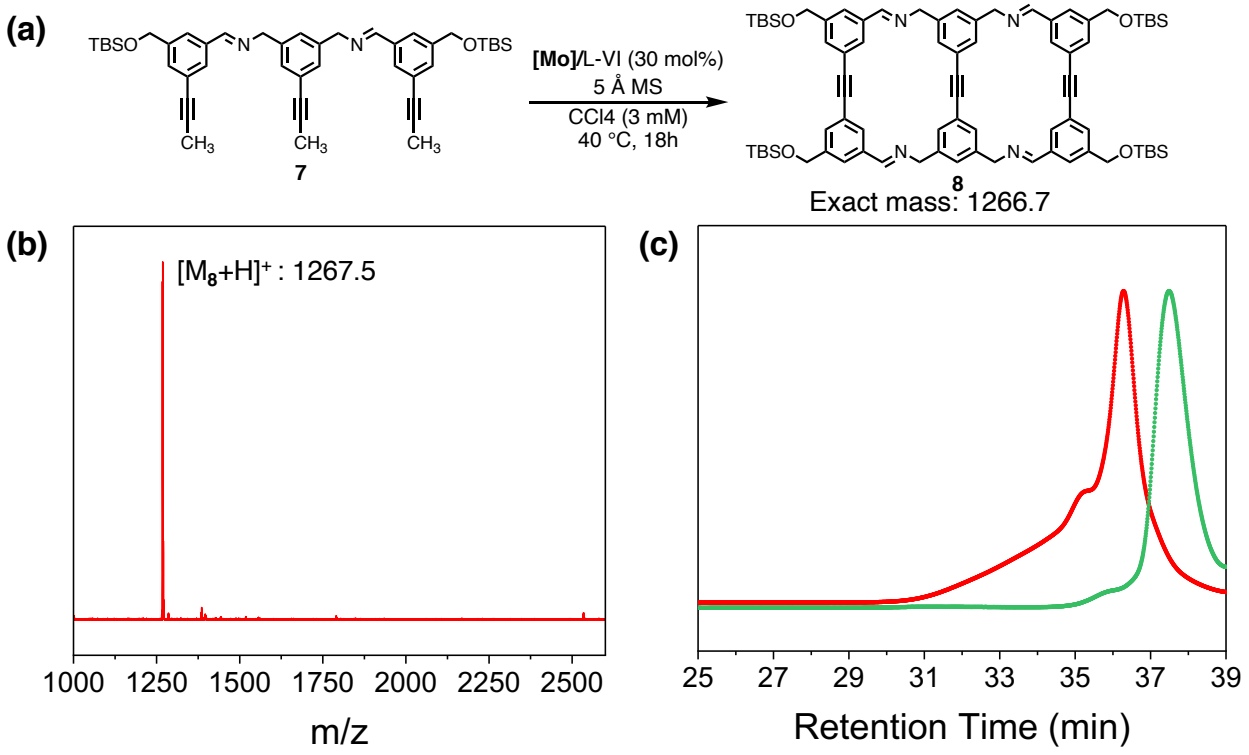

Figure 3.2. MALDI-TOF-MS and SEC results of the dimerization of strand **7** to ladder **8**. a) Reaction conditions. b) MALDI-MS mass spectrum of the reaction mixture. Expected exact mass $[M_8 + H]^+ = 1267.7$ g mol-1. All MALDI-MS data were collected in reflectron positive ion mode using a DCTB matrix. c) SEC chromatograms comparing precursor **7** (green) and the metathesis reaction mixture (red).

To determine whether metathesis operates in parallel with imine formation, we next attempted the synthesis of **8** via simultaneous addition of all reaction components. Precursors **3** and **6**, in a molar ratio of 1:2.2 to avoid excess of primary amine, were combined with a solution of preactivated **VI** in CCl_4 and added to a slurry of 5 Å MS in CCl_4. MALDI-MS characterization revealed primarily low molecular weight species as well as a trace amount of **8** and some metathesis products (Figure 3.3). The absence of high molecular weight species from the spectrum suggests incomplete AM cyclooligomerization, though the presence of the peak corresponding to **8** indicates some catalytic activity. We reasoned that the primary amine groups of **3** deactivated the catalyst, stifling metathesis activity. This explanation is consistent with previous reports of catalyst deactivation by basic amines.[24]

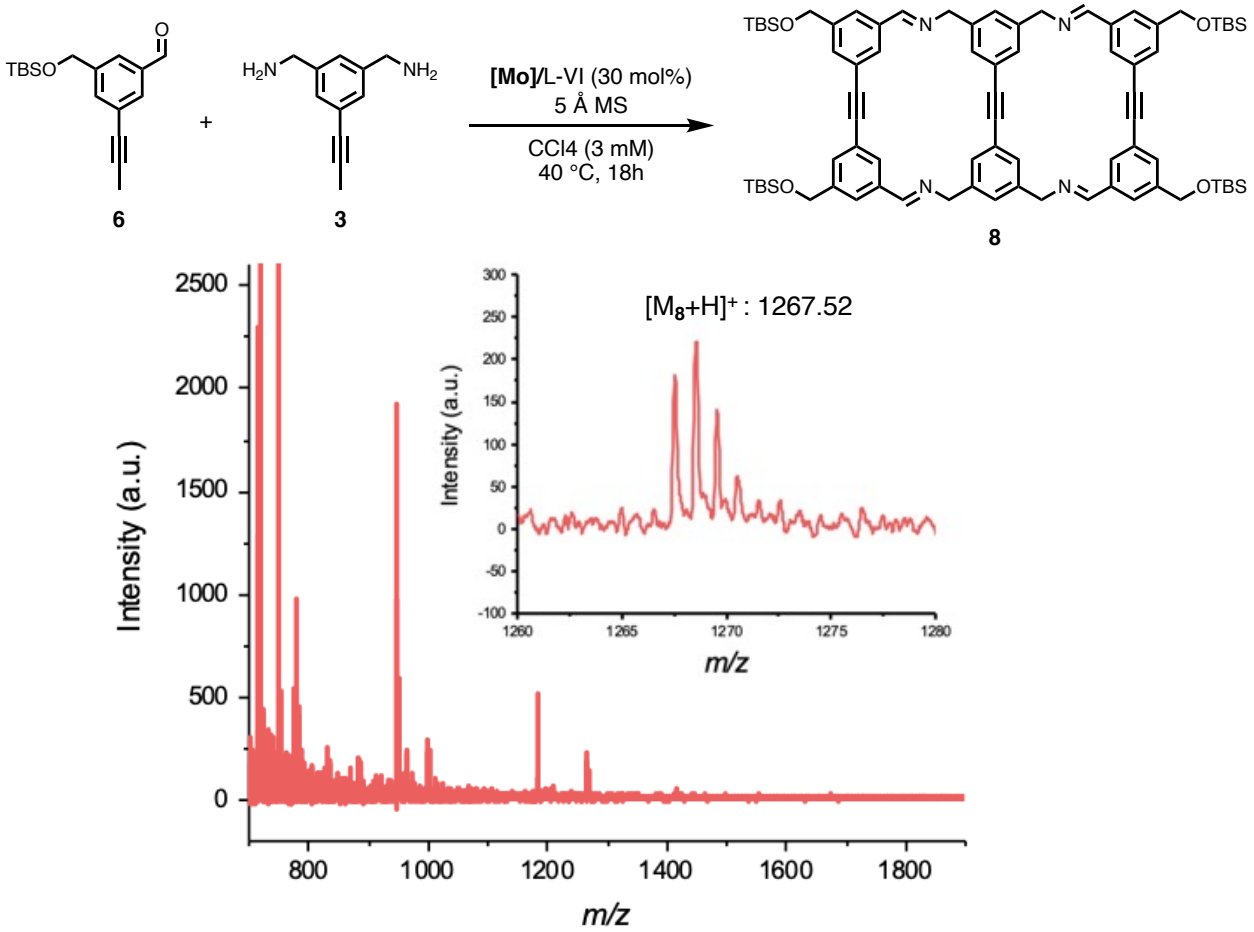

Figure 3.3. MALDI-MS analysis of the attempted ODCC assembly of ladder **8** *via* simultaneous addition of metathesis catalyst and imine-forming substrates **3** and **6**. The peak at m/z = 1268.6 indicates the presence of molecular ladder **8** in the reaction mixture.

To circumvent poisoning of the catalyst, a pre-stir strategy was employed. When diamine **3** and aldehyde **6** (1:2.2 ratio in CCl_4) were allowed to react overnight prior to addition of preactivated catalyst **VI**, the product distribution shifted to favor the target ladder **8**, as indicated by MALDI-MS (Figure 3.4). In contrast to the simultaneous addition experiment, metathesis appears to proceed smoothly when all amine groups are first converted to the corresponding imine. This result supports the notion that AM operates orthogonally to imine formation in one pot and further validates our hypothesis that self-assembly via parallel AM and imine formation is stymied by residual amine. The apparent abundance of the in-register molecular ladder (the putative the

thermodynamic product) in the product distribution also suggests that AM is under thermodynamic control under the reaction conditions.[25]

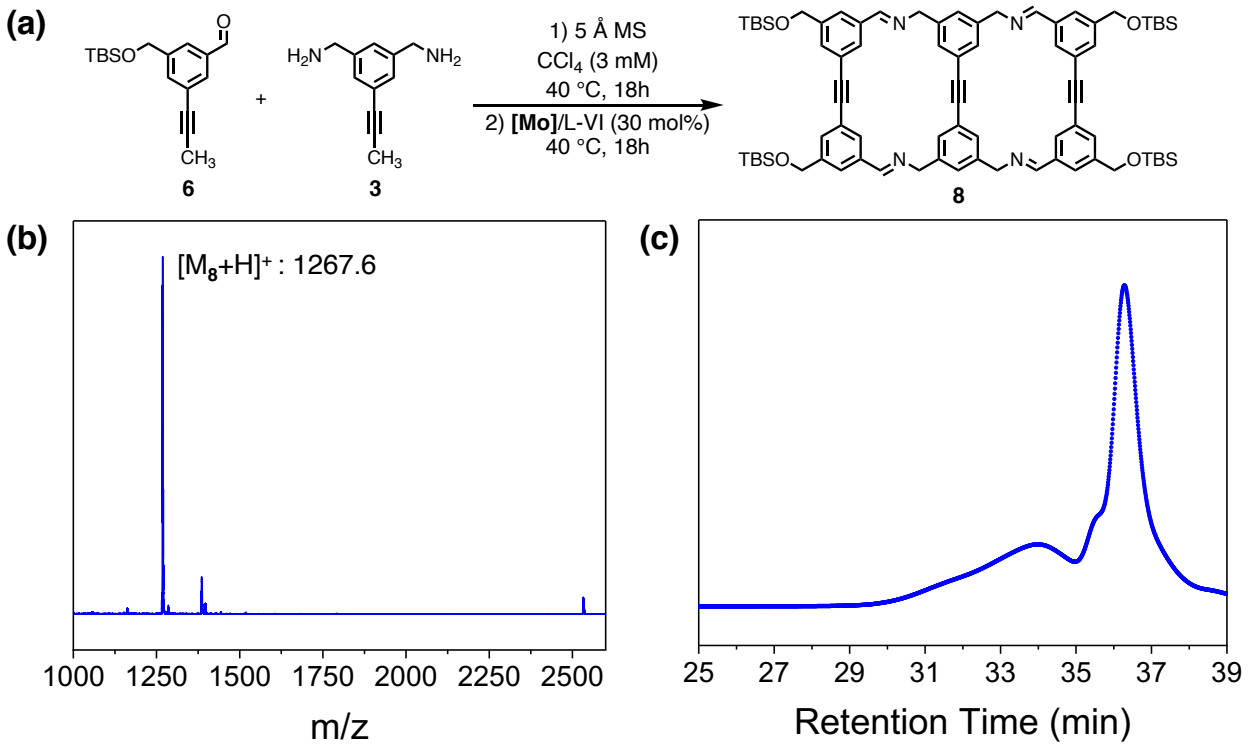

Figure 3.4. Characterization of the reaction mixture from the pre-stir experiment. a) Reaction conditions. b) MALDI-MS mass spectrum of the reaction mixture. c) SEC chromatogram of the reaction mixture. We reason that the broad, high molecular weight shoulder is from longer, out of register oligomers of 7.

With a synthetic route to **8** established, we next investigated the necessity of molecular sieves in the reaction. Given the robustness of canopy-type catalysts to hydrolysis,[3] we reasoned that catalyst **VI** might tolerate water produced as a result of imine formation. The activity of catalyst **VI** in the absence of molecular sieves was previously demonstrated by Zhang and coworkers, albeit only over short timescales and in solvents highly immiscible with water.[6] We feared that in a molar excess of water, and on the timescales required for cyclooligomerization, hydrolytic decomposition of the catalyst would impede error correction. As predicted, metathesis of both strand **7** and pre-stirred **3** and **6** under open air conditions failed. SEC traces of both reaction

mixtures revealed only strand **7**, indicating that metathesis did not occur (Figure 3.5). To investigate whether the catalytic inactivity could have been the result of poisoning by adventitious water, reactions were also run in an inert atmosphere under dynamic vacuum to remove 2-butyne. Conversion to ladder **8** was achieved for strand **7** but not for a pre-stirred mixture of **3** and **6**, suggesting that molecular sieves act not only as efficient scavengers of 2-butyne, but also of moisture produced during the reaction. These results also demonstrate that, despite improved stability of canopy catalysts, even robust species such as **VI** are susceptible to hydrolysis.

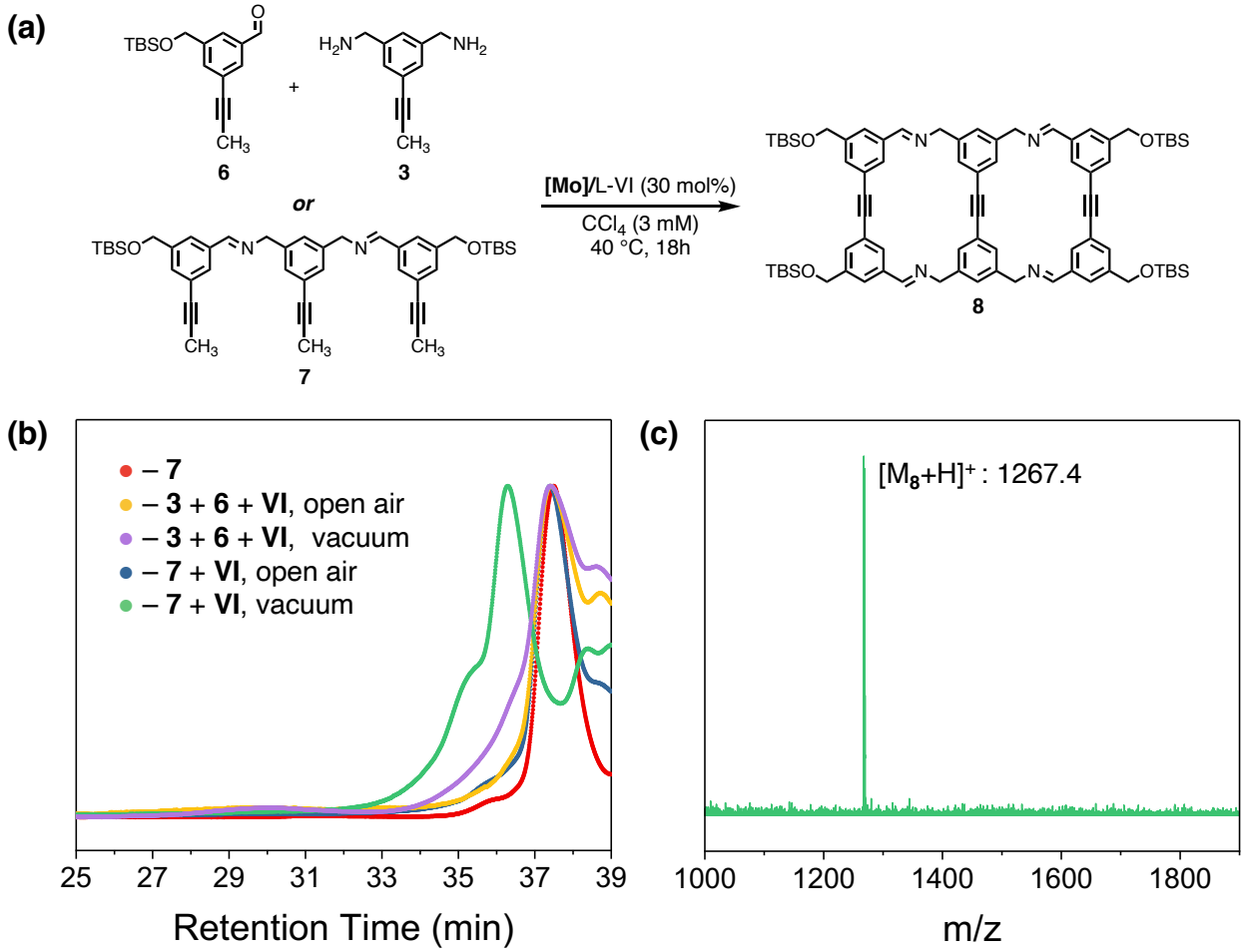

Figure 3.5. Metathesis of strand **7** or precursors **3** and **6** in the absence of molecular sieves. When **7** is subjected to metathesis under dynamic vacuum conditions, ladder **8** is generated. By contrast, when **7** is generated in situ by reaction of **3** and **6**, or when the reaction takes place in open air, metathesis products are not observed. These results suggest that the catalyst is susceptible to deactivation by water. (a) SEC traces of reaction mixtures run under open air or dynamic vacuum

Figure 3.5 (cont) conditions. The trace of strand **7** is included for reference. (b) MALDI mass spectrum of the metathesis reaction mixture of strand **7** under dynamic vacuum conditions.

3.2.2 Compatibility of Alkyne and Imine Exchange Catalysts

Given the success of these preliminary experiments, we next explored the effects of a Lewis acid catalyst on cross-reactivity. Many applications of imine exchange DCC rely on a Lewis acid catalyst such as $Sc(OTf)_3$ not only for acceleration of transimination, but also for in-situ deprotection of acetals.[26] Ideally, AM would tolerate these conditions, though ligand exchange between the Lewis acidic Sc(III) and Mo(VI) metal centers could threaten metathesis activity. Metathesis of **7** with 40 mol% $Sc(OTf)_3$ yielded a multitude of products, as indicated by a broad SEC trace. Multiple peaks were observed by MALDI-MS with masses corresponding to out-of-register oligomers of **7** (Figure 3.6b and c). This misregistration of ladder precursors is indicative of an inability of the metathesis system to "error correct," since products containing fewer constituent building blocks are favored over larger oligomers.[25,27,28] Moreover, many of the out-of-register species bear propyne functional groups, suggesting catalyst deactivation occurs on a competitive timescale with cyclooligomerization. When the reaction mixture was resubjected to metathesis in the absence of $Sc(OTf)_3$, only ladder **8** was observed by MALDI-MS and SEC (Figure 3.6). The apparent error-correction of out-of-register species to **8** further supports our assignment of the in-register ladder as the thermodynamic product of metathesis, as well as our hypothesis that $Sc(OTf)_3$ inhibits metathesis.

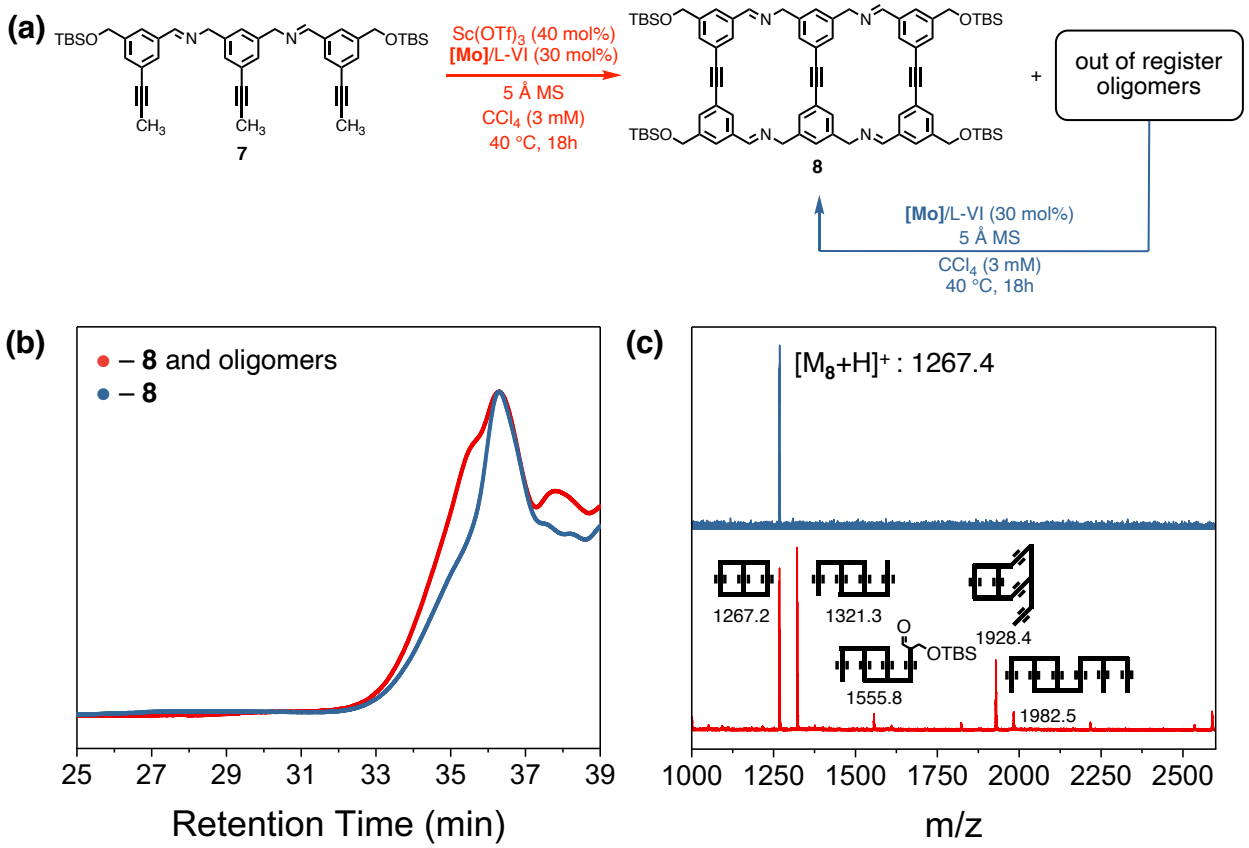

Figure 3.6. Metathesis of ladder precursor **7** in the presence of $Sc(OTf)_3$. (a) Reaction conditions. When **7** is subjected to metathesis in the presence of $Sc(OTf)_3$, high molecular weight oligomers are observed. When the reaction mixture is then resubjected to metathesis, only ladder **8** is observed. (b) SEC chromatograms of the reaction mixture before (red) and after (blue) error-correction. (c) MALDI mass spectra of the assembly reaction mixtures before (red) and after (blue) resubjecting to metathesis. Schematic representations of ladder **8** and out-of-register oligomers generated from metathesis in the presence of $Sc(OTf)_3$ are shown next to the corresponding mass peaks.

To further explore the possible antagonistic effects of Sc(III) on metathesis, we next attempted a one-pot synthesis of **8** from its constituent aldehyde and amine building blocks. Intriguingly, sequential reaction of **3** and **6** via $Sc(OTf)_3$-mediated imine formation followed by AM yielded a different product distribution than previous self-assembly trials. In addition to ladder **8**, MALDI-MS revealed a high molecular weight species tentatively assigned to structure **10**, identified as the cyclic tetramer of ladder precursor **7** (Figure 3.7a and b). SEC analysis further confirmed the shift in product distribution, as well as the presence of low molecular weight species

potentially indicative of incomplete assembly of precursor **7**. Generally, under acidic conditions, the rate of imine formation and hydrolysis is fast and favors the hydrolyzed amine and aldehyde products.[29] Thus, it is possible that in the presence of the Sc(III) catalyst, transimination occurs in parallel with AM, leading to partial deactivation of the metathesis catalyst by the primary amine as well as $Sc(OTf)_3$.

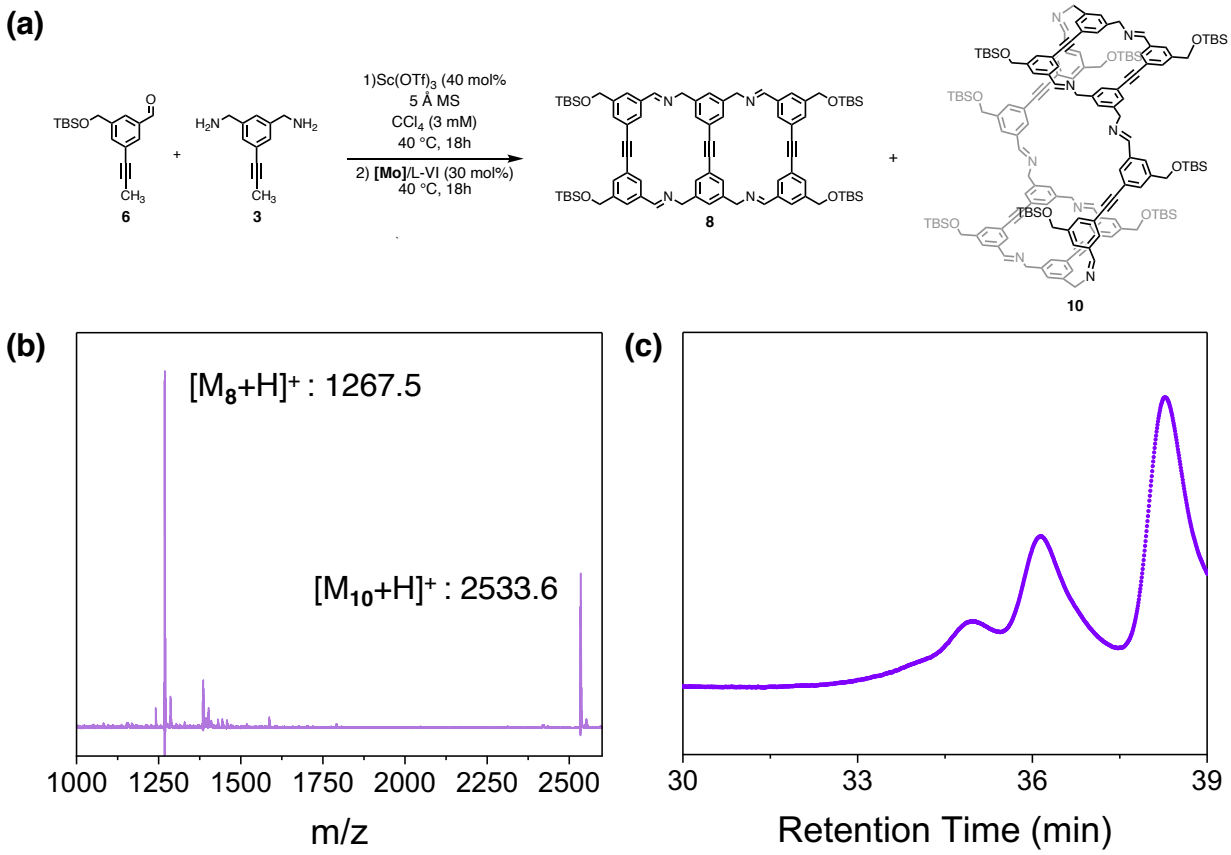

Figure 3.7. Assembly of ladder **8** in the presence of a Lewis Acid catalyst. (a) Reaction conditions and the proposed structure of **10**. (b) MALDI-MS mass spectrum of the assembly reaction mixture. (c) SEC chromatogram of the reaction mixture. The presence of both high and low molecular weight byproducts indicates potential strand misregistration via AM. Expected mass $[M_{10}^{\bullet}]^+$ = 2533.3 g mol^{-1}.

The presence of mass peaks corresponding to **10** in earlier assembly experiments also suggests that this structure may represent a particularly stable kinetic trap for this system, and thus might have error-corrected to **8** at higher temperatures, catalyst loadings, or longer reaction

times.[30] The absence of other oligomers and out-of-register species in the mass spectrum further support this notion and suggests only limited cross-reactivity between the catalysts.

3.2.3 Dynamic Disassembly Experiments

In ODCC with multitopic precursors, access to a particular product distribution may require continuous dynamic exchange for multiple parallel reactions. Thus, we next turned our attention to the nature of imine exchange in our system. Previous studies have demonstrated that amine-imine interchange proceeds even in the absence of an acid catalyst.[31] Therefore, we suspected that imine exchange occurs under our reaction conditions. To probe the equilibrium and dynamic nature of the system, a stationary state perturbation experiment was performed. Precursors **3** and **6** (1:2 ratio) were allowed to react via sequential imine formation and AM, either in the presence or absence of $Sc(OTf)_3$, to generate **8**. Then, the reaction mixtures were charged with 30 equiv of methylamine and stirred at 25 ºC for 18 h. Analysis by ^1H NMR spectroscopy revealed an abundance of ladder disassembly product **9a** and a disappearance of peaks corresponding to metathesis products in both cases (Figure 3.8). Together, these results indicate that imine exchange is dynamic under orthogonal reaction conditions, even in the absence of a molecular Brønsted or Lewis acid catalyst.

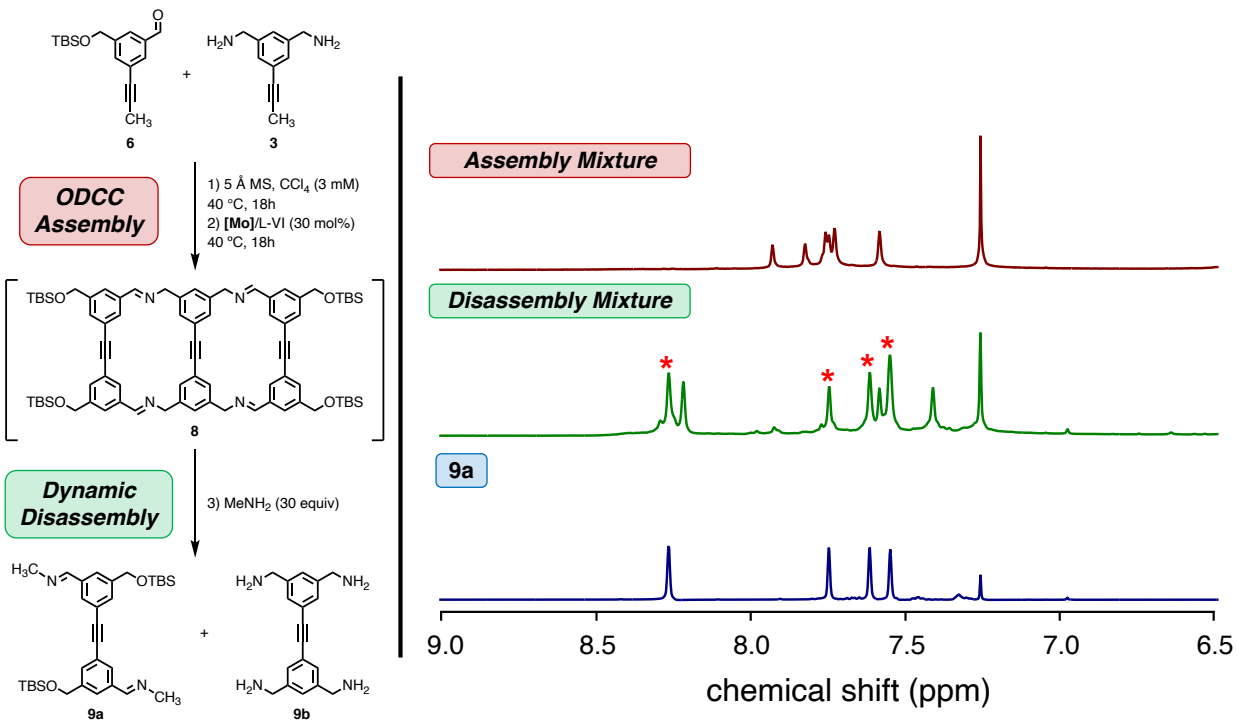

Figure 3.8. Disassembly of ladder **8** proceeds even in the absence of a molecular acid catalyst, indicating amine/imine exchange is dynamic. Left: ODCC assembly and disassembly of ladder **8** via dynamic imine exchange. Right: Comparison of ^{1}H NMR spectra of the assembly mixture (top), the disassembly mixture (middle), and the independently synthesized imine **9a** (bottom). The reaction mixtures were filtered through basic alumina and concentrated to dryness. Peak labels correspond to the disassembly product **9a**. NMR performed in $CDCl_3$, 500 MHz, 25 °C.

The measured success of these experiments indicates the robustness of catalyst **VI** to catalytic imine exchange conditions, as well as the potential for self-assembly by catalytic ODCC using multitopic imine and alkyne-bearing precursors. However, the apparent sensitivity of even the most stable canopy-type catalyst to water and primary amines poses a challenge for future synthetic applications of AM in ODCC. Jia and coworkers recently reported novel Re(V) AM catalysts that are stable to air and moisture as well as polar and protic moieties.[32,33] These systems, which have been demonstrated to promote catalytic metathesis in wet solvent, hold tremendous promise for the evolution of AM in ODCC systems and will require further investigation in the future.

3.3 Conclusion

A one-pot ODCC approach to imine exchange and AM has been developed. The efficacy of the sequential reaction strategy was demonstrated in the synthesis of a 3-rung molecular ladder, as well as its disassembly by transimination in the presence and absence of a Lewis acid catalyst. The protocols developed herein open the door to facile syntheses of well-defined molecular architectures bearing both imine and ethynylene functionalities, expanding the scope of DCC further to increasingly complex materials and chemical systems.

3.4 Supporting Information

3.4.1. General Considerations

All reactions were performed in oven (c.a. 165 ºC) or flame-dried glassware under an atmosphere of dry argon or nitrogen unless otherwise noted. All solvents used were either anhydrous commercial grade (Aldrich/Fisher) or purified by a solvent purification system unless otherwise noted. All alkyne metathesis reactions were conducted in an argon- filled glovebox in oven-dried glassware, using anhydrous (Aldrich), argon-degassed solvents. All reagents were purchased from commercial sources and used without further purification. Molybdenum(VI) propylidyne precatalyst **[Mo]**, (5-iodo-1,3-phenylene)dimethanol, and ligand **L-III** were each prepared according to published literature procedures.[8,34,35] Triphenol ligand **L-VI** was generously gifted to us by the Zhang group and used as received. Molecular sieves (5 Å powdered) were dried in a vacuum oven at 200 ºC for 5 days prior to use in alkyne metathesis reactions.[20] Chromatographic purifications were conducted via MPLC on a Biotage Isolera 1 using Silicycle SiliaSep cartridges (230-400 mesh, 40-63 μm). Column separation conditions are reported in column volumes (CV) of gradient solvent mixtures. ^{1}H and ^{13}C nuclear magnetic resonance spectra (NMR, 500 MHz) were recorded at room temperature (298 K) and chemical shifts were referenced

to the residual solvent peak. Structural assignments were made with additional information from gCOSY, gHSQC, and gHMBC experiments. Elemental analysis was obtained through the Microanalysis Laboratory, School of Chemical Sciences, University of Illinois using an Exeter Analytical CE 440 Analyzer. Mass spectra were obtained through the Mass Spectrometry Facility, School of Chemical Sciences, University of Illinois. High resolution electron impact (EI) mass spectra were obtained on a Micromass 70-VSE TOF spectrometer and electrospray ionization (ESI) mass spectra were obtained on a Waters Synapt G2-Si TOF spectrometer. Matrix-assisted laser desorption/ionization (MALDI) mass spectrometry was performed on a Bruker Daltonics UltrafleXtreme MALDI using DCTB matrix. MALDI spectra were plotted using OriginPro 2018 software. ^{1}H and ^{13}C NMR were processed using MestReNova software v12.0.4-22023. Reported yields are of isolated material which in some cases were corrected for trace residual solvent.

3.4.2 Synthesis and Characterization of Compounds

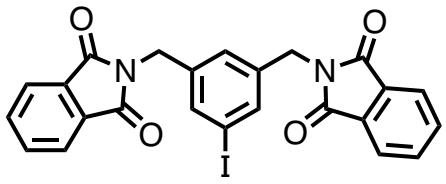

2,2'-(2,2'-(5-iodo-1,3-phenylene)bis(acetyl))dibenzoic acid (1). In a 250 mL round bottom flask charged with stir bar, triphenylphosphine (4.75 g, 18.2 mmol, 2.4 equiv) and (5-iodo-1,3-phenylene)dimethanol (2.00 g, 7.57 mmol, 1 equiv) were combined and dissolved in THF (75 mL). Diisopropyl azodicarboxylate (3.67 g, 18.2 mmol, 2.4 equiv) was added dropwise and the mixture was stirred for 3 h at room temperature. After adding water and stirring briefly, the white precipitate was collected by filtration and washed thoroughly with water (ca. 100 mL) and dried under vacuum to give the product as a white powder (3.64 g, 92% yield). The ^{1}H and ^{13}C NMR spectra corresponded to the values reported in literature for this compound.[36] m.p. = 245–247 ºC; ^{1}H NMR (500 MHz, $CDCl_3$): δ 7.85 (dd, J = 5.5, 3.1 Hz, 4H), 7.72 (dd, J = 5.4, 3.2

Hz, 4H), 7.64 (d, J = 1.4 Hz, 2H), 7.47 (s, 1H), 4.76 (s, 4H); $^{13}C\{^{1}H\}$ NMR (126 MHz, $CDCl_3$): δ 168.0, 138. 9, 136.9, 134.3, 132.2, 128. 5, 123.7, 94.9, 77.4, 77.2, 76.9, 40.8.

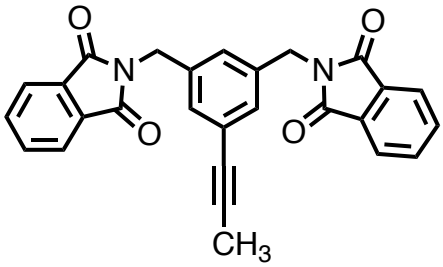

2,2'-((5-(prop-1-yn-1-yl)-1,3-phenylene)bis(methylene))bis(isoindoline-1,3-dione) (2). In a 100 mL Schlenk tube charged with stir bar, iodide 7 (3.42 g, 6.98 mmol, 1 equiv), $Pd(PPh_3)_2Cl_2$ (49 mg, 0.070 mmol, 1 mol %), 1,4 (bisdiphenylphosphino)butane (60 mg, 0.14 mmol, 2 mol%), and but-2-ynoic acid (733 mg, 8.72 mmol, 1.25 equiv) were dissolved in DMSO. To the mixture was added DBU (3.23 g, 20.9 mmol, 3 equiv), then the tube was sealed and the reaction was stirred at 110 °C overnight in an oil bath. After cooling to room temperature, saturated aqueous NH_4Cl was added. The layers were then separated and the aqueous layer was extracted 3x with DCM. The combined organic layers were washed with water and brine, dried with Na_2SO_4, and filtered over celite. The reaction mixture was purified via silica gel chromatography using DCM to afford 2 as a yellow solid (1.38 g, 46% yield). m.p. = 240–243 ºC; ^{1}H NMR (500 MHz, $CDCl_3$): δ 7.85 (dd, J = 5.4, 3.1 Hz, 4H), 7.71 (dd, J = 5.5, 3.1 Hz, 4H), 7.41 (s, 1H), 7.31 (s, 2H), 4.78 (s, 4H), 1.98 (s, 3H); $^{13}C\{^{1}H\}$ NMR (126 MHz, $CDCl_3$): δ 168.0, 137.0, 134.2, 132.2, 130.9, 128.1, 125.1, 123.6, 86.8, 77.4, 77.2, 76.9, 41.2, 4.4; HRMS (ESI) m/z: $[M+Na]^+$ Calcd for $C_{25}H_{20}N_2O_4Na$ 435.1321; Found 435.1335.

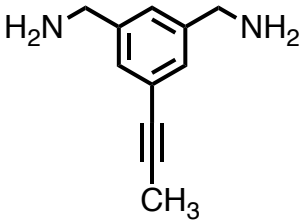

(5-(prop-1-yn-1-yl)-1,3-phenylene)dimethanamine (3). In a three-neck 500 mL round bottom flask charged with stir bar and jacketed condenser, bis-phthalimide 2 (1.34 g, 3.08 mmol, 1 equiv) was dissolved in ethanol (100 mL) and toluene (50 mL). The reaction mixture was then charged with hydrazine hydrate (926 mg, 18.5 mmol, 6 equiv) and stirred at 85 °C overnight in an oil bath. After cooling to room temperature, the mixture was concentrated and redissolved in 10

% NaOH. The aqueous layer was extracted 3x with $CHCl_3$ and separated. The combined organic layers were then acidified with 10% HCl and the aqueous layer was collected, neutralized to pH ~9 with 1M HCl, and extracted 5x with $CHCl_3$. The mixture was then dried over Na_2SO_4, filtered over celite, and concentrated to afford 3 as a yellow oil (420 mg, 78% yield). ^{1}H NMR (500 MHz, $CDCl_3$): δ 7.21 (s, 2H), 7.17 (s, 1H), 3.81 (s, 4H), 2.03 (s, 3H), 1.38 (s, 4H); $^{13}C\{^1H\}$ NMR (126 MHz, $CDCl_3$): δ 143.8, 128. 7, 125.3, 124.4, 85.8, 79.8, 77.4, 77.2, 76.9, 46.3, 4.4; HRMS (ESI) m/z: $[M+H]^+$ Calcd for $C_{11}H_{15}N_2$ 175.1235; Found 175.1234.

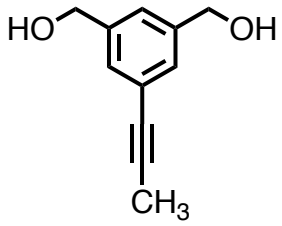

(5-(prop-1-yn-1-yl)-1,3-phenylene)dimethanol (4). In a 500 mL round bottom flask charged with stir bar, 5-iodo-1,3-phenylene)dimethanol (8.3 g, 31 mmol, 1 equiv), $Pd(PPh_3)_2Cl_2$ (1.1 g, 1.6 mmol, 5 mol %), CuI (600 mg, 3.14 mmol, 10 mol%), and triphenylphosphine (412 mg, 1.57 mmol, 5 mol%) were dissolved in triethylamine (100 mL) and toluene (100 mL). The reaction mixture was then cooled to -78 ºC using a dry ice/acetone bath and propyne gas was added to the reaction mixture. (Note: excess propyne was used. The propyne gas was bubbled through the mixture and into the headspace of the reaction from a small lecture bottle via an 18-gauge metal needle with an argon balloon as pressure release. The gas was added in approximately 4 ten-second bursts.) The reaction mixture was allowed to stir at -78 ºC for 5 minutes after which the bath was removed, and the mixture was stirred at 25 ºC for 24 hours. The black reaction mixture was then filtered through a short plug of silica gel with Et_2O and concentrated directly onto celite. The reaction was purified via silica gel flash chromatography with a 10 CV gradient of 0-80% EtOAc/Hexane (CV = column volume) to afford 4 as an off-white solid (5.37g, 97% yield). m.p. = 86–90 ºC. ^{1}H NMR (500 MHz, Acetone-d_6): δ 7.28 (s, 1H), 7.24 (s, 2H), 4.59 (d, J = 6.4 Hz, 4H), 4.24 (t, J = 5.8 Hz, 2H), 2.01 (s, 3H); $^{13}C\{^1H\}$ NMR (126 MHz, Acetone-d_6): δ 203.2, 140.6, 125.7, 121.9, 121.6, 82.8, 77.6, 61.1,

27.3, 27.1, 27.0, 26.8, 26.7, 26.5, 26.4, 0.9; HRMS (EI+) m/z: $[M^{\bullet}]^+$ Calcd for $C_{11}H_{12}O_2$ 176. 0837; Found 176.0840.

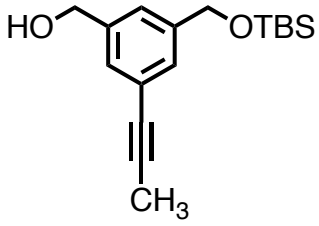

(3-(((tert-butyldimethylsilyl)oxy)methyl)-5-(prop-1-yn-1-yl)phenyl)methanol (5). In a two-neck 100 mL round bottom flask charged with stir bar, diol 4 (717 mg, 4.07 mmol, 1 equiv) was added to a solution of imidazole (277 mg, 4.07 mmol, 1 equiv) in DCM (40 mL). The reaction mixture was charged with TBSCl (624 mg, 4.14 mmol, 1.01 equiv) and allowed to stir at room temperature. After 1 h, the reaction slurry was filtered over celite and the filtrate was concentrated onto silica. The reaction mixture was purified via silica gel flash chromatography using a gradient of 0-10-30-60% EtOAc/Hexanes to afford 5 as a color-less oil which solidified into a white solid upon further drying (752 mg, 64% yield). ^{1}H NMR (500 MHz, $CDCl_3$): δ 9.97 (s, 1H), 7.76 (s, 1H), 6.63 (s, 1H), 7.58 (s, 1H), 4.75 (s, 2H), 2.07 (s, 3H), 0.95 (s, 9H), 0.11 (s, 6H); ^{13}C{^{1}H} NMR (126 MHz, $CDCl_3$): δ 142.0, 141.1, 128.7, 128.5, 124.3, 124.1, 85.9, 79.8, 77.4, 77.2, 76.9, 65.2, 64.7, 26.1, 18.6, 4.5, -5.1; HRMS (EI+) m/z: $[M\text{-}H^-]^+$ Calcd for $C_{17}H_{25}O_2Si$ 289.1624; Found 289.1634.

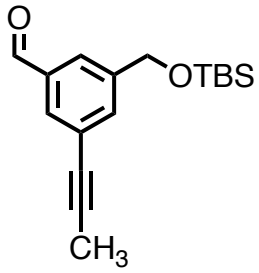

3-(((tert-butyldimethylsilyl)oxy)methyl)-5-(prop-1-yn-1-yl)benzaldehyde (6). In a 50 mL round bottom flask charged with stir bar, alcohol 5 (877 mg, 3.02 mmol, 1 equiv), PCC (976 mg, 4.53 mmol, 1.5 equiv), and celite (1.5 g) were combined in dry DCM (14 mL). The reaction was stirred overnight at room temperature, then passed over a short silica pad with DCM as eluent. The filtrate was further purified via flash column chromatography using a gradient of 0-10% EtOAc/Hexanes to afford 6 as a colorless oil (545 mg, 63% yield). ^{1}H NMR (500 MHz, $CDCl_3$): δ 9.97 (s, 1H), 7.76 (s, 1H), 7.73 (s, 1H), 7.58 (s, 1H), 4.75 (s, 2H), 2.07 (s, 3H), 0.95 (s, 9H), 0.11

(s, 6H); $^{13}C\{^{1}H\}$ NMR (126 MHz, $CDCl_3$): δ 191.8, 142.7, 136.4, 134.6, 131.6, 125.8, 125.1, 87.4, 78.6, 77.3, 77.0, 76.8, 64.0, 25.9, 18.4, 4.4, -5.3; HRMS (EI+) m/z: $[M^{\bullet}]^+$ Calcd for $C_{17}H_{24}O_2Si$ 288.1546; Found 288.1551.

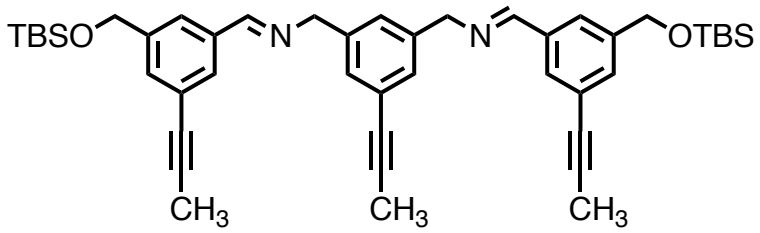

(1E,1'E)-N,N'-((5-(prop-1-yn-1-yl)-1,3-phenylene)bis(methylene))bis(1-(3-(((tert-butyldimethylsilyl)oxy)methyl)-5-(prop-1-yn-1-yl)phenyl)methanimine) (7). In a 2-dram vial charged with magnetic stir bar and 4 Å molecular sieves, diamine 3 (100 mg, 0.57 mmol, 1 equiv) and aldehyde 4 (480 mg, 1.66 mmol, 2.9 equiv) were dissolved in $CHCl_3$ (3 mL) and EtOH (3 mL). Acetic acid (34 μL) was added and the mixture was allowed to stir overnight at 55 °C. After cooling to room temperature, the mixture was diluted with $CHCl_3$ and filtered. The organic layer was washed with methanol and concentrated to afford a colorless oil. The residue, which contained residual aldehyde 4, was further purified by column chromatography using 1:9 triethylamine/hexanes as eluent to afford 7 as a colorless oil (54 mg, 13% yield). Note: NMR indicates the presence of residual 4. The purity of 7 was determined to be 90% by ^{1}H NMR. ^{1}H NMR (500 MHz, $CDCl_3$): δ 8.32 (s, 2H), 7.67 (s, 2H), 7.63 (s, 2H), 7.43 (s, 2H), 7.21 (s, 1H), 4.76 (s, 4H), 4.72 (s, 4H), 2.05 (s, 6H), 2.03 (s, 3H), 0.95 (s, 18H), 0.10 (s, 12H); $^{13}C\{^{1}H\}$ NMR (126 MHz, $CDCl_3$): δ 161.7, 142.2, 139.7, 136.2, 134.8, 131.4, 130.3, 129.8, 127.1, 125.0, 124.6, 86.35, 85. 9, 79.9, 79.5, 77.4, 77.2, 76.9, 64.8, 64.5, 29.9, 26.1, 18.6, 4.5, -5.1; HRMS (ESI) m/z: $[M+H]^+$ Calcd for $C_{45}H_{59}N_2O_2Si_2$ 715.4115; Found 715.4109; Anal. Calcd for $C_{45}H_{58}N_2O_2Si_2$: C, 75.58; H, 8.17; N, 3.92. Found: C, 75.61; H, 8.26; N, 3.81.

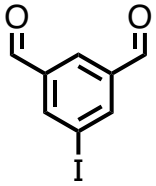

5-Iodoisophthalaldehyde (S1). In a 100 mL round bottom flask charged with magnetic stir bar was added (5-iodo-1,3-phenylene)dimethanol (1.38 g, 5.28 mmol, 1 equiv), pyridinium chlorochromate (3.42 g, 15.8 mmol, 3 equiv), and celite (5.28 g, 1 g per mmol diol). The reagents were dissolved in dry DCM (50 mL) and stirred overnight under an atmosphere of nitrogen, after which the mixture passed over a three-inch silica plug and concentrated to dryness to afford **S1** as a white solid (1.26 g, 92% yield). The ^{1}H and ^{13}C NMR spectra corresponded to the values reported in literature for this compound.[36] ^{1}H NMR (500 MHz, $CDCl_3$): δ 10.02 (s, 2H), 8.45 (s, 2H), 8.32 (s, 1H); $^{13}C\{^{1}H\}$ NMR (126 MHz, $CDCl_3$): δ 189.6, 143.3, 138.5, 130.0, 95.3, 77.4, 77.2, 76.9; HRMS (EI+) m/z: $[M^{\bullet}]^{+}$ Calcd $C_8H_5O_2I$ 259.9334; Found 259.9340.

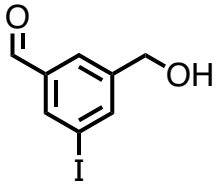

3-(hydroxymethyl)-5-iodobenzaldehyde (S2). In a 25 mL multi-neck round bottom flask charged with magnetic stir bar, **S1** (1.26 g, 4.85 mmol, 1 equiv) was dissolved in THF (7.5 mL) and EtOH (2.5 mL). The mixture was cooled to 0 °C, at which point $NaBH_4$ (64.3 mg, 1.70 mmol, 0.35 equiv) was added. The mixture was stirred for 1 h at room temperature, then concentrated directly onto celite and purified *via* flash chromatography using a gradient of 0-50% EtOAc/Hexanes to afford **S2** as a colorless oil which solidified into a waxy, white solid upon further drying (631 mg, 50% yield). ^{1}H NMR (500 MHz, $CDCl_3$): δ 9.88 (s, 1H), 8.08 (s, 1H), 7.96 (s, 1H), 7.80 (s, 1H), 4.73 (s, 2H), 2.42 (s, 1H); $^{13}C\{^{1}H\}$ NMR (126 MHz, $CDCl_3$): δ 190.9, 144.2, 141.4, 138.0, 137.6, 127.0, 94.9, 77.4, 77.2, 76.9, 63.6; HRMS (EI+) m/z: $[M^{\bullet}]^{+}$ Cacld for $C_8H_7O_2I$ 261.9491; Found 261.9500.

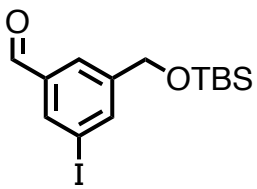

3-(((tert-butyldimethylsilyl)oxy)methyl)-5-iodobenzaldehyde (S3). In a multi- neck 10 mL vial charged with magnetic stir bar was added **S2** (1.16 g, 4.43 mmol, 1 equiv) and imidazole (602 mg, 8.85 mmol, 2 equiv). The

reagents were dissolved in dry DCM (5 mL), then TBSCl (800 mg, 5.3 mmol, 1.2 equiv) was added. The mixture was stirred at room temperature for 2 h, then partitioned between EtOAc and water. The mixture was extracted with EtOAc and the combined organic layers were washed with brine, dried over Mg_2SO_4, and concentrated onto silica. The mixture was purified *via* flash chromatography using a gradient of 0-10% EtOAc/Hexanes to afford **S2** as a colorless oil (1.48 g, 89% yield); ^{1}H NMR (500 MHz, $CDCl_3$): δ 9.91 (s, 1H), 8.08 (s, 1H), 7.93 (s, 1H), 7.78 (s, 1H), 4.75 (s, 2H), 0.95 (s, 9H), 0.12 (s, 6H); $^{13}C\{^1H\}$ NMR (126 MHz, $CDCl_3$): δ 190.8, 144.8, 140.6, 137.9, 136.9, 126.4, 94.5, 77.3, 77.0, 76.8, 63.5, 31.6, 25.9, 22.7, 18.4, 14.1, -5.3; HRMS (EI+) m/z: $[M^{\bullet}]^+$ Cacld for $C_{14}H_{21}IO_2Si$ 376.0356; Found 376.0349.

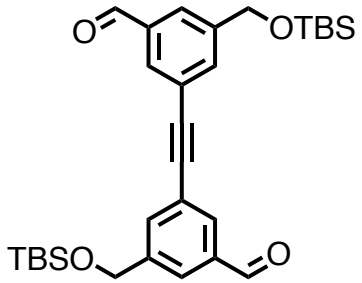

5,5'-(ethyne-1,2-diyl)bis(3-(((tert-butyldimethylsilyl)oxy)methyl)benzaldehyde) (S4). In a 10 mL multi-neck flask equipped with magnetic stir bar and jacketed condenser was added **S3** (250 mg, 0.66 mmol, 1 equiv), $Pd(PPh_3)_2Cl_2$ (28 mg, 40 μmol, 6 mol%), and CuI (13 mg, 66 μmol, 10 mol%). The flask was backfilled with nitrogen three times, then was added, sequentially, toluene (3.3 mL), DBU (600 mg, 3.9 mmol, 6 equiv), trimethylsilylacetylene (33 mg, 33 μmol, 0.5 equiv), and water (5 μL). The mixture was stirred at 80 ºC overnight in an oil bath, then quenched with water and extracted with DCM. The organic layer was washed 1x each with 10% HCl and brine, then dried over Mg_2SO_4. The mixture was further purified *via* flash column chromatography using a gradient of 0-50% EtOAC/Hexanes to afford **S4** as a white foam (28 mg, 16% yield). ^{1}H NMR (500 MHz, $CDCl_3$): δ 10.03 (s, 2H), 7.93 (s, 2H), 7.83 (s, 2H), 7.75 (s, 2H), 4.82 (s, 4H), 0.97 (s, 18H), 0.15 (s, 12H); $^{13}C\{^1H\}$ NMR (126 MHz, $CDCl_3$): δ 191.7, 143.3, 136.7, 134.8, 131.8, 127.0, 124.0,

89.4, 77.4, 77.16, 76.9, 64.1, 26.1, 18.6, -5.1; HRMS (EI+) m/z: $[M^{\bullet}]^+$ Calcd for $C_{30}H_{42}O_4Si_2$ 522.2622; Found 522.2624.

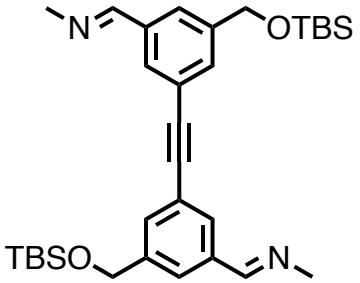

(1E,1'E)-1,1'-(ethyne-1,2-diylbis(5-(((tert-butyldimethylsilyl)oxy)methyl)-3,1-phenylene))bis(N-methylmethanimine) (**9a**). Dialdehyde **S1** (28 mg, 54 μmol, 1 equiv) was dissolved in a minimal amount of $CHCl_3$ (~1 mL). Methylamine (0.53 mL of a 2.0 M THF solution) was added to the mixture, followed by a small drop of acetic acid. The reaction was allowed to stir overnight at room temperature, then passed over a short plug of neutral alumina, dried with Na_2SO_4, filtered, and concentrated to afford 9a as a colorless oil (29 mg, >99% yield). ^{1}H NMR (500 MHz, $CDCl_3$): δ 8.27 (q, *J* = 1.8 Hz, 1H), 7.75 (d, *J* = 1.8 Hz, 1H), 7.62 (d, *J* = 1.6 Hz, 1H), 7.55 (d, *J* = 1.5 Hz, 1H), 4.76 (s, 2H), 3.53 (d, *J* = 1.6 Hz, 3H), 0.96 (s, 9H), 0.12 (s, 6H); ^{13}C{^{1}H} NMR (126 MHz, $CDCl_3$): δ 161.8, 142.4, 136.5, 131.2, 130.0, 125.4, 123.7, 89.4, 77.4, 77.2, 76.9, 64.5, 48.4, 26.1, 18.6, 1.2, -5.1; HRMS (EI+) m/z: $[M^{\bullet}]^+$ Calcd for $C_{32}H_{48}O_2Si_2N_2$ 548.3254; Found 548.3246.

General Procedure for Ladder Assembly from 7

In an argon-filled glovebox, a solution of 7 (10 mg, 14 μmol, 1 equiv) was dissolved in a slurry of 5 Å molecular sieves (120 mg) in CCl_4 (1 mL). In a separate vial, precatalyst **[Mo]** (2.8 mg, 4.2 μmol, 30 mol % relative to 7) and either ligand **L-III** or **L-VI** (each 1.5 mg, 4.2 μmol, 1 equiv relative to **[Mo]**) were combined in 3.6 mL CCl_4 and stirred at 25 or 70 °C, respectively, for 10 minutes in a heating block. The reactant and catalyst mixtures were then combined and stirred overnight at 40 °C. After cooling to room temperature, the mixture was filtered over a short pad of neutral alumina with chloroform as eluent, concentrated, and redissolved in 5 mL of dry THF. The resulting solution was analyzed by MALDI-MS with DCTB as a matrix.

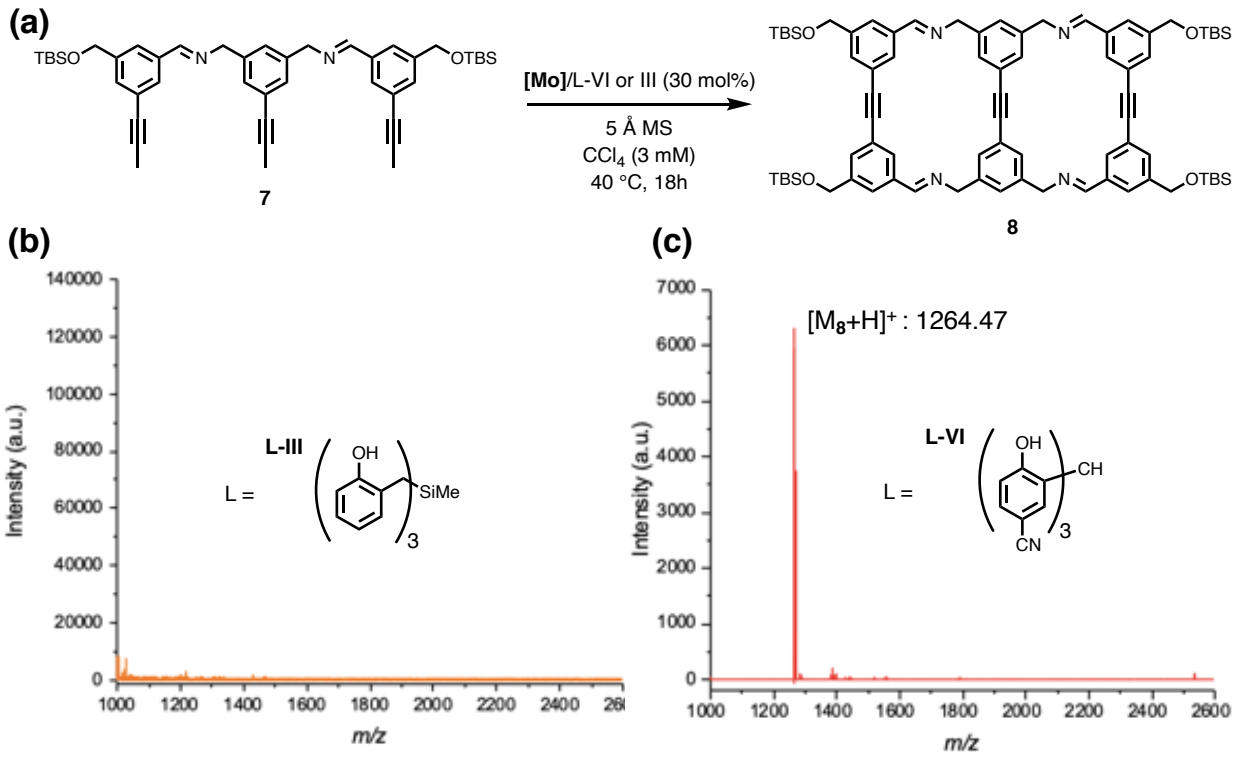

Figure 3.9. MALDI-MS analysis of the AM assembly of ladder precursor **7** using catalysts generated from **[Mo]** and either (a) L-III or (b) L-VI (positive ion mode, DCTB matrix). The mass of molecular ladder **8** is displayed for reference.

General Procedure for ODCC Assembly of Ladder 8 from Diamine 3 and Aldehyde 6

In an argon-filled glovebox, diamine 3 (2.4 mg, 14 µmol, 1 equiv) and aldehyde 6 (8.9 mg, 31 µmol, 2.2 equiv) were each dissolved in 500 µL CCl_4. The mixtures were combined in a slurry of 5 Å molecular sieves (120 mg) in CCl_4 (1 mL) and stirred overnight at 40 °C. In a separate vial, precatalyst **[Mo]** (2.8 mg, 4.2 µmol, 30 mol %) and **L-VI** (1.5 mg, 4.2 µmol, 1 equiv relative to **[Mo]**) were combined in 3.6 mL CCl_4 and stirred at 70 °C for 10 minutes in a heating block. Following catalyst activation, the mixtures were combined and stirred at 40 °C overnight. The reaction mixture was then cooled to room temperature, passed over a short silica plug with chloroform as eluent, and concentrated to dryness. The resultant oil was redissolved in 5 mL dry THF and analyzed by MALDI-MS with DCTB as a matrix.

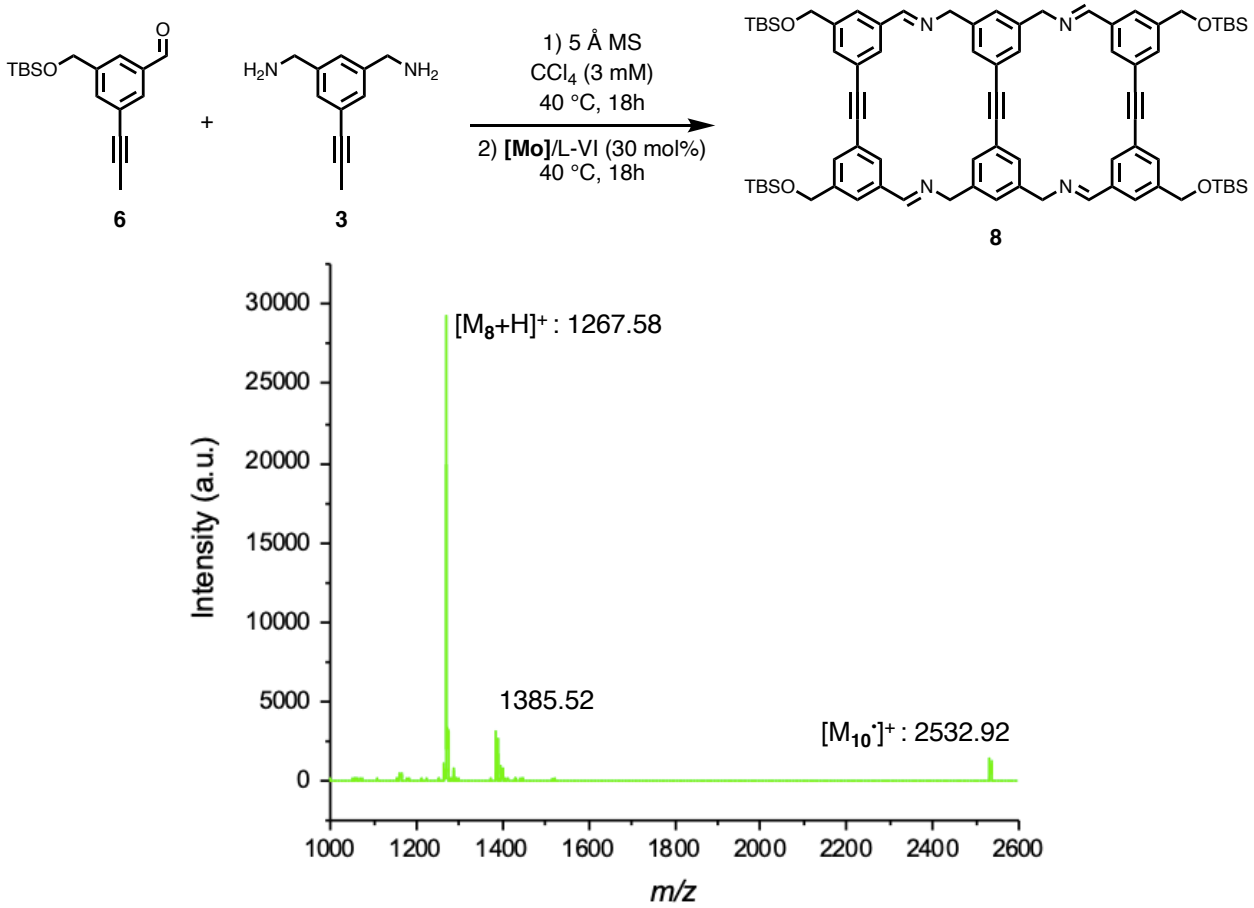

Figure 3.10. MALDI-MS analysis of the assembly of ladder **8** from diamine **3** and aldehyde **6**. Analysis revealed the presence of high molecular weight oligomer **10**, as well as an unidentified species at m/z = 1385.5.

Metathesis of 3 and 6.

In an argon-filled glovebox, diamine 6 (5.0 mg, 28 μmol, 1 equiv) and aldehyde 3 (18.3 mg, 63 μmol, 2.2 equiv) were each dissolved in 500 μL CCl_4. Meanwhile, precatalyst **[Mo]** (5.7 mg, 8.5 μmol, 30 mol%) and **L-VI** (3.1 mg, 8.5 μmol, 1 equiv relative to **[Mo]**) were combined in 8.2 mL CCl_4 and stirred at 70 °C for 10 minutes. Following catalyst activation, the solutions of 3 and 6 were added to a slurry of 5 Å molecular sieves (100 mg) in CCl_4 (200 μL), followed by the catalyst solution. The mixture was stirred at 40 °C overnight in a heating block, then allowed to cool to room temperature and filtered over a short pad of neutral alumina with chloroform as eluent. The

mixture was then concentrated, redissolved in 5 mL dry THF, and analyzed by MALDI-MS with DCTB as a matrix.

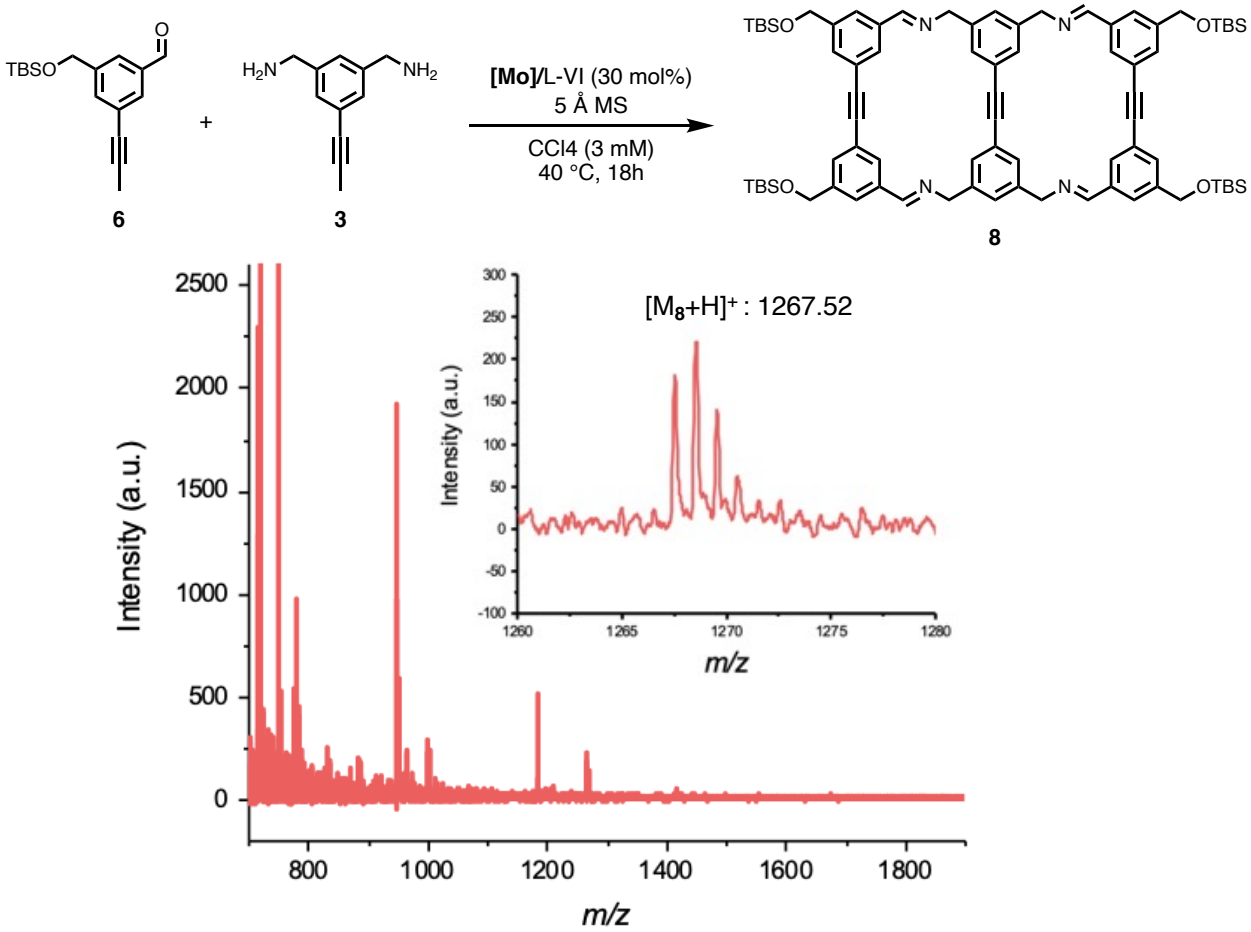

Figure 3.11. MALDI-MS analysis of the attempted ODCC assembly of ladder **8** *via* simultaneous addition of metathesis catalyst and imine-forming substrates **3** and **6**. The peak at m/z = 1268.6 indicates the presence of molecular ladder **8** in the reaction mixture.

Assembly of Ladder 8 without Molecular Sieves

The general procedures for assembly of ladder 8 from strand 7, or from precursors 3 and 6, were followed. For assembly in open air conditions, solutions of substrate and catalyst **VI** were combined, then removed from the glovebox and stirred at 40 °C in a heating block for 18h in a 20 mL reaction vial without a cap. For vacuum-driven reactions, the solutions of substrate and catalyst **VI** were combined in the glovebox, then stirred at 40 °C for 5h, during which a dynamic vacuum was applied to the mixture in 30-minute intervals. The mixture was then stirred overnight in a

heating block inside the glovebox at 40 °C. Reaction mixtures were then filtered over plugs of neutral alumina and concentrated. The resulting oily residues were redissolved in 5 mL dry THF and analyzed by SEC and MALDI-MS.

Assembly of Ladder 8 in the Presence of $Sc(OTf)_3$

The general procedures for assembly of ladder 8 from strand 7, or from precursors 3 and 6, were followed. When solutions of substrate and catalyst were combined, a solution of $Sc(OTf)_3$ (2.8 mg, 5.6 µmol, 40 mol%) in 0.4 mL CCl_4 was also added to the mixture. Following analysis by MALDI-MS and SEC, the residue obtained from reaction of 7 (8 mg) was redissolved in CCl_4 (1 mL) and subjected to the general procedure for the synthesis of ladder 8. After stirring for 18h in a heating block, the mixture was filtered over a pad of neutral alumina, concentrated, and redissolved in THF. The solutions were then analyzed by SEC and MALDI-MS.

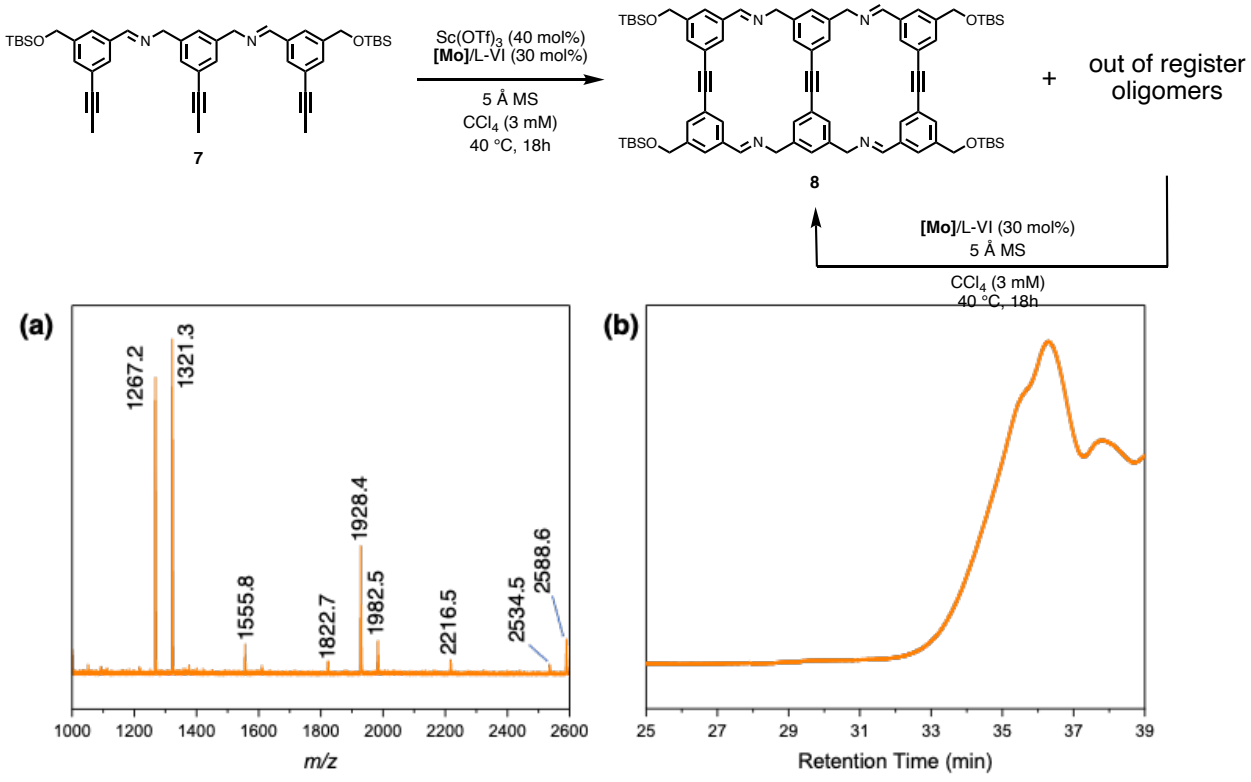

Figure 3.12. Characterization of the metathesis reaction of **7** in the presence of $Sc(OTf)_3$. (a) Normalized MALDI-MS of the initial reaction mixture. The masses of major peaks are indicated.

Figure 3.12 (cont) (b) SEC chromatogram of the initial reaction mixture. The broad shoulder at shorter elution time is attributed to the oligomers of **7** observed by MALDI.

General Procedure for Ladder Disassembly Experiments

Following the general procedure for ODCC assembly of molecular ladder 8, a 100 µL aliquot of the reaction mixture was taken, filtered through a short pad of neutral alumina, concentrated to dryness, and analyzed by ^{1}H NMR. The remaining reaction mixture was charged with methylamine (840 µL of a 2 M solution in THF, 30 equiv relative to 3 or 7) and stirred overnight at room temperature. The mixture was then filtered over neutral alumina and solvent and excess methylamine were removed in vacuo. The mixture was then redissolved in 750 µL $CDCl_3$ and analyzed by ^{1}H NMR.

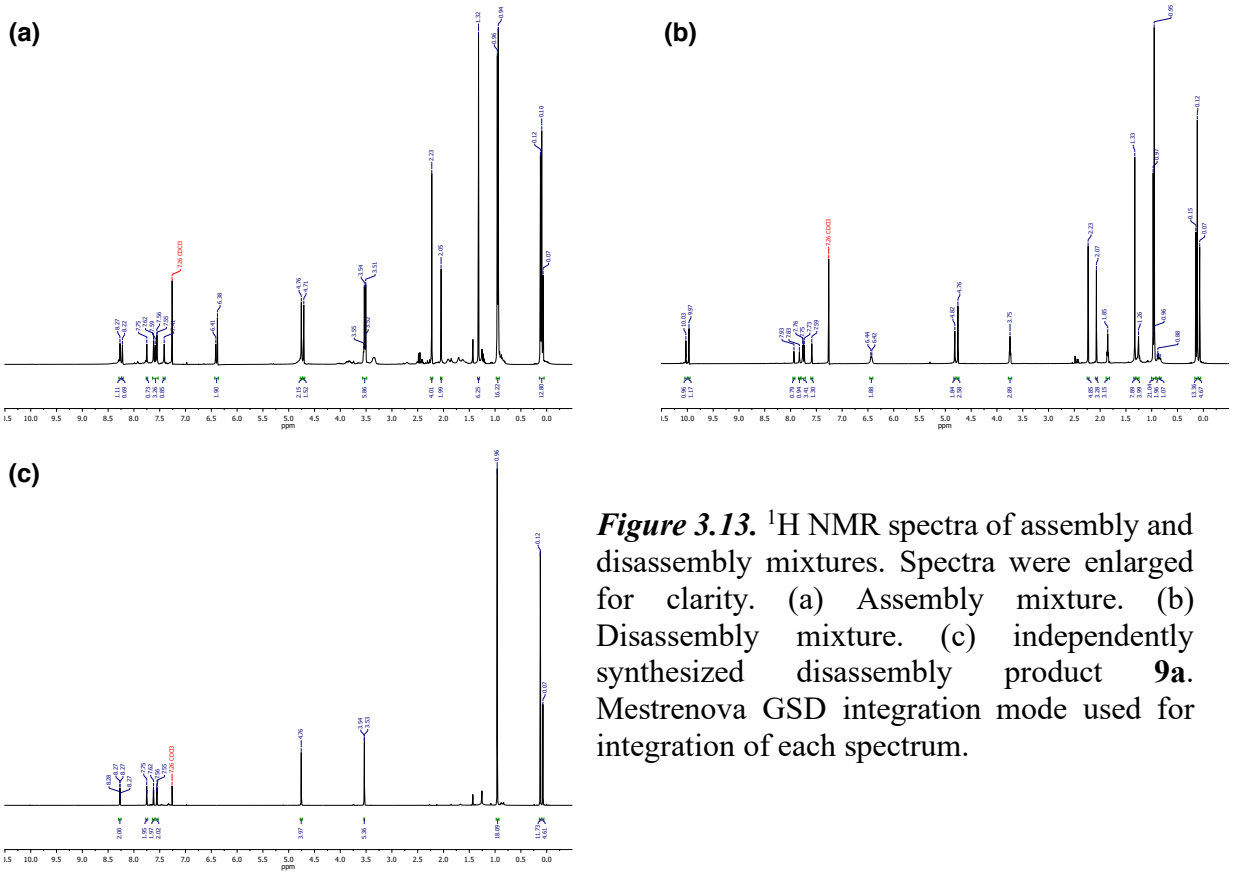

Figure 3.13. ^{1}H NMR spectra of assembly and disassembly mixtures. Spectra were enlarged for clarity. (a) Assembly mixture. (b) Disassembly mixture. (c) independently synthesized disassembly product **9a**. Mestrenova GSD integration mode used for integration of each spectrum.

3.4.3 NMR Spectra

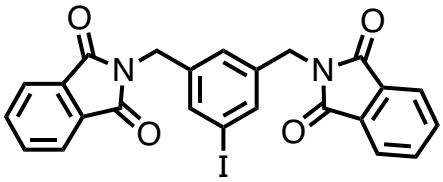

1

(^{1}H NMR, $CDCl_3$, 500 MHz)

1

(^{13}C{^{1}H} NMR, $CDCl_3$, 126 MHz)

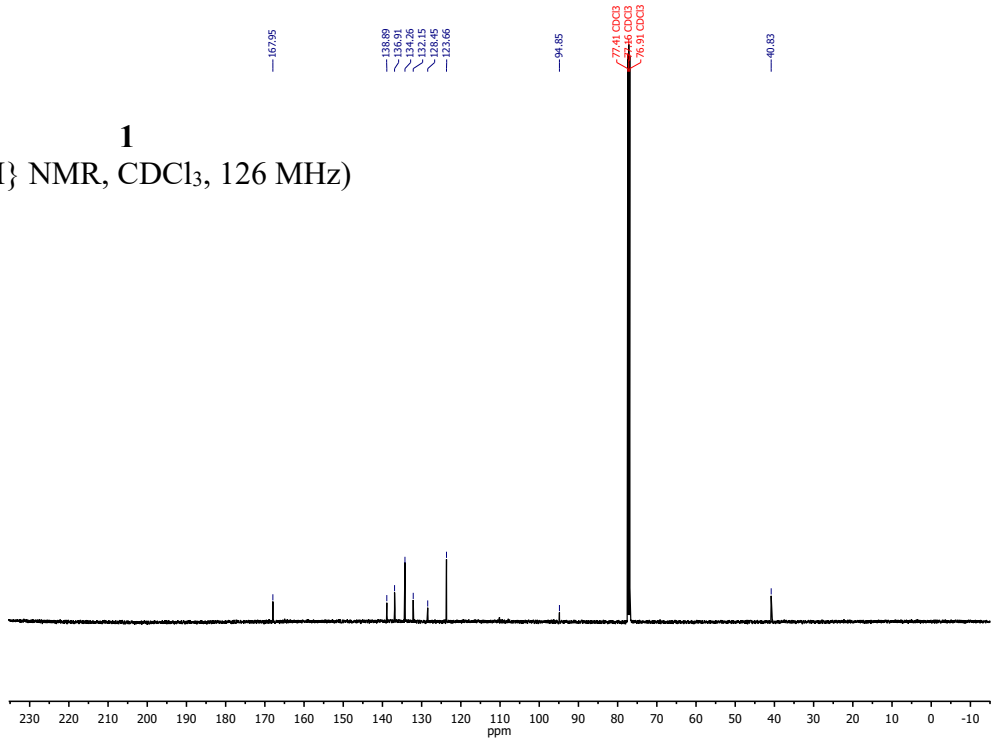

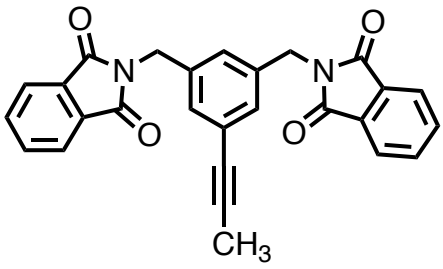

2

(^{1}H NMR, $CDCl_3$, 500 MHz)

2

(^{13}C{^{1}H} NMR, $CDCl_3$, 126 MHz)

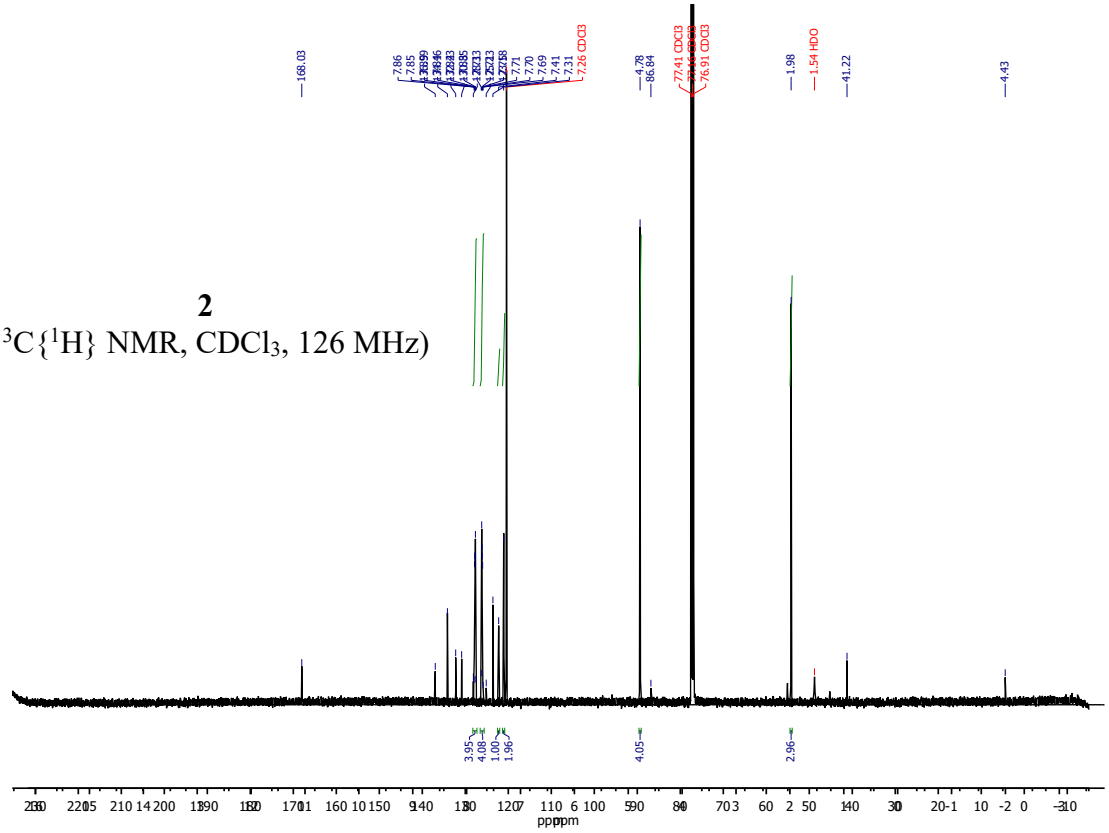

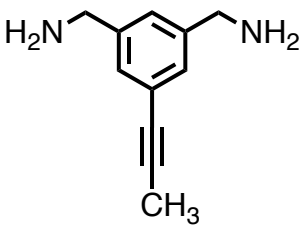

3

(^{1}H NMR, $CDCl_3$, 500 MHz)

3

(^{13}C{^{1}H} NMR, $CDCl_3$, 126 MHz)

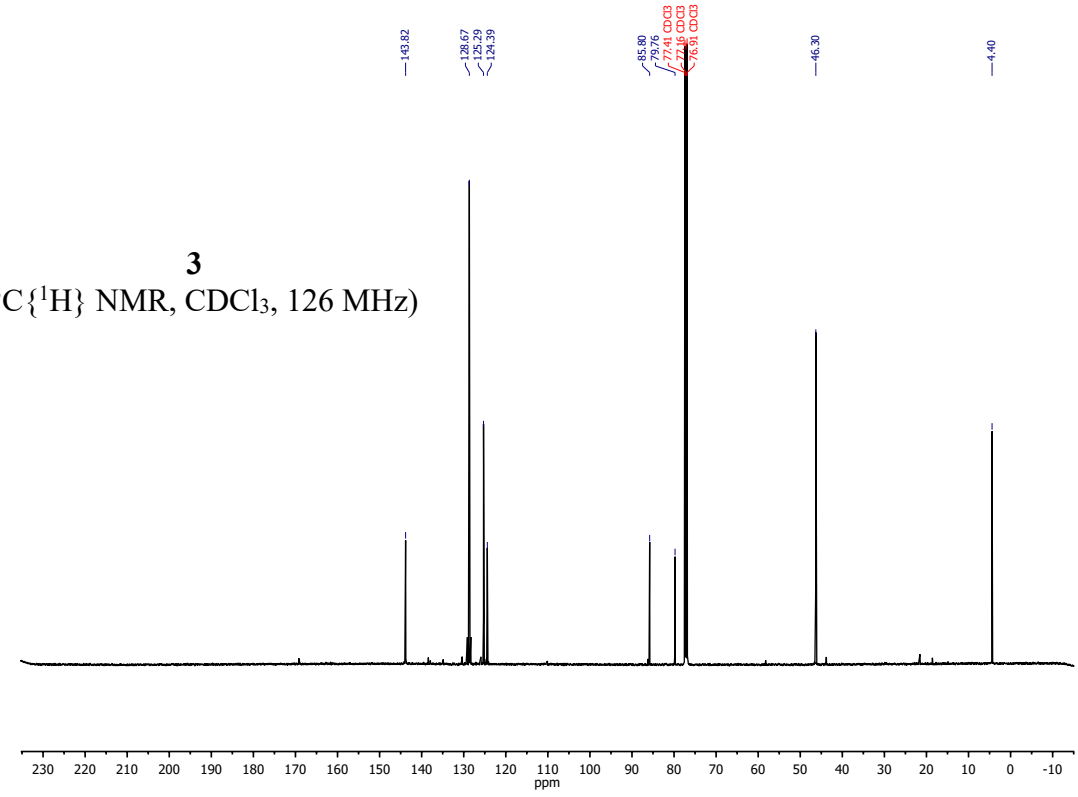

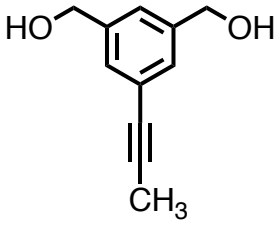

4

(^{1}H NMR, Acetone-*d*$_6$, 500 MHz)

4

(^{13}C{^{1}H} NMR, Acetone-*d*$_6$, 126 MHz)

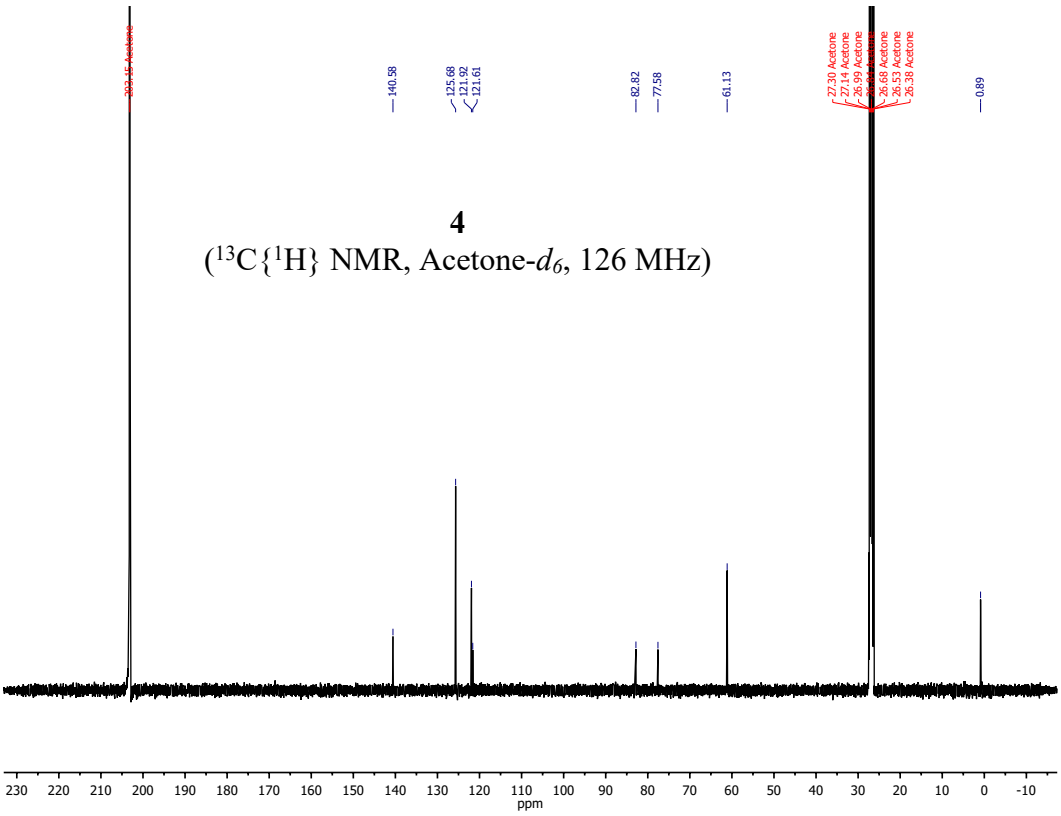

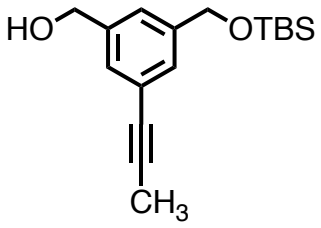

5

(^{1}H NMR, $CDCl_3$, 500 MHz)

5

(^{13}C{^{1}H} NMR, $CDCl_3$, 126 MHz)

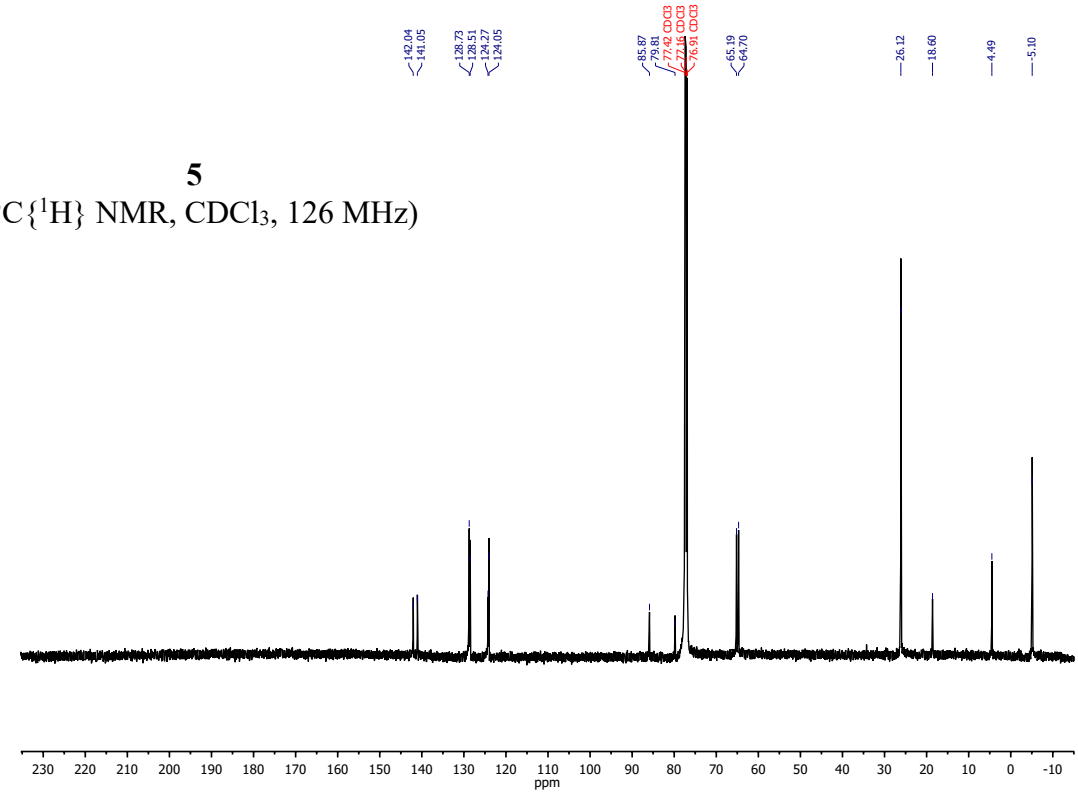

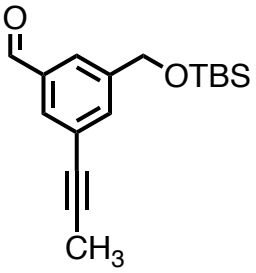

6

(^{1}H NMR, $CDCl_3$, 500 MHz)

6

(^{13}C{^{1}H} NMR, $CDCl_3$, 126 MHz)

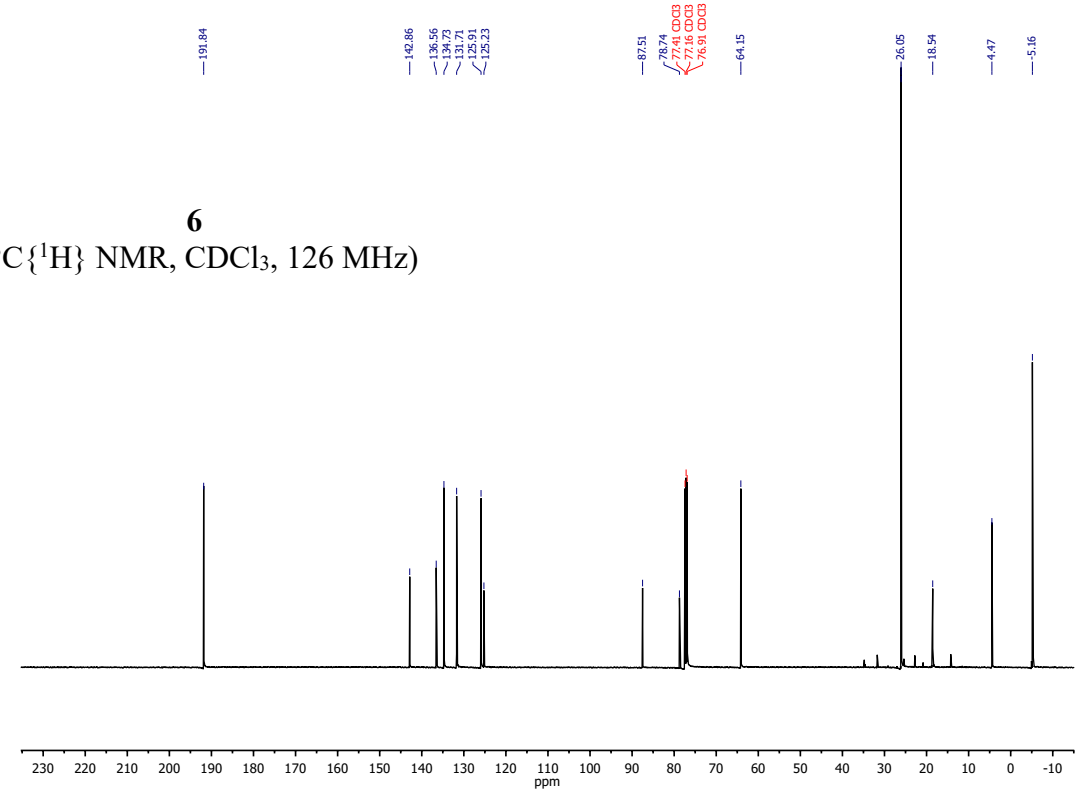

7

(^{1}H NMR, $CDCl_3$, 500 MHz)

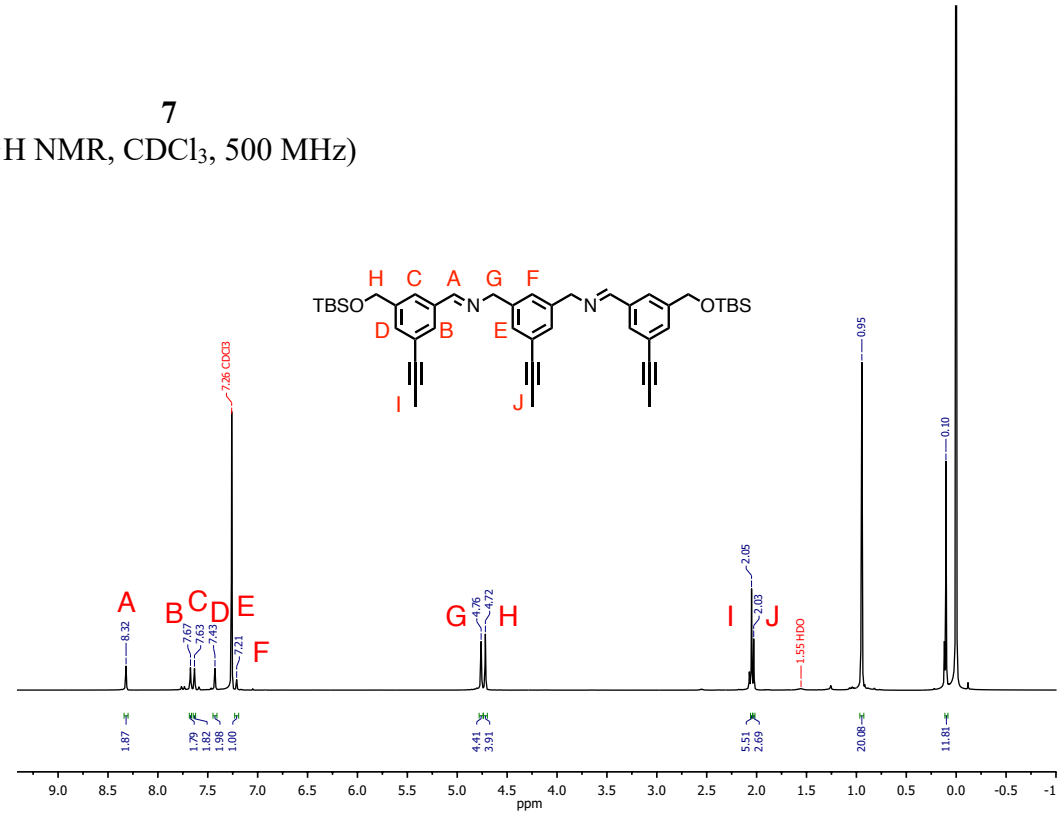

7

(^{13}C{^{1}H} NMR, $CDCl_3$, 126 MHz)

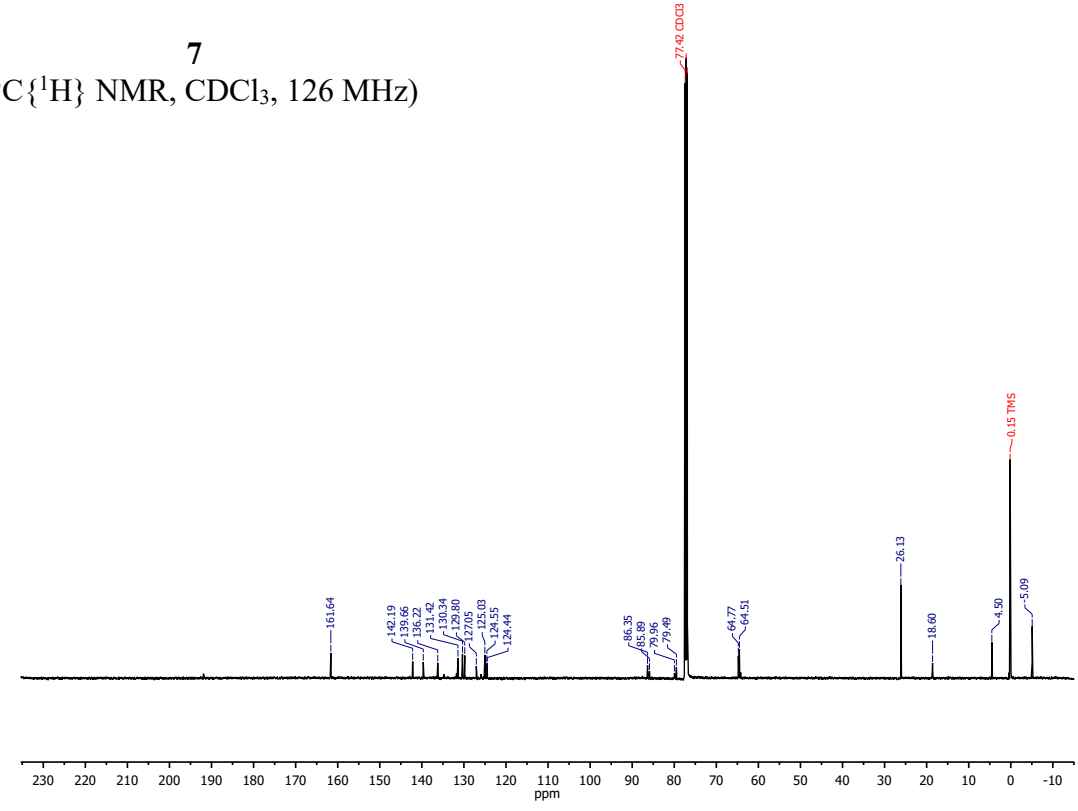

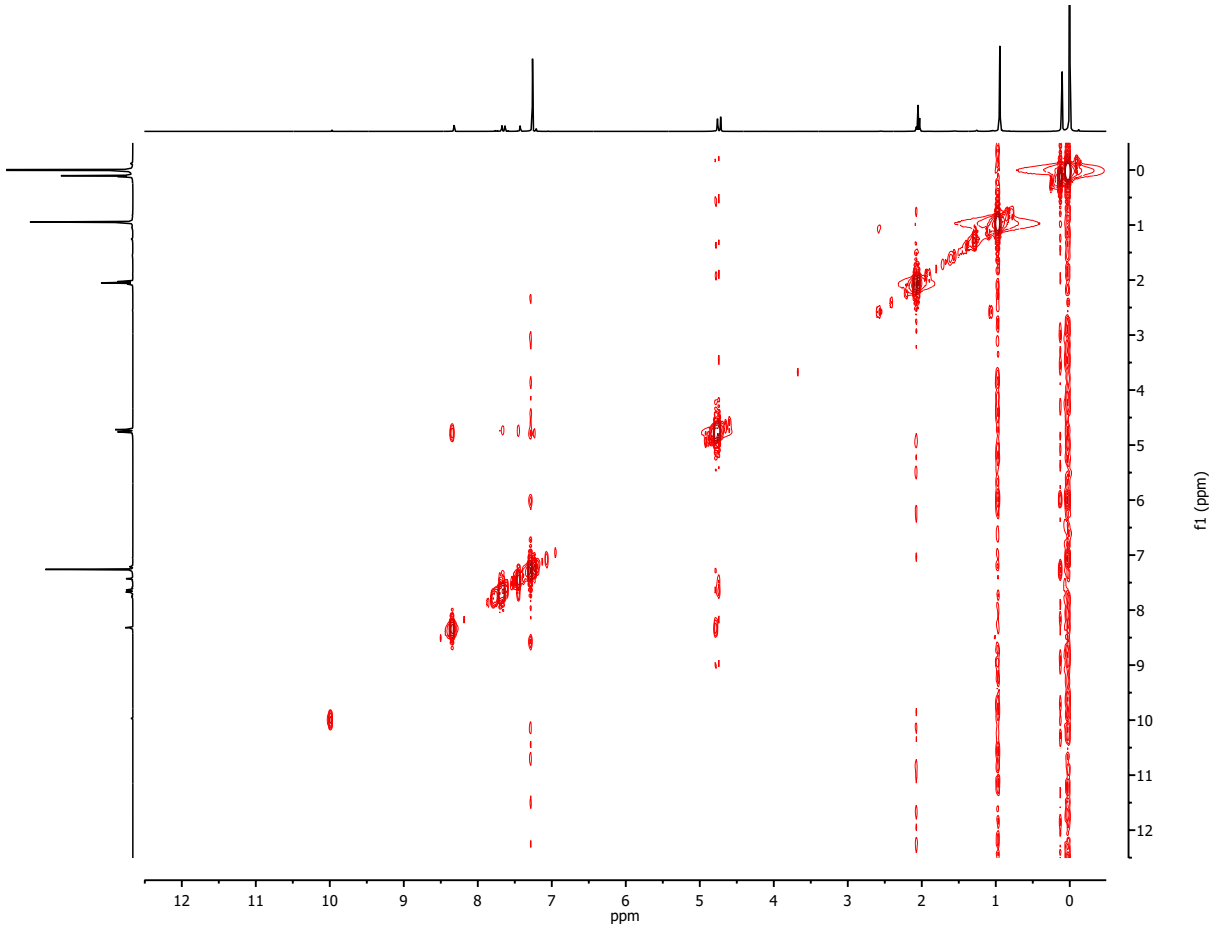

^{1}H-^{1}H COSY spectrum of ladder precursor **7** (500 MHz, $CDCl_3$).

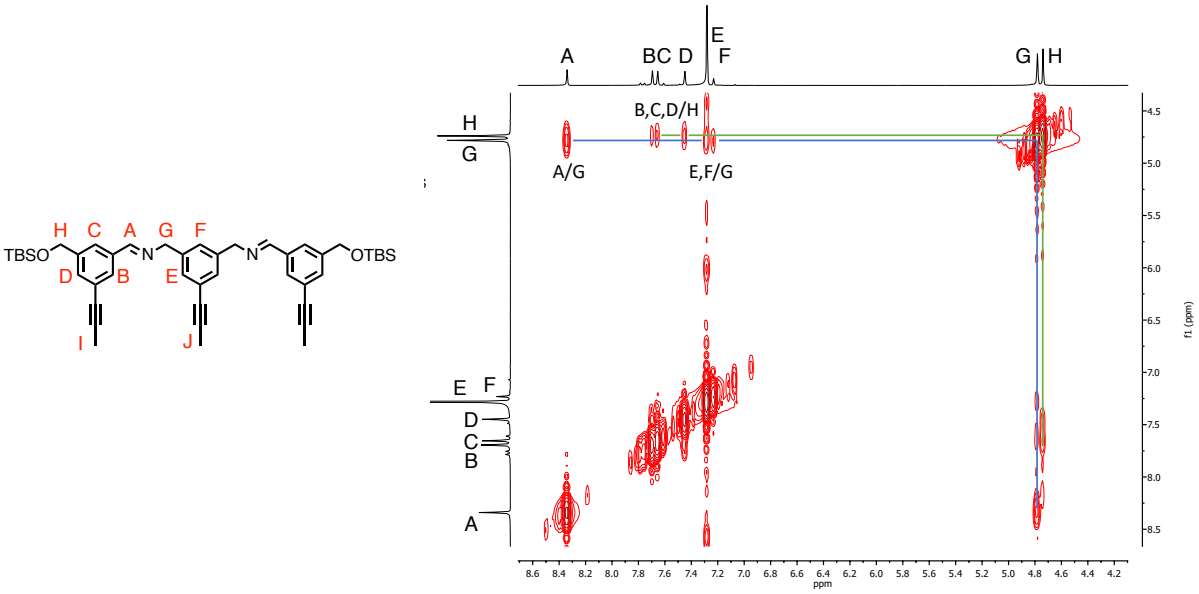

Aromatic and benzylic region of the ^{1}H-^{1}H COSY spectrum of ladder precursor **7** (500 MHz, $CDCl_3$). Correlations used for structural assignment are highlighted.

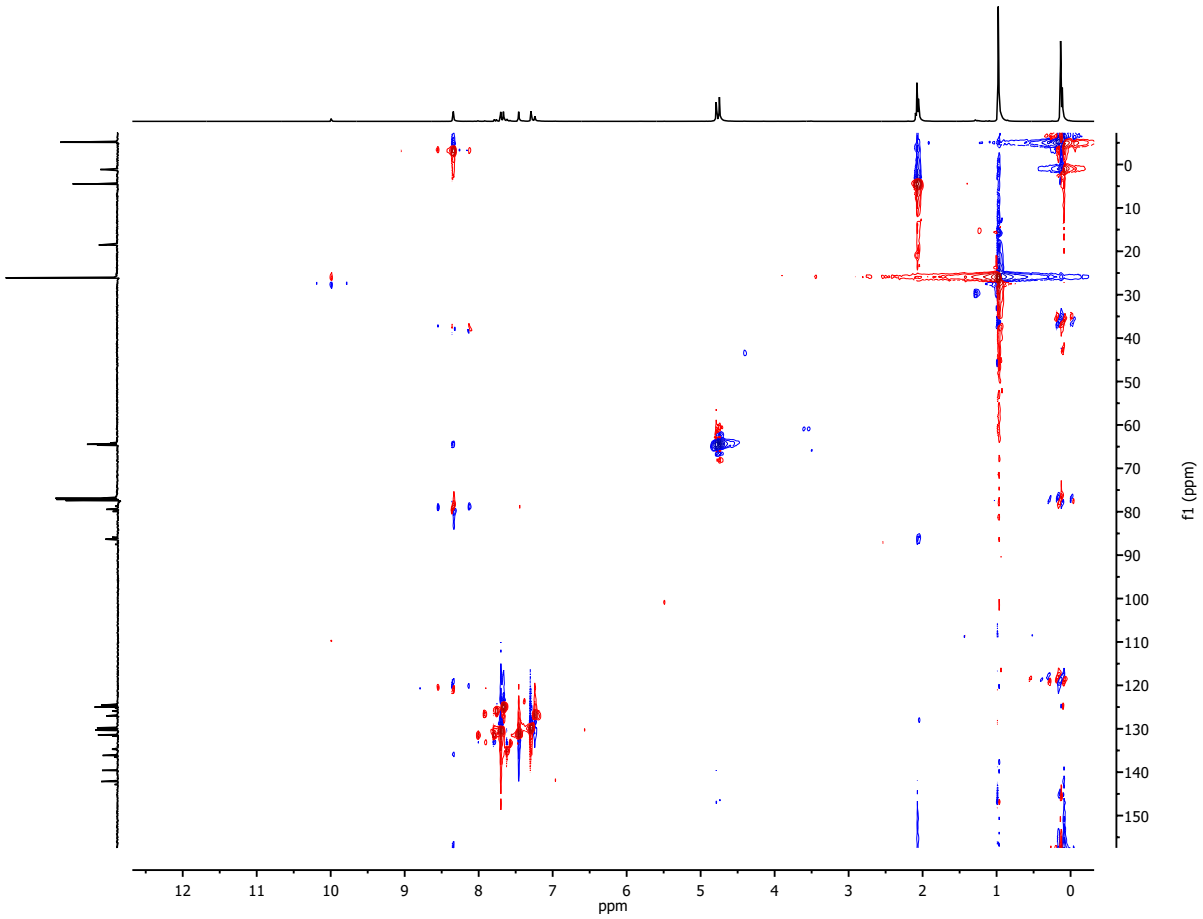

^{1}H-^{13}C HSQC spectrum of ladder precursor **7** (500 MHz, $CDCl_3$).

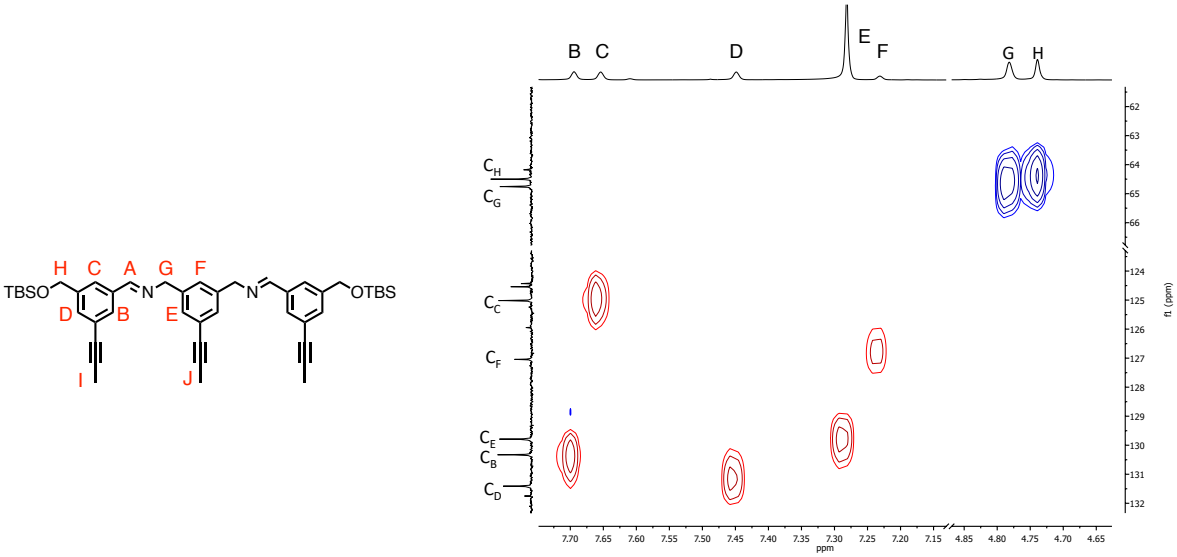

Aromatic and benzylic region of the ^{1}H-^{13}C HSQC spectrum of ladder precursor **7** (500 MHz, $CDCl_3$).

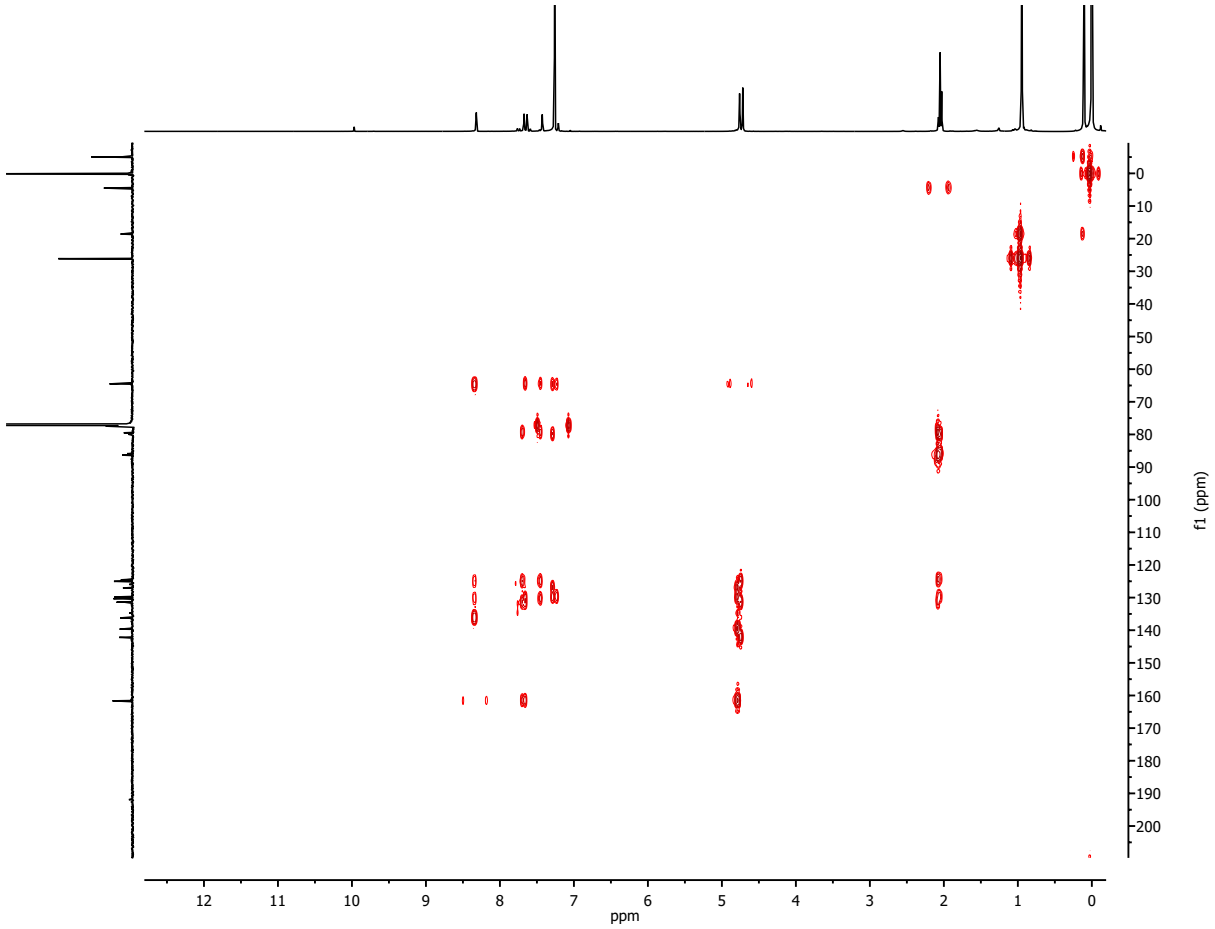

^{1}H-^{13}C HMBC spectrum of ladder precursor **7** (500 MHz, $CDCl_3$).

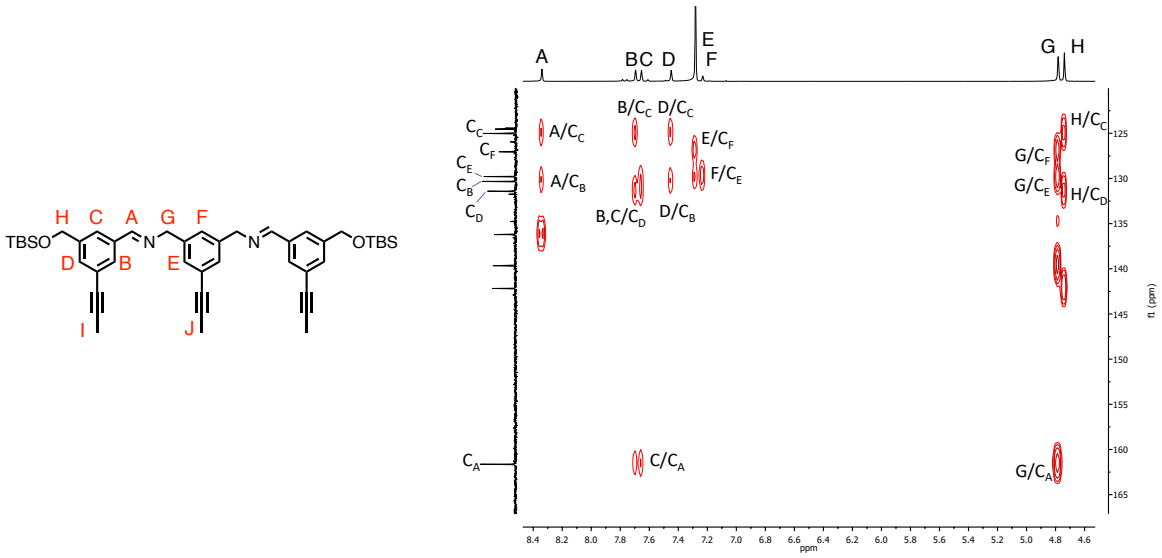

Aromatic and benzylic region of the ^{1}H-^{13}C HMBC spectrum of ladder precursor **7** (500 MHz, $CDCl_3$). Correlations used for structural assignment are highlighted.

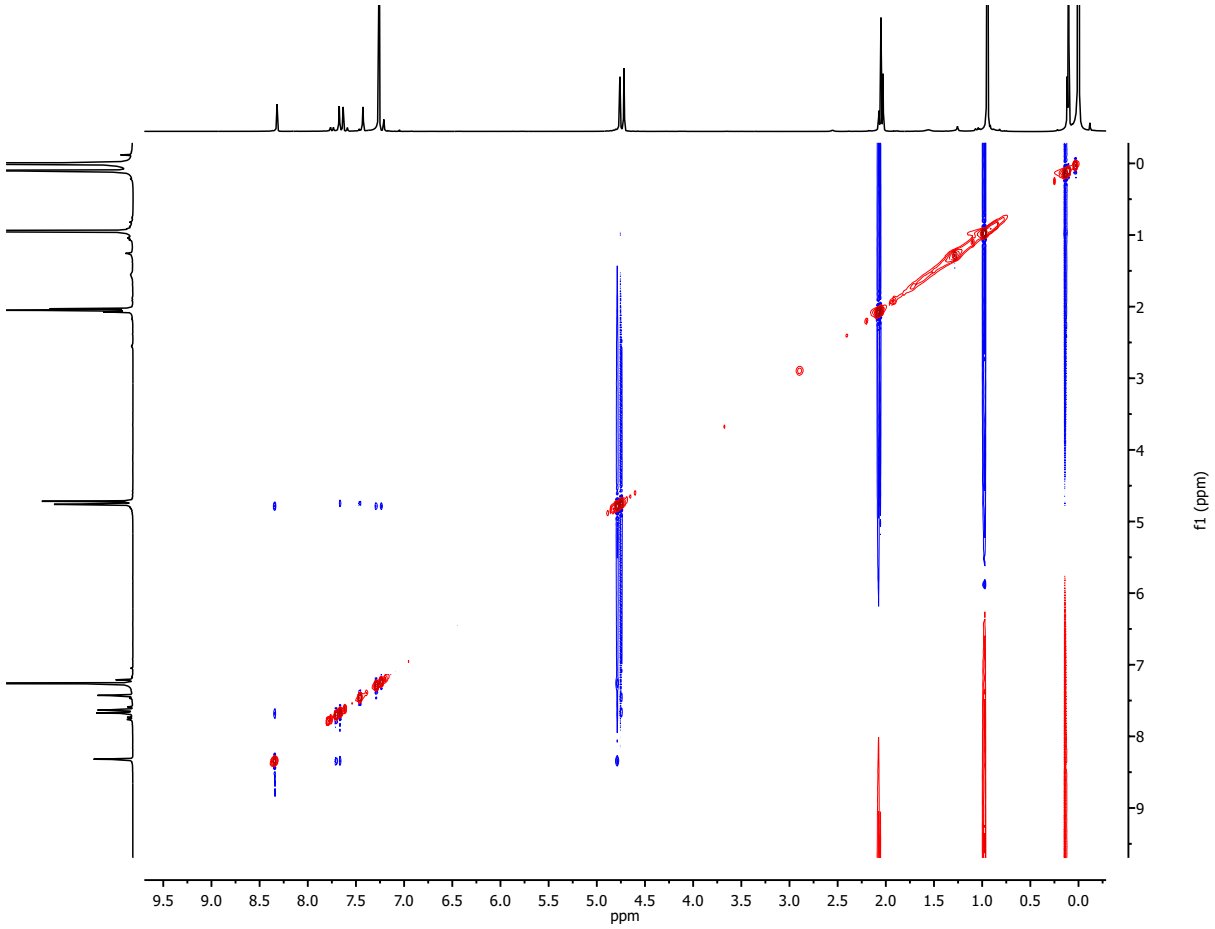

^{1}H-^{1}H NOESY spectrum of ladder precursor **7** (500 MHz, $CDCl_3$).

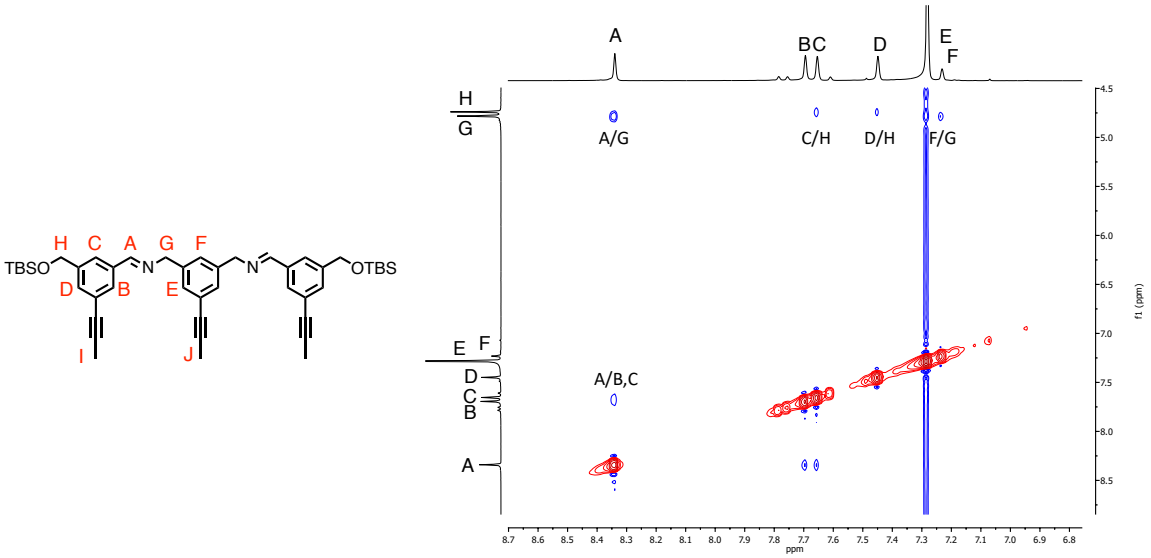

Aromatic and benzylic region of the ^{1}H-^{1}H NOESY spectrum of ladder precursor **7** (500 MHz, $CDCl_3$). Selected correlations used for structural assignment are highlighted.

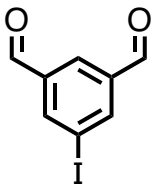

S1

(^{1}H NMR, $CDCl_3$, 500 MHz)

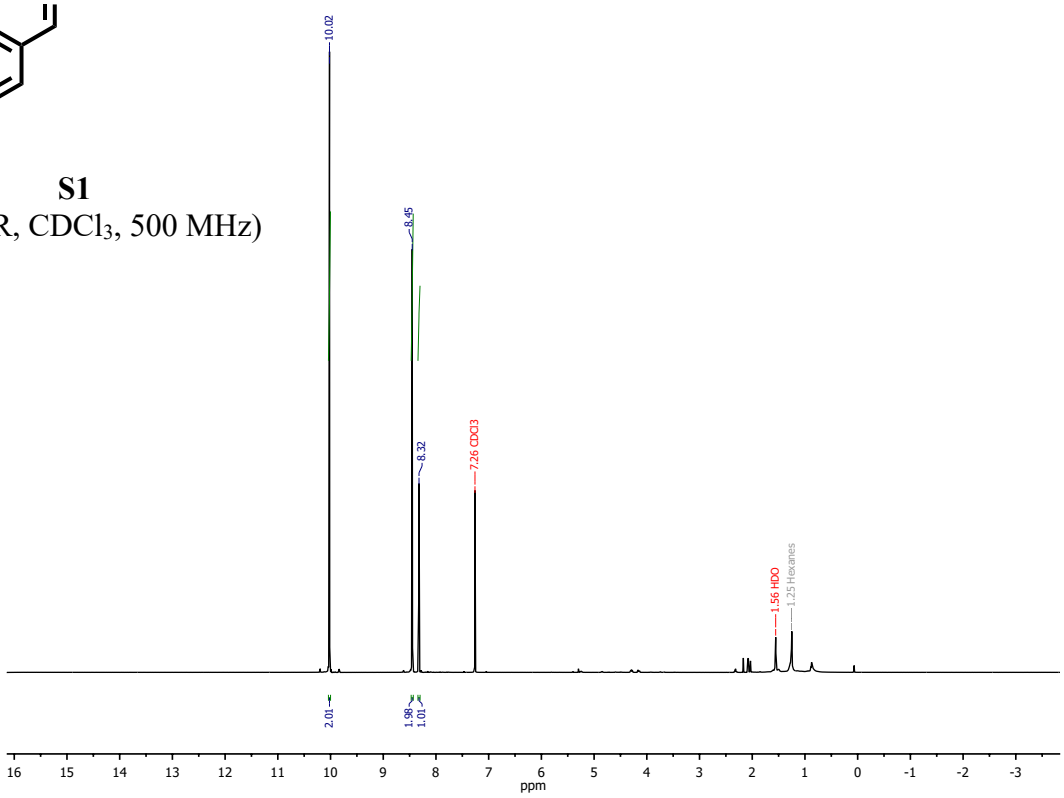

S1

(^{13}C{^{1}H} NMR, $CDCl_3$, 126 MHz)

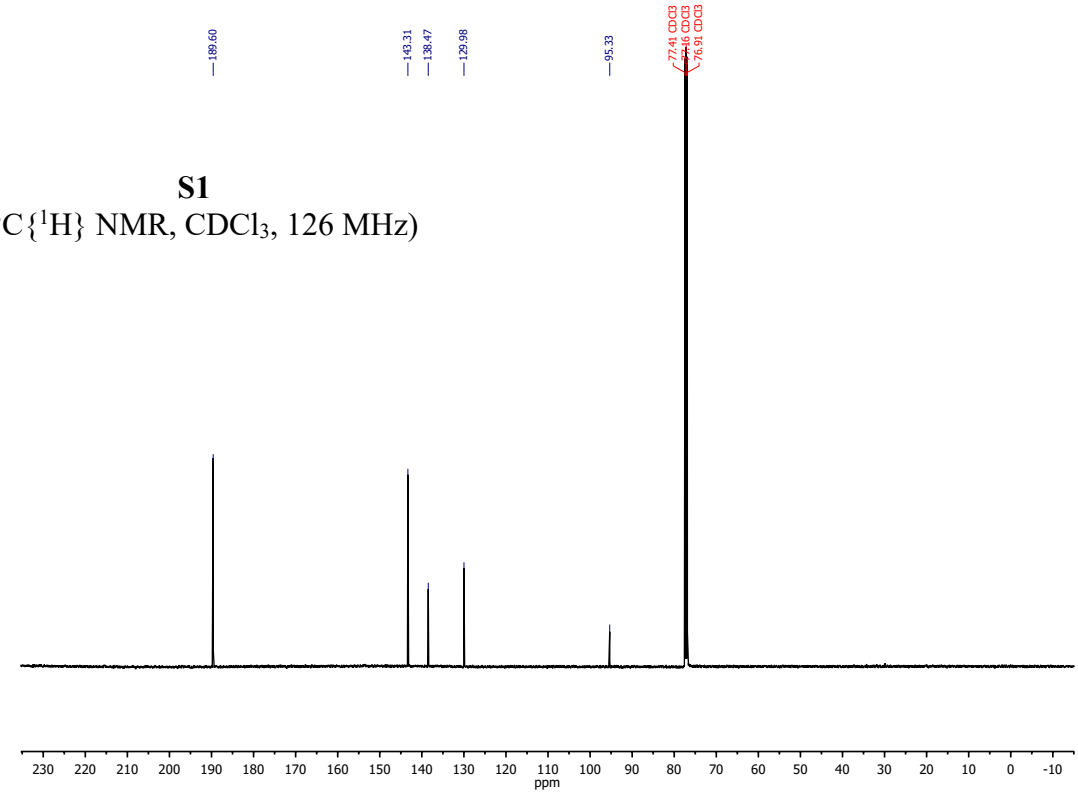

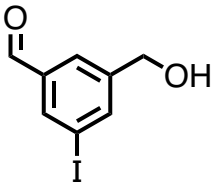

S2
(^{1}H NMR, $CDCl_3$, 500 MHz)

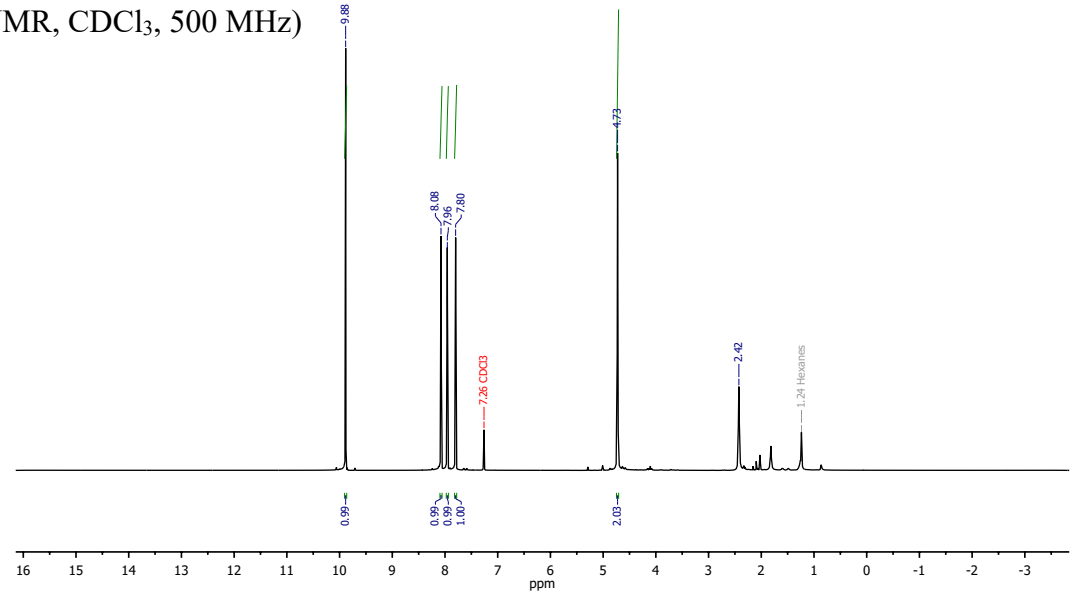

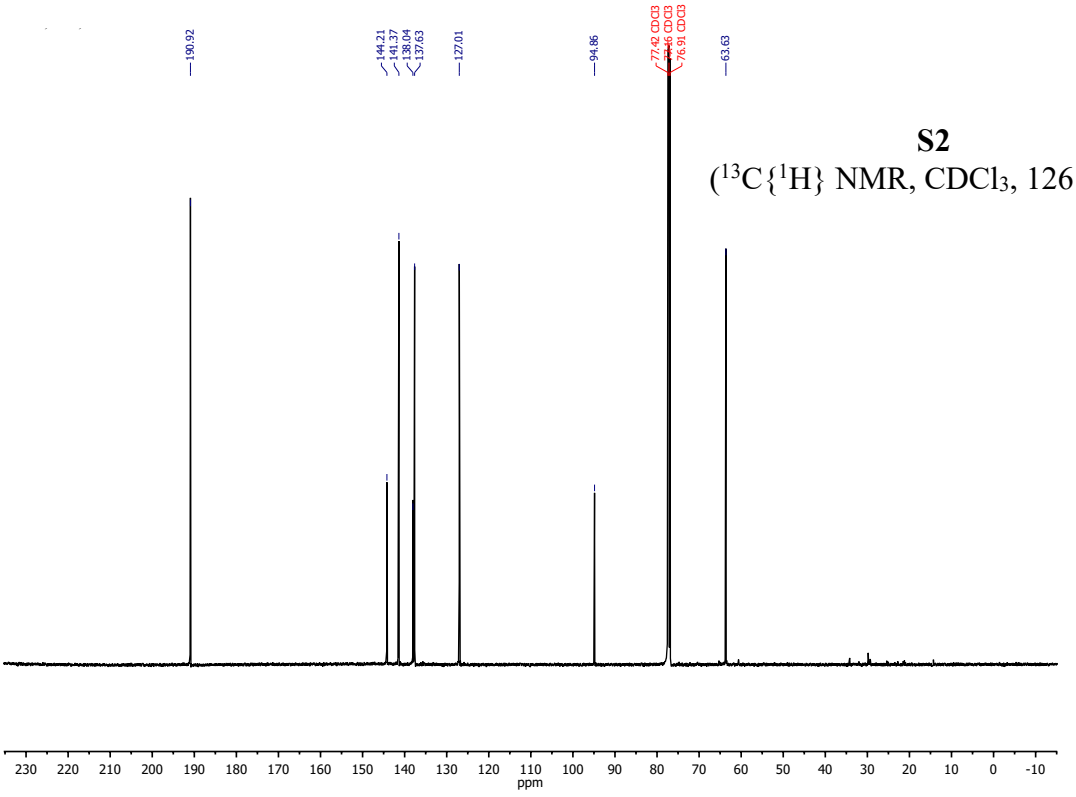

S2
(^{13}C{^{1}H} NMR, $CDCl_3$, 126 MHz)

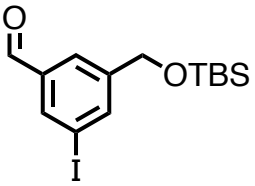

S3

(^{1}H NMR, $CDCl_3$, 500 MHz)

S3

(^{13}C{^{1}H} NMR, $CDCl_3$, 126 MHz)

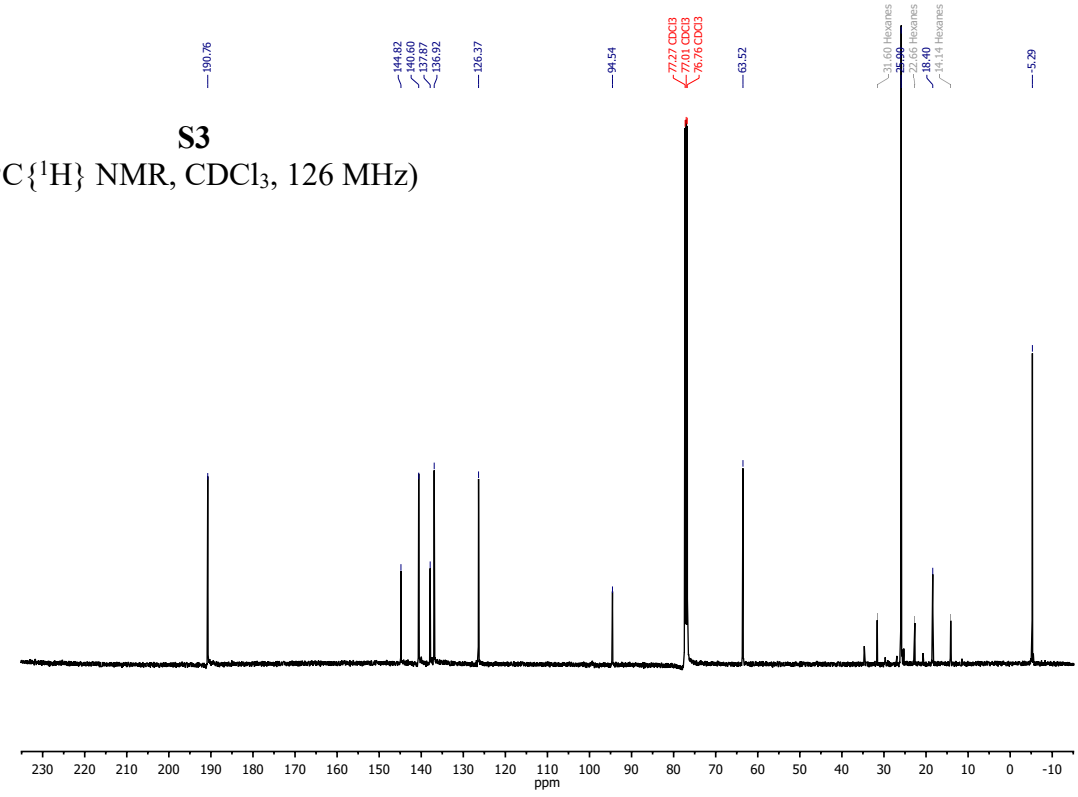

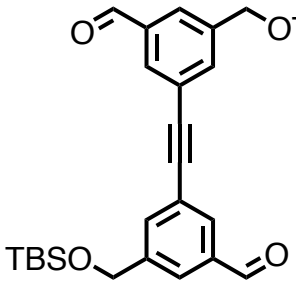

S4

(^{1}H NMR, $CDCl_3$, 500 MHz)

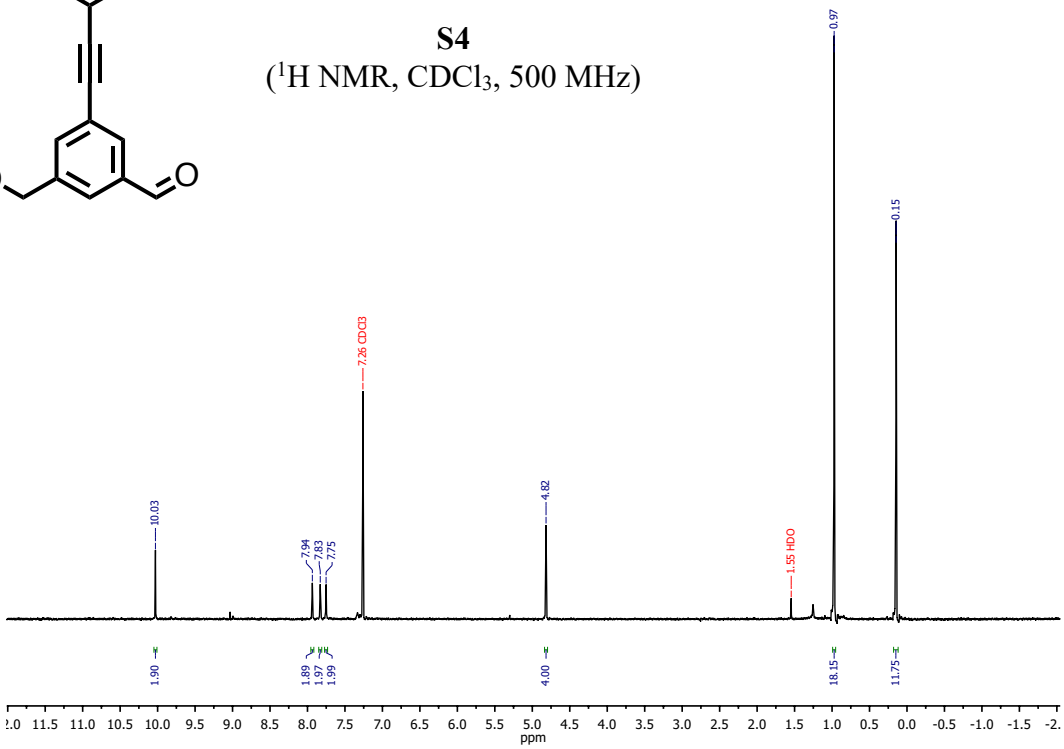

S4

(^{13}C{^{1}H} NMR, $CDCl_3$, 126 MHz)

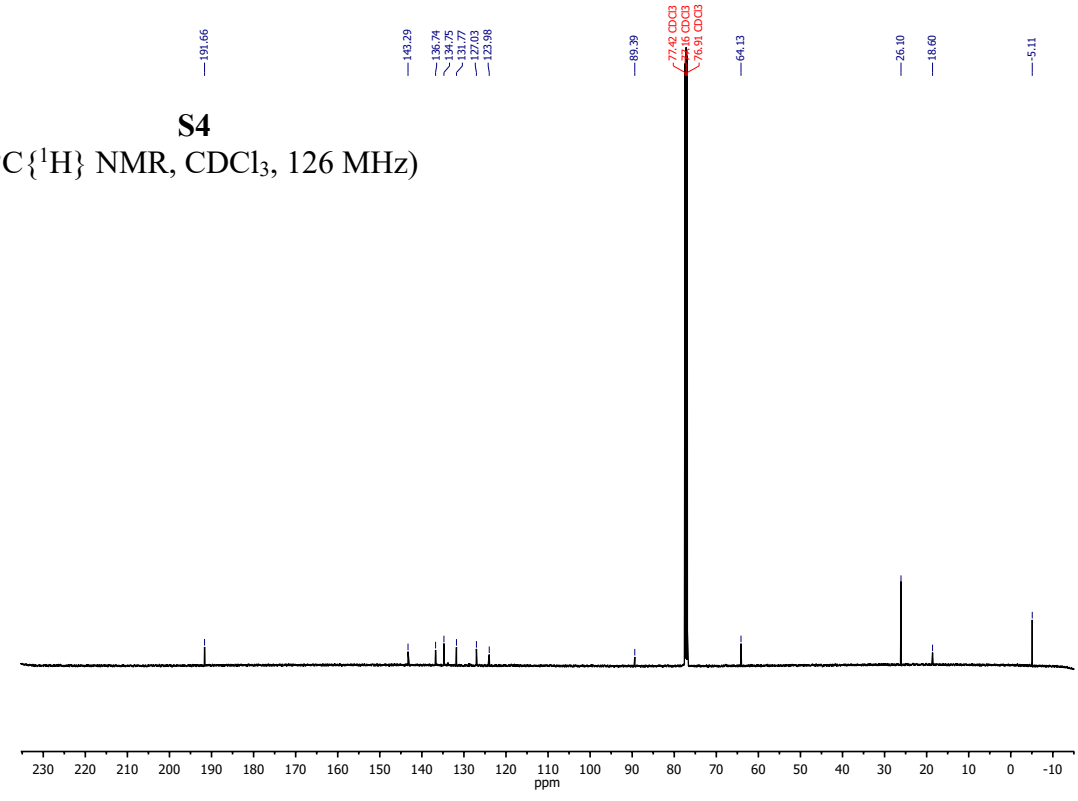

9a

(^{1}H NMR, $CDCl_3$, 500 MHz)

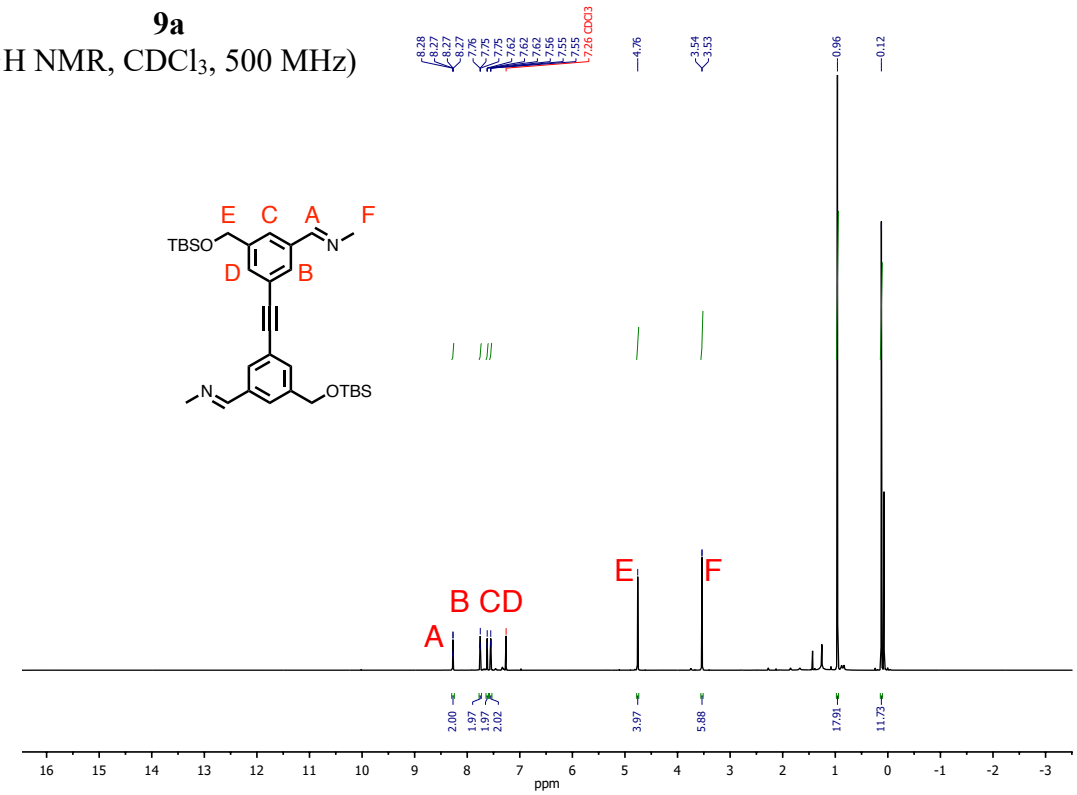

9a

(^{13}C{^{1}H} NMR, $CDCl_3$, 126 MHz)

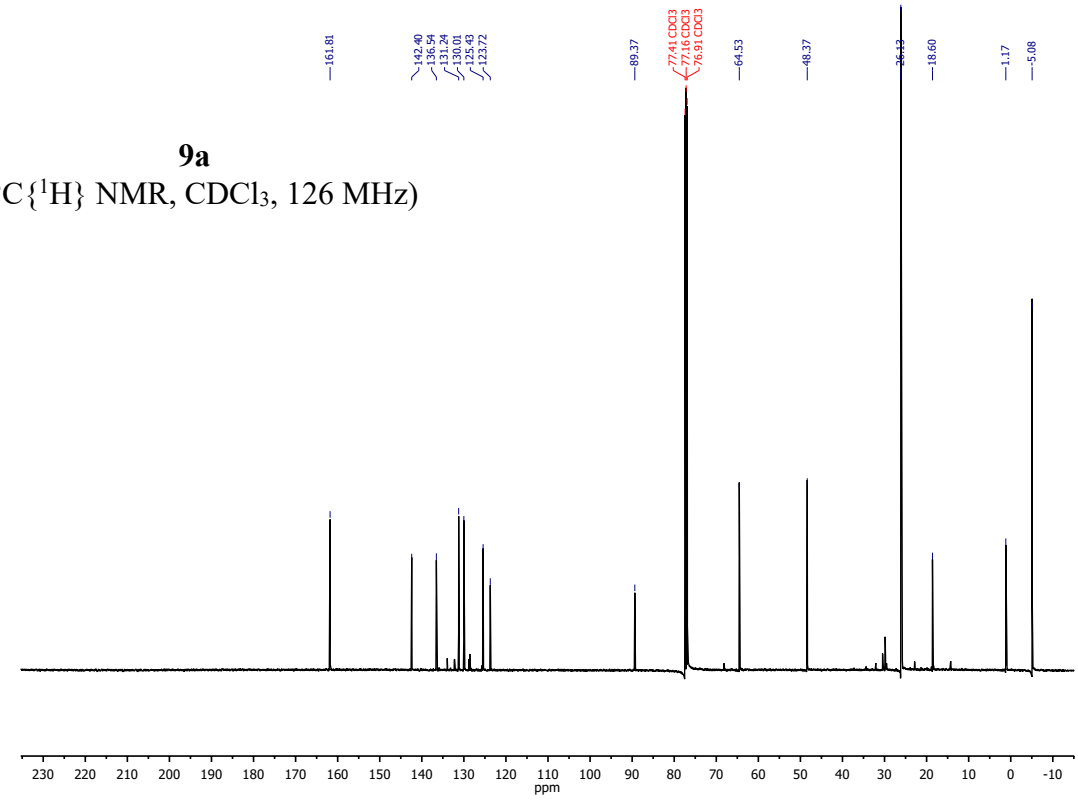

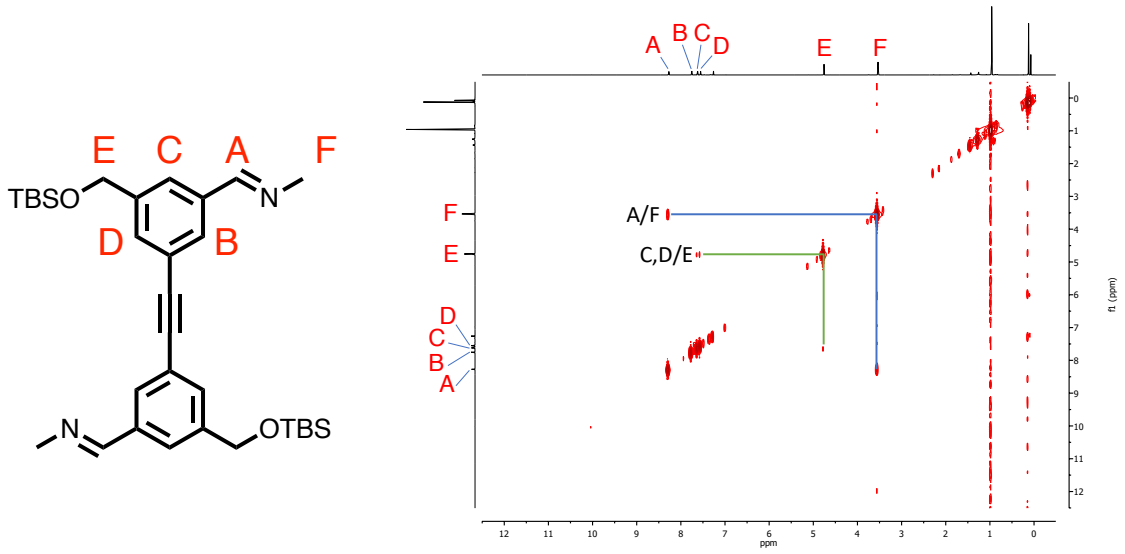

^{1}H-^{1}H COSY spectrum of disassembly product **9a** (500 MHz, $CDCl_3$). Cross-peaks used for structural assignment are highlighted.

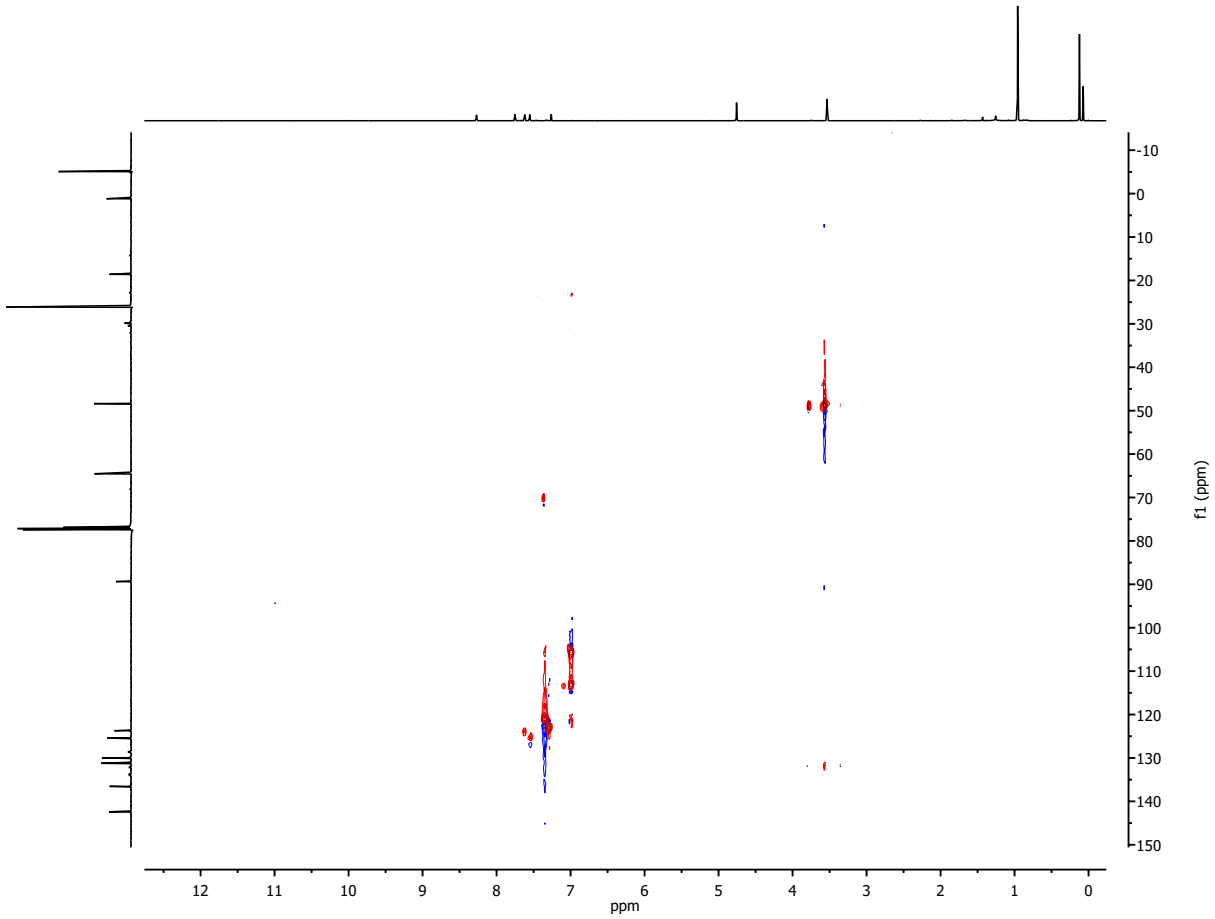

^{1}H-^{13}C HSQC spectrum of disassembly product **9a** (500 MHz, $CDCl_3$).

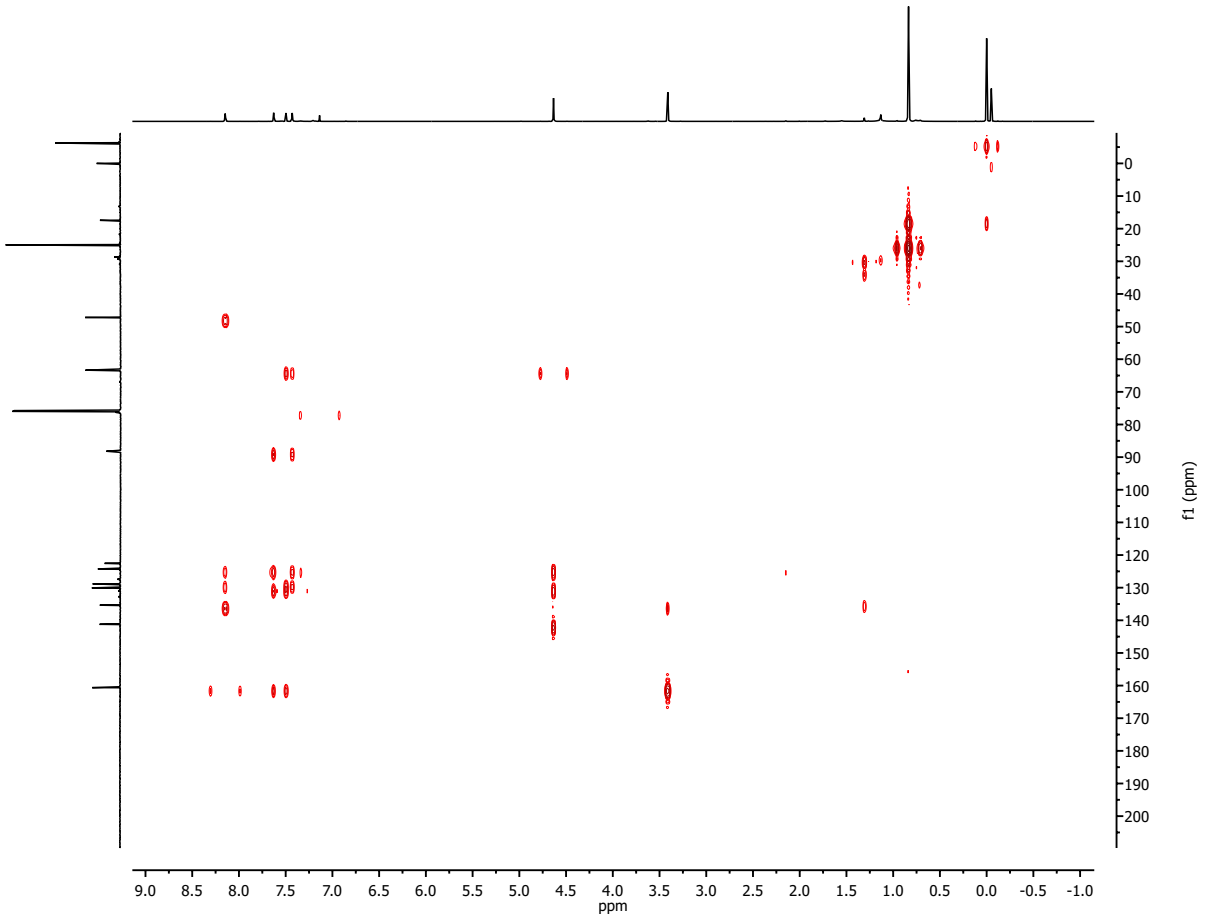

^{1}H–^{13}C HMBC spectrum of disassembly product **9a** (500 MHz, $CDCl_3$).

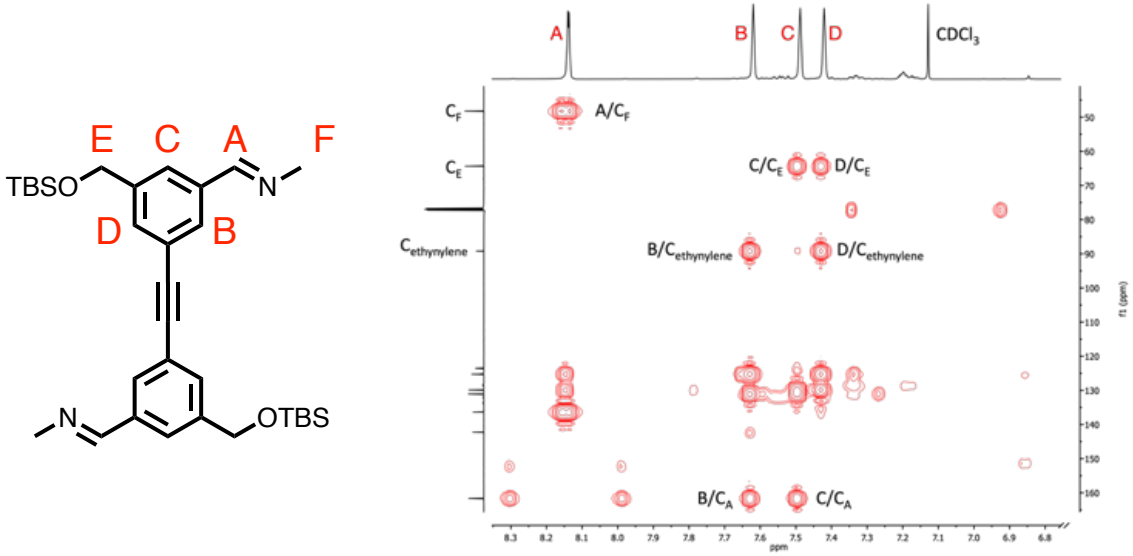

Aromatic and benzylic region of the ^{1}H–^{13}C HMBC spectrum of disassembly product **9a**. Correlations used for structural assignments are highlighted.

3.5 References

(1) Okochi, K. D.; Han, G. S.; Aldridge, I. M.; Liu, Y.; Zhang, W. Covalent Assembly of Heterosequenced Macrocycles and Molecular Cages through Orthogonal Dynamic Covalent Chemistry (ODCC). *Org. Lett.* **2013**, *15* (17), 4296–4299.

(2) Okochi, K. D.; Jin, Y.; Zhang, W. Highly Efficient One-Pot Synthesis of Hetero-Sequenced Shape-Persistent Macrocycles through Orthogonal Dynamic Covalent Chemistry (ODCC). *Chem. Commun.* **2013**, *49* (39), 4418–4420.

(3) Hillenbrand, J.; Leutzsch, M.; Yiannakas, E.; Gordon, C. P.; Wille, C.; Nöthling, N.; Copéret, C.; Fürstner, A. "Canopy Catalysts" for Alkyne Metathesis: Molybdenum Alkylidyne Complexes with a Tripodal Ligand Framework. *J. Am. Chem. Soc.* **2020**, *142* (25), 11279–11294.

(4) Thompson, R. R.; Rotella, M. E.; Du, P.; Zhou, X.; Fronczek, F. R.; Kumar, R.; Gutierrez, O.; Lee, S. Siloxide Podand Ligand as a Scaffold for Molybdenum-Catalyzed Alkyne Metathesis and Isolation of a Dynamic Metallatetrahedrane Intermediate. *Organometallics* **2019**, *38* (21), 4054–4059.

(5) Du, Y.; Yang, H.; Zhu, C.; Ortiz, M.; Okochi, K. D.; Shoemaker, R.; Jin, Y.; Zhang, W. Highly Active Multidentate Ligand-Based Alkyne Metathesis Catalysts. *Chem. - A Eur. J.* **2016**, *22* (23), 7959–7963.

(6) Ge, Y.; Huang, S.; Hu, Y.; Zhang, L.; He, L.; Krajewski, S.; Ortiz, M.; Jin, Y.; Zhang, W. Highly Active Alkyne Metathesis Catalysts Operating under Open Air Condition. *Nat. Commun.* **2021**, *12* (1), 1136.

(7) Jyothish, K.; Zhang, W. Introducing A Podand Motif to Alkyne Metathesis Catalyst Design: A Highly Active Multidentate Molybdenum(VI) Catalyst That Resists Alkyne

Polymerization. *Angew. Chemie Int. Ed.* **2011**, *50* (15), 3435–3438.

(8) Yang, H.; Liu, Z.; Zhang, W. Multidentate Triphenolsilane-Based Alkyne Metathesis Catalysts. *Adv. Synth. Catal.* **2013**, *355* (5), 885–890.

(9) Jyothish, K.; Zhang, W. Towards Highly Active and Robust Alkyne Metathesis Catalysts: Recent Developments in Catalyst Design. *Angew. Chemie Int. Ed.* **2011**, *50* (37), 8478–8480.

(10) Pattillo, C. C.; Moore, J. S. A Tetrahedral Molecular Cage with a Responsive Vertex. *Chem. Sci.* **2019**, *10* (29), 7043–7048.

(11) Anfinsen, C. B. Principles That Govern the Folding of Protein Chains. *Science (80-.).* **1973**, *181* (4096), 223–230.

(12) Bartolec, B.; Altay, M.; Otto, S. Template-Promoted Self-Replication in Dynamic Combinatorial Libraries Made from a Simple Building Block. *Chem. Commun.* **2018**, *54* (93), 13096–13098.

(13) Nowak, P.; Colomb-Delsuc, M.; Otto, S.; Li, J. Template-Triggered Emergence of a Self-Replicator from a Dynamic Combinatorial Library. *J. Am. Chem. Soc.* **2015**, *137* (34), 10965–10969.

(14) Osowska, K.; Miljanić, O. Š. Oxidative Kinetic Self-Sorting of a Dynamic Imine Library. *J. Am. Chem. Soc.* **2011**, *133* (4), 724–727.

(15) Herrmann, A. Dynamic Combinatorial/Covalent Chemistry: A Tool to Read, Generate and Modulate the Bioactivity of Compounds and Compound Mixtures. *Chem. Soc. Rev.* **2014**, *43* (6), 1899–1933.

(16) Cencer, M. M.; Greenlee, A. J.; Moore, J. S. Quantifying Error Correction through a Rule-Based Model of Strand Escape from an [n]-Rung Ladder. *J. Am. Chem. Soc.* **2020**, *142*

(1), 162–168.

(17) Jiang, X.; Laffoon, J. D.; Chen, D.; Pérez-Estrada, S.; Danis, A. S.; Rodríguez-López, J.; Garcia-Garibay, M. A.; Zhu, J.; Moore, J. S. Kinetic Control in the Synthesis of a Möbius Tris((Ethynyl)[5]Helicene) Macrocycle Using Alkyne Metathesis. *J. Am. Chem. Soc.* **2020**, *142* (14), 6493–6498.

(18) Belowich, M. E.; Stoddart, J. F. Dynamic Imine Chemistry. *Chem. Soc. Rev.* **2012**, *41* (6), 2003.

(19) Shen, D.; Rees, L. V. . Adsorption and Diffusion of N-Butane and 2-Butyne in Silicalite-I. *Zeolites* **1991**, *11* (7), 684–689.

(20) Heppekausen, J.; Stade, R.; Goddard, R.; Fürstner, A. Practical New Silyloxy-Based Alkyne Metathesis Catalysts with Optimized Activity and Selectivity Profiles. *J. Am. Chem. Soc.* **2010**, *132* (32), 11045–11057.

(21) Temme, O.; Laschat, S. Effect of Molecular Sieves on the Formation and Acid-Catalysed Mono- and Bis-Cyclization of N-Arylimines: Easy Entry to Polycyclic Ring Systems by a Novel Cascade Reaction. *J. Chem. Soc. Perkin Trans. 1* **1995**, No. 2, 125.

(22) Haack, A.; Hillenbrand, J.; Leutzsch, M.; van Gastel, M.; Neese, F.; Fürstner, A. Productive Alkyne Metathesis with “Canopy Catalysts” Mandates Pseudorotation. *J. Am. Chem. Soc.* **2021**, *143* (15), 5643–5648.

(23) Thompson, R. R.; Rotella, M. E.; Zhou, X.; Fronczek, F. R.; Gutierrez, O.; Lee, S. Impact of Ligands and Metals on the Formation of Metallacyclic Intermediates and a Nontraditional Mechanism for Group VI Alkyne Metathesis Catalysts. *J. Am. Chem. Soc.* **2021**, jacs.1c01843.

(24) Fürstner, A. Alkyne Metathesis on the Rise. *Angew. Chemie Int. Ed.* **2013**, *52* (10), 2794–

2819.

(25) Pattillo, C. C. Synthetic and Mechanistic Studies to Expand the Scope of Alkyne Metathesis Dynamic Covalent Chemistry, University of Illinois, 2019.

(26) Leguizamon, S. C.; Scott, T. F. Sequence-Selective Dynamic Covalent Assembly of Information-Bearing Oligomers. *Nat. Commun.* **2020**, *11* (1), 784.

(27) Yang, A. Understanding Reaction Pathways Leading to Tetrahedral Organic Cages via Alkyne Metathesis, University of Illinois at Urbana-Champaign, 2018.

(28) Moneypenny, T. P.; Yang, A.; Walter, N. P.; Woods, T. J.; Gray, D. L.; Zhang, Y.; Moore, J. S. Product Distribution from Precursor Bite Angle Variation in Multitopic Alkyne Metathesis: Evidence for a Putative Kinetic Bottleneck. *J. Am. Chem. Soc.* **2018**, *140* (17), 5825–5833.

(29) Strom, K. R.; Szostak, J. W. Solid-Phase Synthesis of Sequence-Defined Informational Oligomers. *J. Org. Chem.* **2020**, *85* (21), 13929–13938.

(30) Wei, T.; Furgal, J. C.; Jung, J. H.; Scott, T. F. Long, Self-Assembled Molecular Ladders by Cooperative Dynamic Covalent Reactions. *Polym. Chem.* **2017**, *8* (3), 520–527.

(31) Ciaccia, M.; Cacciapaglia, R.; Mencarelli, P.; Mandolini, L.; Di Stefano, S. Fast Transimination in Organic Solvents in the Absence of Proton and Metal Catalysts. A Key to Imine Metathesis Catalyzed by Primary Amines under Mild Conditions. *Chem. Sci.* **2013**, *4* (5), 2253.

(32) Cui, M.; Bai, W.; Sung, H. H. Y.; Williams, I. D.; Jia, G. Robust Alkyne Metathesis Catalyzed by Air Stable d 2 Re(V) Alkylidyne Complexes. *J. Am. Chem. Soc.* **2020**, *142* (31), 13339–13344.

(33) Cui, M.; Sung, H. H. Y.; Williams, I. D.; Jia, G. Alkyne Metathesis with d 2 Re(V)

Alkylidyne Complexes Supported by Phosphino-Phenolates: Ligand Effect on Catalytic Activity and Applications in Ring-Closing Alkyne Metathesis. *J. Am. Chem. Soc.* **2022**, *144* (14), 6349–6360.

(34) Zhang, W.; Lu, Y.; Moore, J. S. Preparation of a Trisamidomolybdenum(VI) Propylidyne Complex. *Org. Synth.* **2007**, *84*, 163.

(35) Peterle, T.; Ringler, P.; Mayor, M. Gold Nanoparticles Stabilized by Acetylene-Functionalized Multidentate Thioether Ligands: Building Blocks for Nanoparticle Superstructures. *Adv. Funct. Mater.* **2009**, *19* (21), 3497–3506.

(36) Andréasson, J.; Straight, S. D.; Moore, T. A.; Moore, A. L.; Gust, D. Molecular All-Photonic Encoder−Decoder. *J. Am. Chem. Soc.* **2008**, *130* (33), 11122–11128.

CHAPTER 4: TOWARDS REGENERATIVE THERMOSETS USING FRONTAL RING-OPENING OLEFIN METATHESIS POLYMERIZATION

4.1 Introduction

Energy efficient manufacturing of thermoset polymers and polymer-based composites with realistic end-of-life strategies presents one of the most significant scientific and societal challenges for this century. Thermoset polymers and composites possess the necessary chemical and mechanical properties critical for achieving lightweight, durable structures in transportation, civil, and energy infrastructure, but the vast energy input and cure times required for initial manufacture render current approaches to generate these materials unsustainable.[1] Present technologies for manufacturing high-performance thermoset parts typically rely on energy-intensive curing in large, expensive autoclaves or ovens, often operating on the order of several hours.[2] Consequently, there has been much interest in producing these materials with less energy, reducing their cost and environmental impact.

Frontal polymerization (FP) is a promising curing strategy that substantially reduces manufacturing burdens by using the enthalpy of polymerization to provide the energy for materials synthesis, rather than requiring a sustained input of energy from an external source.[3] In frontal polymerization, a solution of a monomer and a latent initiator is activated locally, typically with heat, until the initiator is activated for polymerization of the monomer. Heat released from this initial polymerization event further drives reaction, resulting in a propagating reaction wave that rapidly transforms the available monomer into polymer. Though a multitude of FP chemistries have been developed in recent years, FP manufacturing of materials used for high-performance applications specifically requires chemical systems that are stable and processable at low

temperatures for wide windows (typically several hours), possess high energy density and reactivity, and generate chemically and thermally robust polymer products.

In the last two decades, ring opening metathesis polymerization (ROMP), which exploits reversible C=C bond scission to exchange alkene fragments from two different substrates, has emerged as a versatile reaction motif, particularly in the synthesis of robust materials.[4] The enthalpic driving force behind ROMP is provided by the ring opening of highly strained cyclic alkenes. Thus, neat ROMP systems typically exhibit significant heat generation, making them uniquely suited for FP.[5] Norbornene derivatives in particular have been thoroughly explored for frontal ring-opening metathesis polymerization (FROMP) approaches to manufacturing polymer thermosets. Of these systems, the most attractive for manufacturing of high-performance materials utilizes *endo*-dicyclopentadiene (DCPD) and a thermally activated Grubbs-type ruthenium catalyst.[6,7] In addition to the high energy density, high reactivity, and low viscosity required for FROMP, the polydicyclopentadiene (pDCPD) product generated from FP is a highly cross-linked thermoset with high fracture toughness, impact resistance, stiffness and chemical resistance (Figure 4.1).[8–10]

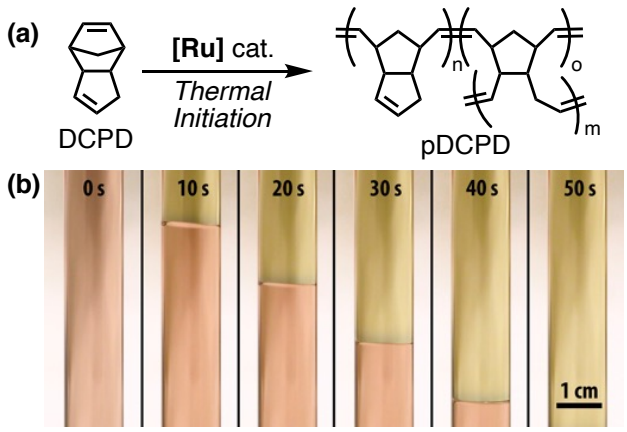

Figure 4.1. FROMP of DCPD in a test tube geometry. (a) Scheme for thermally initiated FROMP of DCPD. (b) Conversion of liquid monomer (pink) to cured thermoset (yellow) takes place through a propagating thermal wave. Adapted from ref. 6. Copyright 2017, American Chemical Society.

Although the high density of covalent crosslinks formed during FROMP leads to excellent thermomechanical properties, this same feature creates challenges for sustainable end-of-life management of thermoset components.[11] When the end-of-life-use of a thermoset component is reached, these materials are often downcycled, incinerated, or discarded in landfills.[12] Existing processes for recycling thermosets often rely on mechanical grinding to facilitate material processing, resulting in a decrease in mechanical properties.[13,14] Fortunately, new end-of-life strategies involving cleavable or dynamic linkages have emerged to address these challenges. The incorporation of a cleavable comonomer into FROMP-generated pDCPD thermosets yields polymers with attributes similar to virgin pDCPD but with a chemically deconstructible polymer network. Work from the Xia and Moore groups demonstrated the FROMP synthesis and degradation of pDCPD thermosets containing 2,3-dihydrofuran (DHF), which yields acid-labile linkages.[15] The Johnson group also demonstrated successful degradation and upcycling into polyurethanes of pDCPD copolymerized with silyl ether moieties (Figure 4.2).[16] Though chemical upcycling is a highly effective strategy for extending the life use of a material, it does not ultimately divert that material from waste streams. Sustainability initiatives for end-of-life management of thermosets would benefit tremendously from the development of new chemical approaches not only to polymer degradation, but also energy-efficient regeneration. Here, regeneration is defined as restoration of the original polymerizable moiety following chemical degradation, enabling reuse of the degradation product in repeated polymerizations.

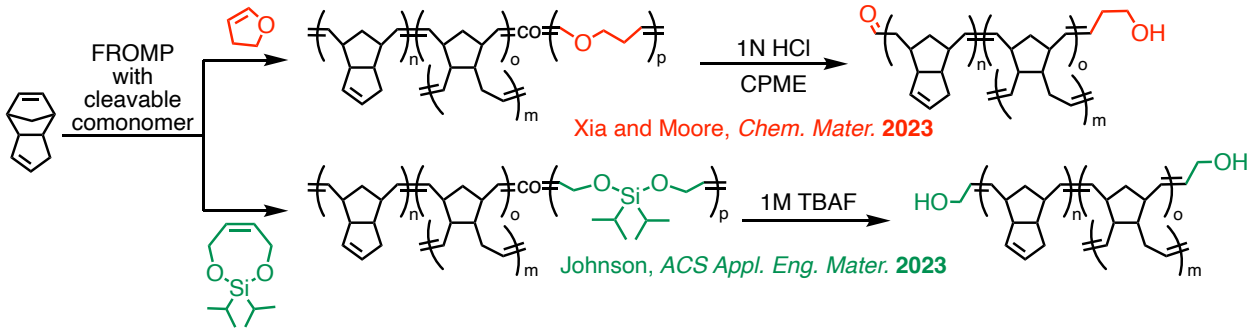

Figure 4.2. Recent strategies for the FROMP synthesis of degradable DCPD copolymers. (top) FROMP with dihydrofuran and subsequent deconstruction yields branched oligomers with terminal aldehyde and alcohol functionalities (b) Cyclic silyl ethers yield alcohol-terminated degradation products, which can be upcycled into polyurethane products.

Because FROMP curing is driven by chemical energy stored in the resin, realizing regenerative thermosets that undergo repeated FROMP requires reactivation of degradation products through the installation of FROMP-able functional groups. To achieve this, we envisioned a strategy in which oligomeric pDCPD degradation products are functionalized with strained cyclic olefins *via* Diels-Alder (DA) cycloaddition, and thus effectively transformed into ROMP-active macromonomers (Figure 4.3a). We reasoned that these degradation products could be solubilized in liquid DCPD to produce a resin suitable for a subsequent generation of FROMP curing. An early attempt by Suslick *et al.* to reactivate oligomeric DPCD (oDCPD) with cyclopentadiene generated in-situ by thermal cracking of DCPD resulted in the addition of an average of 1.3 cyclopentadiene (CP) units per oligomer, as determined by Kendrick mass analysis.[17] It was speculated that cycloaddition occurred selectively at the more reactive chain ends, rather than the polymer backbone or pendant cyclopentene groups. We reasoned that a more potent dienophile functionality would improve the degree of CP incorporation in the reactivation step (Figure 4.3b). To this end, I sought to investigate 1) the compatibility of □icyclopentadiene-1-one (oxaDCPD, **1**), a DCPD derivative possessing an enone moiety in the pendant

cyclopentadiene group, with FROMP conditions and 2) the efficacy of the more potent enone moiety in the reactivation of oligomeric DCPD derivatives *via* DA reaction.

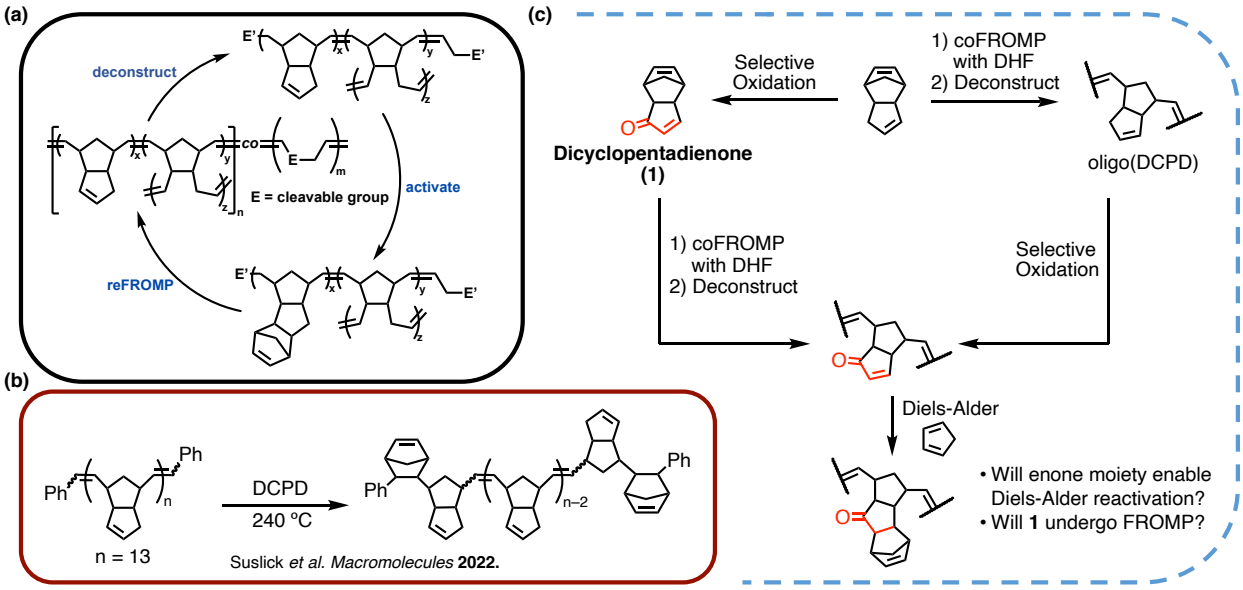

Figure 4.3. Scheme of the reactivation of degradable DCPD thermosets. (a) Proposed reactivation cycle of DCPD thermoset degradation products. (b) Prior work on the Diels-Alder reaction of DCPD oligomers prepared via frontal polymerization. Reaction was assumed to occur only at the chain ends. (c) Proposed path to DCPD oligomers amenable to reactivation through either ketone-functionalized monomers or oligomeric degradation products. The work presented herein concerns the former strategy.

4.2 Synthesis of Precursor 1

Synthetic routes to **1** through both chemical and photochemical oxidation of DCPD have been previously reported.[18–21] We sought to compare the efficiencies of both approaches on multigram scales in order to determine the feasibility of future materials-scale syntheses. Reaction monitoring by gas chromatography-mass spectrometry (GC-MS) of the photochemical oxidation of DCPD with oxygen gas, a reptile lamp as a light source, and tetraphenylporphyrin photosensitizer revealed slow conversion of starting material: a maximum isolated yield of 28% was recorded after six days of continuous irradiation (Figure 4.4). Furthermore, the scale of reaction was limited to 5 grams per batch by the high dilution required for effective

photosensitization. By contrast, a two-step chemical approach using a Riley oxidation to generate the allylic alcohol **2**, followed by oxidation with pyridinium chlorochromate afforded ketone **1** on an 8 gram scale, albeit in lower overall yields and with additional purification steps. It is likely that our unoptimized photochemical setup played a significant role in the sluggish conversion of DCPD in the photochemical case. Neither the penetration depth of the light nor the potential mismatch of emission and absorption profiles of the light source and photosensitizer were investigated. Future attempts to generate **1** or other oxa-congeners of DCPD would likely be improved using dedicated photochemical and flow apparatuses. Electrochemical approaches to allylic oxidation also show promise as potential strategies to access oxidation products of norbornene derivatives.[22]

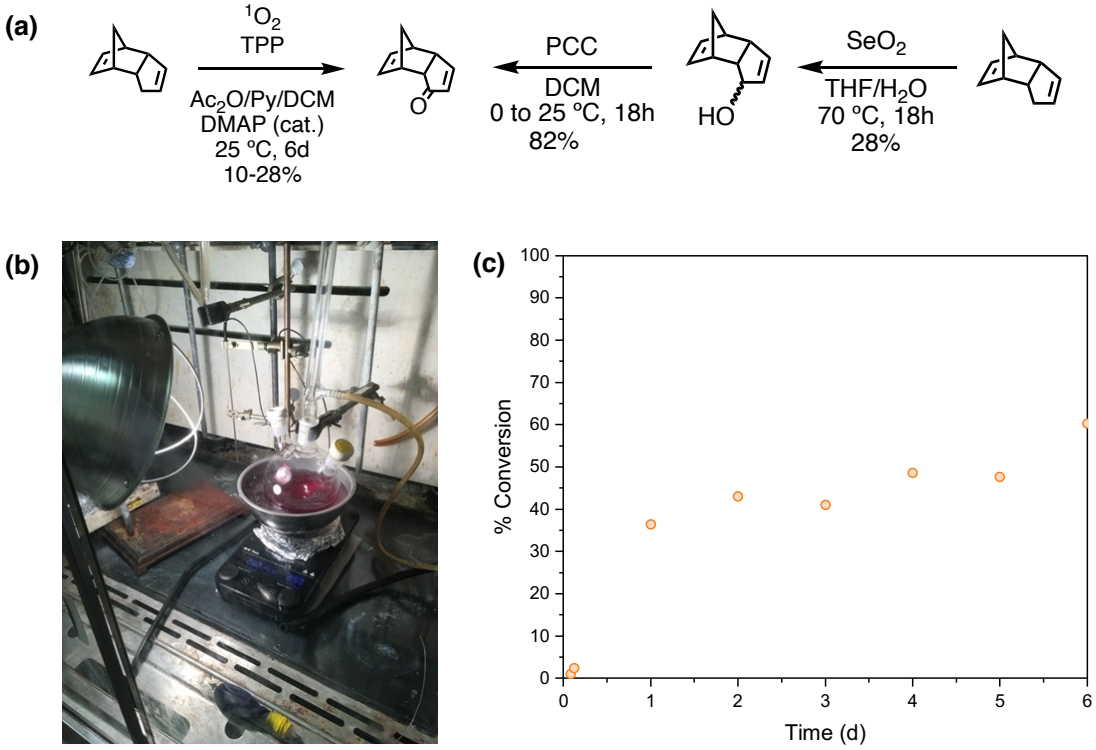

Figure 4.4. Photochemical and chemical synthetic strategies to access **1** from DCPD. (a) Reaction conditions for photochemical allylic oxidation of DCPD (left) and two-step chemical oxidation of DCPD (right). (b) Unoptimized photochemical setup used for photochemical oxidation. (c) Time-dependent conversion of DCPD as monitored by GCMS. Conversion was estimated as the ratio of the product peak area to the sum of the product and substrate peak areas.

4.3 Solution-Phase ROMP Studies of oxaDCPD

Though only a single atom substitution distinguishes **1** from its precursor, we anticipated that this relatively minor functional group change could drastically affect the ability of this species to undergo polymerization. Though a variety of oxa-norbornene derivatives are reported to undergo ROMP in the presence of highly active metathesis catalysts, the formation of oxygen-complexed propagating species is known to slow the rate of polymerization.[23] This effect is pronounced when complexation occurs through the formation of kinetically stable 5- and 6-membered rings, as we might expect for ring-opening metathesis intermediates of **1** and more generally for norbornene derivatives with oxygen atoms attached directly to the 5/6 positions.[23] Therefore, we began our investigation with kinetic ROMP studies of **1** to better understand potential incompatibilities of the monomer with FROMP conditions.

To gain quantitative insight into ROMP behavior of **1**, solution-phase polymerization experiments were performed with Grubbs 2nd generation catalyst (**GC2**). In addition to **1**, DCPD and 1,5-cyclooctadiene (COD) were chosen as reference substrates. At a monomer to initiator loading of 300:1 and concentration of 0.6 mM, DCPD and COD were observed to undergo complete conversion within 15 minutes, as monitored by ^{1}H NMR. By contrast, **1** was observed to reach only 2% conversion after 2 hours (Figure 4.5a). To better understand this discrepancy, experiments were repeated in THF-d_8 at elevated catalyst loadings and reaction concentrations. Under these conditions, complete conversion of **1** was achieved in roughly 30 minutes, accompanied by the appearance of a broad signal at 17.83 ppm. This signal has been shown to correspond to species in which a carbonyl or alcohol oxygen atom attached to the cyclopentylmethylene ligand coordinates to the ruthenium metal center.[24] The relatively slow propagation kinetics of **1**, coupled with the absence of the chelate peak from the corresponding

DCPD and COD spectra, suggest that polymerization of **1** is impeded by the formation of an oxygen-complexed species. This represents a considerable challenge for applications to FROMP, which requires fast, highly enthalpic polymerization conditions to sustain a front. Nonetheless, the ability of **1** to undergo ROMP led us to continue to investigate its suitability for FROMP.

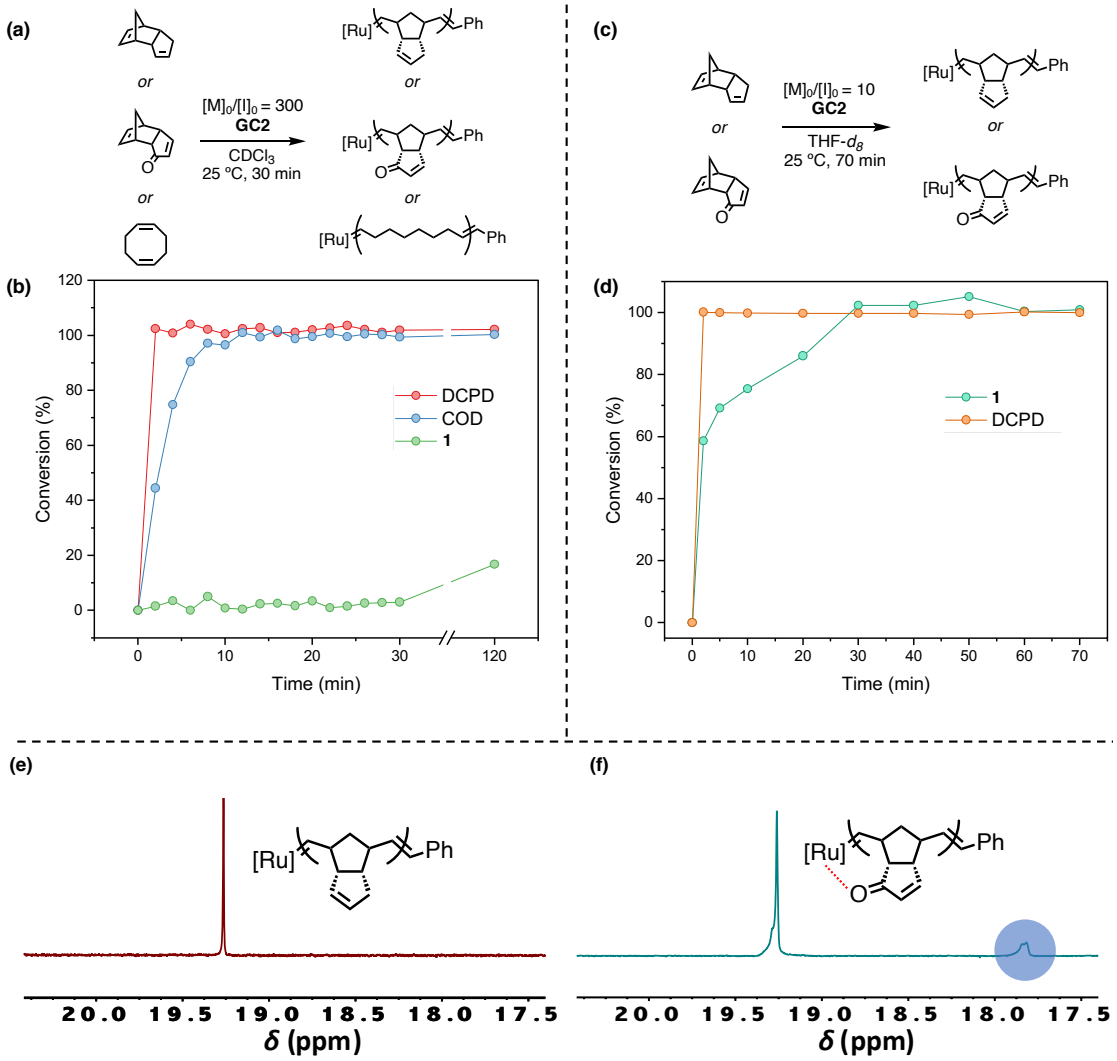

Figure 4.5. Solution-phase kinetic ROMP experiments with different monomers. (a,c) Reaction conditions for ROMP of DCPD, **1**, and COD. (b,d) Time-dependent substrate conversion for the corresponding reaction scheme. (e) Carbene region of the ^{1}H NMR spectrum of the ROMP of DCPD with $[M]_0/[I]_0 = 10$ in THF-d_8. (f) Carbene region at t = 10 min for the polymerization of **1**. The carbene peak at 17.83 ppm is indicative of oxygen chelation.

4.4 Practical Considerations in the FROMP of OxaDCPD Copolymer Mixtures

Though FP has been reported for a several solid-monomer systems,[25,26] typical systems employ liquid monomers or gel resins. Monomer melting is endothermic, which redirects heat away from the polymerization and dampens propagation rates. Furthermore, undesirable geometric perturbations occur with coincident melting and polymerization. These processability challenges generally dictate that solid monomers be dissolved in solvent or liquid comonomer. For example, DCPD is typically mixed with 5 wt% 5-ethylidene-2-norborne to depress the melting point below room temperature. By contrast, processing of the solid, highly crystalline monomer **1** (m.p. = 56 ºC) represented an additional challenge for FROMP applications.

Anticipating that **1** would be unable to undergo FROMP on its own, owing to its slow reaction kinetics and high melting point, we first sought to generate liquid resins of **1**, **GC2**, and a solubilizing comonomer. Attempts to depress the melting point of **1** with small amounts (>10 wt% ENB) were unsuccessful, as evidenced by precipitation events during cooling from 70 ºC. It was determined that formulations of **1** and ENB were only stable in the liquid state above 40 wt% ENB. Gratifyingly, this 60:40 wt% **1**:ENB resin underwent FROMP successfully, albeit with relatively slow front velocities ($v_f = 0.12 \pm 0.09$ mm s^{-1}) (Figure 4.6). We attribute this phenomenon to the sluggish reaction kinetics of **1**. The resultant rubbery polymer product was swelled in DCM over 18 hours, resulting in a 683% increase in mass. This indicates that the structure is likely only lightly crosslinked.

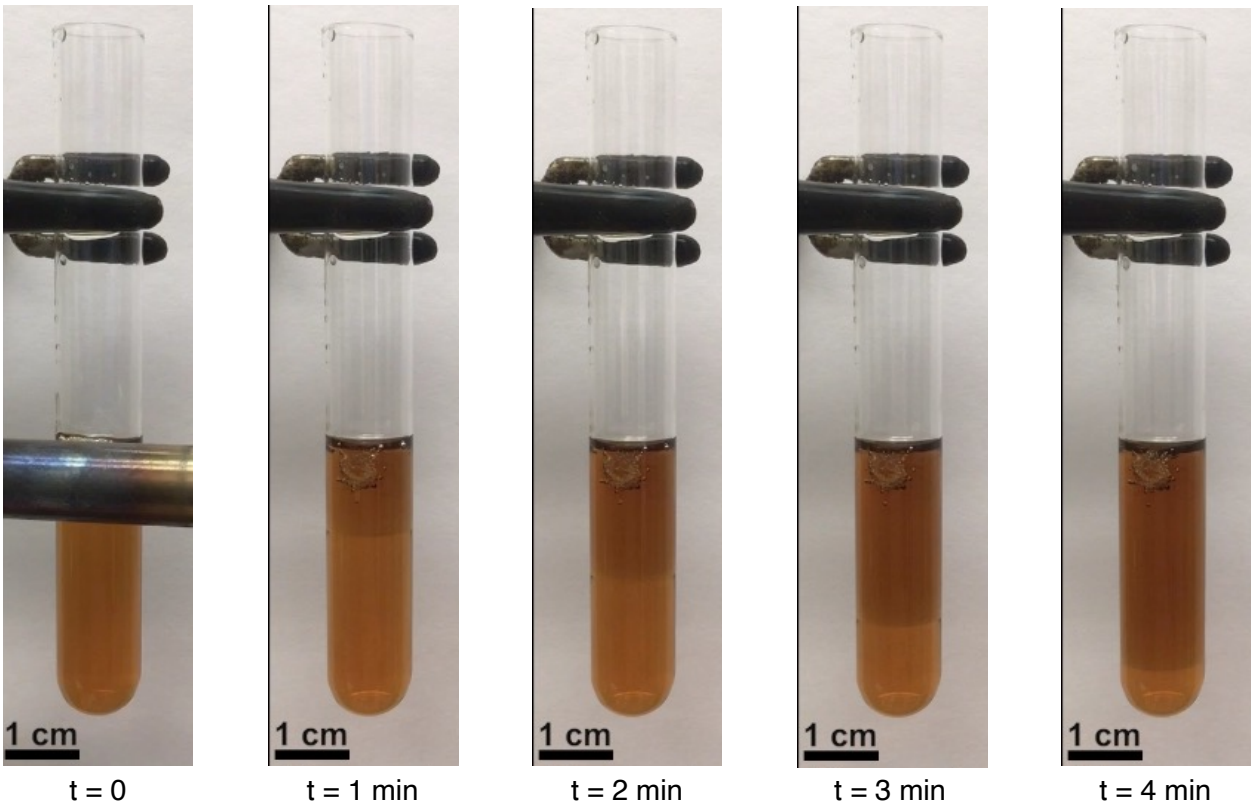

Figure 4.6. FROMP of a 60:40 wt% **1**:ENB using 100 ppm (mol/mol) **GC2** relative to norbornene functionality and 1 equiv tributylphosphite (TBP) relative to catalyst.

In order to better understand the effects of incorporating **1** in polymer thermosets, we next studied formulations of **1** and DCPD. As in the case of ENB formulations, resins were only found to persist in the liquid state at room temperature above 50 wt% DCPD. Front velocities were found to decrease roughly asymptotically with increasing concentration of **1**, reaching a minimum of 0.30 ± 0.01 mm s^{-1}, compared to 8.06 ± 0.06 mm s^{-1} in the case of pure DCPD. Maximum front temperatures, by contrast, did not depreciate considerably with the inclusion of **1** (Figure 4.7). To quantitatively compare these formulations, differential scanning calorimetry (DSC) experiments were performed. In these studies, samples were subjected to a linear heat gradient and the subsequent exothermic events associated with polymerization were quantified. With increasing concentration of **1**, the onset temperature and normalized enthalpy of initial curing events were

found to decrease, from 166.82 ºC and 205.89 J g^{-1} for a resin of 10 wt% **1** to 139.57 ºC and 63.51 J g^{-1} for a resin of 40 wt% **1**. In several cases, this change was accompanied by a secondary exotherm centered around 181 ºC, which increased in intensity with increasing **1** content. Glass transition temperatures (T_g) determined by DSC for these resins were grouped narrowly around 133 ºC, considerably lower than those previously reported for pDCPD (~160 ºC).

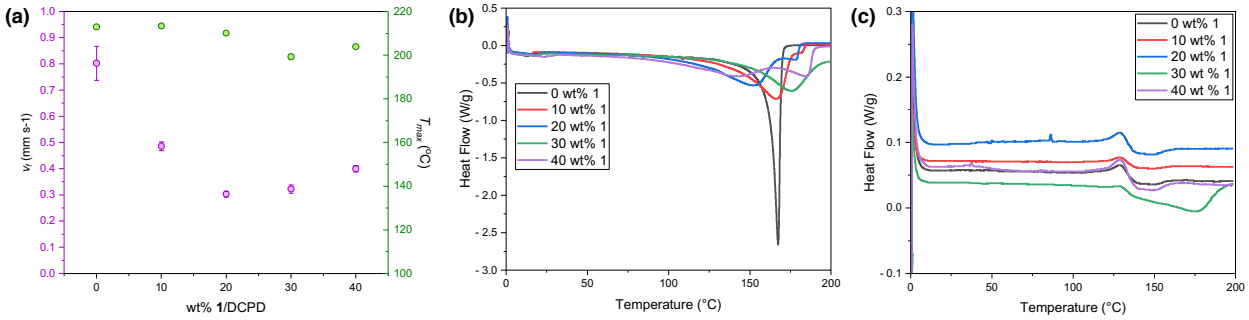

Figure 4.7. Characterization of **1**:DCPD FROMP resins. (a) Frontal velocities (v_f) and maximum front temperatures (T_{max}) of different formulations of **1** and DCPD with 100 ppm **GC2**/TBP relative to norbornene functionality. Representative differential scanning calorimetry (DSC) plots for the first (b) and second (c) heating scan for resins derived by **1** and DCPD.

The apparent relationship between comonomer formulation and bulk cure profile suggests that DCPD and **1** form a eutectic mixture with distinct curing regimes, or undergo a secondary, exothermic chemical reaction at high temperature. The sum of both enthalpies of cure for each resin formulation were similar to those reported previously for pure DCPD. This further supports our observations that comonomer formulations of **1** and DCPD exhibit sufficient exothermicity to engender polymerization, though the two-step cure profile generated by DSC is not likely representative of a frontal cure profile, and thus the thermomechanical properties of the resultant polymers required additional characterization.

To better understand the possible discrepancies between bulk and frontal curing, and to evaluate the thermomechanical properties of different comonomer formulations, dynamic mechanical analysis (DMA) was performed on frontally polymerized resins of DCPD and **1**. It was

observed that the intensity of the tan(δ) peak decreases with increasing concentration of **1**. This may be attributed to an increase in the ratio of amorphous and crystalline domains of the material Surprisingly, thermosets synthesized *via* FROMP all displayed closely grouped T_g values near that of pure pDCPD and roughly 50 ºC lower than those determined by DSC. This data, along with the multi-stage cure profile observed for bulk cure samples, suggests that frontal and bulk polymerization of comonomer formulations of DCPD and **1** generate samples with drastically different thermomechanical properties. DSC studies of frontally cured formulations of **1** and other comonomers are currently underway to investigate this phenomenon. Future explorations of FP systems should consider these discrepancies, as well as the validity of different characterization techniques, when evaluating different comonomer formulations.

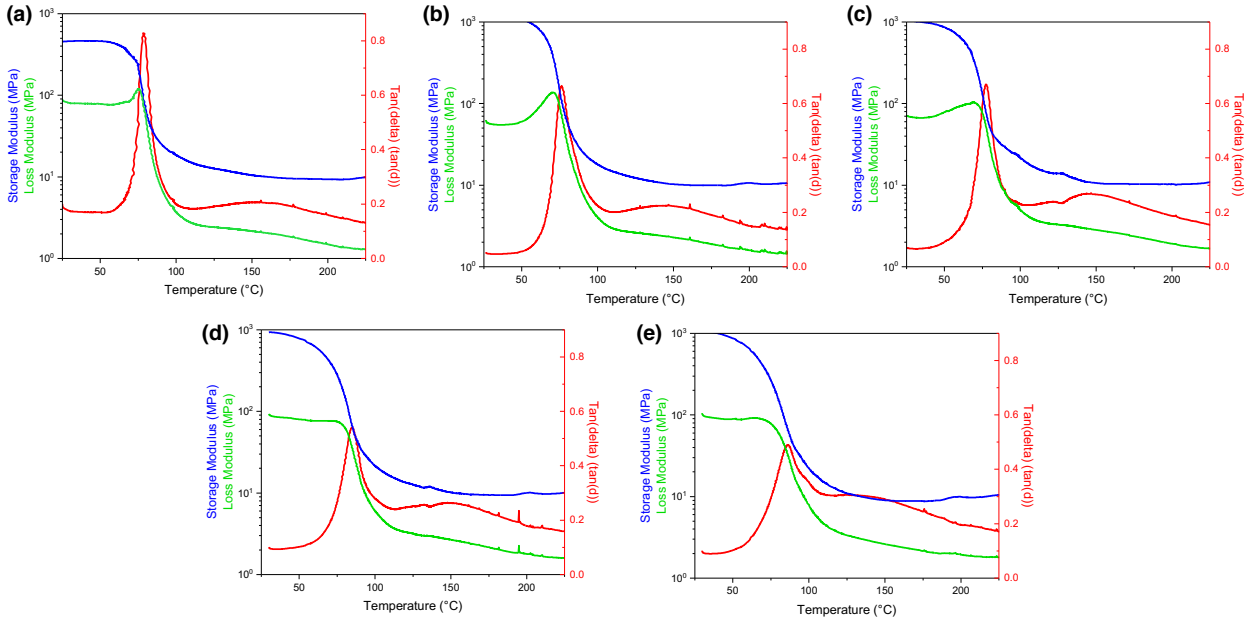

Figure 4.8. Representative DMA plots for polymers generated from FROMP of DCPD and **1**. (a) DMA of pure FP-derived pDCPD. (b-e) DMA plots for polymers generated from 10, 20, 30, and 40 wt% **1**:DCPD, respectively. The storage and loss moduli are given in blue and green, respectively, and the ratio of these curves affords the red tan(δ) trace. The maxima of the tan(δ) curve correspond to transition temperatures within the resultant polymer.

FROMP of neat **1** was not attempted. However, future work should seek to explore efficient bulk cure techniques to access polymers of **1** (**1**$_p$). Recent studies of thermosets generated by reaction injection molding of **1** indicate that **1**$_p$ exhibits higher T_g, enhanced storage modulus, and increased hardness and compression strength compared to pDCPD synthesized *via* the same method.[18] These features were attributed to inter-chain interactions, particularly vinylic C—H•••O=C hydrogen bonds and dipole-dipole interactions between ketone groups. Comparison of this material to thermosets generated by the FROMP of a finely ground powder of **1**, or of the liquid monomer at elevated temperatures, would be useful for future development of sustainable approaches to high-performance polymer materials.

4.5 Diels-Alder Reactions of Oligo(oxaDCPD)

Having established the feasibility of FROMP of comonomer formulations of **1**, we next investigated strategies for reactivation of oligomeric products for FROMP. We expected that reaction conditions for DA of cyclopentadiene and monomer **1** would enable the same transformation of the corresponding oligomers. Thus, we began our investigation with small molecule studies. Following previously reported procedures, **1** was treated with aluminum chloride and freshly distilled CP in toluene at room temperature.[27] Thin layer chromatography (TLC) and GC-MS analysis indicated that the reaction was complete after 90 minutes, furnishing a mixture of diastereomers in 84% yield. Consistent with previous reports, NMR analysis indicated that the product distribution was populated by two stereoisomers: *endo-anti-exo* (major product) and *endo-anti-endo* (minor) (Scheme 4.1).

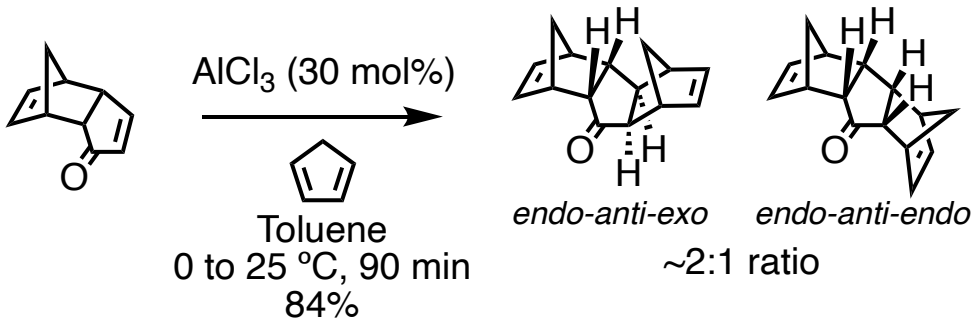

Scheme 4.1. Diels-Alder reaction of **1** with cyclopentadiene furnishes a mixture of diastereomeric tricyclic systems.

Encouraged by the efficiency of the DA reaction, we next attempted to translate this process to ROMP oligomers containing **1**. To simplify analysis of reaction mixtures, oligomers of **1** (**1$_o$**) were used as a model system in place of degradation products of **1**, DCPD, and a cleavable comonomer. **1$_o$** was synthesized *via* solution-phase ROMP using Grubbs 3rd generation catalyst (**GC3**). Low monomer to initiator loadings and high concentrations of a chain transfer agent (*cis*-4-octene) were employed to limit molecular weight. MALDI-TOF analysis and analytical size exclusion chromatography (SEC) revealed a narrowly dispersed product mixture (PDI = 1.1) with M_n = 3909 Da, corresponding to an average degree of polymerization of X_n = 26 for polymers with butene-functionalized chain ends. Unfortunately, attempts at DA using standard conditions resulted in no reaction, as indicated by MALDI mass analysis and SEC. Switching solvent systems to dichloromethane, in which **1$_o$** displayed superior solubility, resulted in a shift in the product distribution, as indicated by the appearance of new aliphatic signals in the ^{1}H NMR spectrum, the presence of a high molecular weight shoulder in the SEC trace of the reaction mixture, as well as the presence of a new set of peaks in the MALDI mass spectrum (Figure 4.9).

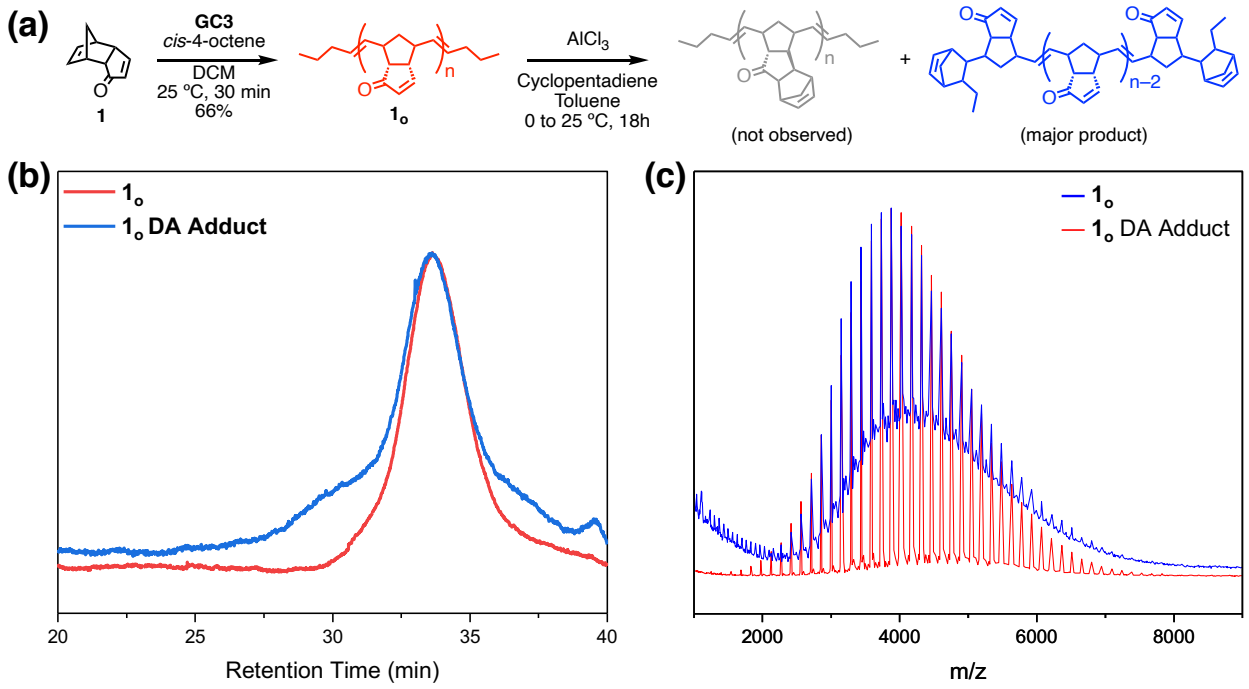

Figure 4.9. Synthesis and attempted post-polymerization modification of $\mathbf{1_o}$. (a) Reaction scheme for oligomerization and subsequent Diels-Alder reaction. (b) SEC traces for $\mathbf{1_o}$ (red) and the DA adduct of $\mathbf{1_o}$ with cyclopentadiene (blue). (c) MALDI-TOF spectra of $\mathbf{1_o}$ (red) and the DA adduct of $\mathbf{1_o}$ with cyclopentadiene (blue).

To unambiguously identify the speciation of the DA product distribution, Kendrick mass analysis was employed (Figure 4.10). It was determined, as in the case of oDCPD, that only one to two CP units were incorporated per polymer chain. We reason that these reactions likely occurred at the sterically accessible chain ends, rather than randomly in the polymer backbone or at the cyclopentenone pendant groups. The difference in DA activity between **1** and $\mathbf{1_o}$ might be attributed to the difference in steric accessibility of the enone functional group. In $\mathbf{1_o}$, we propose that a combination of restricted rotation about the polymer backbone as well as steric crowding by neighboring pendant cyclopentenone functional groups renders the enone moiety inaccessible for dienophilic attack compared to monomer **1**. This is further evidenced by the observation that extended reaction times (18h) fail to furnish more highly CP-functionalized products, suggesting that chain ends readily undergo DA while the polymer backbone and pendant groups are unreactive

under standard conditions. Future studies should seek to elucidate the effects of elevated temperatures and different solvent systems on the reactivity of this system.

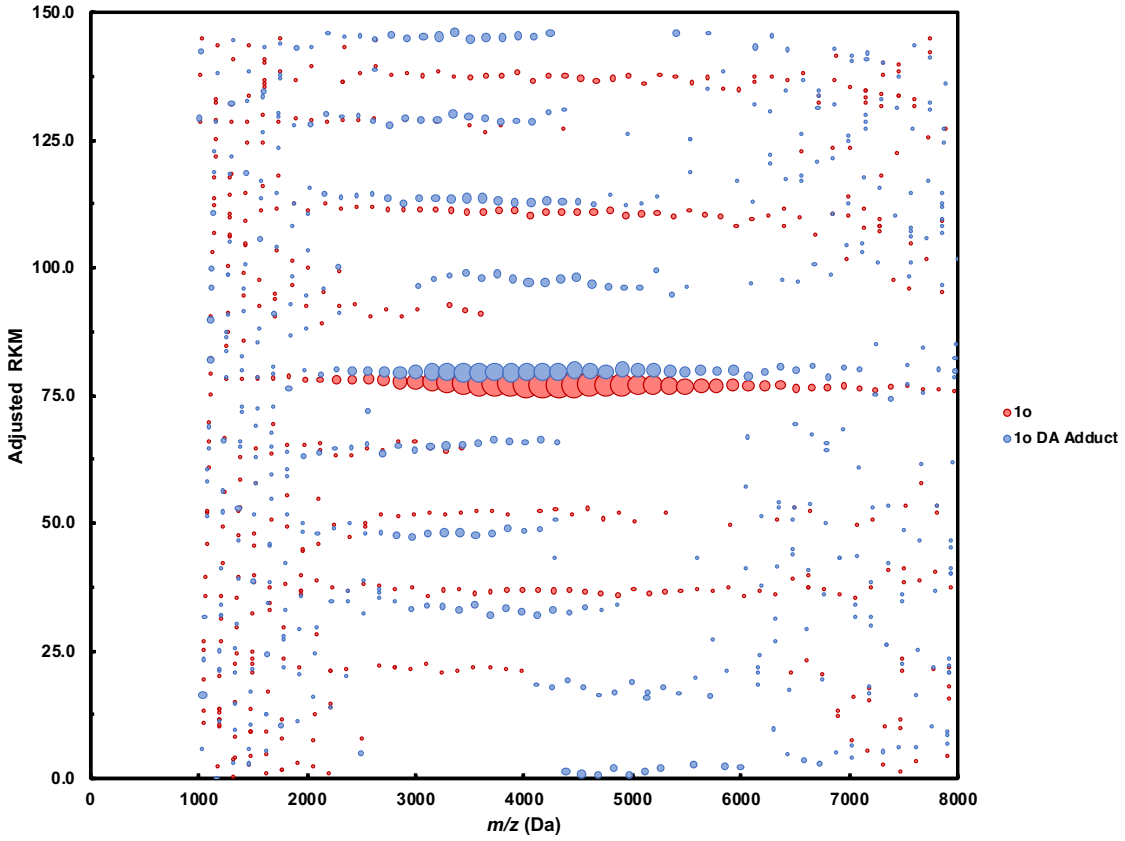

Figure 4.10. Kendrick plots of $\mathbf{1_o}$ and its DA adduct with CP. Species with identical chain-ends possess an identical remainder of Kendrick mass values and therefore horizontally align. The relative intensity of each species was determined from the area under the corresponding MALDI peak and is reflected in the radius of the circular points. The absence of new species from the Kendrick plot, with the exception of distributions whose moduli correspond to $\mathbf{1_o}$ derivatives functionalized with one or two CP units, suggest that DA addition of CP occurs only at the sterically accessible chain ends.

4.6 Conclusions

This chapter reports the synthesis and characterization of a ketone-functionalized derivative of DCPD, its compatibility with established FROMP systems, and the DA activity of its oligomers. Synthetic routes to **1** explored in this chapter highlight the shortcomings of existing (photo)chemical strategies to generate material at scale and point to flow and heterogeneous

catalytic approaches as potential solutions to the challenge of sustainable and efficient manufacturing of functionalized DCPD derivatives. Solution-phase ROMP studies, in combination with FROMP studies of comonomer formulations of **1** and various norbornene derivatives, indicate the far-reaching effects that monomer functionalization can have on reaction kinetics, resin stability, and thermomechanical characteristics of the resultant polymer thermosets. Specifically, the slow ROMP kinetics of **1**, determined to arise from the formation of persistent oxygen chelated species, was observed to translate to frontal polymerization. The crystallinity of **1** also mandated comonomer formulations with ENB and DCPD to enable FROMP. These practical considerations, initially overlooked in the design of **1**, will inform future selection and design of novel FROMP monomers.

Though attempts at reactivation of $\mathbf{1_o}$ with CP were unsuccessful, the studies presented in this chapter nonetheless provide extremely valuable information regarding potential barriers to post-synthetic modification of pDCPD derivatives. The apparent difference in reactivity of oligomer chain ends compared to backbone and pendant functional groups indicate the role polymer chain dynamics likely play in altering monomer reactivity. Explorations of these phenomena, as well as investigations of new strategies for oligomer reactivation, are currently underway.

4.7 Supporting Information

4.7.1 General Considerations

All reactions were performed in oven (c.a. 165 ºC) or flame-dried glassware under an atmosphere of dry argon or nitrogen unless otherwise noted. All solvents used were either anhydrous commercial grade (Aldrich/Fisher) or purified by a solvent purification system unless otherwise noted. All reagents were purchased from commercial sources and used without further purification.

Since DCPD is a solid at room temperature, 5 wt% ENB was added to depress the melting point. All references to DCPD herein refer to this 95:5 DCPD:ENB solution. Chromatographic purifications were conducted via MPLC on a Biotage Isolera 1 using Silicycle SiliaSep cartridges (230-400 mesh, 40-63 μm). Column separation conditions are reported in column volumes (CV) of gradient solvent mixtures. ^{1}H and ^{13}C NMR spectra were recorded on a Carver B500 Bruker Avance III HD NMR spectrometer at room temperature (298 K) and chemical shifts were referenced to the residual solvent peak ($CDCl_3$ ^{1}H NMR δ = 7.26 ppm). Kinetic experiments were performed using a Varian Unity INOVA 600 MHz NMR spectrometer and are referenced to residual solvent peaks ($CDCl_3$ ^{1}H NMR δ = 7.26 ppm and THF-d_8 δ = 3.58 ppm). Mass spectra were obtained through the Mass Spectrometry Facility, School of Chemical Sciences, University of Illinois. High resolution electron impact (EI) mass spectra were obtained on a Micromass 70-VSE TOF spectrometer and electrospray ionization (ESI) mass spectra were obtained on a Waters Synapt G2-Si TOF spectrometer. Matrix-assisted laser desorption/ionization (MALDI) mass spectrometry was performed on a Bruker Daltonics UltrafleXtreme MALDI using DCTB matrix. MALDI, DSC, and DMA traces were plotted using OriginPro 2018 software. ^{1}H and ^{13}C NMR were processed using MestReNova software v12.0.4-22023. Reported yields are of isolated material which in some cases were corrected for trace residual solvent.

4.7.2 Synthesis and Characterization of Compounds

Photochemical Synthesis of 1

1 was synthesized according to previously reported photochemical procedures[18,20,21] with the following modifications: in a 500 mL round bottom flask fitted with reflux condenser and charged with magnetic stir bar, dimethylaminopyridine (244 mg, 2 mmol, 0.02 equiv) and tetraphenylporphyrin (13.5 mg, 22 μmol) were dissolved in dichloromethane (90 mL). To this

solution was added DCPD (13g, 98 mmol, 1 equiv), acetic anhydride (9.55 mL, 100 mmol, 4 equiv), and pyridine (4 mL, 49 mmol, 0.5 equiv). The reaction mixture was purged with oxygen gas for ten minutes, then placed under an oxygen atmosphere. The mixture was allowed to stir for 6 days, during which time the solution was continuously irradiated with a white light-emitting reptile lamp. Reaction progress was monitored *via* GC-MS. The reaction mixture was diluted with DCM and washed with sat. aqueous $NaHCO_3$ until basic, then subsequently washed with 1M HCl until mint green. The organic phase was then washed with sat. aqueous $CuSO_4$ and brine, dried over Na_2SO_4, and filtered over celite. The reaction mixture was purified via silica gel chromatography using DCM to afford **1** as a beige oil which solidifies upon standing at room temperature (4.00 g, 28 % yield). The ^1H and ^{13}C NMR spectra corresponded to the values reported in literature for this compound. m.p. = 56 ºC; ^1H NMR (500 MHz, $CDCl_3$) δ 7.38 (dd, J = 5.7, 2.6 Hz, 1H), 5.96 (d, J = 6.3 Hz, 1H), 5.94 (dd, J = 5.7, 3.0 Hz, 1H), 5.78 (dd, J = 5.7, 3.0 Hz, 1H), 3.41 (s, 1H), 3.22 (s, 1H), 2.96 (s, 1H), 2.80 (t, J = 5.1 Hz, 1H), 1.76 (d, J = 8.4 Hz, 1H), 1.62 (d, J = 8.5 Hz, 1H); $^{13}C\{^1H\}$ NMR (126 MHz, $CDCl_3$) δ 210.89, 164.71, 137.08, 132.71, 132.50, 77.41, 77.16, 76.91, 52.87, 50.37, 48.40, 45.13, 44.19.

Chemical Synthesis of 1

1-Dicyclopentadienol (S1): Synthesized according to previously reported procedures[19,28] with the following modifications: dicyclopentadiene (69 g, 0.5 mol, 1 equiv), was dissolved in a mixture of tetrahydrofuran (250 mL) and water (25 mL). Selenium dioxide (33 g, 0.3 mol, 0.4 equiv), was added, and the solution was stirred and heated under reflux for 18 hours. The resulting dark brown mixture was then filtered from selenium and poured into two liters of water. The heavy dark oil was drawn off and the aqueous solution was extracted with ether. The organic solutions were combined, washed with water and dried over Na_2SO_4. Removal of solvent, followed by vacuum

distillation of the crude product, gave **1-dicyclopentadienol** as a pale yellow, viscous oil (21.4 g, 28% yield). The ^{1}H and ^{13}C NMR spectra corresponded to the values reported in literature for this compound. b.p. = 84 ºC (3 mmHg); ^{1}H NMR (500 MHz, $CDCl_3$): δ 5.91 (dd, J = 5.7, 3.0 Hz, 1H), 5.82 (dd, J = 5.7, 3.0 Hz, 1H), 5.78 – 5.71 (m, 1H), 5.61 – 5.55 (m, 1H), 4.04 (m, 1H), 3.35 (m, 1H), 3.03 (m, 1H), 2.77 (m, 1H), 2.51 (m, 1H), 1.95 (s, 1H), 1.54 (m, 1H), 1.37 (m, 1H); ^{13}C NMR (126 MHz, $CDCl_3$, δ ppm): δ 137.76, 135.41, 134.63, 132.38, 78.92, 54.64, 53.37, 51.23, 44.77, 44.62.

1: In a 2L round bottom flask charged with magnetic stir bar, pyridinium chlorochromate (22g, 101 mmol, 1.5 equiv) was dissolved in dichloromethane (400 mL). A solution of alcohol **S1** (10g, 68 mmol, 1 equiv) was then transferred via cannula to the mixture and the reaction was allowed to stir for 18h at room temperature. The resulting slurry was then filtered over celite, concentrated directly onto silica, and purified via chromatography in 20% ethyl acetate/hexanes to afford **1** as an off-white oil which solidified upon standing at room temperature (8.07 g, 82% yield). The physical characteristics for this material matched exactly those of the product obtained through photochemical oxidation.

General Procedure for Diels-Alder Cycloaddition of 1 and Cyclopentadiene

In an oven-dried 2-dram vial charged with magnetic stir bar, **1** (200 mg, 1.37 mmol, 1 equiv) and $AlCl_3$ (55 mg, 0.41 mmol, 0.3 equiv) were dissolved in dry toluene (2 mL). The reaction was cooled to 0 ºC, at which point freshly distilled cyclopentadiene (0.4 mL, 4.79 mmol, 3.5 equiv) was added and the mixture was allowed to warm to room temperature, at which point a color change from yellow to brown was observed. After stirring for 90 minutes, the reaction was quenched with water and extracted with dichloromethane. The combined organic layers were washed with water and brine, then dried over Na_2SO_4 and concentrated directly onto silica.

Purification by column chromatography in 3% ethyl acetate/hexanes afforded a white solid determined by ^{1}H and ^{13}C NMR to be a mixture of isomers of the Diels-Alder adducts of **1** (243 mg, 84% yield). ^{1}H NMR (500 MHz, $CDCl_3$): δ 6.20 (dd, *J* = 5.9, 3.0 Hz, 2H), 6.15 (ddd, *J* = 16.5, 5.7, 3.0 Hz, 7H), 6.07 (td, *J* = 5.6, 2.9 Hz, 7H), 5.65 (s, 1H), 3.21 (ddt, *J* = 4.5, 2.9, 1.4 Hz, 3H), 3.08 (dtt, *J* = 10.5, 3.5, 1.7 Hz, 8H), 2.96 (p, *J* = 1.6 Hz, 3H), 2.85 – 2.80 (m, 3H), 2.59 (dd, *J* = 8.4, 4.7 Hz, 1H), 2.51 (ddd, *J* = 8.7, 4.3, 2.1 Hz, 3H), 2.45 – 2.38 (m, 2H), 1.94 (d, *J* = 7.8 Hz, 3H), 1.78 (dt, *J* = 7.8, 2.1 Hz, 3H), 1.47 (ddt, *J* = 29.0, 8.3, 1.9 Hz, 4H), 1.40 – 1.23 (m, 11H); $^{13}C\{^{1}H\}$ NMR (126 MHz, $CDCl_3$) δ 222.81, 138.39, 137.33, 137.12, 137.09, 136.14, 135.89, 135.50, 77.28, 77.03, 76.77, 60.47, 60.28, 59.67, 59.16, 51.38, 51.25, 50.10, 49.88, 48.23, 48.03, 47.65, 47.52, 47.36, 46.85, 46.57, 46.49, 45.80, 45.64, 44.62.

General Procedure for Ring Opening Metathesis Oligomerization of 1

In an oven-dried 20 mL scintillation vial charged with magnetic stir bar, Grubbs 3rd generation catalyst (40 mg, 55 µmol, 1 equiv) was dissolved in DCM (8 mL). Then, *cis*-4-octene (5 µL, 0.30 mmol, 5.3 equiv) was added and the mixture was allowed to stir for 30 minutes at room temperature, at which point a solution of **1** (200 mg, 1.37 mmol, 25 equiv) and *cis*-4-octene (1.1 µL, 60 µmol, 1.1 equiv) in DCM (2.4 mL) was added, resulting in a color change from green to brown. The reaction was allowed to stir for an additional 30 minutes, then poured directly into methanol (100 mL) to precipitate the polymer product. Following centrifugation, the solid was collected via filtration through a 0.45 µm nylon membrane filter and washed with additional methanol. The resulting brown powder was dried under high vacuum to afford $\mathbf{1_o}$ (132 mg, 66% yield).

General Procedure for Diels-Alder Cycloaddition of $\mathbf{1_o}$ and Cyclopentadiene

The General Procedure for Diels-Alder Cycloaddition of **1** and Cyclopentadiene was followed with the following modifications: in an oven-dried 2-dram vial charged with magnetic stir bar, $\mathbf{1_o}$ (150 mg) was dissolved in either dry toluene or dry dichloromethane (2 mL). The reaction was cooled to 0 ºC, then and $AlCl_3$ (41 mg, 0.31 mmol) was added in one portion. The reaction was stirred for 30 minutes, at which point freshly distilled cyclopentadiene (0.3 mL, 3.57 mmol) was added and the mixture was allowed to warm to room temperature. After stirring for an additional 90 minutes, the reaction mixture was poured directly into methanol to precipitate the polymer product. The resulting beige powder was isolated by filtration over a 0.45 μm nylon membrane filter and washed with additional methanol, dried under high vacuum, and analyzed by NMR, SEC, and MALDI-MS.

4.7.3 Solution-Phase and Frontal Polymerization Experiments

General Procedure for Kinetic Studies of Solution-Phase ROMP

In an Ar-filled glovebox, a 500 mHz NMR tube was charged with **GC2** (1 mg, 1.2 μmol, 1 equiv), 1,3,5-trimethoxybenzene, and $CDCl_3$ (1.9 mL). After locking and shimming, an initial ^1H NMR spectrum was acquired, the sample was ejected, and 100 μL of stock solution of ROMP monomer (DCPD, COD, or **1**) (3.6 M) in $CDCl_3$ was injected. After 30 s of shimming adjustment, ^1H NMR spectra were acquired every 30 seconds for 30 minutes. An additional spectrum was acquired for each monomer after 2 hours. at 2.5 min, 5 min, 10 min, and every subsequent 10 min at ambient temperature for 120 min. For experiments at elevated catalyst loading, the same procedure was used with the following modifications: a 500 mHz NMR tube was charged with **GC2** (8.5 mg, 0.01 mmol, 1 equiv) and 1,3,5-trimethoxybenzene in THF-d_8 (900 μL). After acquiring an initial ^1H NMR spectrum, 100 μL of stock solution of ROMP monomer (DCPD or **1**) (1 M) in THF-d_8

was injected. ^{1}H NMR spectra were acquired at 2.5 min, 5 min, 10 min, and every subsequent 10 min at ambient temperature for 120 min. Substrate conversion was determined by comparing the integration of a growing polymer peak to that of a monomer peak using the following relationship:

$$Conversion = \frac{H_p}{H_p + H_m}$$

Where H_p and H_m refer to the integration of the polymer and monomer peak, respectively. In the case of the polymerization of **1** at elevated catalyst loadings, a new propagating carbene peak at δ = 17.83 ppm appeared after 10 minutes.

General Procedure for FROMP Formulations of 1 with DCPD or ENB

In an 20 mL scintillation vial, a total of 3g of monomer **1** and DCPD or ENB were combined to generate a mixture between 0 and 40 wt% of **1**. The mixture was melted at 70 ºC, then cooled to room temperature and charged with tributylphosphite (0.6-1.0 µL, 1 mmol per 10,000 mmol norbornene functionality), then Grubbs 2nd generation catalyst (1.8-1.9 mg, 1 equiv relative to phosphite). The solution was then sonicated for 5 minutes and used for FROMP experiments as detailed below.

Front Velocity and Temperature Profile Measurements

The resins described above were transferred to 13 x 100 mm glass test tubes (total resin volume ca. 3 mL). A K-type thermocouple (TMQSS, Omega) was inserted into the center of the test tube such that the tip was ca. 1 cm below the surface of the resin. FP was initiated by direct contact of a hot 40 W soldering iron (Weller, WLC100) to the side of the glass test tube at a height corresponding to the surface of the resin solution. Front propagation was captured on a Canon EOS T3i Rebel camera, which provided UHD 4K video footage (3840 x 2160 @ 30 fps). The front velocities (v_f) were determined for from this recorded footage using the open source physics (OSP) software package Tracker®. Each video was analyzed three times and the front velocity of the

sample was determined by the average of the three analyses. Temperature profiles (and maximum front temperature, T_{max}) were recorded by the inserted thermocouple.

Differential Scanning Calorimetry

Differential scanning calorimetry (DSC) liquid resin cure kinetic measurements were performed with a TA Instruments Q250 differential scanning calorimeter. Resins formulated according to the general procedure for FROMP formulations of 1 with DCPD were transferred into aluminum hermetic DSC pans at room temperature and sealed. The sample mass was determined using an analytical balance and was carefully maintained between 5 mg and 10 mg. The specific heat capacity was determined between 25 °C and 200 °C by comparison with a sapphire standard. Each sample was subjected to 3 thermal cycles (heat, cool, and second heat). The first heat scan occurred from 0 to 200 ºC at a rate of 5 ºC min^{-1}. The second heat scan occurred at a rate of 10 ºC min^{-1} over the same temperature regime. Glass transition temperatures (T_g) were determined from the midpoint of the thermal transition observed in the second heating scan.

wt% 1	Onset Temperature (ºC)	Primary Peak Temperature (ºC)	Primary Peak Enthalpy (J g^{-1})	Secondary Peak Enthalpy (J g^{-1})	Total Enthalpy (J g^{-1})	T_g (º C)
0	162	167.39	238.3	--	238.3	133.96
10	134.69	166.82	205.89	181.87	273.64	133.3
20	108.15	152.53	155.93	178.36	278.25	133.63
30	148.16	175.74	150.3	--	150.3	133.2
40	140.86	139.57	63.51	184.73	309.21	133.63

Table 4.1. DSC data obtained from two heating cycles of resins derived from **1** and DCPD. Transition temperatures were calculated from the mid-point of the thermal transitions in the second heating scan.

Dynamic Mechanical Analysis

Dynamic mechanical analysis (DMA) tests were performed on a TA Instruments DMA 850 with supplied tensile grips under a nitrogen atmosphere. Plaque molds with gauge dimensions of 9.0 x 3.4 x 1.0 mm were fabricated with RTV-630 silicone molding compound; a glass slide (75.0 x 25.0 x 1.0 mm) was clamped atop the open face of the mold, and resins prepared according to the general procedure for FROMP formulations of 1 with DCPD were injected from the top of the mold using a syringe. FP was initiated by direct contact of a hot 40 W soldering iron (Weller, WLC100) to the top of the glass slide. The temperature of the sample was increased linearly at 5 °C min^{-1} from 25 to 250°C for all catalyst systems. Glass transition temperatures (T_g) were determined using the peak of tan(δ).

4.7.4 NMR Spectra

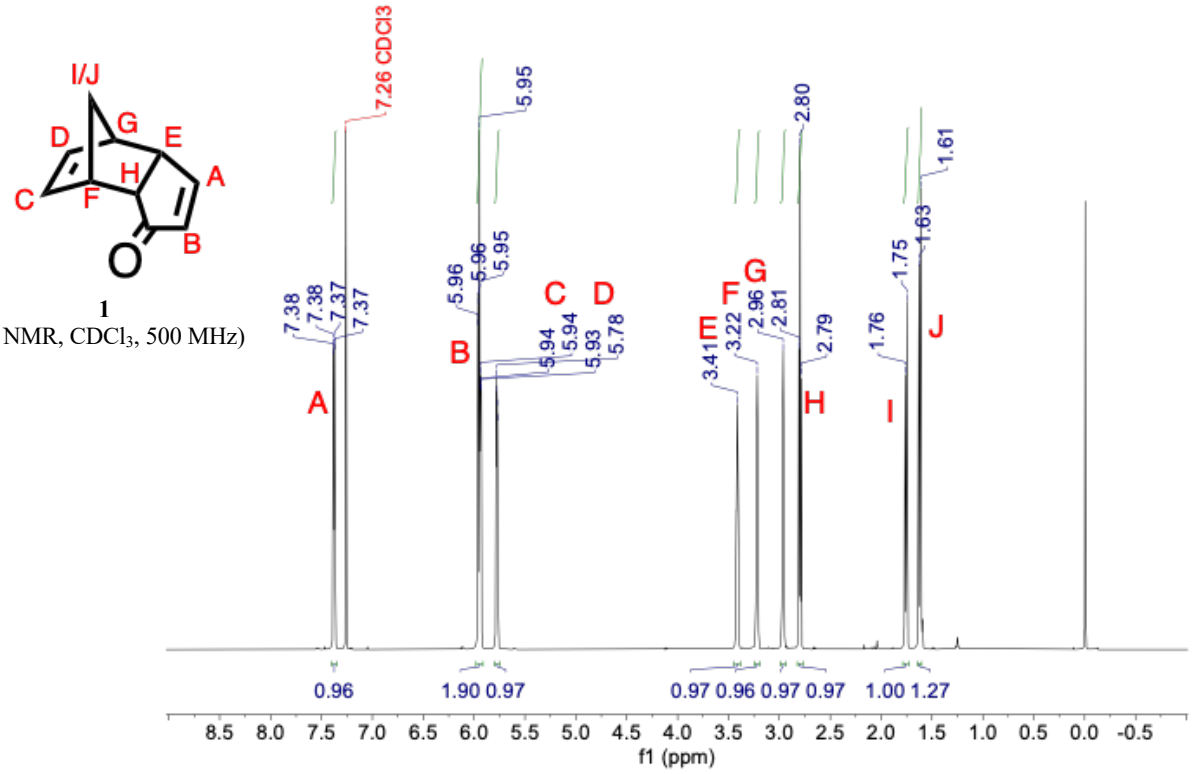

1
(^{1}H NMR, $CDCl_3$, 500 MHz)

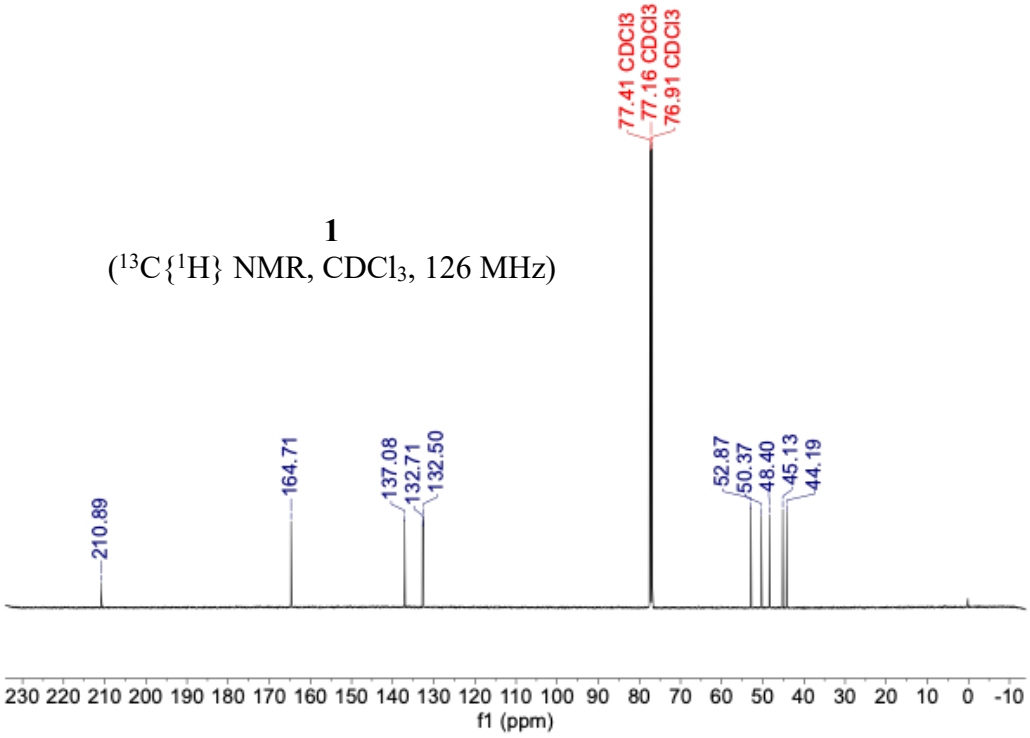

1
(^{13}C{^{1}H} NMR, $CDCl_3$, 126 MHz)

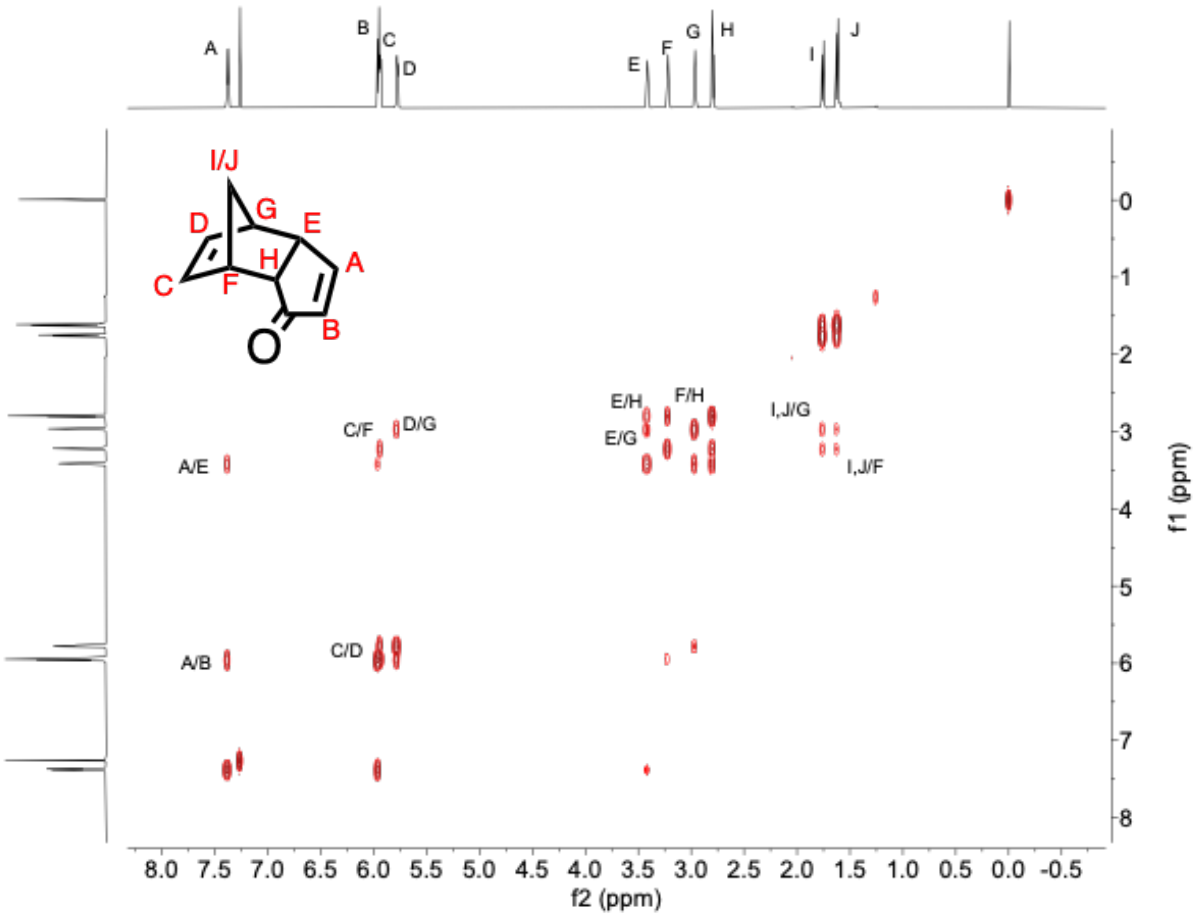

^{1}H-^{1}H COSY spectrum of **1** (500 MHz, $CDCl_3$). Correlations used for structural assignment are highlighted.

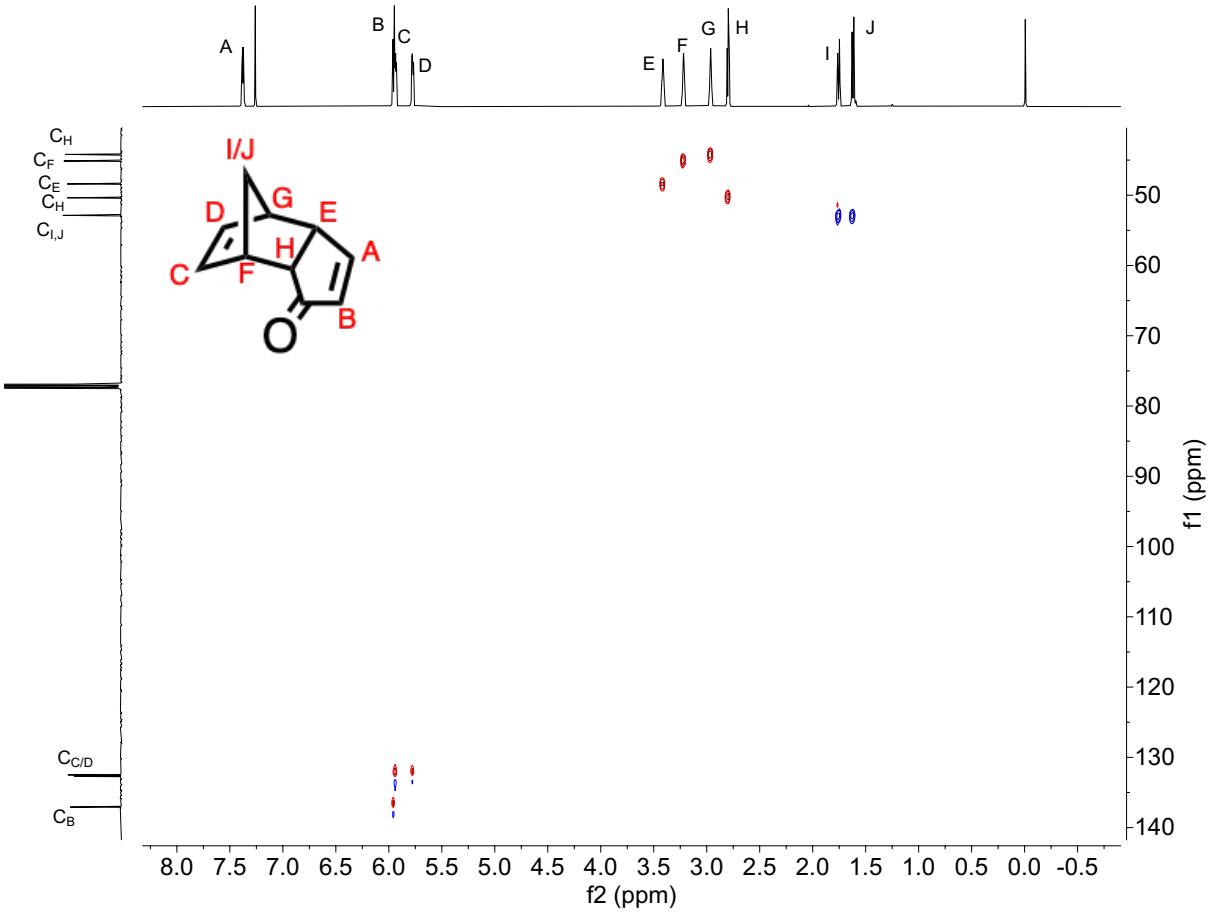

^{1}H-^{13}C HSQC spectrum of **1** (500 MHz, $CDCl_3$). Correlations used for structural assignment are highlighted.

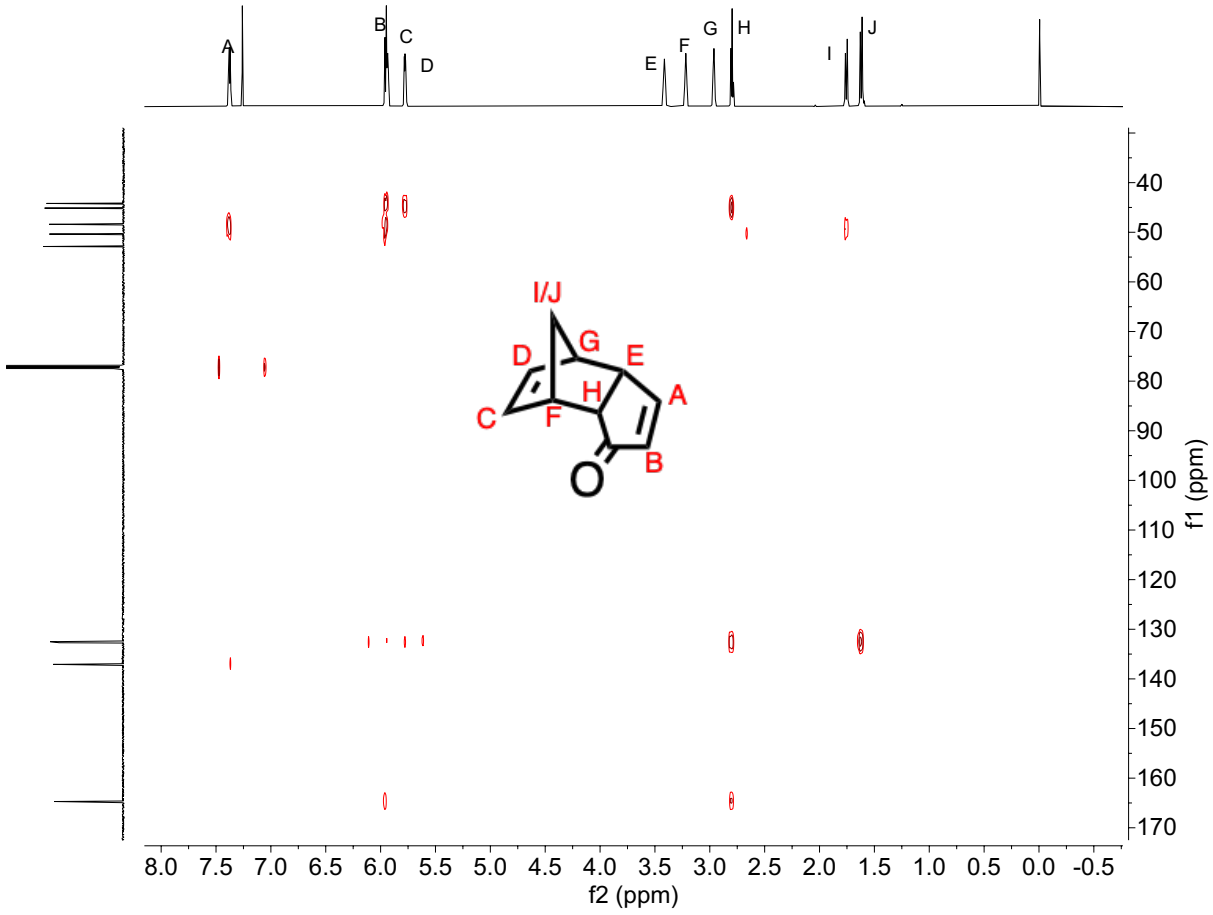

^{1}H-^{13}C HMBC spectrum of **1** (500 MHz, $CDCl_3$).

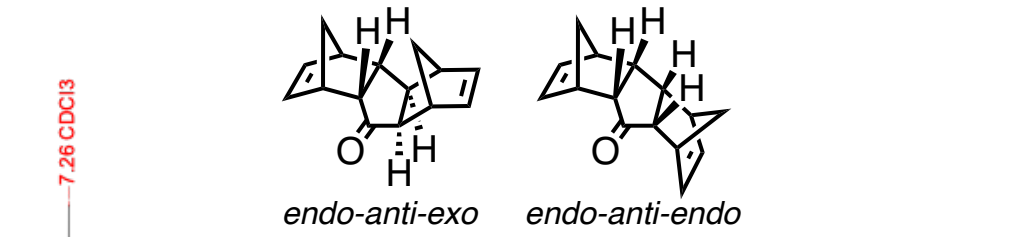

DA Adducts of **1** and CP
(^{1}H NMR, $CDCl_3$, 500 MHz)

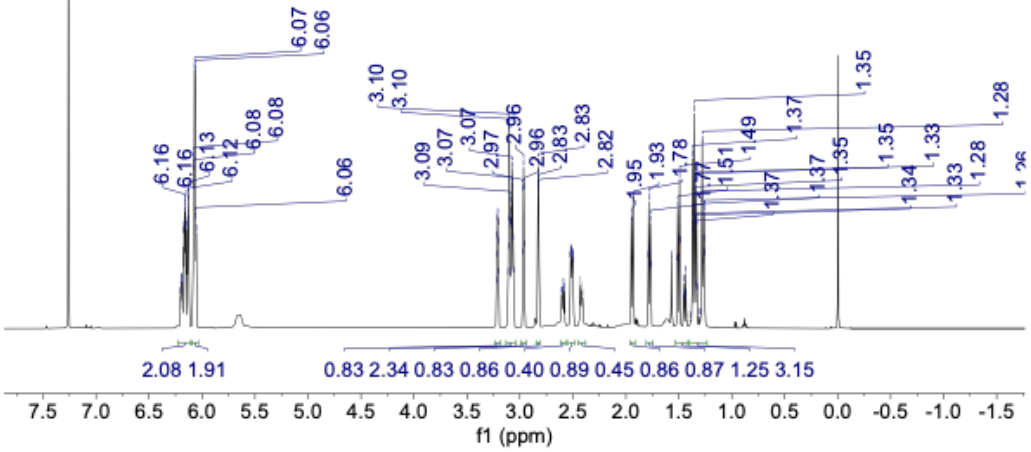

DA Adducts of **1** and CP
($^{13}C\{^{1}H\}$ NMR, $CDCl_3$, 500 MHz)

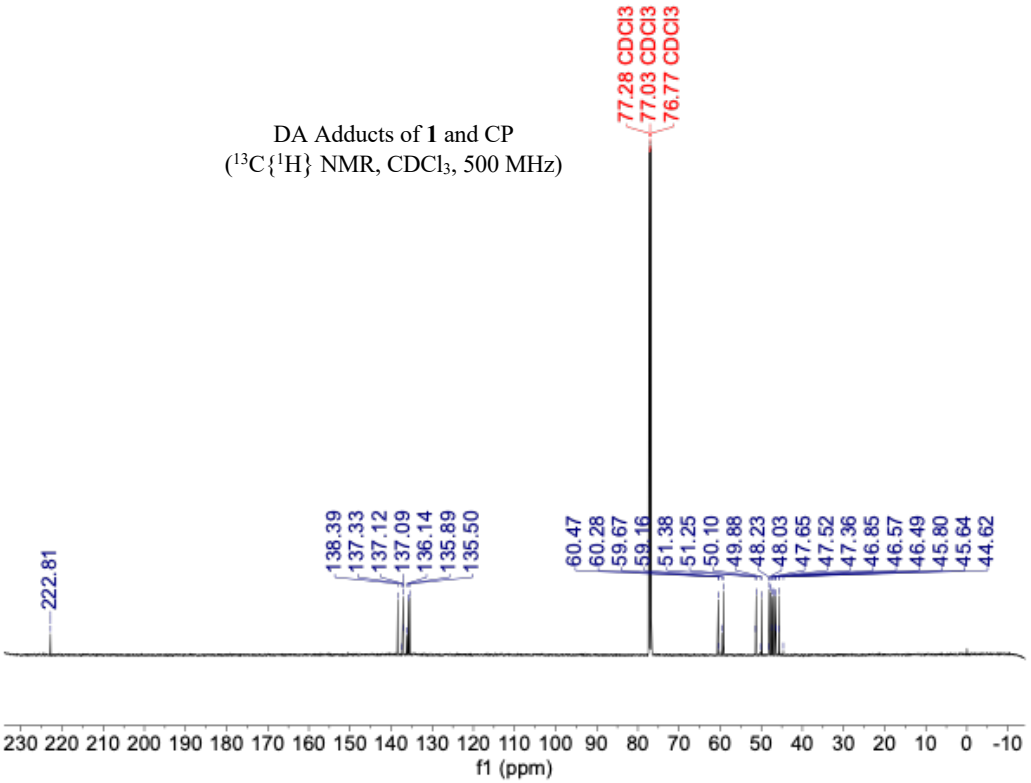

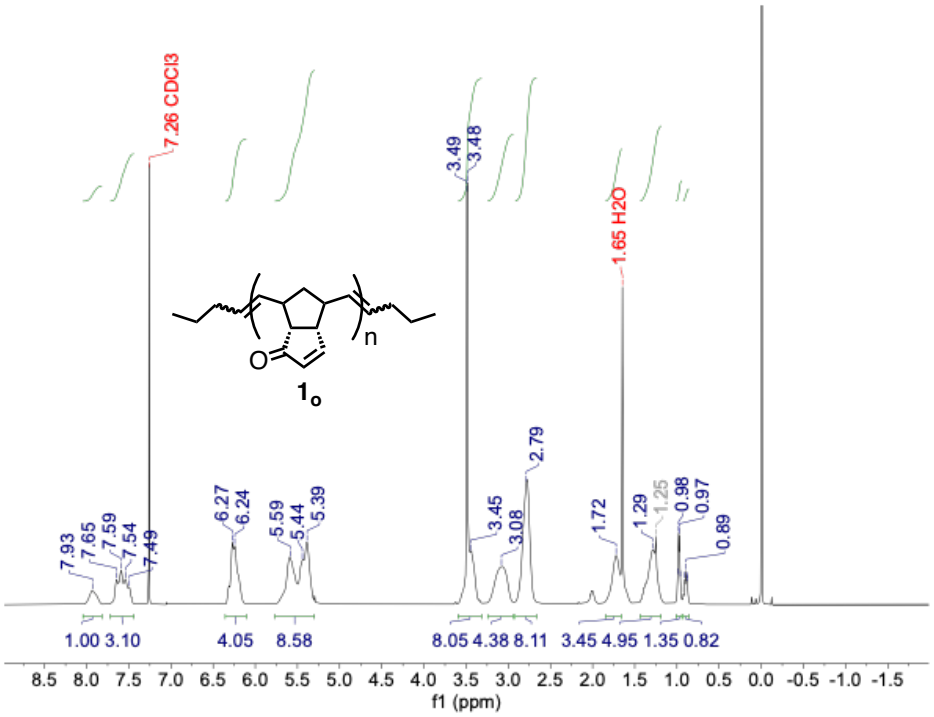

^{1}H NMR ($CDCl_3$, 500 MHz) of $\mathbf{1_o}$.

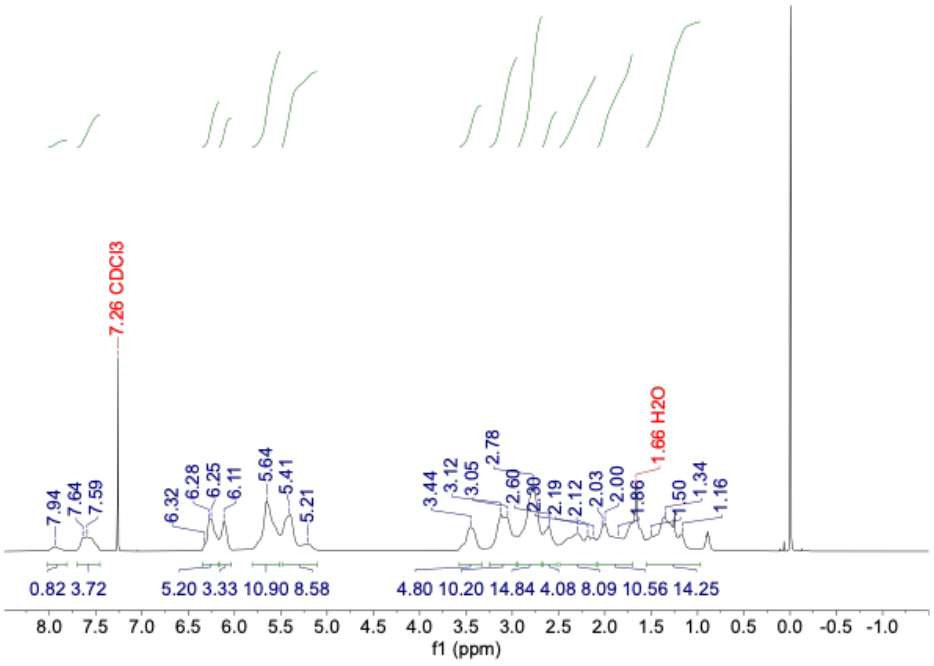

Cru

Crude ^{1}H NMR ($CDCl_3$, 500 MHz) of the product distribution from Diels-Alder reaction of $\mathbf{1_o}$ and CP.

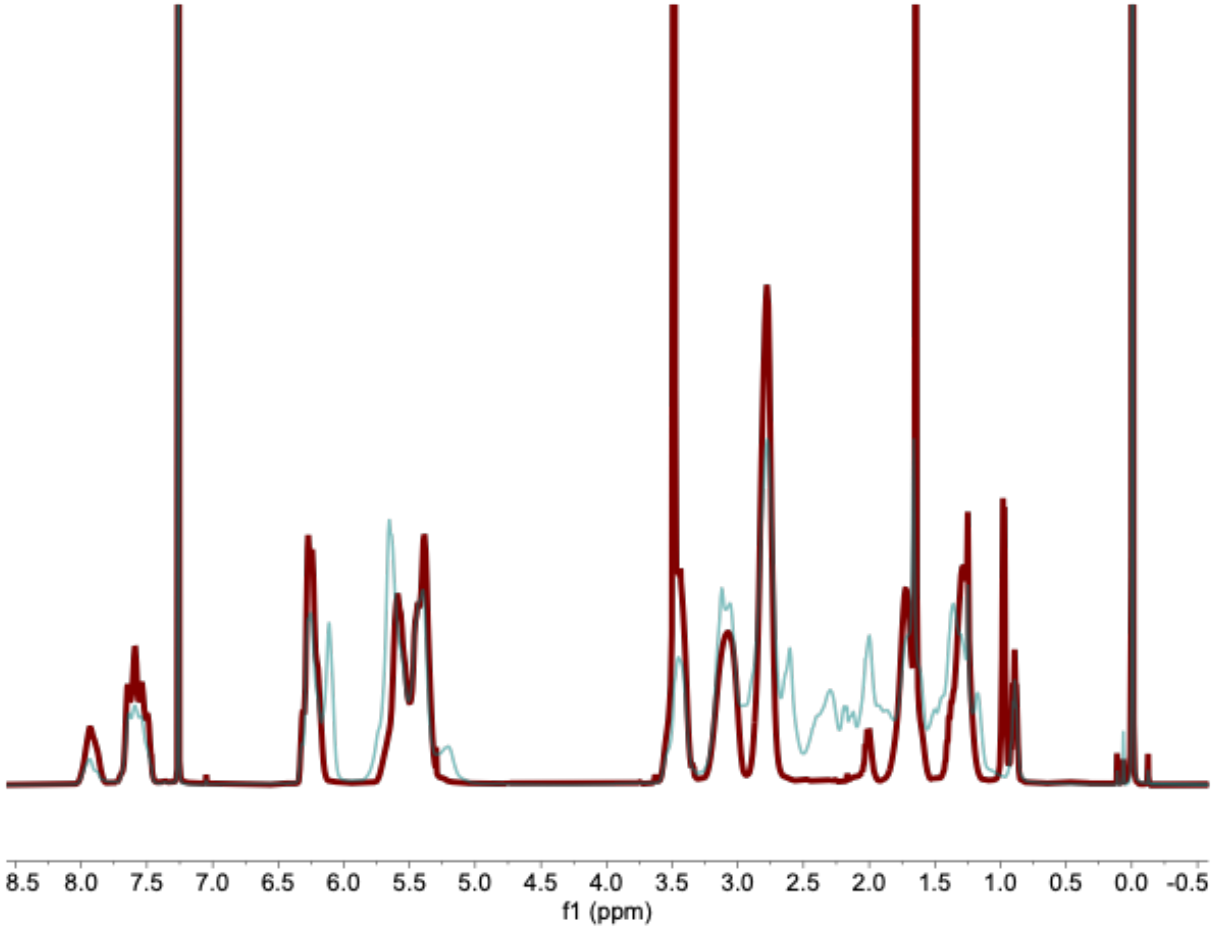

Overlaid spectra of $\mathbf{1_o}$ (red) and the Diels-Alder adduct of $\mathbf{1_o}$ and CP (blue) showing the appearance of new peaks in the alkyl and vinyl regions.

4.8 References

(1) Pascault, J.-P.; Sautereau, H.; Verdu, J.; Williams, R. J. J. *Thermosetting Polymers*; CRC Press, 2002.

(2) Abliz, D.; Duan, Y.; Steuernagel, L.; Xie, L.; Li, D.; Ziegmann, G. Curing Methods for Advanced Polymer Composites - A Review. *Polym. Polym. Compos.* **2013**, *21* (6), 341–348.

(3) Pojman, J. A. Polymer Science: A Comprehensive Reference. In *Polymer Science: A Comprehensive Refernce*; Matyjaszewski, K., Möller, M., Eds.; Elsevier: Amsterdam, 2021; pp 957–980.

(4) Suslick, B. A.; Hemmer, J.; Groce, B. R.; Stawiasz, K. J.; Geubelle, P. H.; Malucelli, G.; Mariani, A.; Moore, J. S.; Pojman, J. A.; Sottos, N. R. Frontal Polymerizations: From Chemical Perspectives to Macroscopic Properties and Applications. *Chem. Rev.* **2023**, *123* (6), 3237–3298.

(5) North, M. ROMP of Norbornene Derivatives of Amino-Esters and Amino-Acids. In *Ring Opening Metathesis Polymerisation and Related Chemistry*; Springer Netherlands: Dordrecht, 2002; pp 157–166.

(6) Robertson, I. D.; Yourdkhani, M.; Centellas, P. J.; Aw, J. E.; Ivanoff, D. G.; Goli, E.; Lloyd, E. M.; Dean, L. M.; Sottos, N. R.; Geubelle, P. H.; Moore, J. S.; White, S. R. Rapid Energy-Efficient Manufacturing of Polymers and Composites via Frontal Polymerization. *Nature* **2018**, *557* (7704), 223–227.

(7) Robertson, I. D.; Dean, L. M.; Rudebusch, G. E.; Sottos, N. R.; White, S. R.; Moore, J. S. Alkyl Phosphite Inhibitors for Frontal Ring-Opening Metathesis Polymerization Greatly Increase Pot Life. *ACS Macro Lett.* **2017**, *6* (6), 609–612.

(8) Vallons, K. A. M.; Drozdzak, R.; Charret, M.; Lomov, S. V.; Verpoest, I. Assessment of the Mechanical Behaviour of Glass Fibre Composites with a Tough Polydicyclopentadiene (PDCPD) Matrix. *Compos. Part A Appl. Sci. Manuf.* **2015**, *78*, 191–200.

(9) Woodson, C. S.; Grubbs, R. H. Polymeric Composites Including Dicyclopentadiene and Related Monomers. 6,310,121 B1, 2001.

(10) Delaude, L.; Noels, A. F. No Title. In *Kirk-Othmer Encyclopedia of Chemical Technology*; Seidel, A., Ed.; John Wiley & Sons, Inc.: Malden, 2007; pp 920–958.

(11) Long, T. E. Toward Recyclable Thermosets. *Science (80-.).* **2014**, *344* (6185), 706–707.

(12) Geyer, R.; Jambeck, J. R.; Law, K. L. Production, Use, and Fate of All Plastics Ever Made. *Sci. Adv.* **2017**, *3* (7).

(13) Post, W.; Susa, A.; Blaauw, R.; Molenveld, K.; Knoop, R. J. I. A Review on the Potential and Limitations of Recyclable Thermosets for Structural Applications. *Polym. Rev.* **2020**, *60* (2), 359–388.

(14) Pickering, S. J. Recycling Technologies for Thermoset Composite Materials—Current Status. *Compos. Part A Appl. Sci. Manuf.* **2006**, *37* (8), 1206–1215.

(15) Davydovich, O.; Paul, J. E.; Feist, J. D.; Aw, J. E.; Balta Bonner, F. J.; Lessard, J. J.; Tawfick, S.; Xia, Y.; Sottos, N. R.; Moore, J. S. Frontal Polymerization of Dihydrofuran Comonomer Facilitates Thermoset Deconstruction. *Chem. Mater.* **2022**, *34* (19), 8790–8797.

(16) Lloyd, E. M.; Cooper, J. C.; Shieh, P.; Ivanoff, D. G.; Parikh, N. A.; Mejia, E. B.; Husted, K. E. L.; Costa, L. C.; Sottos, N. R.; Johnson, J. A.; Moore, J. S. Efficient Manufacture, Deconstruction, and Upcycling of High-Performance Thermosets and Composites. *ACS*

Appl. Eng. Mater. **2023**, *1* (1), 477–485.

(17) Suslick, B. A.; Alzate-Sanchez, D. M.; Moore, J. S. Scalable Frontal Oligomerization: Insights from Advanced Mass Analysis. *Macromolecules* **2022**, *55* (18), 8234–8241.

(18) Godwin, B.; Anvari, M. H.; Olfatbakhsh, T.; Mahbod, M.; Milani, A. S.; DiLabio, G. A.; Wulff, J. E. A Single-Atom Upgrade to Polydicyclopentadiene. *Macromolecules* **2023**, *56* (4), 1592–1600.

(19) Rosenblum, M. Preparation and Thermal Rearrangement of Several Dicyclopentadiene Derivatives. *J. Am. Chem. Soc.* **1957**, *79* (12), 3179–3181.

(20) Álvarez, C.; Peláez, R.; Medarde, M. New Dicyclopentadiene-Based Scaffolds. *Tetrahedron* **2007**, *63* (10), 2132–2141.

(21) Borsato, G.; De Lucchi, O.; Fabris, F.; Lucchini, V.; Frascella, P.; Zambon, A. Synthesis and Evaluation of New Chiral Diols Based on the Dicyclopentadiene Skeleton. *Tetrahedron Lett.* **2003**, *44* (17), 3517–3520.

(22) Horn, E. J.; Rosen, B. R.; Chen, Y.; Tang, J.; Chen, K.; Eastgate, M. D.; Baran, P. S. Scalable and Sustainable Electrochemical Allylic C–H Oxidation. *Nature* **2016**, *533* (7601), 77–81.

(23) Hyatt, M. G.; Walsh, D. J.; Lord, R. L.; Andino Martinez, J. G.; Guironnet, D. Mechanistic and Kinetic Studies of the Ring Opening Metathesis Polymerization of Norbornenyl Monomers by a Grubbs Third Generation Catalyst. *J. Am. Chem. Soc.* **2019**, *141* (44), 17918–17925.

(24) Czelusniak, I.; Heywood, J. D.; Kenwright, A. M.; Khosravi, E. Investigation of Factors Affecting Ruthenium Complexation in ROMP Reactions of Oxygen-Containing Norbornene Derivatives Using Grubbs First Generation Initiator. *J. Mol. Catal. A Chem.*

2008, *280* (1–2), 29–34.

(25) Pojman, J. A.; Nagy, I. P.; Salter, C. Traveling Fronts of Addition Polymerization with a Solid Monomer. *J. Am. Chem. Soc.* **1993**, *115* (23), 11044–11045.

(26) Fortenberry, D. I.; Pojman, J. A. Solvent-Free Synthesis of Polyacrylamide by Frontal Polymerization. *J. Polym. Sci. Part A Polym. Chem.* **2000**, *38* (7), 1129–1135.

(27) Kotha, S.; Keesari, R. R.; Fatma, A.; Gunta, R. Synthetic Strategies to Diverse Polyquinanes via Olefin Metathesis: Access to the Basic Core of Crinipellin, Presilphiperfolanol, and Cucumin. *J. Org. Chem.* **2020**, *85* (2), 851–863.

(28) Saha, S.; Ginzburg, Y.; Rozenberg, I.; Iliashevsky, O.; Ben-Asuly, A.; Gabriel Lemcoff, N. Cross-Linked ROMP Polymers Based on Odourless Dicyclopentadiene Derivatives. *Polym. Chem.* **2016**, *7* (18), 3071–3075.